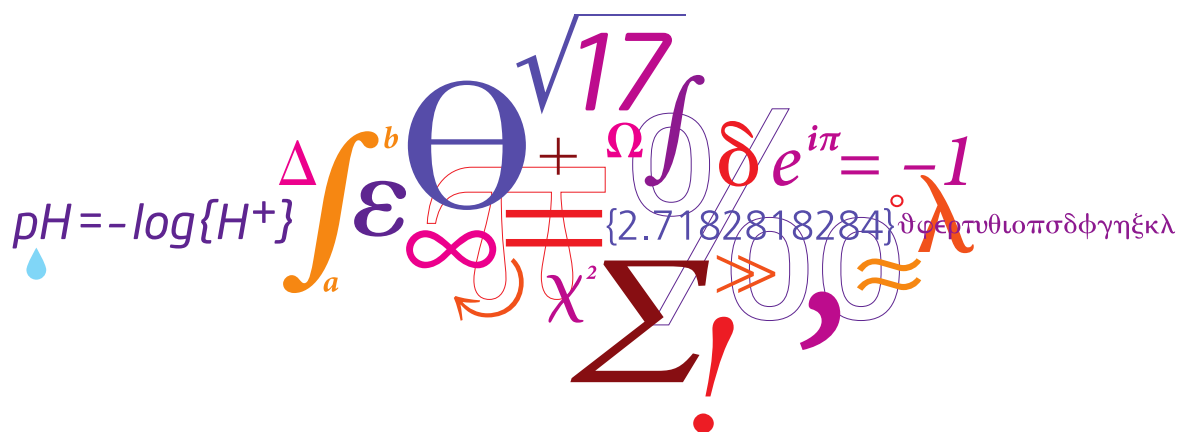

Modeling Study of High Pressure and High Temperature Reservoir Fluids



Farhad Varzandeh

June 26, 2017

Associate Professor Wei Yan

Professor Erling H. Stenby

Center for Energy Resources Engineering (CERE)

Department of Chemistry

Technical University of Denmark (DTU)

Kgs. Lyngby, Denmark

I would like to dedicate this thesis to:

My wife, my love and soul mate, Shahrzad

&

My parents and sister, Asadollah, Fariba, and Shiva

Acknowledgements

This thesis is submitted in partial fulfillment of the requirements for the Ph.D. degree at the Technical University of Denmark (DTU). The work was carried out at the Department of Chemistry, DTU, from December 2013 to March 2017 under the supervision of Associate Professor Wei Yan and Professor Erling H. Stenby. This PhD project was part of the NextOil (New Extreme Oil and Gas in Denmark) project sponsored by Innovation Fund Denmark, Mærsk oil and DONG E&P.

I would like to express my most sincere gratitude to my supervisors, Dr. Wei Yan and Prof. Erling H. Stenby, for supporting me throughout the project and for the many hours we have spent discussing the challenges. I am also grateful for the opportunities I have been given to attend several international conferences, at which I have had the chance to network and discuss with experts in the field. I would also like to thank my other colleagues at CERE and DTU-Kemi, especially Teresa, Anders and my office mates, Diego, Duncan and Christos for their input and assistance throughout this period.

I am grateful to my parents, Asadollah and Fariba, and my sister, Shiva, for their wise counsel and sympathetic ear. Last, but certainly not least, I will thank my wife and my soul mate, Shahrzad for her patience, support, and devotion throughout my Ph.D. studies. My Ph.D. journey would not be as exciting without her presence, encouragements and motivation. Thank you for being by my side in the up and downs of the journey, giving me confidence and making me more than I am.

June 26, 2017

Farhad Varzandeh

Summary

With dwindling easily accessible oil and gas resources, more and more exploration and production activities in the oil industry are driven to technically challenging environments such as unconventional resources and deeper formations. The temperature and pressure can become extremely high, e.g., up to 250 °C and 2400 bar, in the deep petroleum reservoirs. Furthermore, many of these deep reservoirs are found offshore, including the North Sea and the Gulf of Mexico, making the development even more risky. On the other hand, development of these high pressure high temperature (HPHT) fields can be highly rewarding if successfully produced. This PhD project is part of the NextOil (New Extreme Oil and Gas in the Danish North Sea) project which is intended to reduce the uncertainties in HPHT field development. The main focus of this PhD is on accurate description of the reservoir fluid behavior under HPHT conditions to minimize the production risks from these types of reservoirs. In particular, the study has thoroughly evaluated several non-cubic Equations of State (EoSs) which are considered promising for HPHT fluid modeling, showing their advantages and shortcomings based on an extensive comparison with experimental data. In the course of the evaluation, we have developed new petroleum fluid characterization procedures, built large databases for well-defined mixtures and reservoir fluids, and improved the evaluation software and made it more suitable for efficient and large scale comparison.

We have made a comprehensive comparison between cubic and non-cubic EoSs to evaluate whether advanced EoS in non-cubic forms, including both the SAFT-type EoS with strong theoretical basis (e.g. the PC-SAFT EoS) and the empirical BWR-type EoS (e.g. the Soave-BWR EoS), can be advantageous for describing the physical properties and phase equilibrium of reservoir fluids over a wide temperature and pressure range. In addition, we have also compared these models in calculation of heat capacities and Joule-Thomson coefficients for pure components and multicomponent mixtures. Joule-Thomson coefficients are of special interest to the oil industry because of the so called reverse Joule-Thomson effect commonly observed in HPHT fields, where a decrease in pressure results in an increase in temperature, which is just the opposite to the effect at low pressure. In the comparative studies between cubic and non-cubic

models, we also included GERG-2008 which is a wide-range EoS developed for 21 components of natural gases and their binary mixtures and is regarded as the most accurate EoS model for natural gas mixtures.

It was found that the non-cubic models are much better than the cubics in density, compressibility, heat capacity and Joule-Thomson coefficient calculation of the well-defined light and heavy components in reservoir fluids over a wide temperature and pressure range, GERG-2008 being the best with the lowest deviation among all EoS models. GERG-2008 however gives very large deviations for bubble point pressure calculation of some heavy and asymmetric binary systems such as n-butane + n-nonane system. This suggests that this EoS and its binary interaction parameters could still be improved for some of the binary pairs. Soave-BWR gives the closest prediction of the thermal properties to that of GERG-2008 among other EoSs tested in this study. The binary VLE calculation showed that PC-SAFT and Soave-BWR are similar to SRK and PR in correlating the important binary pairs in reservoir fluids. Although Soave-BWR and PC-SAFT give smaller average k_{ij} values than SRK and PR, they are more sensitive to the change in k_{ij} . Phase envelope prediction of synthetic gases showed that all the EoS models were similar for not too asymmetric synthetic gases, with or without the optimal k_{ij} values for SRK, PR, PC-SAFT and Soave-BWR. For highly asymmetric synthetic mixtures, Soave-BWR and GERG-2008 tend to predict phase envelopes different from other models whereas none of the tested models give satisfactory predictions. For heat capacity and Joule-Thomson coefficients, GERG-2008 and Soave-BWR give the closest predictions. All the evaluated EoS models tend to predict a nearly constant Joule-Thomson coefficient at high pressures. For typical reservoir temperatures, the constant is around -0.5 K/MPa.

For non-cubic models like PC-SAFT the characterization method is less mature than the cubic models. A reservoir fluid characterization method for PC-SAFT has been proposed by combining Pedersen's method with a newly developed set of correlations for the PC-SAFT model parameters m , $m\varepsilon/k$ and $m\sigma^3$. In addition, we further improved the characterization method for PC-SAFT by adjusting the correlations with a large PVT database. We have further improved the correlations and more importantly, we have established a general approach to characterizing reservoir fluids for any EoS. The approach consists in developing correlations of model parameters first with a database for well-defined components and then adjusting the correlations with a large PVT database. The adjustment is made to minimize the deviation in key PVT properties like saturation pressures, densities at reservoir temperature and Stock Tank

Oil (STO) densities, while keeping the n-alkane limit of the correlations unchanged. Apart from applying this general approach to PC-SAFT, we have also shown that the approach can be applied to classical cubic models like SRK and PR. In addition, we discussed how to develop a PNA based characterization for PC-SAFT and also utilize a large PVT database to further improve the characterization. With the developed characterization methods, we have made a comparison in PVT calculation involving 17 EoS-characterization combinations and 260 reservoir fluids. PC-SAFT with the new general characterization method is shown to give the lowest AAD% and maximum deviation in calculation of saturation pressure, density and STO density, among all the tested characterization methods for PC-SAFT. Application of the new characterization method to SRK and PR improved the saturation pressure calculation in comparison to the original characterization method for SRK and PR. Using volume translation together with the new characterization approach for SRK and PR gives comparable results for density and STO density to that of original characterization for SRK and PR with volume translation. For the PVT database used in this study, cubic EoSs seem to have better performance than PC-SAFT in calculation of saturation pressure; PC-SAFT and cubics with volume translation show comparable results in calculation of density and STO density. As a preliminary attempt to integrate more analytical information in characterization, we discussed how to modify the existing algorithms to utilize data from both simulated distillation and true boiling point distillation, and in particular, the component distribution information from the simulated distillation. Some analyses have been made on the impact of including more detailed analytical information.

Finally, to improve Soave-BWR for mixture calculation, we have tried to develop several new sets of mixing rules for this EoS. The new mixing rules were developed based on some theoretical considerations as well as the previous mixing rules for non-cubic EoS models. In addition, it was tried to create some hybrid mixing rules by combining a new set of mixing rules and the original mixing rules for Soave-BWR. It was shown that some problems with the original Soave-BWR mixing rules can be fixed by the new mixing rules although the overall performance is not significantly improved. Development of mixing rules for non-cubic EoS models is still a semi-empirical process, requiring extensive testing to evaluating their performance. We have developed the code in a structured manner so that the new mixing rules can be quickly tested. It can facilitate further extensive screening of new mixing rules for Soave-BWR or even other non-cubic EoS models.

Resumé

Med faldende forekomster af nemt tilgængelige olie og ressourcer finder flere og flere udforsknings- og produktions aktiviteter i olie industrien sted i teknisk udfordrende miljøer, så dybere formationer eller som utraditionelle ressourcer. Temperatur og tryk kan blive meget højt, fx op til 250 °C og 2400 bar, i dybe petroleums reservoirer. Ydermere er mange af disse dybe reservoirer beliggende off-shore, som i Nordsøen eller den mexicanske golf, hvilket gør udviklingen endnu mere risikabel. Fordelen ved udviklingen af disse højt tryk, høj temperatur (HPHT) felter er, på den anden side, et højt udbytte, hvis succesfuldt. Dette PhD projekt er en del af NextOil (New Extreme Oil and Gas in the Danish North Sea) projektet, der har til formål at reducere usikkerhederne i HPHT felt udviklingsprocessen. Hoved fokus er på nøjagtigt beskrivelse af reservoir olierne opførsel under HPHT betingelser for at minimere risikoen ved produktion fra denne type reservoirer. Studiet har i særdeleshed grundigt evalueret flere ikke-kubiske tilstandsligninger (EoS) der er betragtet som lovende for HPHT olie modellering, og viser deres fordele og hvor de har problemer baseret på en omfattende sammenligning med eksperimentel data. I forbindelse med evalueringen har vi udviklet en ny olie karakteriserings procedure, bygget store databaser for klart-definerede blandinger og reservoir olier, samt forbedret evaluerings softwaren og gjort den bedre egnet for effektiv sammenligning på en større skala.

Vi har lavet en omfattende sammenligning mellem kubiske og ikke kubiske EoS'er for at evaluere om avancerede ikke kubiske EoS'er, inklusive både EoS'er i stil med SAFT med stærk teoretisk baggrund og empiriske EoS'er i stil med BWR (for eksempel Soave-BWR EoS), bedre kan beskrive de fysiske egenskaber og fasevægt af reservoir olier over et bredt temperatur og tryk spænd. Ud over dette har vi også sammenlignet disse modeller ved udregning af varme kapaciteter og Joule-Thomson koefficienter for såvel rene komponenter som multikomponent blandinger. Joule-Thomson koefficienter har særligt interesse i olie industrien på grund af den såkaldte omvendte Joule-Thomson effekt normalt set i HPHT felter, hvor et fald i tryk vil resultere i en stigning i temperatur, hvilket er direkte modsat af effekten ved lavt tryk. I dette sammenligningsstudie mellem kubiske og ikke kubiske modeller, har vi også inkluderet GERG-2008, som er

en EoS udviklet for 21 komponenter af natur gas og deres respektive binære blandinger. Den anses generelt som den mest præcise EoS model for naturgas blandinger.

Vi fandt at de ikke-kubiske modeller virkede langt bedre end de kubiske i forhold til densitet, kompressibilitet, varme kapacitet og Joule-Thomson koefficient beregninger for veldefinerede reservoir olier, såvel lette som tunge, over et bredt temperatur og tryk spænd. GERG-2008 var bedst med de laveste afvigelser af alle EoS modellerne. GERG-2008 giver imidlertid meget store afvigelser i boblepunkts tryk beregninger for nogle tunge og asymmetriske binære systemer som for eksempel n-butan+ n-nonan systemet. Dette indikerer at denne EoS og dens binære interaktions parametre kan forbedres for nogle af de binære par. Soave-BWR giver den næste bedre forudsigelse af de termiske egenskaber blandt de undersøgte EoS'er efter GERG-2008. Binære VLE beregninger viser at PC-SAFT og Soave-BWR er meget lig SRK og PR for korrelation af vigtige binære par i reservoir olier. Selvom Soave-BWR og PC-SAFT giver mindre k_{ij} værdier i gennemsnit end SRK og PR, så er de også mere sensitive i forhold til ændringer i k_{ij} . Forudsigelsen af boblepunktskurven i et temperatur mod tryk diagram for syntetiske gaser viste at alle EoS modellerne opfører sig sammenligneligt for ikke alt for asymmetriske syntetiske gaser, både med og uden optimale k_{ij} værdier for SRK, PR, PC-SAFT og Soave-BWR. For meget asymmetriske syntetiske blandinger, har Soave-BWR og GERG-2008 tendens til at forudsige boblepunktskurven i et temperatur mod tryk diagram forskelligt fra de andre modeller, men ingen af de testede modeller giver tilfredsstillende forudsigelser. For varme kapacitet og Joule-Thomson koefficienter giver GERG-2008 og Soave-BWR de bedste forudsigelser. Alle de evaluerede EoS modeller tendenser til at forudsiger en nærmest konstant Joule-Thomson koefficient ved højt tryk. Ved typiske reservoir temperaturer er konstanten omkring -0.5 K/MPa.

For ikke kubiske modeller som PC-SAFT er karakteriserings metoderne mindre modne end de er for kubiske modeller. En reservoir olie karakteriserings metode for PC-SAFT er blevet forlagt ved at kombinere Pedersen's metode med et ny udviklet sæt af korrelationer for PC-SAFT modellens parametre, m , $m\varepsilon/k$ og $m\sigma^3$. Udover dette har vi forbedret karakteriseringen for PC-SAFT yderligere ved at justere korrelationerne ved brug af en stor PVT database. Vi har udviklet yderligere på korrelationerne og endnu mere vigtigt, så har vi udviklet en general tilgang til karakterisering af reservoir olier for enhver EoS. Denne tilgang er baseret på udvikling af korrelationer af model parametre, først med en database for veldefinerede komponenter og siden ved at justere korrelationerne til en stor PVT database. Ændringerne er lavet for at minimere afvigelsen i vigtige PVT egenskaber som damptryk, densitet ved reservoir temperatur

og “Stock Tank Oil” (STO) densitet, mens n-alkan begrænsningen for korrelationerne er bevaret uændret. Udover at anvende denne generelle tilgang på PC-SAFT, har vi også vist at den kan bruges med klassiske kubiske modeller som SRK og PR. Vi diskuterer også hvordan man kan udvikle en PNA baseret karakterisering for PC-SAFT og samtidig gøre brug af en stor PVT database til yderligere optimering af karakteriseringen. Med den udviklede karakteriserings metode, har vi lavet en sammenligning af PVT beregninger ved brug af 17 EoS-karakteriseringens kombinationer og 260 reservoir olier. PC-SAFT med den nye generelle karakteriserings metode er fundet til at give den laveste AAD% og maksimum afvigelse ved beregning af damptryk, densitet og STO densitet, sammenlignet med PC-SAFT med alle de andre testede karakteriserings metoder. Brug af den nye karakteriserings metode for SRK og PR forbedrede damptryk beregningen sammenlignet med den originale karakteriserings metode for SRK og PR. Ved brug af en volumen translation sammen med den nye karakteriserings metode for SRK og PR giver sammenlignelige resultater for densitet og STO densitet med den originale karakterisering for SRK og PR med volumen translation. For PVT databasen brugt i dette studie synes de kubiske EoS'er at gøre det bedre end PC-SAFT når det kommer til beregning af damptrykket, mens kubiske EoS'er med volumen translation og PC-SAFT opnår sammenlignelige resultater i beregningen af densitet og STO densitet. Som et tidligt forsøg på at integrere mere analytisk information i karakteriseringen har vi diskuteret hvordan man kan modificere de eksisterende algoritmer to at gøre brug af data fra både simuleret destillation og “true boiling point” destillation, og i særdeleshed, informationen om sammensætningen fra den simulerede destillation. Noget analyse er lavet omkring påvirkningen af at inkludere mere detaljeret analytisk information.

Slutteligt, for at forbedre Soave-BWR for blandings beregninger, har vi prøvet at udvikle indtil flere nye set af blandings regler for denne EoS. De nye blandings regler er udviklet baseret på teoretiske betragtninger samt tidligere blandings regler for ikke kubiske EoS modeller. Ud over dette har vi forsøgt at skabe nogle hybrid blandingsregler ved at kombinere et nyt sæt blandings regler med originale blandingsregler for Soave-BWR. Det er vist at nogle problemer ved de originale Soave-BWR blandingsregler kan rettes med de nye blandingsregler, men den samlede præstation er dog ikke væsentligt forbedret. Udvikling af blandingsregler for ikke kubiske EoS modeller er stadig en semiempirisk proces der kræver grundige tests for at evaluere deres kunnen. Vi har udviklet koden i en struktureret facon således at nye blandingsregler hurtigt kan testes. Det kan derfor bruges til yderligere omfattende screening af nye blandingsregler for Soave-BWR eller endda andre ikke kubiske EoS modeller.

Contents

List of Figures	xvi
List of Tables	xxvi
List of Symbols	xxx
1 Introduction	1
1.1 Thermodynamic Models Considered for HPHT Modeling	3
1.2 Scope and Outline of This Research	5
2 Cubic and Non-Cubic Equations of State	8
2.1 Cubic Equations of State	9
2.1.1 Soave-Redlich-Kwong EOS (SRK)	9
2.1.2 Peng-Robinson EOS (PR)	10
2.1.3 Volume Shift	11
2.2 PC-SAFT EoS	12
2.3 Soave-BWR EoS	14
2.4 GERG-2008 EoS	17
3 Phase Behavior of Well Defined Systems	19
3.1 Density and Compressibility of Pure Components	22

3.1.1	Density and Saturated Liquid Density Calculations	23
3.1.2	Isothermal Compressibility Calculations	33
3.1.3	Sample Binary Density and Multicomponent Gas Mixture Z Factor	34
3.2	Binary VLE and Regression of Binary Interaction Parameters	38
3.3	Phase Envelopes of Multicomponent Mixtures	49
3.4	Conclusions	67
4	Petroleum Fluid Characterization and PVT Modeling	69
4.1	Methods of Petroleum Hydrocarbon Analysis	72
4.1.1	Overview	72
4.1.2	True Boiling Point Distillation (TBP)	73
4.1.3	Simulated Distillation by Gas Chromatography (SimDist)	73
4.1.4	Two-Dimensional Gas Chromatography (GC \times GC)	76
4.1.5	Critical Information Obtained from Various Analytical Methods	79
4.2	Overview of C_{7+} Characterization Procedure	80
4.2.1	Molar Distribution	81
4.2.2	Parameter Estimation for Thermodynamic Models	86
4.2.3	Lumping	86
4.3	Characterization for SRK, PR and Soave-BWR	87
4.4	Characterization for PC-SAFT	88
4.5	Considerations in a General Characterization Approach	93
4.6	General Characterization Approach for PC-SAFT	94
4.7	Application of The General Approach to SRK and PR	98
4.8	A PNA Based Characterization Method for PC-SAFT	101
4.9	C_{7+} Characterization using More Detailed Analytical Information	106
4.10	Results and Discussions	109

4.10.1	Petroleum Fluid Database	109
4.10.2	Deviations in Saturation Pressure, Density and STO Density . .	109
4.10.3	Simulation of DL and CME Tests	112
4.10.4	Impact of Compositional Characterization on PVT Modeling . .	121
4.11	Conclusions	134
5	Heat Capacity and Joule-Thomson Coefficient	136
5.1	Isobaric Heat Capacity Calculations	138
5.2	Joule-Thomson Coefficient Calculations	138
5.3	Results and Discussions	139
5.3.1	Systematic Comparison of Different EoSs for C_p and μ_{JT} of Pure and Multicomponent Systems	141
5.3.2	Heat Capacity and Joule-Thomson Coefficient Calculations for Light and Heavy n-alkanes	148
5.3.3	Joule-Thomson Inversion Curve	156
5.4	Conclusions	159
6	New Mixing Rules for Soave-BWR	161
6.1	Equations of State Mixing Rules	161
6.1.1	Classical Mixing Rules	163
6.1.2	Mixing Rules for The Virial Family of EoS	166
6.2	Development of New Mixing Rules for Soave-BWR	172
6.2.1	Mixing Rules using the van der Waals (vdW) Approach	172
6.2.2	LKP Mixing Rules (LKP)	174
6.2.3	Other Hybrid Mixing Rules	174
6.2.4	Implementation of the New Mixing Rules	175
6.2.5	Preliminary Evaluation of The New Mixing Rules	176

6.3	Results and Discussions	182
6.3.1	Density Calculations	182
6.3.2	Binary VLE and Regression of Binary Interaction Parameters .	184
6.3.3	Phase Envelopes of Multicomponent Mixtures	186
6.4	Conclusions	194
7	Conclusions and Future Work	196
7.1	Conclusions	196
7.1.1	Phase Behavior Study of Well-Defined Components	196
7.1.2	Reservoir Fluid Characterization and PVT Modeling	197
7.1.3	Heat Capacities and Joule-Thomson Coefficients	199
7.1.4	New Mixing Rules for Soave-BWR	200
7.2	Future Work	201
7.2.1	Further Development of Soave-BWR EoS	201
7.2.2	Fluid Characterization using More Detailed Analytical Information	202
	Bibliography	203
	Appendix A Parameter Estimation for Thermodynamic Models	218
A.1	Acentric Factor Correlations	218
A.2	Critical Temperature and Pressure Correlations	219
A.3	Comparison of Critical Properties Correlations	224
	Appendix B PVT Database and Deviations in Saturation Pressure, Density and STO Density	228
B.1	Petroleum Fluid Database	228
B.2	Deviations in Saturation Pressure, Density and STO Density	236
B.3	PVT Results using General Characterization Approach for PC-SAFT .	249

B.4 Deviation in Compressibility Calculations	262
Appendix C C_p and μ_{JT} Calculated using Different EoSs for Light and Heavy n-alkanes	264
Appendix D Academic Activities	272
D.1 Peer Reviewed Journal Articles	272
D.2 Conference Presentations	272
D.3 Teaching Assistance/Supervisory of M.Sc. Projects	274

List of Figures

1.1	HPHT classification system from [2]. The classification boundaries represent stability limits of common well-service-tool components, elastomeric seals and electronic devices.	2
3.1	AAD% in calculated density for different EoS within 150-500 K and 0-2000 bar.	25
3.2	Contour map of deviation in the calculated densities for methane by different EoSs. The relative deviations (%) are labeled on the contour lines. The green and the red circles indicate the conditions for the minimum and the maximum deviations, respectively.	28
3.3	AAD% in the calculated saturated liquid density for different EoSs. . .	29
3.4	Average AAD% in the calculated density and saturated liquid density of the “main components” using different EoSs.	31
3.5	Density vs. pressure for n-C9 using GERG-2008 (blue lines) and Soave-BWR (red lines) at different temperatures: 303.15 K (solid lines), 323.15 K (dotted lines), 373.15 K (dashed line), 473.15 K (dash-dot lines), 523.15 K (long-dashed lines), and 573.15 K (long-dashed double dots lines). The experimental data is taken from [60].	32
3.6	Contour map of deviation in the calculated density (a) and compressibility (b) for methane using GERG-2008. The relative deviations (%) are labeled on the contour lines. The blue dashed lines show negative deviations and solid black lines show positive deviations. The green and the red circles indicate the conditions for the minimum and the maximum deviations, respectively.	34

3.7	Contour map of deviation in the compressibility of methane using SRK (a), PR (b), SRK with volume translation (c), PR with volume translation (d), PC-SAFT (e), and Soave-BWR (f).	35
3.8	AAD% in the calculated densities of the binary system methane (1) + n-decane (2) using GERG-2008, PC-SAFT and Soave-BWR with regressed k_{ij} within 278.15-463.15 K and 1-1400 bar. The experimental data is taken from [61].	36
3.9	Density vs. pressure using GERG-2008 (blue lines) and Soave-BWR with regressed k_{ij} (red lines) for two mixtures of methane and n-decane at different temperatures. 22.27 mol% C ₁ and 323.2 K (\diamond , solid lines), 22.27 mol% C ₁ and 463.2 K (Δ , dashed lines), 70.85 mol% C ₁ and 323.2 K (\square , dash-dot lines), and 70.85 mol% C ₁ and 463.2 K (\circ , long-dashed lines). The experimental data is taken from [61].	36
3.10	Experimental and simulated results using GERG-2008 (blue lines) and Soave-BWR with regressed k_{ij} (red lines) for Z factor of the gas mixture A from [62] at different temperatures: 290 K (solid lines), 315 K (dashed lines), and 340 K (long-dashed lines).	37
3.11	AAD% in bubble point pressure and vapor phase composition for the binary pairs of N ₂ , CO ₂ , H ₂ S and C ₁ using different EoSs with 0 k_{ij} and regressed k_{ij}	46
3.12	Deviations in bubble point pressure calculation as a function of temperature using GERG-2008 (blue markers) and Soave-BWR with 0 k_{ij} (red markers) for different binary mixtures of n-butane (1) + n-nonane (2). 74.9 mol% nC ₄ (\blacksquare), 50.2 mol% nC ₄ (\blacktriangle), 26.2 mol% nC ₄ (\blacklozenge), and 21.4 mol% nC ₄ (\bullet). The experimental data is taken from [65].	47
3.13	Bubble point pressures at different temperatures using GERG-2008 (blue lines) and Soave-BWR with 0 k_{ij} (red lines) for binary mixtures of nC ₄ and nC ₉ . 74.9 mol% nC ₄ (\square , solid lines), 50.2 mol% nC ₄ (Δ , dashed lines), 26.2 mol% nC ₄ (\diamond , dash-dot lines), and 21.4 mol% nC ₄ (\circ , dotted lines). The experimental data is taken from [65].	47
3.14	Phase envelopes for Gas 5 with (a) zero k_{ij} 's and (b) the optimal k_{ij} 's.	52
3.15	Phase envelopes for Gas 6 with (a) zero k_{ij} 's and (b) the optimal k_{ij} 's.	53

3.16	Phase envelopes for Gas 10 with (a) zero k_{ij} 's and (b) the optimal k_{ij} 's.	54
3.17	Phase envelopes for Gas 11 with (a) zero k_{ij} 's and (b) the optimal k_{ij} 's.	55
3.18	Phase envelopes for (a) Gas 12, and (b) Gas 16 with optimal k_{ij} 's.	56
3.19	Phase envelopes for Gas 17 with (a) zero k_{ij} 's and (b) the optimal k_{ij} 's.	57
3.20	Phase envelopes for Gas 18 with (a) zero k_{ij} 's and (b) the optimal k_{ij} 's.	58
3.21	Phase envelopes for Gas 22 with (a) zero k_{ij} 's and (b) the optimal k_{ij} 's.	59
3.22	Phase envelopes for Gas 24 with (a) zero k_{ij} 's and (b) the optimal k_{ij} 's.	60
3.23	Phase envelopes for Gas 25 with (a) zero k_{ij} 's and (b) the optimal k_{ij} 's.	61
3.24	Phase envelopes for Gas 26 with (a) zero k_{ij} 's and (b) the optimal k_{ij} 's.	62
3.25	Phase envelopes for Gas 27 with (a) zero k_{ij} 's and (b) the optimal k_{ij} 's.	63
3.26	Phase envelopes for Gas 28 with (a) zero k_{ij} 's and (b) the optimal k_{ij} 's.	64
3.27	Phase envelope for binary mixtures of methane + n-decane (40.31 mol% C_1) using different EoSs with optimal k_{ij} 's. The experimental data is taken from [61].	65
3.28	Phase envelope for binary mixtures of methane + n-decane (60.21 mol% C_1) using different EoSs with optimal k_{ij} 's. The experimental data is taken from [61].	66
3.29	Phase envelope for binary mixtures of methane + n-decane (84.97 mol% C_1) using different EoSs with optimal k_{ij} 's. The experimental data is taken from [61].	66
4.1	Sample SimDist results up to around C_{40} for an oil sample.	75
4.2	Isolating the paraffinic group within each SCN fraction for the oil sample in Figure 4.1.	75
4.3	Contour plot of the GC×GC separation of a heavy gas oil from [102]. The shaded band is presented as a 3D-plot in Figure 4.4.	77
4.4	3D-plot of a part of the GC×GC separation of a heavy gas oil from [102] (the shaded part of Figure 4.3).	78

4.5	Change of σ for non n-alkanes with the relative difference in specific gravity SG . σ_p and SG_p are for the n-alkanes at the same boiling point temperatures.	91
4.6	Change of ε for non n-alkanes with the relative difference in specific gravity SG . ε_p and SG_p are for the n-alkanes at the same boiling point temperatures.	92
4.7	Change of m for non n-alkanes with the relative difference in specific gravity SG . m_p and SG_p are for the n-alkanes at the same boiling point temperatures.	93
4.8	The recommended characterization procedure (steps A and B) and its application to PVT calculation.	95
4.9	T_c and P_c correlations as a function of ΔSG for the pure components in DIPPR database.	99
4.10	Comparison between original and simplified Twu's method in calculation of critical temperature and pressure vs. experimental data from DIPPR. 100	
4.11	SG vs. T_b for n-alkanes and other hydrocarbons in DIPPR database. The black dashed line passes through the representative aromatic group listed in Table 4.3.	103
4.12	Phase envelope diagram for Fluid 7 from [128] using PC-SAFT and the "trial" PNA Approach.	104
4.13	Density vs. pressure for the oil mixture from [87] - a) Comparison between cubics with and without volume translation and non-cubic models including PC-SAFT with the new general characterization method, b) Comparison between different characterization methods for PC-SAFT. 114	
4.14	Gas compressibility factor vs. pressure for the oil mixture from [87] - a) Comparison between cubics with and without volume translation and non-cubic models including PC-SAFT with the new general characterization method, b) Comparison between different characterization methods for PC-SAFT.	115

4.15	Oil formation volume factor vs. pressure for the oil mixture from [87] - a) Comparison between cubics with and without volume translation and non-cubic models including PC-SAFT with the new general characterization method, b) Comparison between different characterization methods for PC-SAFT.	117
4.16	Solution gas-oil ratio vs. pressure for the oil mixture from [87] - a) Comparison between cubics with and without volume translation and non-cubic models including PC-SAFT with the new general characterization method, b) Comparison between different characterization methods for PC-SAFT.	118
4.17	Oil compressibility vs. pressure for the oil mixture from [87] - a) Comparison between cubics with and without volume translation and non-cubic models including PC-SAFT with the new general characterization method, b) Comparison between different characterization methods for PC-SAFT.	119
4.18	Oil compressibility vs. pressure for fluid 73 from the database - Comparison between cubics with and without volume translation and non-cubic models including PC-SAFT with the new general characterization method.	120
4.19	SimDist results for the light crude oil from the Danish North Sea (DK oil sample).	122
4.20	Simulated distillation calibration chromatogram.	122
4.21	Simulated distillation for the DK oil sample up to C ₄₀	123
4.22	Isolating the paraffinic group within each SCN fraction for the DK oil sample.	124
4.23	Mole% of the sample black oil calculated from wt% of TBP distillation using MW^{Exp} and MW^{KF}	129
4.24	Phase envelopes of black oil and gas condensate samples using TBP distillation data.	130
4.25	Phase envelopes of black oil and gas condensate samples using SimDist data.	131
4.26	Density of black oil sample at 388.75 K using TBP distillation data with MW^{Exp} (black) and MW^{KF} (red).	132

4.27	Density of black oil sample at 388.75 K using SimDist data with MW^{Exp} (black) and MW^{KF} (red).	132
4.28	Density of gas condensate sample at 388.75 K using TBP distillation data with MW^{Exp} (black) and MW^{KF} (red).	133
4.29	Density of gas condensate sample at 388.75 K using SimDist data with MW^{Exp} (black) and MW^{KF} (red).	133
5.1	Heat capacity prediction for methane at different temperatures using REFPROP. The experimental data is taken from [154].	140
5.2	Joule-Thomson coefficient prediction for methane at different temperatures using REFPROP. The experimental data is taken from [154].	140
5.3	AAD% in the heat capacity of the “main components” within 250-500 K and 5-1500 bar using different EoSs. The model predictions are compared with REFPROP results.	141
5.4	MAD in the Joule-Thomson coefficient of the “main components” within 250-500 K and 5-1500 bar using different EoSs. The model predictions are compared with REFPROP results.	142
5.5	AAD% in the heat capacity of binary and multicomponent mixtures within 250-500 K and 5-1500 bar using different EoSs. The model predictions are compared with REFPROP results (REFPROP uses GERG-2008 for mixtures).	143
5.6	MAD in the Joule-Thomson coefficient of binary and multicomponent mixtures within 250-500 K and 5-1500 bar using different EoSs. The model predictions are compared with REFPROP results (REFPROP uses GERG-2008 for mixtures).	144
5.7	Heat capacity vs. pressure using GERG-2008 (blue lines) and Soave-BWR (red lines) for C_1 at different temperatures: 250 K (solid lines), 275 K (dashed lines), 300 K (dash-dot lines), 350 K (dotted lines). The experimental data is taken from [154].	145

- 5.8 Heat capacity vs. pressure using GERG-2008 (blue lines) and Soave-BWR with regressed k_{ij} (red lines) for C₁-C₂ mixture from [154] at different temperatures: 250 K (solid lines), 275 K (dashed lines), 300 K (dash-dot lines), 350 K (dotted lines). 145
- 5.9 Heat capacity vs. pressure using GERG-2008 (blue lines) and Soave-BWR with regressed k_{ij} (red lines) for the natural gas mixture from [154] at different temperatures: 250 K (solid lines), 275 K (dashed lines), 300 K (dash-dot lines), 350 K (dotted lines). 146
- 5.10 Joule-Thomson coefficient vs. pressure using GERG-2008 (blue lines) and Soave-BWR (red lines) for C₁ at different temperatures: 250 K (solid lines), 275 K (dashed lines), 300 K (dash-dot lines), 350 K (dotted lines). The experimental data is taken from [154]. 147
- 5.11 Joule-Thomson coefficient vs. pressure using GERG-2008 (blue lines) and Soave-BWR with regressed k_{ij} (red lines) for C₁-C₂ mixture from [154] at different temperatures: 250 K (solid lines), 275 K (dashed lines), 300 K (dash-dot lines), 350 K (dotted lines). 147
- 5.12 Joule-Thomson coefficient vs. pressure using GERG-2008 (blue lines) and Soave-BWR with regressed k_{ij} (red lines) for the natural gas mixture from [154] at different temperatures: 250 K (solid lines), 275 K (dashed lines), 300 K (dash-dot lines), 350 K (dotted lines). 148
- 5.13 Absolute Average Deviation (AAD) in calculation of C_p of the n-alkanes studied in this work using different EoSs at 0.1 MPa and 10 MPa. . . . 152
- 5.14 C_p of n-alkanes as a function of the carbon number at (a) 0.1 MPa and at (b) 10 MPa. 333.15 K (\diamond), 373.15 K (\square), 403.15 K (\triangle) and 438.15 K (\circ). SRK (solid line), PR (dashed line), PC-SAFT (dash-dot line) and Soave-BWR (long dashed line). 153
- 5.15 C_p of n-alkanes up to nC₃₆ as a function of the carbon number at (a) 0.1 MPa and at (b) 10 MPa. 333.15 K (\diamond), 373.15 K (\square), 403.15 K (\triangle) and 438.15 K (\circ). SRK (solid line), PR (dashed line), PC-SAFT (dash-dot line) and Soave-BWR (long dashed line). 153
- 5.16 Absolute Average Deviation (AAD) in the calculation of the Joule-Thomson coefficient of the n-alkanes studied in this work using different EoSs at 0.1 MPa and 10 MPa. 155

- 5.17 Joule-Thomson coefficient of n-alkanes as a function of the carbon number at (a) 0.1 MPa and at (b) 10 MPa. 333.15 K (\diamond), 373.15 K (\square), 403.15 K (\triangle) and 438.15 K (\circ). SRK (solid line), PR (dashed line), PC-SAFT (dash-dot line) and Soave-BWR (long dashed line). 155
- 5.18 Joule-Thomson coefficient of n-alkanes up to nC₃₆ as a function of the carbon number at (a) 0.1 MPa and at (b) 10 MPa. 333.15 K (\diamond), 373.15 K (\square), 403.15 K (\triangle) and 438.15 K (\circ). PC-SAFT (dash-dot line) and Soave-BWR (long dashed line). 156
- 5.19 Calculated inversion curve for Joule-Thomson coefficient of (a) methane, (b) ethane and (c) propane through SRK, PR, PC-SAFT and Soave-BWR. Experimental data from Perry's handbook [156] (\circ) and Bessières et al. [137] (\diamond). P_r is the reduced pressure and T_r the reduced temperature. 157
- 5.20 Predicted inversion curves for different n-alkanes using SRK, PR, PC-SAFT and Soave-BWR. P_r is the reduced pressure and T_r the reduced temperature. 158
- 5.21 Predicted inversion curves for the n-alkanes studied in this work, obtained from the PC-SAFT EoS. n-hexane (solid line), n-octane (dashed line), n-decane (dash-dot line), n-dodecane (long dashed line), n-tetradecane (long dashed double dots line) and n-hexadecane (dotted line). p_r is the reduced pressure and T_r the reduced temperature. 159
- 6.1 $P - xy$ diagram for C₁-C₂ at 270 K with (a) zero k_{ij} and (b) the optimal k_{ij} . Soave ($-\cdot-$), vdW ($---$), LKP (\cdots), vdW-B ($- -$), vdW-DEF ($-\cdot\cdot-$), vdW-D ($- -$). The experimental data is taken from [169]. 177
- 6.2 $P - xy$ diagram for C₁-C₁₀ at 410.9 K with (a) zero k_{ij} and (b) the optimal k_{ij} . Soave ($-\cdot-$), vdW ($---$), LKP (\cdots), vdW-B ($- -$), vdW-DEF ($-\cdot\cdot-$), vdW-D ($- -$). The experimental data is taken from [170]. 178
- 6.3 Excess volume for the binary system methane (1) + n-decane (2) at 463.15 K. (\blacksquare) 40 MPa, (\blacklozenge) 60 MPa, (\blacktriangle) 80 MPa, (\bullet) 100 MPa, (\times) 120 MPa and ($+$) 140 MPa. Soave ($-\cdot-$), vdW ($---$), vdW-D ($- -$), all with 0 k_{ij} . The experimental data is taken from [61]. 180

6.4	Excess volume for the binary system methane (1) + n-decane (2) at 463.15 K. (■) 40 MPa, (◆) 60 MPa, (▲) 80 MPa, (●) 100 MPa, (×) 120 MPa and (+) 140 MPa. Soave (— · —), vdW (—), vdW-D (eq. (6.67)) (— —), all with 0 k_{ij} . The experimental data is taken from [61].	181
6.5	Excess volume for the binary system methane (1) + n-decane (2) at 463.15 K. (■) 40 MPa, (◆) 60 MPa, (▲) 80 MPa, (●) 100 MPa, (×) 120 MPa and (+) 140 MPa. Soave (— · —), vdW (—), vdW-D (eq. (6.67)) (— —), LKP (· · ·), all with regressed k_{ij} . The experimental data is taken from [61].	182
6.6	AAD% in the calculated densities of the binary system methane (1) + n-decane (2) using Soave, vdW, LKP, vdW-D (eq. (6.67)) with regressed k_{ij} within 278.15-463.15 K and 1-1400 bar. The experimental data is taken from [61].	183
6.7	Density vs. pressure using vdW (green lines) and Soave (red lines) both with regressed k_{ij} for two mixtures of methane and n-decane at different temperatures. 22.27 mol% C ₁ and 323.2 K (◇, solid lines), 22.27 mol% C ₁ and 463.2 K (△, dashed lines), 70.85 mol% C ₁ and 323.2 K (□, dash-dot lines), and 70.85 mol% C ₁ and 463.2 K (○, long-dashed lines). The experimental data is taken from [61].	183
6.8	AAD% in bubble point pressure and vapor phase composition for binary pairs of N ₂ , CO ₂ , H ₂ S and C ₁ using Soave-BWR with different mixing rules with regressed k_{ij}	186
6.9	Phase envelopes for Gas 6 with the optimal k_{ij} 's.	187
6.10	Phase envelopes for Gas 17 with the optimal k_{ij} 's.	188
6.11	Phase envelopes for Gas 22 with the optimal k_{ij} 's.	188
6.12	Phase envelopes for Gas 24 with the optimal k_{ij} 's.	189
6.13	Phase envelopes for Gas 25 with the optimal k_{ij} 's.	189
6.14	Phase envelopes for Gas 28 with the optimal k_{ij} 's.	190
6.15	Phase envelopes for Gas 26 with the optimal k_{ij} 's.	190
6.16	Phase envelopes for Gas 27 with the optimal k_{ij} 's.	191

6.17	Phase envelopes for Gas 27 with the optimal k_{ij} 's - New k_{ij} is used for LKP.	191
6.18	Phase envelope for binary mixtures of methane + n-decane (40.31 mol% C ₁) using Soave-BWR with different mixing rules with optimal k_{ij} 's. The experimental data is taken from [61].	192
6.19	Phase envelope for binary mixtures of methane + n-decane (60.21 mol% C ₁) using Soave-BWR with different mixing rules with optimal k_{ij} 's. The experimental data is taken from [61].	193
6.20	Phase envelope for binary mixtures of methane + n-decane (84.97 mol% C ₁) using Soave-BWR with different mixing rules with optimal k_{ij} 's. The experimental data is taken from [61].	193
A.1	AAD% in T_c using different correlations.	226
A.2	AAD% in P_c using different correlations.	226
A.3	AAD% in ω using different correlations set.	227

List of Tables

3.1	Applicable ranges for the reference EoS models for various components.	23
3.2	AAD% and maximum absolute deviation in the calculated phase density of pure components within 150-500 K and 0-2000 bar.	24
3.3	AAD0% in the calculated phase density of pure components within applicable range of reference EoS.	24
3.4	Trends in the temperature volume translation parameters: the parameters that are not monotonic decreasing with temperature are marked with “N” while the others are kept blank.	26
3.5	AAD% and maximum deviations in the calculated saturated liquid density for different EoSs.	27
3.6	AAD% and maximum deviations in the calculated saturated liquid density and density within 150-500 K and 0-2000 bar using CPA EoS. .	30
3.7	AAD% in the calculated high pressure liquid densities for heavy normal alkanes.	32
3.8	AAD0% and maximum absolute deviations in the calculated compressibility of the “main components”.	33
3.9	AAD% in the calculated gas Z factor of gas mixture A from [62] using different EoSs. The results are compared with GERG-2008 predictions.	37
3.10	Deviation in bubble point pressure and vapor phase composition by GERG-2008 and Soave-BWR with 0 and regressed k_{ij} values (experimental data from [63–65]).	39

3.11	Deviations in bubble point pressures and vapor phase compositions predicted by SRK, PR, PC-SAFT and Soave-BWR (experimental data from [63, 64]).	40
3.12	Regressed k_{ij} values for the four EoS models and their deviations in calculated bubble point pressures and vapor phase compositions (experimental data from [63, 64]).	43
3.13	Statistics for the four EoS models in binary VLE calculation: sensitivities and average k_{ij}	48
3.14	Interaction parameters for N_2-C_{7+} , CO_2-C_{7+} , H_2S-C_{7+} , and CH_4-C_{7+} for SRK, PR, PC-SAFT and Soave-BWR.	49
3.15	An overview of the phase envelopes tested in this study.	50
4.1	Information provided by different analytical methods.	79
4.2	Typical input information for reservoir fluid characterization.	80
4.3	Representative aromatic components and their parameters for the new PNA approach.	104
4.4	Summary of AAD% and maximum deviations in the calculated saturation pressures, reservoir fluid densities and STO densities using SRK, PR, Soave-BWR and PC-SAFT with different characterization methods.	110
4.5	AAAD% in calculated saturation pressure, density, STO density and other properties of the oil from [87] using SRK, PR, Soave-BWR and PC-SAFT EoS with different characterization methods.	113
4.6	AAAD% in calculated compressibility of all the reservoir fluids in the database using different EoSs.	121
4.7	Weight% of SCN fractions up to C_{24+} from TBP distillation and SimDist (with/without PA distribution) for the DK oil sample.	125
4.8	Weight%, MW and SG of the components for the low GOR (Black Oil) case used in compositional characterization. For both TBP distillation and SimDist (with/without PA distribution).	126

4.9	Weight%, MW and SG of the components for the high GOR (Gas Condensate) case used in compositional characterization. For both TBP distillation and SimDist (with/without PA distribution).	128
5.1	Mole fraction of different binary and multicomponent mixtures used for heat capacity and Joule-Thomson coefficient calculations.	143
5.2	Heat capacity values at constant pressure, C_p , of the n-alkanes studied in this work in $Jg^{-1}K^{-1}$	149
5.3	Joule-Thomson coefficient of the studied n-alkanes, μ_{JT} , in $K.MPa^{-1}$	150
5.4	Absolute Average Deviation (AAD) and maximum deviation (Max. Dev.) in the C_p calculation of the n-alkanes studied in this work at 0.1 and 10 MPa using different EoSs.	151
5.5	Absolute Average Deviation (AAD) and maximum deviation (Max. Dev.) in the Joule-Thomson coefficient calculation of the n-alkanes studied in this work at different pressures using different EoSs.	154
6.1	Regressed k_{ij} values for the four EoS models and their deviations in calculated bubble point pressures and vapor phase compositions (experimental data from [63, 64]).	185
A.1	AAD% in the calculated critical properties of pure components using different correlations set.	225
B.1	An overview of the reservoir fluid systems tested.	228
B.2	Summary of AAD% in predicted saturation pressures, reservoir fluid densities and stock tank oil densities (PC-SAFT eq. (4.31) and eqs. (4.34)–(4.35)).	236
B.3	Summary of AAD% in predicted saturation pressures, reservoir fluid densities and stock tank oil densities (PC-SAFT with new general characterization eqs. (4.39)–(4.40)).	249

B.4	AAD% in calculated compressibility using different EoSs including PC-SAFT with the new characterization method (eqs. (4.39)–(4.40)). The fluids without density data or few data above saturation pressure are eliminated from table.	262
C.1	Heat capacity at constant pressure, C_p , calculated using SRK EoS in $\text{Jg}^{-1}\text{K}^{-1}$	264
C.2	Heat capacity at constant pressure, C_p , calculated using PR EoS in $\text{Jg}^{-1}\text{K}^{-1}$	265
C.3	Heat capacity at constant pressure, C_p , calculated using PC-SAFT EoS in $\text{Jg}^{-1}\text{K}^{-1}$	266
C.4	Heat capacity at constant pressure, C_p , calculated using Soave-BWR EoS in $\text{Jg}^{-1}\text{K}^{-1}$	267
C.5	Joule-Thomson coefficient, μ_{JT} , calculated using SRK EoS in K.MPa^{-1}	268
C.6	Joule-Thomson coefficient, μ_{JT} , calculated using PR EoS in K.MPa^{-1}	269
C.7	Joule-Thomson coefficient, μ_{JT} , calculated using PC-SAFT EoS in K.MPa^{-1}	270
C.8	Joule-Thomson coefficient, μ_{JT} , calculated using Soave-BWR EoS in K.MPa^{-1}	271

List of Symbols

Greek Letters

- μ_{JT} Joule-Thomson coefficient
- ω Acentric factor
- ρ Density
- σ Segment diameter - parameter of PC-SAFT
- ε Segment-Segment interaction - parameter of PC-SAFT

Latin Symbols

- \tilde{a} Reduced Helmholtz free energy
- \tilde{a}^{assoc} Reduced Helmholtz free energy, association contribution
- \tilde{a}^{disp} Reduced Helmholtz free energy, dispersion contribution
- \tilde{a}^{hc} Reduced Helmholtz free energy, hard chain contribution
- \tilde{a}^{id} Reduced Helmholtz free energy, ideal gas contribution
- $AAD\%$ Percent absolute average deviation
- b Co-volume
- B, D, E, F Parameters of Soave-BWR EoS
- c Volume translation (correction term)

d	Mean diameter for PC-SAFT
k	Boltzman constant - PC-SAFT
k_{ij}	Binary interaction parameter between component i and j
m	Segment number - parameter of PC-SAFT
MW	Molecular weight
N	Avogadro number - PC-SAFT
P	Pressure
P_c	Critical pressure
P_r	Reduced pressure
R	Universal gas constant
SG	Specific gravity
T	Temperature
T_b	True boiling point temperature
T_c	Critical temperature
T_r	Reduced temperature
v	Molar volume
w_i	Weight fraction
x_i	Mole fraction of component i
Z	Compressibility factor
Z_{RA}	Rackett compressibility factor
EoS	Equation of State
HPHT	High Pressure-High Temperature

PNA Paraffins-Naphthenes-Aromatics

SCN Single Carbon Number

STO Stock Tank Oil

TBP True Boiling Point

1 | Introduction

Increase in global oil demand and declining known oil resources have derived a need to find untapped reservoirs. Oil companies are exploring various remote and harsh locations such as deep waters in Gulf of Mexico, remote arctic regions, unexplored deep deserts, etc. Quite often, the depth of new oil/gas wells being drilled has increased considerably to reach these new resources. The increase in the well depth, results in the increase in the bottomhole temperature and pressure to extreme values (i.e. up to 250 °C and 2400 bar) [1]. The oil and gas industry has contended with elevated temperatures and pressures for years; however, there are no industry-wide standards that define High pressure/High temperature (HPHT) conditions and the associated interrelationship between temperature and pressure. In an effort to clarify those definitions, Schlumberger used guidelines that organize HPHT wells into three categories, selected according to commonly encountered technology thresholds [2]. As shown in Figure 1.1, reservoirs having temperatures higher than 150 °C and pressures higher than 700 bar are classified as HPHT reservoirs Figure 1.1. There are some fields in Danish sector of the North Sea that are considered as HPHT (e.g. Hejre, Svane, Amalie, and Gita).

HPHT reservoirs are technically and economically risky to develop, but highly rewarding if successfully produced. Some of the challenges associated with these reservoirs are for example, the effect of temperature on mud composition, logging tools and electronics and the effect of pressure on design of appropriate drilling and production equipment such as blow out preventers, risers, etc. [3]. A vital HPHT-well parameter is the length of time that tools, materials and chemical products must withstand the HPHT conditions. For example, logging and testing tools, drilling muds and stimulation fluids are exposed to HPHT environments for a limited time, but packers, sand screens, reservoir monitoring equipment and cement systems must survive for many years (even beyond the well's productive life). Accordingly, this time factor has a major impact on how scientists and engineers approach product development [2].

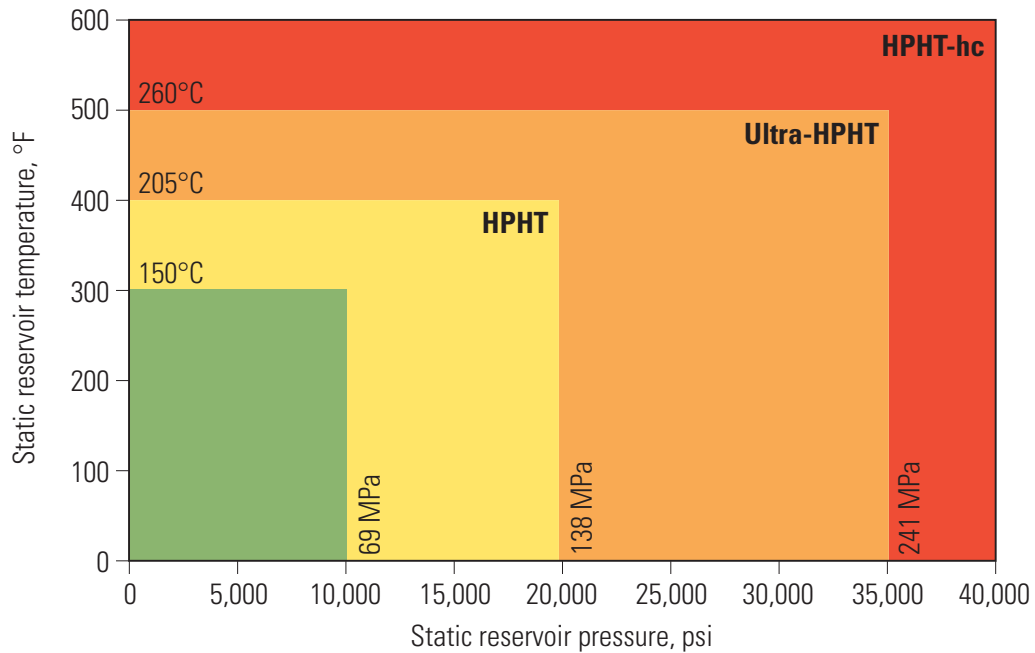


Figure 1.1 HPHT classification system from [2]. The classification boundaries represent stability limits of common well-service-tool components, elastomeric seals and electronic devices.

In addition to the operational challenges mentioned above, accurate knowledge of the reservoir fluid behavior under HPHT conditions is required to minimize the production risks. The density and viscosity of natural gas and crude oil at reservoir conditions are critical fundamental properties required for accurate assessment of the amount of recoverable petroleum within a reservoir and the modeling of the flow of these fluids through the porous media. These properties are also used to design appropriate drilling and production equipment such as blow out preventers, risers, etc. Compressibility is another important derivative property in the HPHT reservoirs as it is the main mechanism that yields production in HPHT reservoirs. Thermo-physical properties, such as Joule-Thomson coefficients, are among other important properties that need to be estimated with high accuracy at HPHT conditions as the pressure drop can result in an increase in the temperature. This behavior is known as the “reverse” Joule-Thomson effect and usually happens at high pressure and temperature conditions.

With the current state of art, there is no accurate database for these fluid properties at extreme conditions. In addition, there are neither equations of state for some of the properties such as density and compressibility that can be used to predict these fundamental properties of multicomponent hydrocarbon mixtures over a wide range of

temperature and pressure. Presently, oil companies are using correlations based on lower temperature and pressure databases that exhibit an unsatisfactory predictive capability at extreme conditions (e.g. as great as $\pm 50\%$). From the perspective of these oil companies that are committed to safely producing these resources, accurately predicting flow rates, and assuring the integrity of the flow, the absence of an extensive experimental database at extreme conditions and models capable of predicting these properties over an extremely wide range of temperature and pressure (including extreme conditions) makes their task even more daunting [4].

1.1 Thermodynamic Models Considered for HPHT Modeling

In the oil and gas industry, there is an obvious contrast between the upstream and the downstream with regards to adopting newly developed equations of state. In the downstream, these new EoS models are usually quickly accepted while in the upstream, the most widely used EoS models are still the cubic equations of state (CEoS), specifically the Soave-Redlich-Kwong (SRK) EoS [5] and the Peng-Robinson (PR) EoS [6]. These two CEoSs are the most used models in PVT modeling of reservoir fluids and almost the exclusively used models in compositional reservoir simulations. There are many reasons for the phenomenon: in contrast to the large variety of chemicals in the downstream, hydrocarbons are the major components of concern in the upstream; CEoSs are generally believed to provide enough accuracy in routine PVT modeling; as a main user of PVT modeling results, compositional reservoir simulation has much bigger uncertainties in its geology and fluid flow parts, making the accuracy of PVT modeling a less important issue in many situations; last but not the least, compositional reservoir simulations are already time-consuming compared with black oil reservoir simulations, using a more complicated thermodynamic model will further increase the computation time and therefore a strong justification for doing that is needed. Despite all the above reasons for sticking to the traditional models for PVT modeling, the upstream industry does have the needs to try more complex thermodynamic models as more exploration and production activities are carried out at deeper reservoirs, which means higher pressures and higher temperatures. HPHT reservoirs are risky to develop and require substantial investment, especially if they are offshore. To make the exploration and production viable, it is preferred to make more careful evaluation based on more accurate PVT modeling of HPHT reservoir fluids.

In this area, using non-cubic EoSs which provide a better density description can be advantageous.

To evaluate the performance of different thermodynamic models capable of more accurate description of the phase equilibrium and physical properties calculations for HPHT reservoir fluids, we have focused on three non-cubic EoSs in this research: The Perturbed Chain Statistical Associating Fluid Theory (PC-SAFT) EoS [7, 8], which has a solid basis of statistical mechanics; Soave's modification of the Benedict-Webb-Rubin (Soave-BWR) EoS [9], which is a virial type equations of state and despite its empirical nature, it provides a highly accurate density description even around the critical point; and GERG-2008 which is a wide-range EoS developed for 21 components of natural gases and their binary mixtures and is adopted as an ISO Standard (ISO 20765-2) reference equation suitable for natural gas applications [10]. PC-SAFT has received more attention due to its rigorous theoretical basis. It has shown promising performance in comparison with cubic EoSs for calculation of complex phase behavior, high pressure density, and second-order derivative properties, such compressibility and speed of sound [7, 11–14]. GERG-2008 is considered as a standard reference equation suitable for natural gas applications where highly accurate thermodynamic properties are required. However, due to its limitation to only 21 components of natural gas systems and its complexity, it is difficult to apply the equation to reservoir fluids. Soave-BWR can be considered as a simpler version of GERG-2008 although it was proposed before GERG-2008 and actually simplified from another EoS. In the general sense, Soave-BWR and GERG-2008 all belong to the same family of multiple parameter virial family equations of state. Soave-BWR is much simpler and its accuracy is also compromised, but a systematic comparison with GERG-2008 had not been performed before this study. It is beneficial to have a systematic comparison between the commonly used cubic models and these potential non-cubic models to reveal the strengths and weaknesses of these non-cubic models of our interest. More importantly, we can through the comparative study establish a platform which facilitates future EoS evaluation involving various aspects of phase equilibrium and physical properties and large databases for pure components and mixtures.

1.2 Scope and Outline of This Research

In chapter 2 we will briefly review all the EoS models used in our research. A comprehensive comparison will then be presented in chapter 3 between three non-cubic models, PC-SAFT, Soave-BWR and GERG-2008 and two cubic models, SRK and PR, in description of pure components saturated liquid density, density and compressibility in a wide temperature and pressure range, calculation of binary Vapor-Liquid-Equilibria (VLE) and density, prediction of multicomponent phase envelopes and gas compressibility factor for several well-defined systems. In addition, due to importance of thermo-physical properties, the performance of the mentioned models in calculation of heat capacity and Joule-Thomson coefficient for pure components and multicomponent mixtures over a wide pressure and temperature range is presented in chapter 5 where, the calculation results are compared with available experimental data in the literature and special emphasis has been given to the reverse Joule-Thomson effects at HPHT conditions.

To apply any cubic or non-cubic EoS model to PVT calculation of a reservoir fluid, we need to use reservoir fluid characterization which is to represent the reservoir fluid with an appropriate number of pseudo-components and assign appropriate model parameters to these components. Reservoir fluid characterization for cubic EoSs like SRK [5] and PR [6] is relatively mature. For example, the method of Pedersen et al. [15, 16] and that of Whitson et al. [17, 18] are amongst the widely used characterization methods in the upstream oil industry. The model parameters needed for SRK, PR and Soave-BWR are T_c , P_c , and ω , which can be generated by the methods of Pedersen et al. [15, 16] and that of Whitson et al. [17, 18]. For non-cubic models like PC-SAFT, their respective model parameters should be generated for the pseudo-components in the C_{7+} fractions but characterization for non-cubics is less mature.

In chapter 4, a reservoir fluid characterization method for PC-SAFT is proposed by combining Pedersen's method with newly developed set of correlations for the PC-SAFT model parameters m , $m\varepsilon/k$ and $m\sigma^3$. In addition, we further improved the characterization method for PC-SAFT by adjusting the correlations with a large PVT database. We have further improved the correlations and more importantly, we have established a general approach to characterizing reservoir fluids for any EoS. The approach consists in developing correlations of model parameters first with a database for well-defined components and then adjusting the correlations with a large PVT database. The adjustment is made to minimize the deviation in key PVT properties

like saturation pressures, densities at reservoir temperature and Stock Tank Oil (STO) densities, while keeping the n-alkane limit of the correlations unchanged. Apart from applying this general approach to PC-SAFT, we have also shown that the approach can be applied to classical cubic models like SRK and PR. In addition, we discussed how to develop a PNA based characterization for PC-SAFT and also utilize a large PVT database to further improve the characterization. In the end, we have made a comprehensive comparison in PVT calculation involving 17 EoS-characterization combinations and 260 reservoir fluids.

Petroleum fluid characterization usually uses a subset of the available analytical data. Meanwhile, modern analytical techniques allow more detailed compositional data that can be potentially used in characterization. There is little discussion on how to utilize a more complete set of the analytical data and more detailed compositional information in characterization. In chapter 4, we present our attempt to include more detailed analytical information in characterization and evaluate its impact on PVT modeling. We tried to establish a procedure to utilize more analytical information from conventional analytical techniques including simulated distillation (SimDist) and true boiling point (TBP) distillation, and then apply the procedure to one low GOR system and one high GOR system to investigate the impact of compositional characterization.

We have included a large amount of data, either experimental ones collected from the open literature and confidential reports, or synthetic ones generated by the most reliable reference EoS models in our comparative study. Furthermore, to make a fair comparison between all the selected models, we have attempted to treat them in the same manner. For example, all the optimal binary interaction parameters are regressed for SRK, PR, PC-SAFT, and Soave-BWR models and then used in the subsequent predictions for multicomponent phase envelopes and PVT modeling. In the PVT modeling part, the parameters for the pseudo-components in C_{7+} are generated by essentially the same characterization procedure with differences only in the correlations for model parameters, and no parameter tuning using the experimental PVT data has been performed for a particular model. In the comparative study, particular treatments in favor of a specific model have been avoided so that the results can reveal the advantages as well as limitations of the compared models with as little bias as possible.

Most mixing rules currently in use for EoS models are either semi-empirical or empirical and it is especially the case for non-cubic models including Soave-BWR. To address

some of the challenges with Soave-BWR EoS, in chapter 6, we describe several new mixing rules tested for Soave-BWR. The mixing rules proposed for Soave-BWR are based on some theoretical considerations as well as the previous mixing rules for non-cubic EoS models. In addition, we also tried to create some hybrid mixing rules to test their effects. A preliminary evaluation is used to screen out some of these mixing rules. Several selected ones are used in the final evaluation using more phase equilibrium and density data.

Finally, it is obvious that non-cubic EoS models are less matured in PVT modeling than cubic models. Even for PC-SAFT which has been frequently used in recent asphaltene precipitation modeling [19, 20, 12, 21–27], there are few systematic studies, at least to our knowledge, about its comparison with SRK and PR in basic PVT modeling. In our opinion, the basic PVT modeling issue should be addressed before the non-cubic models can be really accepted for routine use in the upstream of the oil and gas industry. With a better understanding of the strengths and weaknesses of the non-cubic models, it is easier for the engineers to decide whether and when to use these models and where to improve these models.

2 | Cubic and Non-Cubic Equations of State

Accurate description of the fluid phase behavior and physical properties of different systems is of great importance in the oil and gas industry. Several types of Equations of State (EoSs) have been successfully applied to hydrocarbon reservoir fluids. The simplest is the semi-empirical van der Waals (vdW) EoS, which is an improvement of the ideal gas equation by considering the intermolecular attractive and repulsive forces [28]:

$$P = \frac{RT}{v-b} - \frac{a}{v^2} \quad (2.1)$$

In this equation $\frac{a}{v^2}$ is the attractive term, b is the repulsive term, and v is the molar volume. The repulsive term b is also considered as the apparent volume of the molecules and is called co-volume. Several equations with many parameters have also been used to describe the phase behavior. Due to the large number of parameters, these equations have higher flexibility than the vdW type EoSs and describe volumetric behavior of mainly the pure components with higher accuracy.

We have focused on three non-cubic EoSs in this research: The Perturbed Chain Statistical Associating Fluid Theory (PC-SAFT) EoS [7, 8], which has a solid basis of statistical mechanics; Soave's modification of the Benedict-Webb-Rubin (Soave-BWR) EoS [9], which gives accurate density description even around the critical point; and GERG-2008 which is a wide-range EoS developed for 21 components of natural gases and their binary mixtures and is adopted as an ISO Standard (ISO 20765-2) reference equation suitable for natural gas applications [10].

Most equations of state are originally developed for the pure components. As a result, some mixing rules should be used to determine their parameters when applying them to

the multicomponent systems. Some of the mixing rules for different EoSs are reviewed in chapter 6 where new mixing rules for Soave-BWR are presented and tested.

In this chapter, we describe the cubic and non-cubic EoS models that have been used in this study.

2.1 Cubic Equations of State

2.1.1 Soave-Redlich-Kwong EOS (SRK)

Redlich and Kwong [29] modified the attractive term of the vdW EoS as:

$$P = \frac{RT}{v-b} - \frac{a}{T_r^{0.5}v(v+b)} \quad (2.2)$$

Soave [5] replaced the temperature dependency of the attractive term in eq. (2.2) by a more general function α :

$$P = \frac{RT}{v-b} - \frac{a_c\alpha}{v(v+b)} \quad (2.3)$$

where

$$a_c = 0.42747 \frac{R^2 T_c^2}{P_c} \quad (2.4)$$

$$b = 0.08664 \frac{RT_c}{P_c} \quad (2.5)$$

$$\alpha = \left(1 + m(1 - T_r^{0.5})\right)^2 \quad (2.6)$$

In the latter equation, m is a function of acentric factor as follows:

$$m = 0.480 + 1.574\omega - 0.176\omega^2 \quad (2.7)$$

The SRK EoS could also be written in the polynomial form as follows:

$$A = \frac{a\alpha P}{R^2 T^2} \quad (2.8)$$

$$B = \frac{bP}{RT} \quad (2.9)$$

$$Z^3 - Z^2 + Z(A - B - B^2) - AB = 0 \quad (2.10)$$

Although SRK does not provide reliable liquid density, it is quite capable of predicting vapor-liquid equilibria.

2.1.2 Peng-Robinson EOS (PR)

Peng and Robinson [6] modified the attractive term of the vdW EoS mainly to improve the prediction of liquid density compared to SRK:

$$P = \frac{RT}{v-b} - \frac{a_c \alpha}{v(v+b) + b(v-b)} \quad (2.11)$$

where

$$a_c = 0.457235 \frac{R^2 T_c^2}{P_c} \quad (2.12)$$

$$b = 0.077796 \frac{RT_c}{P_c} \quad (2.13)$$

$$\alpha = \left(1 + m(1 - T_r^{0.5})\right)^2 \quad (2.14)$$

In the equation for α , m is a function of acentric factor as follows:

$$m = 0.37464 + 1.5422\omega - 0.26992\omega^2 \quad (2.15)$$

The polynomial form of PR is:

$$Z^3 - (1 - B)Z^2 + Z(A - 2B - 3B^2) - (AB - B^2 - B^3) = 0 \quad (2.16)$$

where A and B are calculated using eqs. (2.8) and (2.9).

To apply SRK and PR to the multicomponent mixtures, the following mixing rules are used:

$$b = \sum_{i=1}^n \sum_{j=1}^n x_i x_j b_{ij} = \sum_{i=1}^n \sum_{j=1}^n x_i x_j \left(\frac{b_i + b_j}{2} \right) = \sum_{i=1}^n x_i b_i \quad (2.17)$$

$$a = \sum_{i=1}^n \sum_{j=1}^n x_i x_j a_{ij} = \sum_{i=1}^n \sum_{j=1}^n x_i x_j \sqrt{a_i a_j} (1 - k_{ij}) \quad (2.18)$$

In these equations, arithmetic average is used for the repulsive force between molecules i and j (b_{ij}), which has the characteristic of volume, and geometric average is used for the attractive force between molecules i and j (a_{ij}), which is of an energy nature. The mixing rule used for b suggests that the pure-component molar volumes at high

pressures should be additive. The parameter k_{ij} in eq. (2.18) is the binary interaction parameter between component i and j . For two identical components, k_{ij} is zero by definition, while for two different non-polar compounds, k_{ij} is equal to or close to zero. For a binary pair containing one polar and one non-polar components, nonzero k_{ij} 's are often appropriate. More information about different mixing rules for different EoSs can be found in chapter 6.

2.1.3 Volume Shift

Peneloux et al. [30] introduced the volume shift concept for SRK by subtracting the predicted molar volume by a constant correction term to improve the predicted liquid molar volume and density:

$$v^{cor} = v^{EoS} - c \quad (2.19)$$

In this equation v^{cor} is the corrected molar volume, v^{EoS} is the molar volume calculated by the cubic EoSs, and c is the volume translation or volume-shift parameter calculated as follows:

$$c = 0.40768 \frac{RT_c (0.29441 - Z_{RA})}{P_c} \quad (2.20)$$

where

$$Z_{RA} = 0.29056 - 0.08775\omega \quad (2.21)$$

The parameter c has no influence on the gas-liquid phase equilibrium calculation results, as it only multiplies the fugacity of each component in both phases by an equal amount, resulting in the same value of equilibrium ratio. It can also be easily used for the mixtures by the following mixing rule:

$$c = \sum_{i=1}^n x_i c_i \quad (2.22)$$

where x_i is the mole fraction of component i in the mixture.

The Peneloux volume translation concept is not limited to SRK, and Jhaveri and Youngren [31] applied it to the PR EoS. For non-hydrocarbon and hydrocarbon components lighter than C₇, the volume-shift parameter for PR is calculated as follows:

$$c = 0.50033 \frac{RT_c (0.25969 - Z_{RA})}{P_c} \quad (2.23)$$

where Z_{RA} is the Rackett compressibility factor defined in eq. (2.21).

2.2 PC-SAFT EoS

The PC-SAFT EoS proposed by Gross and Sadowski [7, 8] is one of the successful modifications of the original SAFT EoS [32]. Unlike SAFT, PC-SAFT uses the mixture of hard-sphere chains as the reference system and then introduces the dispersive attractions. PC-SAFT is proposed to model asymmetric and highly non-ideal systems. PC-SAFT can be expressed in terms of the reduced Helmholtz energy \tilde{a} :

$$\tilde{a} \equiv \frac{A}{NkT} = \tilde{a}^{id} + \tilde{a}^{hc} + \tilde{a}^{disp} + \tilde{a}^{assoc} \quad (2.24)$$

where \tilde{a}^{id} is the ideal gas contribution, \tilde{a}^{hc} is the contribution of the hard-sphere chain reference system, \tilde{a}^{disp} is the dispersion contribution arising from the square well attractive potential and \tilde{a}^{assoc} is the association contribution based on Wertheim's theory [8, 32]. When PC-SAFT is applied to a system only consisting of non-associating components, as the case in this study, the \tilde{a}^{assoc} term in eq. (2.24) disappears. Without the association term, the expression used in eq. (2.24) is comparable to a conventional cubic EoS, with $\tilde{a}^{id} + \tilde{a}^{hc}$ corresponding to the repulsive contribution in a cubic EOS and \tilde{a}^{disp} corresponding to the attractive contribution. However, the repulsive and attractive contributions in a cubic EOS are empirical while \tilde{a}^{hc} and \tilde{a}^{disp} in the PC-SAFT are theoretically derived from statistical mechanics. \tilde{a}^{hc} in PC-SAFT takes into account both the hard sphere contribution and the chain contribution:

$$\tilde{a}^{hc} = \bar{m}\tilde{a}^{hs} + \tilde{a}^{chain} = \bar{m}\tilde{a}^{hs} - \sum_i x_i(m_i - 1) \ln g_{ii}^{hs} \quad (2.25)$$

where \bar{m} is the mean segment number in the mixture:

$$\bar{m} = \sum_i x_i m_i \quad (2.26)$$

The hard-sphere term is given by the mixture version of the Carnahan-Starling EoS for hard-spheres

$$\tilde{a}^{hs} = \frac{1}{\zeta_0} \left[\frac{3\zeta_1\zeta_2}{1-\zeta_3} + \frac{3\zeta_2^3}{\zeta_3(1-\zeta_3)^2} + \left(\frac{\zeta_2^3}{\zeta_3^2} - \zeta_0 \right) \ln(1-\zeta_3) \right] \quad (2.27)$$

with ζ_n defined by

$$\zeta_n = \frac{\pi}{6} \rho \sum_i x_i m_i d_i^n \quad n \in \{0, 1, 2, 3\} \quad (2.28)$$

and d_i is the temperature-dependent segment diameter of component i [33]

$$d_i = \sigma_i \left[1 - 0.12 \exp \left(-3 \frac{\varepsilon_i}{kT} \right) \right] \quad (2.29)$$

The radial distribution function at contact g_{ij}^{hs} in eq. (2.25) is given by

$$g_{ij}^{hs} = \frac{1}{1 - \zeta_3} + \left(\frac{d_i d_j}{d_i + d_j} \right) \frac{2\zeta_2}{(1 - \zeta_3)^2} + \left(\frac{d_i d_j}{d_i + d_j} \right)^2 \frac{2\zeta_2^2}{(1 - \zeta_3)^2} \quad (2.30)$$

The dispersive term \tilde{a}^{disp} is modeled using a second order perturbation theory on chain molecules rather than hard spheres, which makes it different from other versions of SAFT. \tilde{a}^{disp} is given by

$$\tilde{a}^{disp} = -2\pi\rho I_1(\eta, \bar{m}) \overline{m^2 \varepsilon \sigma^3} - \pi\rho\bar{m} C_1(\eta, \bar{m}) I_2(\eta, \bar{m}) \overline{m^2 \varepsilon^2 \sigma^3} \quad (2.31)$$

where the integrals I_1 and I_2 , and the compressibility expression C_1 are functions of \bar{m} and the packing fraction η (or ζ_3). The van der Waals one-fluid mixing rules are applied to the dispersion term, resulting in

$$\overline{m^2 \varepsilon \sigma^3} = \sum_i \sum_j x_i x_j m_i m_j \left(\frac{\varepsilon_{ij}}{kT} \right) \sigma_{ij}^3 \quad (2.32)$$

$$\overline{m^2 \varepsilon^2 \sigma^3} = \sum_i \sum_j x_i x_j m_i m_j \left(\frac{\varepsilon_{ij}}{kT} \right)^2 \sigma_{ij}^3 \quad (2.33)$$

with the conventional Berthelot-Lorentz combining rules for ε_{ij} and σ_{ij} :

$$\varepsilon_{ij} = \sqrt{\varepsilon_{ii} \varepsilon_{jj}} (1 - k_{ij}) \quad (2.34)$$

$$\sigma_{ij} = (\sigma_i + \sigma_j)/2 \quad (2.35)$$

Despite the complex form of the PC-SAFT EoS, there are only three model parameters for a non-associating component, the chain length m , the segment diameter σ and the segment energy ε .

von Solms et al. [34] simplified the original PC-SAFT EoS by assuming that all the segments in the mixture have the same mean diameter d , which gives a mixture volume

fraction identical to that of the actual mixture. The mean diameter d is given by

$$d = \left(\frac{\sum_i x_i m_i d_i^n}{\sum_i x_i m_i} \right)^{1/3} \quad (2.36)$$

This modification simplifies the \tilde{a}^{hs} and g^{hs} terms to

$$\tilde{a}^{hs} = \frac{4\eta - 3\eta^2}{(1 - \eta)^2} \quad (2.37)$$

$$g^{hs} = \frac{1 - \eta/2}{(1 - \eta)^3} \quad (2.38)$$

The simplified PC-SAFT EoS is identical to the original PC-SAFT EoS for pure components and equally accurate for mixtures [34]. The main advantage of the simplified version is that it somewhat reduces the computation times for non-associating systems and markedly for associating systems. The simplified version of PC-SAFT is used in all our calculations.

2.3 Soave-BWR EoS

The Benedict-Webb-Rubin (BWR) equation of state [35] belongs to the so-called virial type equations of state. Despite its empirical nature, it provides a highly accurate density description than many other types of EoS models. The original BWR takes the following functional form:

$$Z = \frac{P}{RT\rho} = 1 + B\rho + C\rho^2 + D\rho^5 + E\rho^2(1 + F\rho^2) \exp(-F\rho^2) \quad (2.39)$$

where ρ is the density, and B , C , D , E and F are the five model parameters.

A recent modification of the BWR EoS is given by Soave in 1995 [36]:

$$Z = \frac{P}{RT\rho} = 1 + B\rho + C\rho^2 + D\rho^4 + E\rho^2(1 + F\rho^2) \exp(-F\rho^2) \quad (2.40)$$

where the exponent five of the density in the original equation was changed to four. In 1999, Soave [9] further simplified the equation by dropping the $C\rho^2$ term:

$$Z = \frac{P}{RT\rho} = 1 + B\rho + D\rho^4 + E\rho^2(1 + F\rho^2)\exp(-F\rho^2) \quad (2.41)$$

Although the number of terms in the equation is reduced, with proper parametrization, the new version of Soave-BWR, i.e., eq. (2.41), turned out to be better than the old version, i.e., eq. (2.40). The Soave-BWR EoS used in our calculations refers to the 1999 version.

There are four parameters in Soave-BWR, B , D , E and F . Their values at the critical point are linked to a new set of notations defined by

$$b = B(T_c)\rho_c \quad (2.42)$$

$$d = D(T_c)\rho_c^4 \quad (2.43)$$

$$e = E(T_c)\rho_c^2 \quad (2.44)$$

$$f = F\rho_c^2 \quad (2.45)$$

The above four values b , d , e and f can be determined from the three critical constraints $P_c = Z_c\rho_cRT_c$ and $(\partial P/\partial\rho)_{T_c} = (\partial^2 P/\partial\rho^2)_{T_c} = 0$, plus an empirical constraint $f = 0.77$ as follows:

$$e = (2 - 5Z_c) / [(1 + f + 3f^2 - 2f^3)\exp(-f)] \quad (2.46)$$

$$d = [1 - 2Z_c - e(1 + f - 2f^2)\exp(-f)] / 3 \quad (2.47)$$

$$b = Z_c - 1 - d - e(1 + f)\exp(-f) \quad (2.48)$$

The temperature dependence of B , D , E and F were determined by correlating partly “synthetic” and partly experimental data, including vapor pressures for T_r between 0.4 and 1.0 and ω between 0.0 and 0.9, saturated liquid densities for T_r greater than 0.4 and compressed liquid densities at $P_r = 10$, and gas-phase densities of C₁ to C₄ alkanes. The resulting temperature functions for B , D and E are expressed in terms of the reduced temperature and the acentric factor, while F is treated as temperature independent.

The following equations show how the Soave-BWR parameters are determined:

$$B = \left(\frac{RT_c}{P_c}\right) \beta = \left(\frac{RT_c}{P_c}\right) \left[\beta_c + 0.422 \left(1 - \frac{1}{T_r^{1.6}}\right) + 0.234\omega \left(1 - \frac{1}{T_r^3}\right) \right] \quad (2.49)$$

$$D = \left(\frac{RT_c}{P_c}\right)^4 \delta = \left(\frac{RT_c}{P_c}\right)^4 \delta_c \left[1 + d_1 \left(\frac{1}{T_r} - 1\right) + d_2 \left(\frac{1}{T_r} - 1\right)^2 \right] \quad (2.50)$$

$$E = \left(\frac{RT_c}{P_c}\right)^2 \varepsilon = \left(\frac{RT_c}{P_c}\right)^2 \left[\varepsilon_c + e_1 \left(\frac{1}{T_r} - 1\right) + e_2 \left(\frac{1}{T_r} - 1\right)^2 + e_3 \left(\frac{1}{T_r} - 1\right)^3 \right] \quad (2.51)$$

$$F = \left(\frac{RT_c}{P_c}\right)^2 \phi = \left(\frac{RT_c}{P_c}\right)^2 f Z_c^2 \quad (2.52)$$

where:

$$d_1 = 0.4912 + 0.6478\omega \quad (2.53)$$

$$d_2 = 0.3000 + 0.3619\omega \quad (2.54)$$

$$e_1 = 0.0841 + 0.1318\omega + 0.0018\omega^2 \quad (2.55)$$

$$e_2 = 0.0750 + 0.2408\omega - 0.0140\omega^2 \quad (2.56)$$

$$e_3 = -0.0065 + 0.1798\omega - 0.0078\omega^2 \quad (2.57)$$

$$f = 0.77 \quad , \quad \beta_c = bZ_c \quad , \quad \delta_c = dZ_c^4 \quad , \quad \varepsilon_c = eZ_c^2 \quad (2.58)$$

Soave developed the mixing rules for T_c , P_c and ω based on the mixing rules used for the classical CEoS models like SRK and PR. The developed mixing rules calculate the mixture T_c , P_c and ω in such a way that the corresponding mixing parameters a and b in SRK or PR are as close as possible to their values calculated by the van der Waals mixing rules. The final mixing rules for T_c , P_c and ω are:

$$T_{cm} = S_1 / \left(\sqrt{S_2} + \sqrt{S_3} \right)^2 \quad (2.59)$$

$$P_{cm} = T_{cm} / S_3 \quad (2.60)$$

$$m_m = \sqrt{S_2 / S_3} \quad (2.61)$$

$$S_1 = \sum_i \sum_j x_i x_j (1 - k_{ij}) \frac{T_{ci} T_{cj}}{\sqrt{P_{ci} P_{cj}}} (1 + m_i) (1 + m_j) \quad (2.62)$$

$$S_2 = \sum_i \sum_j x_i x_j (1 - k_{ij}) \sqrt{\frac{T_{ci} T_{cj}}{P_{ci} P_{cj}}} m_i m_j \quad (2.63)$$

$$S_3 = \sum_i x_i \frac{T_{ci}}{P_{ci}} \quad (2.64)$$

m in eqs. (2.61)–(2.63) is a function of ω and a simple proportionality relationship is used for it:

$$m = \mu\omega \quad (2.65)$$

with an empirical value 1.25 given to μ . A linear mixing rule is used for Z_c :

$$Z_{cm} = \frac{\sum_i (x_i Z_{c_i} T_{c_i} / P_{c_i})}{\sum_i (x_i T_{c_i} / P_{c_i})} \quad (2.66)$$

In summary, there are four parameters for each component in Soave-BWR, T_c , P_c , ω and Z_c . For n-alkanes, a good approximation of Z_c is given by

$$Z_c = 0.2908 - 0.099\omega + 0.04\omega^2 \quad (2.67)$$

which is also used by Soave in generating the “synthetic” saturated liquid densities [5, 36]. Soave also pointed out that for some compounds, it is important to use Z_c as an independent parameter to reproduce both vapor pressures and liquid densities accurately. However, our experiences show that at least for phase equilibrium of highly asymmetric binary pairs in reservoir fluids, setting Z_c as an independent parameter does not offer much advantage, and in fact sometimes adverse effects. Therefore, it is decided to use eq. (2.66) to calculate Z_c , which reduces the number of model parameters to just three.

2.4 GERG-2008 EoS

GERG-2008 is based on a multi-fluid mixture model and is valid over the temperature range of 60 K to 700 K and up to 700 bar [10]. GERG-2008 is explicit in the Helmholtz free energy as a function of density ρ , temperature T , and composition x (mole fraction) and the structure of this EoS in the dimensionless reduced form is as follows:

$$\alpha(\delta, \tau, \bar{x}) = \alpha^0(\rho, T, \bar{x}) + \sum_{i=1}^n x_i \alpha_{0i}^r(\delta, \tau) + \Delta\alpha^r(\delta, \tau, \bar{x}) \quad (2.68)$$

where δ is the reduced mixture density and τ is the inverse reduced mixture temperature according to:

$$\delta = \frac{\rho}{\rho_r(\bar{x})} \quad (2.69)$$

$$\tau = \frac{T_r(\bar{x})}{T} \quad (2.70)$$

In these equations, T_r and ρ_r are the reducing functions, and are only dependent on the composition of the mixture. In eq. (2.68), $\alpha(\delta, \tau, \bar{x})$ is the dimensionless form of the reduced Helmholtz free energy and is defined as $\alpha = a/(RT)$. The dimensionless form of the Helmholtz free energy for the ideal-gas mixture is $\alpha^0(\rho, T, \bar{x})$ and is defined as follows:

$$\alpha^0(\rho, T, \bar{x}) = \sum_{i=1}^n x_i (\alpha_{0i}^0(\rho, T) + \ln x_i) \quad (2.71)$$

where n is the number of components in the mixture, α_{0i}^0 is the dimensionless form of the Helmholtz free energy in the ideal-gas state of component i , and x_i is mole fraction of the mixture components. The term $x_i \ln x_i$ accounts for the entropy of mixing.

The last two terms on the right hand side of eq. (2.68) represent the residual part of the reduced Helmholtz free energy of the mixture, where $\sum_{i=1}^n x_i \alpha_{0i}^r(\delta, \tau)$ is the residual part of the reduced Helmholtz free energy of component i , and $\Delta\alpha^r(\delta, \tau, \bar{x})$ is the contribution to the reduced residual Helmholtz free energy due to mixing at constant δ and τ which is the summation over all binary specific and generalized departure functions $\Delta\alpha_{ij}^r(\delta, \tau, \bar{x})$ developed for the respective binary mixtures. \bar{x} is the vector of mole fractions. To apply the GERG-2008 EoS to the mixtures, the following mixing rules are used:

$$\frac{1}{\rho_r(\bar{x})} = \sum_{i=1}^n x_i^2 \frac{1}{\rho_{c,i}} + \sum_{i=1}^{n-1} \sum_{j=i+1}^n 2x_i x_j \beta_{v,ij} \gamma_{v,ij} \cdot \frac{x_i + x_j}{\beta_{v,ij}^2 x_i + x_j} \cdot \frac{1}{8} \left(\frac{1}{\rho_{c,i}^{1/3}} + \frac{1}{\rho_{c,j}^{1/3}} \right)^3 \quad (2.72)$$

$$T_r(\bar{x}) = \sum_{i=1}^n x_i^2 T_{c,i} + \sum_{i=1}^{n-1} \sum_{j=i+1}^n 2x_i x_j \beta_{T,ij} \gamma_{T,ij} \cdot \frac{x_i + x_j}{\beta_{T,ij}^2 x_i + x_j} \cdot (T_{c,i} T_{c,j})^{0.5} \quad (2.73)$$

In these correlations, $\rho_{c,i}$ and $T_{c,i}$ are critical density and critical temperature of component i and the four binary parameters $\beta_{v,ij}$, $\gamma_{v,ij}$, $\beta_{T,ij}$, and $\gamma_{T,ij}$ are fitted to the binary mixtures data. More information about GERG-2008 and its earlier version, GERG-2004, the experimental data used for their development, and the value of the binary parameters can be found in the original GERG articles [10, 37–40]. The developed mixing rules have the so-called Michelsen–Kistenmacher syndrome [41]. This means the mixture parameters, including the composition-dependent parameters of multi-fluid mixtures, calculated from mixing rules might not be invariant when a component is split into a number of identical sub-components. The developers of GERG-2008 were aware of this limitation but decided to use these empirical mixing rules as they give better accuracy in description of the available data for the thermal and caloric properties of multicomponent mixtures.

3 | Phase Behavior of Well Defined Systems

Accurate description of PVT, including phase equilibrium and physical properties, is always needed for development of natural gas and petroleum reservoir fluids. It is especially a crucial problem for reservoirs at HPHT conditions, where the importance for density and compressibility in production forecast is more pronounced. Equations of State (EoS) are commonly used to describe phase equilibrium and physical properties over a wide range of pressure, temperature and mixture composition. As classical cubic EoS models (SRK and PR) do not satisfy the demands on the accuracy of some thermodynamic properties, such as density and compressibility, over the entire region of interest (especially at high pressures), it becomes more attractive to use non-cubic EoSs (PC-SAFT, Soave-BWR and GERG-2008) for description of these properties over a wide temperature and pressure range. PC-SAFT has received more attention due to its rigorous theoretical basis. It has shown promising performance in comparison to cubic EoSs for calculation of complex phase behavior, high pressure density, and second-order derivative properties, such as compressibility and speed of sound [7, 11–14]. Among the non-cubic models, GERG-2008 is a new wide-range EoS for natural gases and other mixtures of 21 natural gas components. It is considered as a standard reference equation suitable for natural gas applications where highly accurate thermodynamic properties are required. However, due to its limitation to only 21 components of natural gas systems and its complexity, it cannot be generalized to reservoir oil fluids. There are few systematic comparisons between GERG-2008 and other EoSs in the literature. It is beneficial to have a comprehensive comparison between engineering cubic and non-cubic EoS models and GERG-2008 using an extensive database for various aspects in modeling of phase equilibrium and physical properties. We will present such a comparative study here, not only to provide the detailed comparison results, but also to establish a platform that can facilitate future evaluation of EoS models.

Dauber and Span [42, 43] applied GERG-2008 to simulation of liquefied natural gas process and made comparison with cubic EoSs including SRK and PR. Recently, Perez-Sanz et al. [44] measured the speed of sound for a synthetic coal mine methane as well as second virial acoustic coefficient, adiabatic coefficient and heat capacity. They validated their measurements by comparing their results with GERG-2008 predictions, where they found good agreement between GERG-2008 and experimental measurements for speed of sound, heat capacity and adiabatic coefficient. However, a large disagreement was observed for the second virial acoustic coefficient. Yuan et al. [45] used the Aspen Plus software [46] to compare SRK, PR, the Lee-Kesler-Plocker (LKP) equation [47] and GERG-2008 in calculating gas density, saturated liquid density, specific heat capacity, enthalpy and vapor-liquid equilibrium of some gas mixtures at conditions relevant to gas liquefaction processes. They found that SRK, PR and LKP give large deviations from the experimental data for some of the properties or under certain conditions, which may lead to inaccurate results for the simulation and optimization of the liquefaction processes. In contrast, GERG-2008 shows higher accuracy in calculation of the thermodynamic properties and phase equilibrium over the temperature and pressure range tested. They recommended GERG-2008 as the basis for predicting physical parameters in natural gas liquefaction processes.

There are several studies on the comparison between non-cubic models, including PC-SAFT and Soave-BWR, and other cubic models in the recent literature. In order to provide a comprehensive understanding of the potentials and limitations of the advanced SAFT family EoS and their improvements over classical models, Villiers et al. [14, 48] studied the performance of SRK, PR, CPA, SAFT, and PC-SAFT on derivative properties for different component families. They concluded that, in general, the performance of PC-SAFT is superior in correlating most of the second-order derivative properties of investigated alkanes. Liang et al. [49] made an extensive comparison of SRK, CPA and PC-SAFT for calculation of the speed of sound in n-alkanes where they observed none of the models could describe the speed of sound with satisfactory accuracy when they are used without fitting their parameters to the experimental data. After integrating the speed of sound data into both tuning of the universal constants and the pure component parameters estimation, Liang et al. obtained better results for PC-SAFT. Polishuk [50–53] has made several comparisons between cubic EoSs, Soave-BWR, PC-SAFT and SAFT+Cubic in calculation of different thermodynamic properties of pure and multicomponent systems including the derivative properties such as speed of sound and heat capacity. He pointed out some limitations of cubic EoSs, such as poorer high pressure speed of sound and density results predicted by

PR as compared to PC-SAFT and SAFT+Cubic EoSs [53]. In addition, he showed the advantage of Soave-BWR in modeling the pure compound vapor pressures and phase envelope, which are the particular type of data for which the model has been developed. However, he mentioned that the Soave-BWR model fails to estimate other thermodynamic properties, such as the high-pressure densities, sound velocities and isentropic compressibilities accurately [50].

In this chapter, we present a comprehensive comparison between cubic EoS (SRK and PR) and non-cubic EoS (PC-SAFT, Soave-BWR and GERG-2008) in description of pure components saturated liquid density, density and compressibility in a wide temperature and pressure range, calculation of binary Vapor-Liquid-Equilibria (VLE) and density, prediction of multicomponent phase envelopes and gas compressibility factor for several well defined systems. In addition to covering various aspects related to the basic PVT modeling, and due to importance of thermo-physical properties, the performance of the mentioned models in calculation of heat capacity and Joule-Thomson coefficient for pure components and multicomponent mixtures over a wide pressure and temperature range is presented in chapter 5 where, the calculation results are compared with available experimental data in the literature and special emphasis has been given to the reverse Joule-Thomson effects at HPHT conditions.

A large amount of data has been included in this study, including both experimental ones collected from the open literature and synthetic ones generated by the most reliable reference EoS models. All the binary interaction parameters for GERG-2008 were regressed from experimental data [10]. In order to make a fair comparison between the selected models, we have determined the optimal values of binary interaction parameters for SRK, PR, Soave-BWR, and PC-SAFT and then used them in the subsequent calculations of binary density, multicomponent phase envelopes and other thermal properties. In this comparative study, we tried to avoid any particular treatments in favor of a specific model and the reported calculation results are pure predictions.

3.1 Density and Compressibility of Pure Components

This section is mainly dedicated to the comparison between GERG-2008, Soave-BWR, PC-SAFT, and SRK and PR with and without volume translation for calculation of phase density and compressibility of pure components over a wide temperature and pressure range (150-500 K and 0-2000 bar), and for calculation of saturated liquid density of these pure components. The tested temperature and pressure range can cover most of the conditions in the upstream and downstream processes. In addition, a sample calculation of methane and n-decane binary mixture density at different compositions, as well as gas compressibility factor (Z) of a multicomponent natural gas mixture at different temperatures using different EoSs are presented.

High accuracy reference EoS models [54] are used to generate “synthetic” density and compressibility data. As it was mentioned in the previous chapter, GERG-2008 has been developed for 21 components of natural gases and their mixtures and for hydrocarbons up to nC_{10} . We exclude H_2 , O_2 , CO , H_2O , He and Ar from the 21 components to form the “main components” group (Table 3.1). The split is based on two reasons. First, the “main components” are more commonly encountered in the upstream of oil and gas production especially in the modeling of reservoir fluids. Second, the other components are not included in the development of other EoS (SRK, PR, PC-SAFT and Soave-BWR) and the comparison including all the components can be biased against other EoSs. In our comparison between SRK, PR, PC-SAFT and Soave-BWR we also included some components that were not used in development of GERG-2008 but were important in the upstream of oil and gas (i.e. nC_{11} , nC_{12} , Benzene and Toluene).

Table 3.1 summarizes the list of components and the applicable ranges of the reference EoS models used in this study. Since the applicable ranges of some reference EoS models cannot cover the whole range of 150-500 K and 0-2000 bar, we consider two types of absolute average deviations (AAD) in the comparison. AAD% is calculated in the whole temperature and pressure range of interest, i.e., neglecting the applicable ranges of the reference EoS models, and AAD0% is calculated only with the data points within the applicable ranges of the reference models. For saturated liquid density, comparison is made in the reduced temperature (T_r) range from 0.35 to 1.0. Based on Table 3.1, for the components where the lowest applicable reduced temperature

($T_{r,min}$) is higher than $T_r = 0.35$, $T_{r,min}$ is used as the lower boundary for the reduced temperature.

Table 3.1 Applicable ranges for the reference EoS models for various components.

Component	T_{min} (K)	T_{max} (K)	P_{max} (bar)	ρ_{max} (mol/L)	$T_{r,min}$
Main Components					
N ₂	63.15	2000	22000	53.15	0.50
CO ₂	216.59	2000	8000	37.24	0.71
H ₂ S	187.70	760	170000	29.12	0.50
CH ₄	90.69	625	10000	40.07	0.48
C ₂ H ₆	90.37	675	9000	22.42	0.30
C ₃ H ₈	85.53	650	10000	20.60	0.23
nC ₄ H ₁₀	134.90	575	2000	13.86	0.32
iC ₄ H ₁₀	113.73	575	350	12.90	0.28
nC ₅ H ₁₂	143.47	600	1000	11.20	0.31
iC ₅ H ₁₂	112.65	500	10000	13.30	0.24
nC ₆ H ₁₄	177.83	600	1000	8.85	0.35
nC ₇ H ₁₆	182.55	600	1000	7.75	0.34
nC ₈ H ₁₈	216.37	600	1000	6.69	0.38
nC ₉ H ₂₀	219.70	600	8000	6.06	0.37
nC ₁₀ H ₂₂	243.50	675	8000	5.41	0.39
Other Components					
nC ₁₁ H ₂₄	247.54	700	5000	4.97	0.39
nC ₁₂ H ₂₆	263.60	700	7000	4.53	0.40
Benzene	278.67	750	5000	11.45	0.50
Toluene	178.00	700	5000	10.58	0.30

3.1.1 Density and Saturated Liquid Density Calculations

Table 3.2 and Figure 3.1 present the deviations in pure components phase density within 150-500 K and 0-2000 bar using SRK and PR (with/without volume translation (VT)), PC-SAFT, Soave-BWR, and GERG-2008. Both AAD% and maximum absolute deviations (%) are presented in Table 3.2. Table 3.3 summarizes the AAD0% in pure components phase density within applicable range of reference EoS. On average, GERG-2008 gives the lowest AAD% and AAD0% in phase density calculation of pure components. When GERG-2008 is used within the applicable ranges of reference EoSs, the average AAD0% is 0.03% for the “main components”, while the average AAD0% for other EoSs are greater than 1.0%. Soave-BWR gives the lowest AAD0% (1.03%) compared to other EoSs (PC-SAFT, SRK and PR (with/without VT)) for the main

components. PR increases the deviation to 6% and SRK gives the highest deviation around 9%. The AAD% for different components are typically smaller than 2% for Soave-BWR and PC-SAFT with Soave-BWR a bit better for components not heavier than C₂. The AAD% for SRK are relatively small for components not heavier than C₂, and actually comparable to those for PC-SAFT. But the AAD% increases quickly for heavier components, reaching around 10% for nC₆ and around 20% for nC₁₂. On the other hand, PR gives larger deviations for light components but smaller deviations for heavier ones than SRK.

Table 3.2 AAD% and maximum absolute deviation in the calculated phase density of pure components within 150-500 K and 0-2000 bar.

Components	SRK		PR		SRK-VT		PR-VT		PC-SAFT		Soave-BWR		GERG-2008	
	AAD%	Max Dev.	AAD%	Max Dev.	AAD%	Max Dev.	AAD%	Max Dev.	AAD%	Max Dev.	AAD%	Max Dev.	AAD%	Max Dev.
N ₂	2.24	7.01	9.35	13.62	0.84	8.02	0.72	5.13	3.23	4.91	0.57	2.63	0.024	0.159
CO ₂	4.88	21.00	5.04	13.28	1.68	19.64	1.13	16.06	1.23	20.90	0.74	3.81	0.161	1.368
H ₂ S	3.04	16.48	7.61	9.51	1.09	15.70	0.86	11.28	0.47	6.72	0.38	3.45	0.006	0.006
CH ₄	1.29	16.47	8.78	12.43	1.09	16.82	0.77	12.93	1.35	6.11	0.88	4.08	0.025	0.123
C ₂ H ₆	2.07	19.91	8.52	11.85	1.14	19.78	1.05	15.73	2.07	5.73	0.64	4.15	0.111	0.296
C ₃ H ₈	3.28	20.60	7.42	12.01	1.05	20.25	1.08	15.82	1.71	3.86	1.44	4.57	0.057	0.927
nC ₄ H ₁₀	5.21	20.07	5.51	12.82	0.96	19.45	1.06	15.82	1.61	8.38	1.81	3.46	0.070	0.891
iC ₄ H ₁₀	4.23	21.24	6.48	13.44	1.01	20.87	1.11	16.79	2.23	6.55	2.17	4.48	0.166	0.627
nC ₅ H ₁₂	7.67	22.71	3.62	13.60	0.90	21.40	1.03	16.42	1.22	15.71	1.70	4.73	0.006	0.007
iC ₅ H ₁₂	5.85	26.58	5.00	18.97	0.92	26.10	1.08	21.61	1.56	8.37	2.78	4.72	0.006	0.006
nC ₆ H ₁₄	10.16	23.14	3.00	14.44	0.87	21.34	1.09	16.66	1.42	6.91	1.35	3.39	0.006	0.006
nC ₇ H ₁₆	12.37	20.09	3.37	11.05	0.83	15.65	1.04	10.43	1.57	5.85	1.29	3.51	0.006	0.006
nC ₈ H ₁₈	14.46	22.26	4.84	13.46	0.83	12.11	1.08	7.00	1.77	6.93	1.04	3.22	0.006	0.006
nC ₉ H ₂₀	16.54	24.60	7.02	16.06	0.83	9.85	1.08	5.17	2.20	7.92	0.85	3.38	0.006	0.006
nC ₁₀ H ₂₂	18.33	26.56	9.02	18.25	0.81	8.17	1.07	3.69	2.05	8.27	0.78	3.44	0.006	0.006
nC ₁₁ H ₂₄	18.38	26.70	9.08	18.40	0.86	6.00	1.17	3.24	2.09	9.31	2.61	4.74	-	-
nC ₁₂ H ₂₆	21.48	29.60	12.54	21.63	0.82	5.56	1.11	3.09	2.01	10.14	0.63	2.84	-	-
Benzene	8.70	15.92	3.36	6.84	0.56	11.47	0.70	6.90	0.73	3.05	1.03	3.12	-	-
Toluene	11.08	17.90	2.74	8.57	0.58	9.60	0.74	5.18	1.04	4.88	0.79	1.62	-	-
Average	9.01	20.99	6.44	13.70	0.93	15.15	1.00	11.00	1.66	7.92	1.24	3.65	0.04	0.30
Average - Main Comps.	7.44	20.58	6.31	13.65	0.99	17.01	1.02	12.70	1.71	8.21	1.23	3.80	0.04	0.30

Table 3.3 AAD0% in the calculated phase density of pure components within applicable range of reference EoS.

Components	SRK	PR	SRK-VT	PR-VT	PC-SAFT	Soave-BWR	GERG-2008
	AAD0%	AAD0%	AAD0%	AAD0%	AAD0%	AAD0%	AAD0%
N ₂	2.24	9.35	0.84	0.72	3.23	0.57	0.024
CO ₂	4.26	5.39	2.02	1.28	0.87	0.78	0.057
H ₂ S	2.89	7.54	1.35	0.91	0.56	0.37	0.006
CH ₄	1.29	8.78	1.09	0.77	1.35	0.88	0.025
C ₂ H ₆	2.07	8.52	1.14	1.05	2.07	0.64	0.111
C ₃ H ₈	3.28	7.42	1.05	1.08	1.71	1.44	0.057
nC ₄ H ₁₀	5.21	5.51	0.96	1.06	1.61	1.81	0.070
iC ₄ H ₁₀	5.56	5.29	2.78	1.95	0.76	0.84	0.078
nC ₅ H ₁₂	7.35	3.78	1.02	0.92	0.69	1.01	0.006
iC ₅ H ₁₂	5.85	5.00	0.92	1.08	1.56	2.78	0.006
nC ₆ H ₁₄	8.63	2.63	0.89	0.97	0.74	0.87	0.006
nC ₇ H ₁₆	10.67	2.02	0.79	0.90	0.70	0.74	0.006
nC ₈ H ₁₈	11.98	2.10	0.71	0.94	0.73	0.56	0.006
nC ₉ H ₂₀	14.04	4.22	0.79	1.08	1.76	1.13	0.006
nC ₁₀ H ₂₂	15.22	5.53	0.76	1.07	1.57	1.09	0.006
nC ₁₁ H ₂₄	15.18	5.48	0.82	1.24	1.48	2.77	-
nC ₁₂ H ₂₆	17.92	8.53	0.75	1.14	1.29	0.82	-
Benzene	6.02	4.92	0.74	0.61	0.78	0.63	-
Toluene	9.91	1.95	0.58	0.72	0.81	0.68	-
Average	7.87	5.47	1.05	1.03	1.28	1.07	0.03
Average - Main Components	6.70	5.54	1.14	1.05	1.33	1.03	0.03

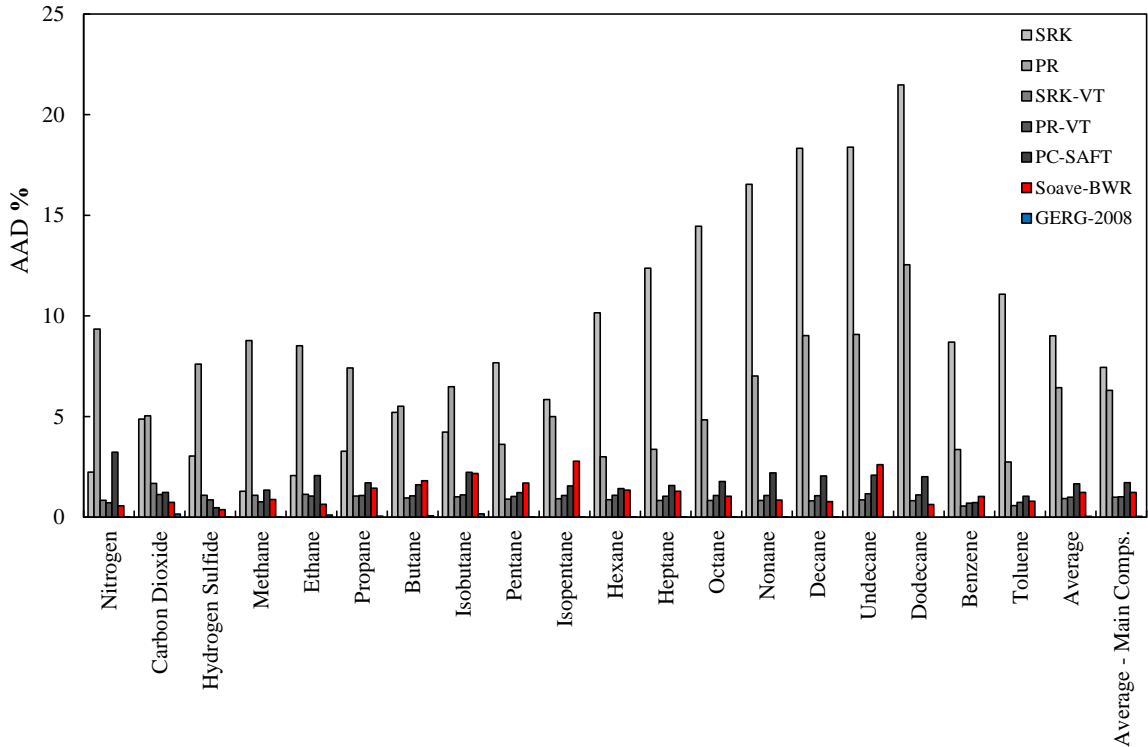


Figure 3.1 AAD% in calculated density for different EoS within 150-500 K and 0-2000 bar.

As mentioned in the previous chapter, volume translation can be used to improve density calculation especially for liquid phases. The volume translation parameter is normally treated as temperature independent [30] since temperature dependent volume translation can lead to negative heat capacity at extreme high pressures [55] and sometimes crossing $P-v$ isotherms [56]. Here we have adopted temperature dependent volume translation in order to improve the density calculation results for cubic EoSs as much as we can. The temperature dependent volume translation parameters are calculated at different temperatures. At each temperature, the volume translation parameter is determined by matching the density from the reference EoS at 1000 bar. In this manner, better density results at high pressures can be expected. This temperature dependent volume translation still suffers negative heat capacity at infinite pressures [55] but not necessarily the problem of crossing isotherms [56]. Table 3.4 shows the trends in the volume translation parameters for different components and models. If the volume translation parameter is monotonically decreasing with temperature, the problem of crossing isotherms will not happen; otherwise, it will. It can be seen that for SRK and PR, the trends are fine for most hydrocarbons. CO_2 and H_2S give the problematic trends for all the four models. For Soave-BWR and PC-SAFT, the trends are problematic with many hydrocarbons. But on the other hand, Soave-BWR and

PC-SAFT already give very accurate density results and the translation is not really necessary; therefor the volume translation has been applied only to the cubic models. It is possible to force the volume translation parameter to follow a certain trend while minimizing the density calculation deviation but no such effort is made here.

Table 3.4 Trends in the temperature volume translation parameters: the parameters that are not monotonic decreasing with temperature are marked with “N” while the others are kept blank.

Components	SRK	PR	PC-SAFT	Soave-BWR
N ₂			N	N
CO ₂	N	N	N	N
H ₂ S	N	N	N	N
CH ₄	N			N
C ₂ H ₆				N
C ₃ H ₈			N	N
nC ₄ H ₁₀			N	N
iC ₄ H ₁₀			N	
nC ₅ H ₁₂			N	
iC ₅ H ₁₂			N	
nC ₆ H ₁₄			N	
nC ₇ H ₁₆			N	N
nC ₈ H ₁₈			N	N
nC ₉ H ₂₀			N	N
nC ₁₀ H ₂₂			N	N
nC ₁₁ H ₂₄			N	N
nC ₁₂ H ₂₆			N	N
Benzene			N	
Toluene			N	N

The results with temperature dependent volume translation for the cubic models are also presented in Tables 3.2–3.3 and Figure 3.1. For fluid density over a wide temperature and pressure range, the temperature-dependent volume transition greatly improves the results for SRK and PR. However, it should be noted that the maximum absolute deviations for SRK and PR (even after using volume translation) are much larger than those for PC-SAFT and Soave-BWR, showing the importance of the functional form of an EoS.

For methane, we further show the contour maps of the deviations within 150-500 K and 0-2000 bar in Figure 3.2 using SRK and PR (with/without VT), PC-SAFT and Soave-BWR. PR gives the worst prediction of density for methane among the other models, mainly due to its poor density results for the methane gas phase. Using volume

translation for PR significantly improves its prediction results and PR-VT gives the smallest average deviation among other EoSs (except for GERG-2008), however its maximum deviation is relatively large. Soave-BWR gives slightly higher deviation than PR-VT but it has very small minimum and maximum deviations. PC-SAFT and SRK have similar average deviations, which are slightly higher than that of Soave-BWR. However, SRK gives much larger negative deviations, i.e., under predicting the densities, at temperatures and pressures close to the critical point. SRK with volume translation gives slightly better prediction of density compared to PC-SAFT. The low average density deviation of SRK is largely attributed to its good performance for the methane gas phase. Compared with SRK, PC-SAFT gives smaller maximum values in density deviations.

The deviations in saturated liquid density are presented in Table 3.5 and Figure 3.3. Among all the models, Soave-BWR and GERG-2008 give accurate prediction of saturated liquid density for the main components while GERG-2008 is slightly better than Soave-BWR in terms of both average and maximum deviation. After using volume translation for the cubic EoSs, the improvement is obvious for SRK and modest for PR. Compared to Soave-BWR and PC-SAFT, SRK and PR give larger deviations in saturated liquid density even with temperature dependent volume translation. This is because volume translation simply shifts the $P - v$ isotherm but does not change its slope. If the improvement of density is focused on one region (high pressures in this case), there is no guarantee that density in other regions can be improved to a similar extent. Temperature dependent volume translation can be designed to match the saturated liquid density but this usually leads to the problem of crossing $P - v$ isotherms [56].

Table 3.5 AAD% and maximum deviations in the calculated saturated liquid density for different EoSs.

Components	SRK		PR		SRK-VT		PR-VT		PC-SAFT		Soave-BWR		GERG-2008	
	AA%D%	Max Dev.	AA%D%	Max Dev.	AA%D%	Max Dev.	AA%D%	Max Dev.	AA%D%	Max Dev.	AA%D%	Max Dev.	AA%D%	Max Dev.
N ₂	4.41	20.02	9.58	13.34	4.96	20.56	3.86	15.69	2.30	3.22	1.18	1.31	0.060	0.561
CO ₂	12.66	24.91	4.39	16.94	9.60	23.79	5.73	19.27	2.58	14.47	1.47	3.20	0.040	0.075
H ₂ S	6.50	19.37	7.11	10.69	4.62	18.74	2.81	14.11	0.68	3.05	1.19	3.93	0.070	0.006
CH ₄	4.94	21.05	9.04	12.78	5.25	21.34	3.76	16.67	0.91	5.55	0.85	3.07	0.050	0.195
C ₂ H ₆	6.92	22.82	6.96	14.48	4.98	22.69	3.44	18.02	0.84	2.84	0.44	1.61	0.100	0.165
C ₃ H ₈	8.36	23.82	5.71	15.52	5.24	23.53	3.49	18.77	0.71	4.34	0.21	0.74	0.170	0.282
nC ₄ H ₁₀	9.72	25.02	4.66	16.78	5.46	24.43	3.61	19.58	0.90	6.79	0.55	1.12	0.210	0.765
iC ₄ H ₁₀	9.10	24.11	5.05	15.83	5.40	23.76	3.56	18.93	0.59	5.51	0.57	1.54	0.290	0.527
nC ₅ H ₁₂	11.63	27.02	3.32	18.98	5.84	26.06	3.82	21.23	1.75	7.35	0.34	1.04	0.110	0.006
iC ₅ H ₁₂	10.06	26.54	4.48	18.46	5.65	26.03	3.74	21.23	1.42	3.47	1.17	1.50	0.090	0.006
nC ₆ H ₁₄	13.07	25.49	2.94	16.97	5.82	23.92	3.91	18.93	1.28	12.40	0.32	4.72	0.220	0.007
nC ₇ H ₁₆	14.70	25.62	3.79	17.40	6.09	23.79	3.95	18.67	1.64	13.64	0.55	6.83	0.170	0.006
nC ₈ H ₁₈	15.84	25.78	5.06	17.62	6.29	23.52	4.03	18.36	1.48	16.77	0.63	8.39	0.150	0.007
nC ₉ H ₂₀	17.56	30.51	7.03	22.80	6.71	28.15	4.42	23.17	1.12	12.11	0.54	3.94	0.110	0.006
nC ₁₀ H ₂₂	18.37	30.18	7.94	22.39	6.77	27.54	4.31	22.41	1.27	10.75	0.72	6.77	0.130	0.006
nC ₁₁ H ₂₄	17.78	32.34	7.30	24.66	6.38	29.86	4.21	24.73	1.26	12.08	2.18	6.77	-	-
nC ₁₂ H ₂₆	20.10	33.38	9.93	26.02	6.67	30.27	4.17	25.34	1.52	9.47	1.03	4.51	-	-
Benzene	11.66	25.81	4.04	17.72	7.16	24.85	4.18	20.12	1.26	9.27	1.73	1.23	-	-
Toluene	13.27	27.06	2.85	19.02	6.01	25.59	3.81	20.79	1.42	9.55	2.11	1.43	-	-
Average	11.93	25.83	5.85	17.81	6.05	24.65	3.94	19.79	1.31	8.56	0.94	3.35	0.13	0.17
Average - Main Components	10.92	24.82	5.80	16.73	5.91	23.86	3.90	19.00	1.30	8.15	0.72	3.31	0.13	0.17

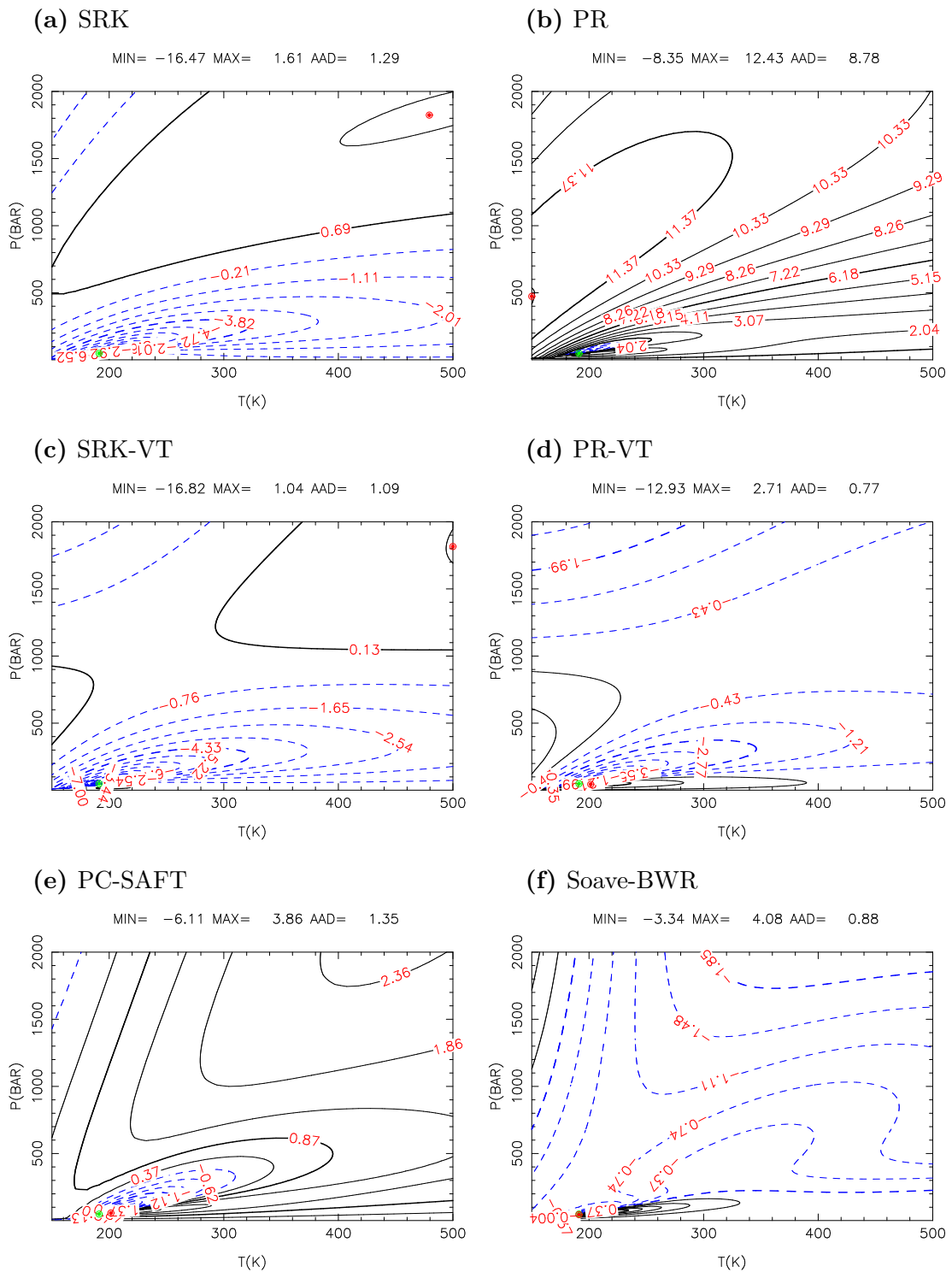


Figure 3.2 Contour map of deviation in the calculated densities for methane by different EoSs. The relative deviations (%) are labeled on the contour lines. The green and the red circles indicate the conditions for the minimum and the maximum deviations, respectively.

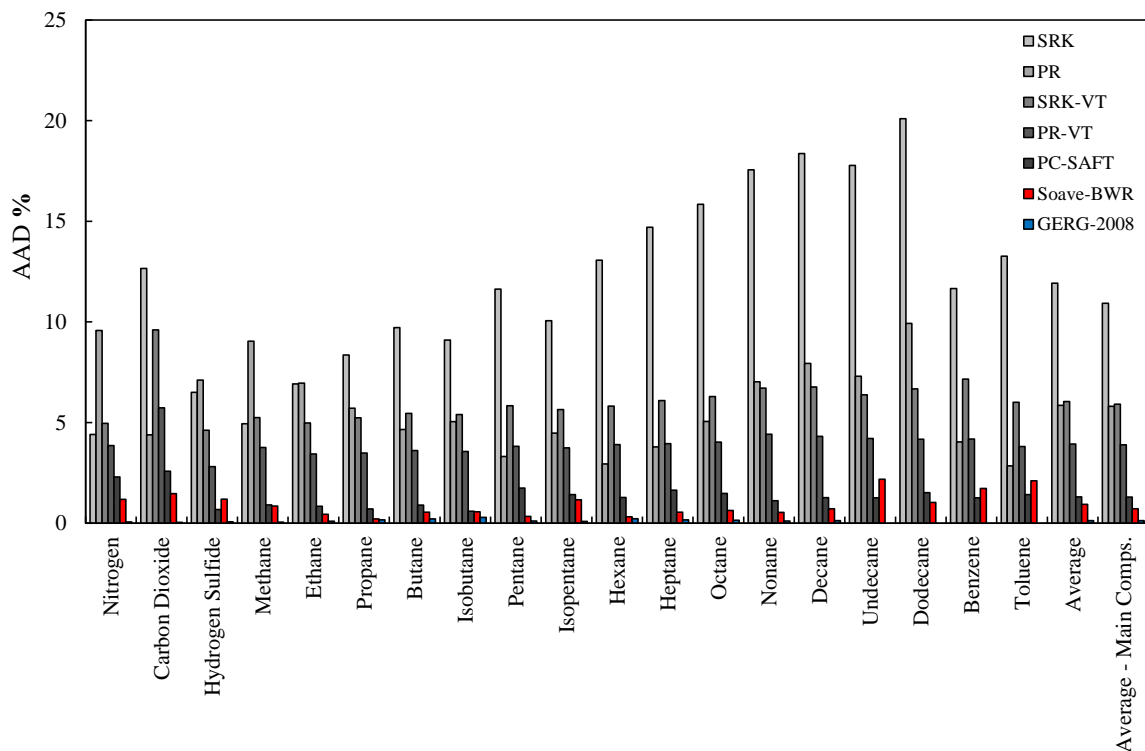


Figure 3.3 AAD% in the calculated saturated liquid density for different EoSs.

Unlike PC-SAFT, both SRK and PR reproduce the experimental critical points. If we relax this requirement and obtain their model parameters by fitting saturated density and vapor pressures, the results can be improved. The Cubic-Plus-Association (CPA) EoS [57, 58] for non-associating compounds is actually SRK with model parameters fitted to vapor pressure and saturated liquid density data. By use of the CPA model parameters from [59], we have obtained the deviations in phase density and saturated liquid density for CPA as listed in Table 3.6. CPA gives much better prediction results than SRK and PR but the deviations, especially the maximum absolute deviations, are still larger than those for non-cubic models. This indicates that in addition to parameter determination, the functional form of an EoS is another important factor for density description. It should also be noted that PC-SAFT does not reproduce experimental critical temperatures and pressures, which leads to larger density deviations around critical points. Actually, we observe that the maximum absolute deviations for PC-SAFT usually appear around the critical temperature and pressure for many components. In contrast, Soave-BWR does not have such a problem.

Table 3.6 AAD% and maximum deviations in the calculated saturated liquid density and density within 150-500 K and 0-2000 bar using CPA EoS.

Components	CPA		CPA	
	AAD% Density	Max Dev.	AAD% Sat. Density	Max Dev.
N ₂	3.94	5.84	3.04	21.00
CO ₂	3.18	14.77	2.19	30.67
H ₂ S	1.87	35.97	2.09	16.70
CH ₄	2.62	6.54	2.97	19.98
C ₂ H ₆	3.24	10.47	2.18	21.48
C ₃ H ₈	4.45	8.25	2.43	31.31
nC ₄ H ₁₀	5.50	17.60	4.12	29.81
iC ₄ H ₁₀	3.69	7.65	2.00	18.57
nC ₅ H ₁₂	2.86	19.13	1.73	30.87
iC ₅ H ₁₂	-	-	-	-
nC ₆ H ₁₄	2.92	8.82	2.03	40.40
nC ₇ H ₁₆	3.00	9.51	1.87	29.32
nC ₈ H ₁₈	3.24	10.51	1.68	25.74
nC ₉ H ₂₀	3.82	11.86	2.15	40.75
nC ₁₀ H ₂₂	4.41	13.16	1.75	21.92
nC ₁₁ H ₂₄	5.32	14.51	2.31	37.02
nC ₁₂ H ₂₆	5.86	15.19	2.36	39.82
Benzene	2.73	7.60	1.90	20.23
Toluene	2.63	8.10	1.61	28.15
Average	3.63	12.53	2.25	27.99
Average - Main Components	3.48	12.86	2.30	27.04

Figure 3.4 illustrates the average AAD% in density and saturated liquid density of the main components for all the EoSs studied here. GERG-2008 gives the lowest deviation for both density and saturated liquid density, while SRK and PR without volume translation give the largest deviation. Using the Peneloux volume translation [30] improves the predictions of cubics and both SRK and PR give slightly lower deviation than PC-SAFT and Soave-BWR in the calculated density. For saturated liquid density, the cubic models are still poorer than the non-cubic ones, even after using volume translation. It can be seen that Soave-BWR gives lower deviation than PC-SAFT in both density and saturated liquid density of the pure components and has the closest predictions to that of GERG-2008 in saturated liquid density calculations. In short, if we want accurate density description over a wide temperature and pressure range, non-cubic models (GERG-2008, Soave-BWR and PC-SAFT) are better than cubic models (SRK and PR) even if temperature dependent volume translation is applied to the latter two.

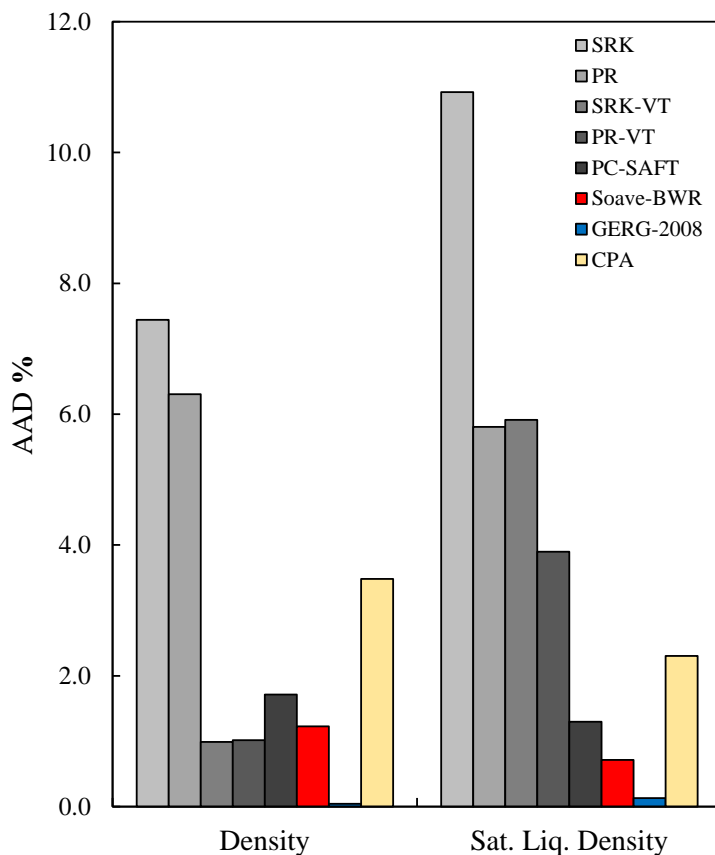


Figure 3.4 Average AAD% in the calculated density and saturated liquid density of the “main components” using different EoSs.

In order to compare the performance of the cubic and non-cubic models for the liquid density data up to extremely high pressures, we used the experimental data from Doolittle [60] for heavy n-alkanes nC₇, nC₉, nC₁₁, nC₁₃, nC₁₇, and nC₂₀. The pressure ranges from 0 to 5000 bar and the temperature ranges from 303 to 573 K (nC₂₀ from 373 K). Table 3.7 presents the AAD% in the calculated high pressure liquid densities. The comparison of density calculation for SRK, PR, PC-SAFT and Soave-BWR shows that Soave-BWR and PC-SAFT have clear advantages over the classical cubic EoSs (even after using volume translation for the cubic models) for both light and heavy components in reservoir fluids. PC-SAFT almost always gives the smallest deviations for those heavy n-alkanes. Soave-BWR is the second best and gives just slightly higher deviations. SRK and PR are much poorer, giving 6.5% and 3.6% deviations, respectively after using volume translation. Non-cubic models have therefore great potential for PVT modeling where high accuracy in density is required. GERG-2008 seems to have the best prediction of density over the whole pressure range especially at higher pressures, however, it can only be used for nC₇ and nC₉. Figure 3.5 shows the

accuracy of GERG-2008 in density predictions for nC₉ at different temperatures and up to 5000 bar compared to Soave-BWR. As illustrated, both models give accurate description of density at all temperatures and pressures up to 300 bar. Soave-BWR starts over predicting the density at higher pressures and the deviation increases as the temperature increases.

Table 3.7 AAD% in the calculated high pressure liquid densities for heavy normal alkanes.

EoS	nC ₇	nC ₉	nC ₁₁	nC ₁₃	nC ₁₇	nC ₂₀	Average
SRK	11.58	14.45	17.13	19.68	26.80	29.32	19.83
PR	2.97	4.70	7.58	10.45	18.42	21.26	10.90
SRK-VT	4.17	4.28	5.63	7.07	6.52	11.51	6.53
PR-VT	1.07	1.39	2.49	3.75	4.48	8.35	3.59
PC-SAFT	1.95	1.74	1.80	1.60	1.94	2.47	1.92
Soave-BWR	2.14	1.57	1.99	1.85	3.15	3.93	2.44
GERG-2008	0.55	0.34	-	-	-	-	0.45

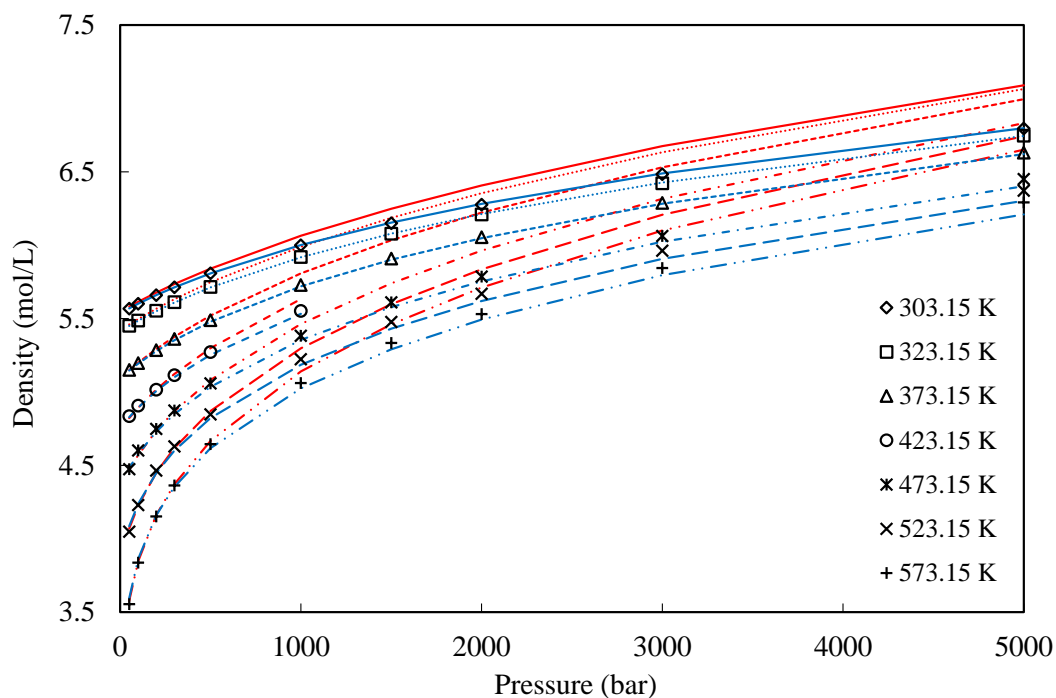


Figure 3.5 Density vs. pressure for n-C₉ using GERG-2008 (blue lines) and Soave-BWR (red lines) at different temperatures: 303.15 K (solid lines), 323.15 K (dotted lines), 373.15 K (dashed line), 473.15 K (dash-dot lines), 523.15 K (long-dashed lines), and 573.15 K (long-dashed double dots lines). The experimental data is taken from [60].

3.1.2 Isothermal Compressibility Calculations

Isothermal compressibility is a measure of the relative volume change of a fluid with pressure at constant temperature and is defined with the following equation:

$$\beta = -\frac{1}{V} \left(\frac{\partial V}{\partial P} \right)_T = \frac{1}{\rho} \left(\frac{\partial \rho}{\partial P} \right)_T \quad (3.1)$$

In order to evaluate how different EoSs perform in calculation of this derivative property, the AAD0% and maximum deviations in the calculated compressibility of the 15 “main components” are presented in Table 3.8. As can be seen, GERG-2008 gives significantly lower deviation than other EoSs both in terms of average AAD0% and maximum deviation. SRK and PR give the largest deviation in the calculated compressibility. Even using volume translation does not improve their performances significantly. In fact, using volume translation makes the predictions even worse for some of the heavier n-alkanes especially for SRK. PC-SAFT and Soave-BWR have better performance than the cubics, while Soave-BWR gives lower deviation than PC-SAFT in compressibility calculation.

Table 3.8 AAD0% and maximum absolute deviations in the calculated compressibility of the “main components”.

Component	SRK		PR		SRK-VT		PR-VT		PC-SAFT		Soave-BWR		GERG-2008	
	AAD0%	Max Dev.	AAD0%	Max Dev.	AAD0%	Max Dev.	AAD0%	Max Dev.	AAD0%	Max Dev.	AAD0%	Max Dev.	AAD0%	Max Dev.
N ₂	6.01	33.74	7.84	33.31	5.84	35.59	6.90	42.01	3.09	14.31	2.77	8.57	0.220	1.027
CO ₂	12.87	79.18	13.80	67.73	9.90	69.36	11.67	61.87	4.71	61.73	2.49	20.56	1.065	7.291
H ₂ S	12.26	55.32	12.51	46.31	10.28	50.80	11.14	36.41	4.26	29.95	3.43	30.66	0.006	0.019
CH ₄	8.69	77.34	10.20	70.33	8.53	75.22	10.26	56.61	3.41	24.51	3.28	19.13	0.175	1.301
C ₂ H ₆	15.94	84.54	17.06	75.03	16.27	79.22	18.86	63.48	5.81	27.86	5.65	17.79	0.846	2.324
C ₃ H ₈	20.81	89.26	22.08	78.06	22.12	81.47	24.60	68.66	11.05	35.16	10.41	20.97	0.914	4.743
nC ₄ H ₁₀	25.03	95.42	26.64	83.10	27.43	85.49	29.16	75.58	15.40	49.92	12.95	21.07	0.547	5.667
iC ₄ H ₁₀	28.16	90.82	24.20	76.96	22.56	81.41	20.69	68.52	17.35	49.96	9.09	18.85	1.538	6.311
nC ₅ H ₁₂	21.41	99.05	22.45	85.16	21.76	86.33	23.17	79.98	21.52	59.73	11.92	22.60	0.006	0.008
iC ₅ H ₁₂	28.27	97.79	29.99	85.42	31.27	86.53	32.25	78.98	21.22	60.33	16.05	25.52	0.006	0.009
nC ₆ H ₁₄	20.00	106.60	20.84	93.29	21.41	91.94	21.39	90.42	15.97	44.10	10.71	18.50	0.006	0.007
nC ₇ H ₁₆	21.19	101.69	21.93	83.76	23.33	83.69	21.96	83.62	21.21	51.40	13.29	21.11	0.006	0.006
nC ₈ H ₁₈	20.67	97.09	21.38	79.31	23.87	77.52	20.70	82.29	18.66	41.01	12.29	20.53	0.006	0.006
nC ₉ H ₂₀	31.52	110.34	32.86	87.79	37.59	86.14	30.90	94.41	20.27	48.87	16.92	25.82	0.006	0.006
nC ₁₀ H ₂₂	31.19	93.78	32.42	70.51	37.91	68.28	29.37	80.49	21.46	43.22	17.18	27.50	0.006	0.006
Average	20.27	87.47	21.08	74.40	21.34	75.93	20.87	70.89	13.69	42.80	9.89	21.28	0.360	1.920

In Figure 3.6, we further show the contour maps of the deviations in density and compressibility of methane within 150-500 K and 0-2000 bar using GERG-2008. Figure 3.7 also presents the contour maps of the deviations in compressibility of methane using SRK and PR (with/without volume translation), PC-SAFT and Soave-BWR. The results show that using volume translation slightly worsens the compressibility predictions of PR for methane.

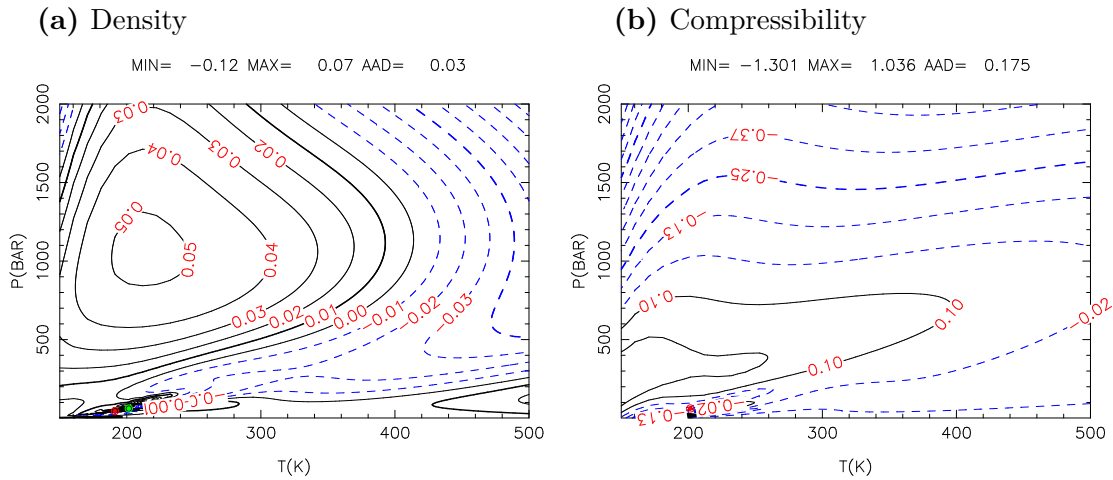


Figure 3.6 Contour map of deviation in the calculated density (a) and compressibility (b) for methane using GERG-2008. The relative deviations (%) are labeled on the contour lines. The blue dashed lines show negative deviations and solid black lines show positive deviations. The green and the red circles indicate the conditions for the minimum and the maximum deviations, respectively.

3.1.3 Sample Binary Density and Multicomponent Gas Mixture Z Factor

Regueira et al. [61] compared the performance of SRK, PR, PC-SAFT and Soave-BWR in density calculation of different binary mixtures of methane and n-decane within 278.15-463.15 K and 1-1400 bar. They observed that the non-cubic models give better prediction of density than cubic ones. Although Soave-BWR is better than PC-SAFT in density and saturated liquid density of pure components (Figure 3.4), Regueira et al. [61] showed that Soave-BWR gives poorer results in density calculation of methane and n-decane binary mixture.

Figure 3.8 illustrates the AAD% in the calculated density as a function of the methane mole fraction (x_1) in the binary mixture of methane and n-decane using non-cubic models (PC-SAFT, Soave-BWR and GERG-2008). The regressed binary interaction parameters k_{ij} 's used for Soave-BWR and PC-SAFT were -0.0311 and 0.0172, respectively. For Soave-BWR, the density results become less accurate as methane mole fraction increases in the binary mixture, while for GERG-2008 the deviation increases only up to $x_1 = 0.7085$. On average, GERG-2008 with AAD% around 0.7% seems to give better prediction of density compared to Soave-BWR with AAD% around 3.2%. PC-SAFT gives slightly higher deviation than GERG-2008 (around 0.8%), which shows it is largely comparable to GERG-2008. In fact, PC-SAFT has better prediction of

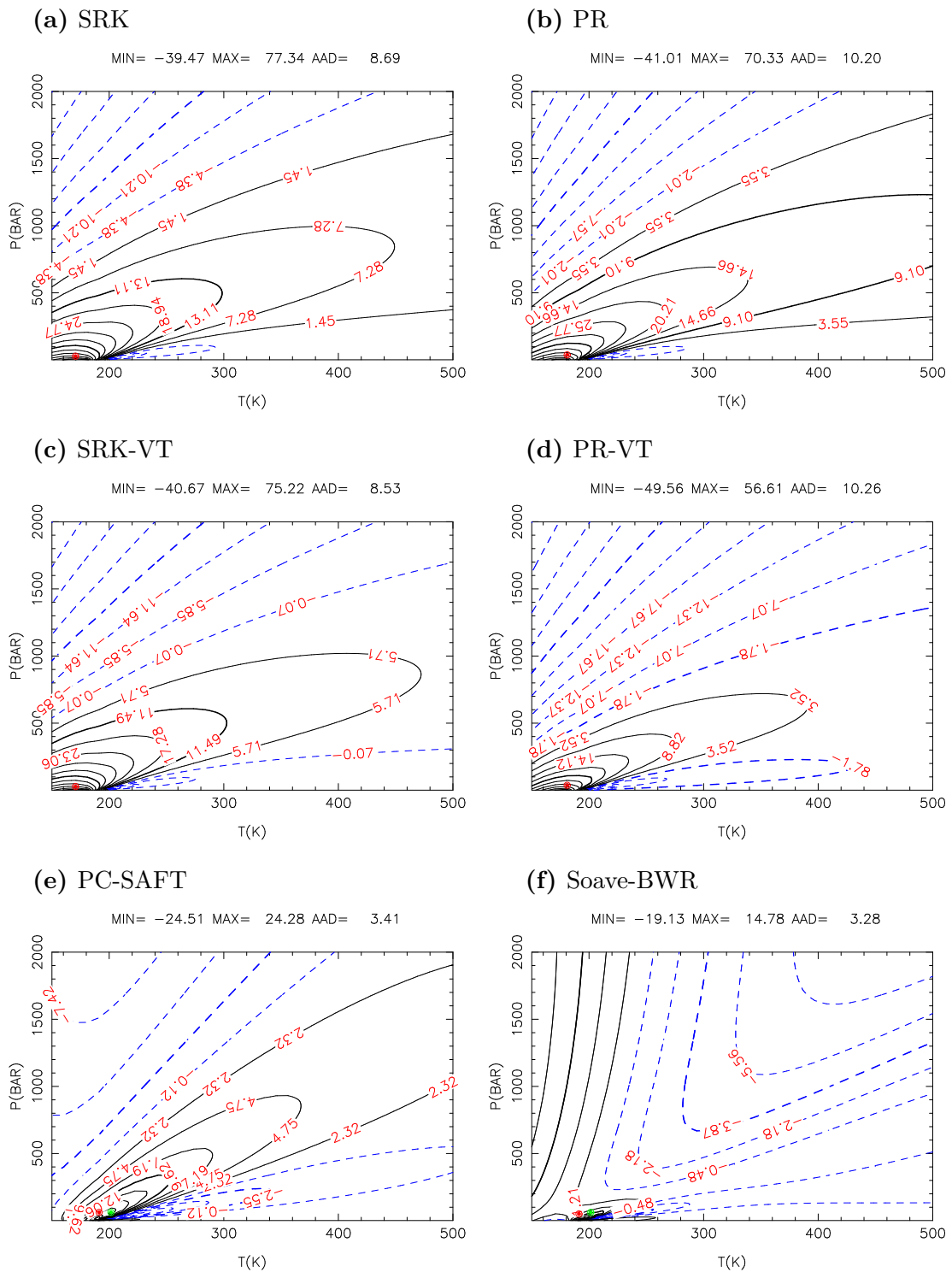


Figure 3.7 Contour map of deviation in the compressibility of methane using SRK (a), PR (b), SRK with volume translation (c), PR with volume translation (d), PC-SAFT (e), and Soave-BWR (f).

density for $x_1 = 0.6017$ and $x_1 = 0.7085$ compared to GERG-2008. Figure 3.9 shows how the density predictions differ for Soave-BWR and GERG-2008 for two mixtures of methane and n-decane at different temperatures. Soave-BWR under predicts the density especially at higher temperatures.

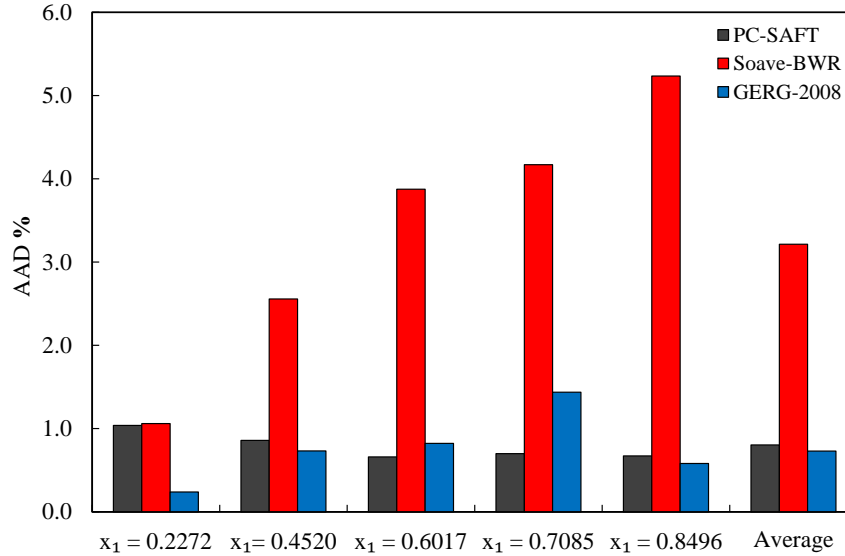


Figure 3.8 AAD% in the calculated densities of the binary system methane (1) + n-decane (2) using GERG-2008, PC-SAFT and Soave-BWR with regressed k_{ij} within 278.15-463.15 K and 1-1400 bar. The experimental data is taken from [61].

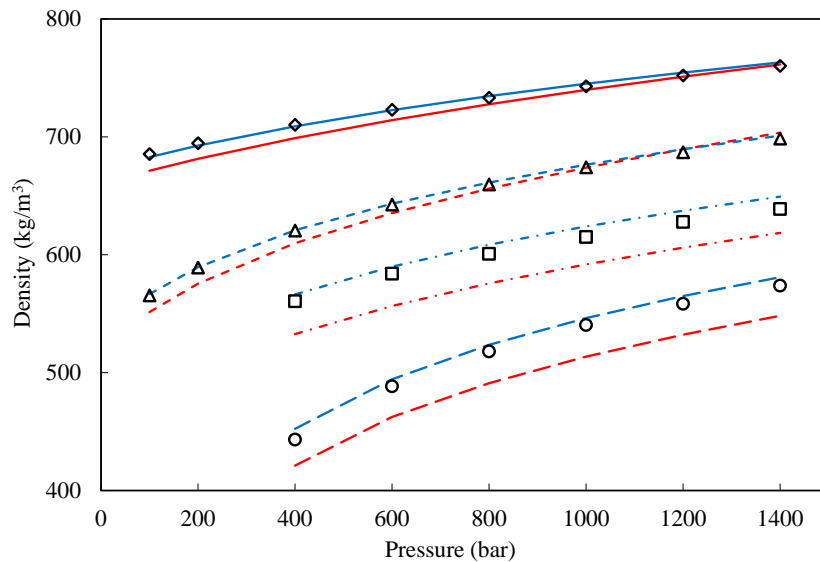


Figure 3.9 Density vs. pressure using GERG-2008 (blue lines) and Soave-BWR with regressed k_{ij} (red lines) for two mixtures of methane and n-decane at different temperatures. 22.27 mol% C₁ and 323.2 K (\diamond , solid lines), 22.27 mol% C₁ and 463.2 K (\triangle , dashed lines), 70.85 mol% C₁ and 323.2 K (\square , dash-dot lines), and 70.85 mol% C₁ and 463.2 K (\circ , long-dashed lines). The experimental data is taken from [61].

Table 3.9 summarizes the deviation in calculation of the Z factor of a gas mixture from Mollerup and Angelo [62] at three different temperatures using different EoSs. As the prediction results using GERG-2008 was very accurate and close to the experimental measurements, the comparison in Table 3.9 was made with the predictions from GERG-2008. The k_{ij} 's used for SRK, PR, Soave-BWR and PC-SAFT are presented in the next section (Tables 3.11–3.12). SRK and PR give the largest deviation in calculation of the Z factor even after using volume translation, with PR being slightly poorer than SRK. The non-cubic models have better accuracy in prediction of Z factor than cubics, while Soave-BWR is better than PC-SAFT. The deviation for almost all the models seems to decrease as the temperature increases. Figure 3.10 shows how Soave-BWR is compared to the GERG-2008. Both models give almost accurate prediction of the experimental data, especially at pressures lower than 600 bar.

Table 3.9 AAD% in the calculated gas Z factor of gas mixture A from [62] using different EoSs. The results are compared with GERG-2008 predictions.

EoS	290 K	315 K	340 K	Average
SRK	2.05	1.99	1.93	1.99
PR	5.28	4.83	4.46	4.86
SRK-VT	1.75	1.58	1.44	1.59
PR-VT	1.90	1.72	1.54	1.72
PC-SAFT	0.87	0.78	0.84	0.83
Soave-BWR	0.40	0.26	0.19	0.28

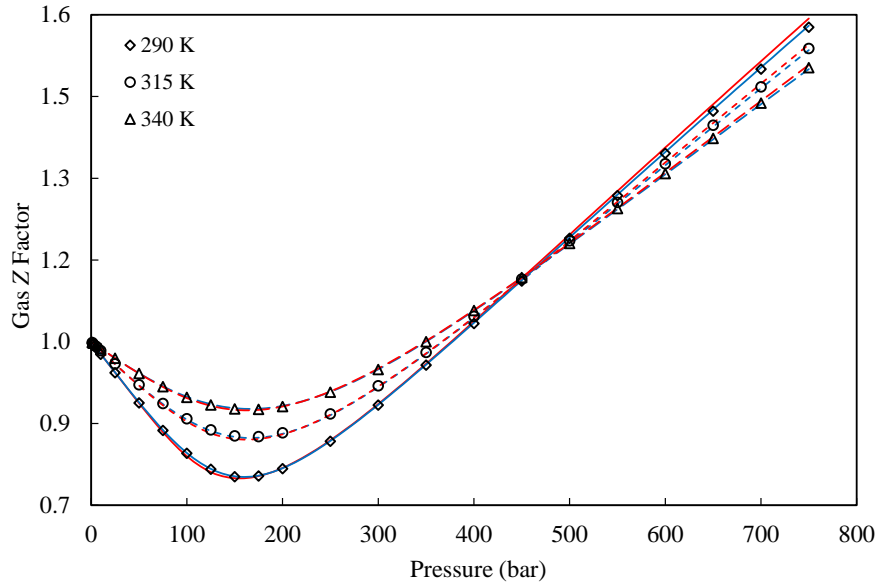


Figure 3.10 Experimental and simulated results using GERG-2008 (blue lines) and Soave-BWR with regressed k_{ij} (red lines) for Z factor of the gas mixture A from [62] at different temperatures: 290 K (solid lines), 315 K (dashed lines), and 340 K (long-dashed lines).

3.2 Binary VLE and Regression of Binary Interaction Parameters

The major components in reservoir fluids include N_2 , CO_2 , H_2S , and various hydrocarbons. The binary interaction parameters k_{ij} 's are usually considered equal to zero between symmetric hydrocarbons, while they are usually non-zero for the asymmetric hydrocarbons, and binary pairs of hydrocarbons and non-hydrocarbons such as N_2 , CO_2 , H_2S . It is very common in petroleum engineering calculations to set the binary interaction parameters between two hydrocarbon components to zero except that one of them is methane.

To apply different EoSs including PC-SAFT and Soave-BWR to reservoir fluids, optimal binary interaction parameters should be regressed. It was mentioned in section 2.4 that the four binary parameters $\beta_{v,ij}$, $\gamma_{v,ij}$, $\beta_{T,ij}$, and $\gamma_{T,ij}$ in GERG-2008 EoS have already been fitted to the available binary data and their values can be found in [10]. To have a fair comparison between GERG-2008 and other EoS models, we regressed the k_{ij} values for SRK, PR, Soave-BWR and PC-SAFT to minimize the deviation in bubble point pressures, as suggested in DECHEMA [63].

The binary VLE data are taken from the DECHEMA Chemical Data Series VI [63], The Polish Academy of Science-TRC Floppy Book Series [64], and Mansfield and Outcalt [65]. Although optimal k_{ij} 's for SRK and PR are already regressed in DECHEMA, these values are regressed again with the complete data from both DECHEMA and TRC series so that a comparison with Soave-BWR, PC-SAFT, and GERG-2008 can be easily made. It should also be noted that k_{ij} 's are treated as temperature independent in the regression. In some advanced cubic models [66–71], temperature dependent k_{ij} 's are used for a better phase equilibrium description. However, we stick to temperature independent ones here for an easy and fair comparison between the cubic and the non-cubic models.

For Soave-BWR, we regressed the k_{ij} 's firstly for all the heavier binary pairs to evaluate its performance compared to GERG-2008, however as it is preferred to use 0 k_{ij} values between heavier hydrocarbon mixtures, in another scenario we only used regressed k_{ij} 's for binary mixtures of N_2 , CO_2 , H_2S , and CH_4 . In the second scenario, we regressed the k_{ij} 's for all the four EoS models, i.e. SRK, PR, Soave-BWR and PC-SAFT.

Table 3.10 presents the binary pairs studied and the temperature ranges used for the first scenario. Bubble point pressure calculation is performed and the comparison

is therefore on the calculated bubble point pressure and vapor phase composition. The Absolute Average Deviations (AAD%) in bubble point pressure and vapor phase composition of heavy binary mixtures are presented in Table 3.10. The average deviation in DP/P (%) for Soave-BWR with regressed k_{ij} 's is around 2.4%. However, as it was mentioned earlier, we prefer to use 0 k_{ij} for the heavy hydrocarbon pairs. Soave-BWR with 0 k_{ij} 's still gives lower deviation in both bubble point pressure (3.3%) and vapor phase composition (1.3%) compared to GERG-2008, which has around 4.5% average deviation in DP/P (%) and 1.5% in DY_1 (mol%).

Table 3.10 Deviation in bubble point pressure and vapor phase composition by GERG-2008 and Soave-BWR with 0 and regressed k_{ij} values (experimental data from [63–65]).

System		Temp. Range		Soave-BWR (0 k_{ij})		Soave-BWR (Regressed k_{ij})			GERG-2008		
COMP1	COMP2	T_{min} (K)	T_{max} (K)	DP/P (%)	DY_1 (mol%)	k_{ij}	DP/P (%)	DY_1 (mol%)	DP/P (%)	DY_1 (mol%)	
C ₂	C ₃	128	368	2.43	0.84	-0.0035	2.34	0.90	2.36	0.97	
	iC ₄	311	394	2.75	0.93	-0.0138	1.16	1.01	1.53	1.17	
	nC ₄	229	403	1.89	0.70	-0.0043	2.32	0.69	1.64	0.64	
	nC ₅	278	444	1.79	1.17	-0.0036	1.44	1.13	1.71	1.60	
	nC ₆	298	450	8.52	1.40	-0.0149	7.93	1.25	9.85	1.65	
	nC ₇	230	505	3.74	0.38	-0.0132	1.95	0.36	4.28	1.10	
	nC ₈	185	373	3.99	2.27	-0.0071	2.60	2.26	3.31	2.28	
	nC ₁₀	185	511	8.33	0.59	-0.0207	4.06	0.52	3.02	0.79	
	C ₃	iC ₄	267	394	1.41	0.34	-0.0032	1.26	0.33	1.20	0.32
		nC ₄	260	413	1.61	0.56	-0.0006	1.59	0.56	1.49	0.57
nC ₅		337	444	3.06	0.60	0.0137	1.05	0.80	1.03	0.84	
nC ₆		273	483	1.39	-	-0.0045	1.19	-	3.10	-	
nC ₇		332	513	1.14	-	-0.0044	0.95	-	1.09	-	
nC ₈		340	546	2.19	1.67	-0.0080	1.44	1.51	2.75	3.25	
nC ₉		377	377	8.16	0.04	-0.0245	0.70	0.11	0.29	0.08	
nC ₁₀		210	511	4.73	0.72	-0.0081	3.71	0.61	2.48	0.54	
iC ₄		nC ₄	273	344	12.17	1.14	-0.0035	12.28	1.02	11.97	1.02
nC ₄		nC ₅	298	458	0.75	6.94	0.0049	0.72	6.11	0.75	6.87
	nC ₆	253	497	2.41	-	-0.0079	2.65	-	2.73	-	
	nC ₇	337	526	0.89	0.28	0.0003	0.90	0.28	1.26	0.51	
	nC ₈	270	375	4.31	-	-0.0005	4.30	-	7.73	-	
	nC ₉	270	370	4.26	-	-0.0051	3.07	-	53.60	-	
	nC ₁₀	311	511	1.52	-	-0.0012	1.35	-	1.56	-	
	iC ₅	nC ₅	328	385	2.01	9.39	0.0116	1.20	9.20	1.96	9.38
	nC ₆	nC ₆	301	335	0.67	0.33	0.0016	0.36	0.45	1.84	0.83
	nC ₅	nC ₆	298	309	3.30	1.01	0.0056	2.88	0.93	3.02	0.99
		nC ₇	404	513	1.14	0.64	0.0050	0.84	0.52	1.04	0.73
nC ₈		304	314	3.85	0.43	0.0000	3.85	0.43	4.06	0.46	
nC ₁₀		318	334	1.33	0.24	0.0012	1.25	0.24	1.20	0.24	
nC ₆	nC ₇	287	369	1.33	0.75	-0.0016	1.31	0.83	1.88	0.61	
	nC ₈	287	388	7.89	0.72	-0.0202	4.61	1.87	11.40	1.51	
nC ₇	nC ₈	313	394	1.33	0.86	0.0021	1.25	0.65	1.32	0.59	
	nC ₁₀	349	392	1.10	0.36	-0.0030	0.70	0.56	0.62	0.75	
Average				3.25	1.31		2.40	1.30	4.52	1.49	

The binary pairs studied for the second scenario are presented in Tables 3.11–3.12 and the temperature ranges for those binary data can be found in Table 3.11. First, pure prediction calculation with zero k_{ij} 's is made and the results from SRK, PR, PC-SAFT and Soave-BWR are compared in Table 3.11. SRK, PR and PC-SAFT give similar deviations in the predicted bubble point pressures and vapor phase compositions, while Soave-BWR gives the smallest deviations in the predictive calculation.

Table 3.11 Deviations in bubble point pressures and vapor phase compositions predicted by SRK, PR, PC-SAFT and Soave-BWR (experimental data from [63, 64]).

System		Temp. Range		SRK		PR		PC-SAFT		Soave-BWR		
COMP1	COMP2	T_{min} (K)	T_{max} (K)	DP/P (%)	DY_1 (mol%)	DP/P (%)	DY_1 (mol%)	DP/P (%)	DY_1 (mol%)	DP/P (%)	DY_1 (mol%)	
C ₁	CO ₂	153	301	11.20	3.13	11.16	3.09	8.35	2.09	11.41	3.46	
	H ₂ S	193	367	15.76	4.54	16.00	4.66	14.31	3.63	15.30	5.11	
	C ₂	130	283	1.69	0.49	1.40	0.31	2.03	0.51	1.42	0.35	
	C ₃	90	361	5.70	0.87	6.12	0.98	4.00	0.65	3.51	0.65	
	iC ₄	110	378	3.36	1.18	3.83	1.38	3.92	1.00	3.20	1.04	
	nC ₄	115	411	5.27	0.98	6.30	1.06	5.81	0.85	3.88	0.76	
	iC ₅	344	444	9.72	4.30	9.77	4.34	10.63	3.89	9.75	3.08	
	nC ₅	176	450	5.47	1.10	6.78	0.99	6.83	0.90	3.97	1.42	
	nC ₆	183	444	13.94	0.29	15.71	0.32	10.13	0.30	5.95	0.55	
	nC ₇	200	511	10.68	0.48	11.80	0.45	8.92	0.30	11.86	0.67	
	nC ₈	223	423	13.79	0.49	15.05	0.49	12.28	0.43	10.05	0.21	
	nC ₉	223	423	13.60	0.31	15.07	0.32	12.39	0.26	14.68	0.28	
	nC ₁₀	244	583	10.35	0.42	11.37	0.41	10.83	0.44	17.72	1.21	
	nC ₁₂	257	318	15.62	-	16.61	-	12.48	-	26.76	-	
	nC ₁₄	321	433	18.28	-	18.85	-	19.16	-	17.59	-	
	nC ₁₆	289	704	14.41	0.79	15.02	1.08	14.54	0.63	21.67	4.84	
	nC ₂₀	305	371	12.61	-	11.25	-	14.59	-	18.59	-	
	nC ₂₄	321	388	9.79	-	15.43	-	16.21	-	15.79	-	
nC ₃₂	343	343	20.47	-	16.10	-	12.19	-	-	-		
nC ₃₆	346	347	27.20	-	23.74	-	2.60	-	-	-		
N ₂	CO ₂	218	301	3.97	0.71	2.74	0.56	3.50	1.50	5.42	1.45	
	H ₂ S	228	344	17.53	6.05	17.51	6.24	15.73	7.25	17.43	5.67	
	C ₁	78	184	6.97	1.76	7.48	2.05	8.12	1.96	7.63	1.99	
	C ₂	111	290	9.60	1.43	6.85	1.68	7.87	1.91	8.03	1.32	
	C ₃	120	353	12.33	1.41	13.19	1.48	13.03	1.77	12.57	1.46	
	iC ₄	255	394	17.04	2.67	18.88	3.18	16.83	3.83	11.14	1.91	
	nC ₄	250	411	14.41	2.18	14.70	2.29	14.85	2.44	9.58	2.58	
	iC ₅	278	377	14.70	2.67	16.85	3.10	20.01	4.74	5.57	1.34	
	nC ₅	277	378	14.47	1.66	16.51	2.02	18.73	2.96	7.14	1.01	
	nC ₆	311	444	21.66	1.61	22.55	1.73	24.47	1.83	10.71	1.49	
	nC ₇	305	497	17.91	4.54	18.05	5.08	17.81	5.48	7.09	1.86	
	nC ₈	322	344	26.68	-	27.06	-	27.39	-	7.77	-	
	nC ₉	344	344	27.52	-	28.50	-	-	-	4.48	-	
	nC ₁₀	311	411	19.02	0.11	22.28	0.13	24.53	0.17	15.39	0.09	
	nC ₁₂	344	367	21.15	-	23.44	-	24.15	-	10.41	-	
	nC ₁₆	463	703	16.32	1.06	16.11	1.13	19.41	1.06	13.49	3.41	
	CO ₂	H ₂ S	225	366	11.71	3.96	12.34	4.01	12.99	4.19	12.54	3.95
		C ₂	207	302	15.46	6.09	15.83	6.08	14.49	5.67	15.72	5.95

Continued on next page

Table 3.11 – continued from previous page.

System		Temp. Range		SRK		PR		PC-SAFT		Soave-BWR	
COMP1	COMP2	T_{min} (K)	T_{max} (K)	DP/P (%)	DY_1 (mol%)	DP/P (%)	DY_1 (mol%)	DP/P (%)	DY_1 (mol%)	DP/P (%)	DY_1 (mol%)
CO ₂	C ₃	233	361	15.37	4.07	15.24	3.96	15.01	3.82	14.02	3.53
	iC ₄	273	398	13.71	3.30	13.61	3.14	12.62	2.76	9.79	1.99
	nC ₄	228	419	14.88	3.49	14.75	3.28	13.96	3.23	12.48	2.32
	iC ₅	278	453	16.27	3.19	16.31	3.12	15.76	2.74	12.16	1.82
	nC ₅	253	463	12.15	3.49	12.27	3.52	12.00	3.06	10.39	2.01
	nC ₆	273	393	15.70	1.44	15.69	1.28	17.06	1.47	14.53	0.72
	nC ₇	311	502	17.44	2.41	17.64	2.19	16.84	2.16	7.90	0.68
	nC ₈	216	466	15.30	1.23	15.38	1.09	15.29	1.36	11.63	0.40
	nC ₉	343	343	20.02	1.00	19.28	0.84	17.77	1.48	8.77	0.08
	nC ₁₀	236	594	19.36	1.79	18.75	1.61	18.47	1.81	7.73	0.49
	nC ₁₂	254	267	10.54	-	10.77	-	7.78	-	5.40	-
	nC ₁₃	255	339	11.62	-	11.95	-	13.03	-	4.96	-
	nC ₁₄	269	311	12.61	-	14.26	-	15.07	-	2.81	-
	nC ₁₅	270	305	0.55	-	1.13	-	2.82	-	3.50	-
	nC ₁₆	463	664	16.06	1.81	14.62	1.68	16.64	1.43	11.99	1.05
	nC ₁₉	293	304	0.13	-	8.67	-	3.24	-	5.51	-
	nC ₂₀	300	373	10.96	-	13.78	-	3.52	-	7.09	-
	nC ₂₁	302	338	10.24	-	13.81	-	3.80	-	7.19	-
	nC ₂₂	315	373	22.93	-	21.48	-	29.67	-	8.99	-
	nC ₂₄	373	573	9.17	0.07	7.74	0.12	18.39	0.14	11.84	0.01
nC ₂₈	348	423	12.95	-	11.59	-	23.94	-	12.44	-	
nC ₃₂	336	573	11.78	0.02	10.95	0.03	21.17	0.03	15.66	0.00	
nC ₃₆	373	423	7.76	-	9.18	-	23.41	-	27.59	-	
H ₂ S	C ₂	200	283	12.54	5.77	13.10	6.06	13.35	5.97	12.97	6.09
	C ₃	217	367	10.78	4.54	10.81	4.41	10.92	4.13	8.93	3.89
	iC ₄	278	398	6.36	2.44	6.02	2.31	6.11	2.19	2.79	1.56
	nC ₄	367	418	5.97	2.19	5.73	2.06	5.49	2.46	3.75	1.29
	iC ₅	323	413	8.94	3.13	9.03	3.00	8.94	3.05	4.20	1.86
	nC ₅	278	444	12.04	1.87	11.81	1.89	11.40	1.81	4.13	1.13
	nC ₆	323	423	12.40	1.50	11.56	1.46	11.84	1.20	2.79	0.43
	nC ₇	311	478	15.25	1.80	14.90	1.62	13.25	0.96	3.64	0.88
	nC ₁₀	278	444	11.16	0.17	9.27	0.27	13.91	0.21	14.42	0.18
	nC ₁₅	423	423	8.35	0.12	7.93	0.23	9.58	0.04	-	-
Average				13.08	2.08	13.48	2.11	13.26	2.12	10.11	1.79

Table 3.12 provides the regression results including the regressed k_{ij} 's. The results for GERG-2008 have also been presented in this table for the binary pairs of N₂, CO₂, H₂S, CH₄ and hydrocarbons up to nC₁₀. After regression, SRK and PR show similar average deviations in DP/P (%) (around 4.4%) and in DY_1 (mol%) (around 1%). PC-SAFT gives slightly better results, around 4.0% in DP/P (%) and 0.9% in DY_1 (mol%). Soave-BWR gives a similar deviation (1.0%) in DY_1 (mol%) but the largest deviation (5.3%) in DP/P (%) among the four models. The comparison shows that the four models are comparable in binary VLE calculation. The non-cubic models do not show clear advantages although PC-SAFT gives slightly lower average

deviations than SRK and PR. The model that gives the best prediction with 0 k_{ij} , i.e., Soave-BWR, is not necessarily the one that can give the best description after parameter tuning. In fact, it is slightly worse than the others. It should also be noted that although the k_{ij} value usually increases with the carbon number, as in the case for SRK, PR and PC-SAFT, the trend does not seem to be valid for Soave-BWR. For example, the k_{ij} for a CH₄-hydrocarbon pair up to C₃ is almost zero for Soave-BWR but its value for iC₄ and heavier hydrocarbons becomes negative – the value for C₃₂ decreases to -0.087. This unusual trend will affect application of Soave-BWR to oil systems since generalization of the k_{ij} with heavy hydrocarbon can be difficult. To be fair, Soave-BWR has not been intensively studied as the SAFT-family EoS models. Compared with the Benedict-Webb-Rubin-Starling (BWRS) EoS evaluated in the DECHEMA [63], Soave-BWR is a dramatic improvement both in VLE accuracy and simplicity. There is, however, still a room to further improve this model.

The comparison between all the four models with regressed k_{ij} and GERG-2008 (with optimal k_{ij} 's) for the binary pairs of N₂, CO₂, H₂S, CH₄ and hydrocarbons up to nC₁₀ shows that GERG-2008 gives the poorest results both for the bubble point pressure and vapor phase composition. The average deviation in DP/P (%) for GERG-2008 is 6.4% which is around 2% higher than the deviation for other EoSs. Figure 3.11 summarizes the comparison results. SRK, PR, PC-SAFT and Soave-BWR with 0 k_{ij} 's give poorer results than GERG-2008 (with optimal k_{ij} 's). However, using regressed k_{ij} 's significantly improves the results of SRK, PC, PC-SAFT and Soave-BWR both in bubble point pressure and vapor phase composition. Soave-BWR and PR seems to give the lowest deviation in bubble point pressure while PC-SAFT gives slightly lower deviation in vapor phase composition for the binary pairs of N₂, CO₂, H₂S, CH₄ and hydrocarbons up to nC₁₀. The good performance of Soave-BWR for the binary pairs of N₂, CO₂, H₂S, CH₄ and hydrocarbons up to nC₁₀ shows that the higher deviation in bubble point pressure for Soave-BWR is largely due to its poor bubble point predictions for binary pairs of N₂, CO₂, H₂S, CH₄ and hydrocarbons heavier than nC₁₀.

Table 3.12 Regressed k_{ij} values for the four EoS models and their deviations in calculated bubble point pressures and vapor phase compositions (experimental data from [63, 64]).

System	COMP1	COMP2	SRK	PR	PC-SAPT	Soave-BWR	GERG-2008								
	k_{ij}	DY_1 (mol%)	DP/P (%)	k_{ij}	DP/P (%)	DY_1 (mol%)	DP/P (%)	DY_1 (mol%)	DP/P (%)	DY_1 (mol%)					
C ₁	CO ₂	0.0993	1.99	0.78	0.0985	1.94	0.75	0.0328	2.31	1.30	0.0804	1.97	0.84	2.42	1.08
	H ₂ S	0.0879	4.09	1.80	0.0859	4.29	1.69	0.0411	3.95	1.66	0.0692	3.93	1.66	4.24	2.08
	C ₂	-0.0030	1.55	0.45	0.0017	1.35	0.32	-0.0058	1.47	0.39	0.0002	1.41	0.36	1.73	0.45
	C ₃	0.0180	3.77	0.76	0.0188	2.77	0.79	0.0034	4.30	0.70	0.0024	2.99	0.65	2.77	0.84
	iC ₄	0.0054	3.06	1.13	0.0108	2.75	1.28	0.0061	2.90	0.93	-0.0079	2.62	1.01	2.40	0.99
	nC ₄	0.0100	4.26	0.89	0.0168	3.78	0.87	0.0041	5.27	0.80	-0.0044	4.19	0.78	5.00	0.96
	iC ₅	0.0267	8.84	4.02	0.0253	8.94	4.07	0.0236	8.71	3.39	-0.0142	8.72	3.16	9.65	3.85
	nC ₅	0.0213	2.36	1.00	0.0270	2.24	0.81	0.0121	3.28	0.77	-0.0076	3.05	1.25	3.53	1.48
	nC ₆	0.0355	3.77	0.20	0.0417	3.90	0.17	0.0114	5.58	0.17	-0.0048	5.71	0.43	5.79	0.77
	nC ₇	0.0280	7.45	0.43	0.0335	7.54	0.36	0.0103	6.56	0.29	-0.0149	9.25	0.58	11.85	1.26
N ₂	nC ₈	0.0410	3.97	0.36	0.0451	4.15	0.35	0.0159	5.93	0.35	-0.0149	5.17	0.26	9.09	0.32
	nC ₉	0.0449	2.68	0.24	0.0485	3.03	0.28	0.0151	4.85	0.29	-0.0184	6.64	0.24	9.89	0.28
	nC ₁₀	0.0411	4.29	0.31	0.0409	4.30	0.26	0.0172	6.51	0.33	-0.0311	7.06	0.82	9.10	1.17
	nC ₁₂	0.0442	7.11	-	0.0500	6.88	-	0.0103	5.88	-	-0.0315	12.22	-	-	-
	nC ₁₄	0.0703	1.43	-	0.0693	1.35	-	0.0329	4.96	-	-0.0425	5.89	-	-	-
	nC ₁₆	0.0586	5.34	0.65	0.0561	5.39	0.86	0.0189	4.11	0.79	-0.0441	9.60	1.51	-	-
	nC ₂₀	0.0534	13.00	-	0.0541	13.61	-	0.0172	3.69	-	-0.0405	11.42	-	-	-
	nC ₂₄	0.0298	7.20	-	0.0500	12.83	-	0.0223	3.99	-	-0.0110	12.80	-	-	-
	nC ₃₂	-0.0728	2.96	-	-0.0559	2.86	-	0.0160	3.25	-	-0.0866	12.89	-	-	-
	nC ₃₆	-0.0868	8.87	-	-0.0763	7.25	-	-0.0040	1.07	-	-0.0400	-	-	-	-
	CO ₂	-0.0196	2.27	0.70	-0.0067	2.61	0.70	-0.0046	2.93	1.47	0.0163	2.55	1.61	1.49	0.45
	H ₂ S	0.1802	5.20	1.42	0.1852	5.51	1.27	0.1082	9.76	1.15	0.1041	9.07	1.48	6.65	1.25
	C ₁	0.0307	2.34	1.27	0.0326	2.13	1.15	0.0258	2.12	1.14	0.0246	2.09	1.14	1.79	1.19
	C ₂	0.0392	4.17	0.71	0.0504	4.04	0.54	0.0472	3.30	0.48	0.0333	2.69	0.84	2.00	0.51
	C ₃	0.0838	8.55	0.67	0.0944	8.56	0.50	0.0669	8.04	0.32	0.0447	7.86	0.81	5.64	0.85
	iC ₄	0.1021	4.64	1.40	0.1065	4.41	1.23	0.0734	4.72	1.21	0.0361	3.47	1.44	4.11	1.37
nC ₄	0.0974	4.95	2.22	0.1037	4.71	1.78	0.0711	4.46	1.64	0.0341	3.90	3.14	4.12	2.64	
iC ₅	0.0962	4.42	1.52	0.1022	4.14	1.50	0.0727	4.09	1.64	0.0148	3.16	1.08	6.37	1.72	
nC ₅	0.0934	4.59	0.96	0.1000	4.58	0.80	0.0665	4.97	0.99	0.0145	4.30	0.98	6.48	1.11	
nC ₆	0.1496	7.11	1.57	0.1548	6.26	1.21	0.0853	5.03	0.75	0.0280	5.26	1.74	12.29	1.36	

Continued on next page

Table 3.12 – continued from previous page.

System	COMP1	COMP2	SRK		PR		PC-SAFT		Soave-BWR		GERG-2008			
			k_{ij}	DP/P (%)	DY_1 (mol%)	k_{ij}	DP/P (%)	DY_1 (mol%)	k_{ij}	DP/P (%)	DY_1 (mol%)	DP/P (%)	DY_1 (mol%)	
CO ₂	nC7	0.1402	8.16	6.90	2.08	0.0751	5.91	1.88	0.0086	5.85	1.92	23.80	2.67	
	nC8	0.1834	4.75	4.31	-	0.0877	4.46	-	0.0143	4.74	-	49.35	-	
	nC9	0.1896	2.58	2.35	-	0.0852	2.48	-	0.0048	3.80	-	8.96	-	
	nC10	0.1079	5.32	4.97	0.10	0.0540	6.39	0.15	-0.0414	4.64	0.08	12.80	0.17	
	nC12	0.1612	8.35	8.40	-	0.0683	8.06	-	-0.0180	10.46	-	-	-	
	nC16	0.2504	5.05	3.02	1.02	0.0921	1.77	0.35	-0.0778	7.82	1.80	-	-	
	H ₂ S	0.1014	1.25	0.999	1.34	0.97	0.0627	1.16	0.87	0.0733	1.53	0.88	1.31	1.05
	C ₂	0.1315	2.46	2.48	2.17	2.13	0.0662	2.76	2.47	0.0937	2.48	2.11	2.83	2.34
	C ₃	0.1443	3.12	3.15	0.83	0.89	0.0751	2.98	0.55	0.0802	3.07	0.53	3.35	0.98
	iC ₄	0.1269	2.62	1.05	0.1181	1.16	0.0631	2.23	0.89	0.0602	1.90	0.76	2.50	1.22
	nC ₄	0.1395	3.13	1.20	0.1315	1.29	0.0672	2.79	1.08	0.0675	2.52	1.14	2.98	1.20
	iC ₅	0.1321	3.15	1.26	0.1219	1.35	0.0671	1.65	1.01	0.0550	1.53	0.57	3.41	0.77
	nC ₅	0.1274	4.37	1.45	0.1198	1.49	0.0665	3.60	1.01	0.0541	3.64	0.67	5.40	1.01
	nC ₆	0.1320	4.59	0.56	0.1236	0.64	0.0726	3.63	0.61	0.0538	3.18	0.50	6.09	1.00
	nC ₇	0.1096	4.93	1.23	0.0977	1.38	0.0527	6.21	1.11	0.0209	6.57	0.68	6.08	1.23
	nC ₈	0.1238	6.31	0.12	0.1155	0.10	0.0699	6.90	0.15	0.0389	5.52	0.16	10.20	0.38
	nC ₉	0.1151	1.86	0.11	0.1054	0.26	0.0600	1.96	0.09	0.0205	2.43	0.03	4.19	0.45
	nC ₁₀	0.1237	4.72	0.58	0.1115	0.68	0.0662	4.25	0.55	0.0177	5.45	0.53	9.78	1.25
	nC ₁₂	0.1019	1.50	-	0.0948	1.09	0.0687	0.58	-	0.0219	0.98	-	-	-
	nC ₁₃	0.0953	3.23	-	0.0967	2.52	0.0725	3.21	-	0.0179	2.52	-	-	-
	nC ₁₄	0.1086	1.51	-	0.0959	1.27	0.0718	3.58	-	0.0049	2.54	-	-	-
	nC ₁₅	0.1084	0.79	-	0.0979	0.85	0.0700	1.27	-	0.0103	1.43	-	-	-
	nC ₁₆	0.1178	4.08	0.53	0.1028	4.13	0.0599	5.51	0.24	-0.0113	11.38	0.88	-	-
	nC ₁₉	0.1113	2.19	-	0.0978	2.64	0.0625	4.50	-	0.0071	4.69	-	-	-
	nC ₂₀	0.1051	3.12	-	0.0912	3.43	0.0612	4.87	-	0.0060	6.05	-	-	-
	nC ₂₁	0.1011	3.35	-	0.0875	3.51	0.0590	4.80	-	0.0086	5.43	-	-	-
	nC ₂₂	0.0936	5.70	-	0.0791	6.03	0.0561	4.82	-	-0.0018	9.15	-	-	-
	nC ₂₄	0.0560	5.66	0.06	0.0333	7.70	0.0517	3.36	0.06	-0.0293	15.89	0.02	-	-
	nC ₂₈	0.0421	9.10	-	0.0307	9.19	0.0497	3.83	-	-0.0205	11.39	-	-	-
	nC ₃₂	0.0284	9.79	0.02	0.0154	10.21	0.0471	4.33	0.05	-0.0305	11.12	0.00	-	-
	nC ₃₆	-0.0145	6.88	-	-0.0264	6.91	0.0424	2.90	-	-0.0567	11.19	-	-	-

Continued on next page

Table 3.12 – continued from previous page.

System	SRK		PR		PC-SAFT		Soave-BWR		GERG-2008						
	COMP2	k_{ij}	DP/P (%)	DY_1 (mol%)	k_{ij}	DP/P (%)	DY_1 (mol%)	k_{ij}	DP/P (%)	DY_1 (mol%)					
H ₂ S	C ₂	0.0870	1.26	1.27	0.0834	1.37	1.56	0.0581	1.31	1.37	0.0605	1.51	1.62	0.83	1.41
	C ₃	0.0838	1.87	1.82	0.0791	1.88	1.81	0.0538	2.09	1.59	0.0486	1.95	1.73	1.75	1.65
	iC ₄	0.0594	2.34	1.63	0.0542	2.11	1.69	0.0384	1.99	1.10	0.0160	1.97	1.29	1.87	0.93
	nC ₄	0.0979	1.85	1.44	0.0894	1.86	1.47	0.0504	1.83	0.70	0.0364	1.84	0.87	1.96	0.85
	iC ₅	0.0781	3.93	1.93	0.0707	3.96	2.00	0.0474	3.24	1.56	0.0182	3.38	1.47	2.63	1.09
	nC ₅	0.0692	2.84	1.66	0.0625	2.50	1.73	0.0454	1.69	1.26	0.0152	1.50	1.22	3.12	1.44
	nC ₆	0.0691	2.18	0.60	0.0599	2.07	0.73	0.0404	3.06	0.39	0.0016	2.73	0.44	1.85	0.69
	nC ₇	0.0790	5.04	1.08	0.0691	4.60	1.19	0.0475	4.57	0.85	0.0043	3.65	0.90	4.24	1.18
	nC ₁₀	0.0447	3.94	0.19	0.0352	3.75	0.27	0.0387	3.28	0.15	-0.0336	4.31	0.13	6.96	0.13
	nC ₁₅	0.0067	7.88	0.13	-0.0110	8.22	0.21	0.0287	3.48	0.10	0.0000	-	-	-	-
	Average		4.41	1.01	1.01	4.38	1.00	1.00	3.96	0.87	0.87	5.30	0.99	6.39	1.15
	Average - up to nC ₁₀		3.94	1.09	1.08	3.78	1.08	1.08	4.03	0.95	0.95	3.93	1.01	6.39	1.15

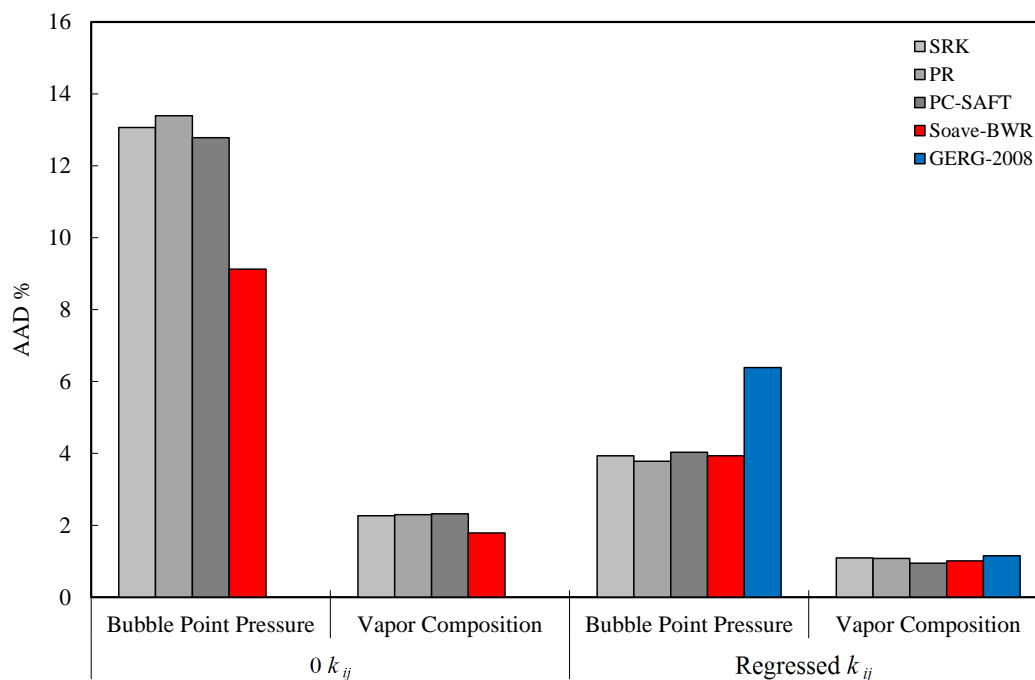


Figure 3.11 AAD% in bubble point pressure and vapor phase composition for the binary pairs of N_2 , CO_2 , H_2S and C_1 using different EoSs with 0 k_{ij} and regressed k_{ij} .

GERG-2008 seems to give very large deviations in bubble point pressures for mixtures of N_2 and heavy n-alkanes, and some other hydrocarbon binary pairs such as n-butane and n-nonane. Figure 3.12 shows the deviation in bubble point pressure calculation for different mixtures of nC_4 and nC_9 in the temperature range of 270 K to 370 K using GERG-2008 and Soave-BWR. The experimental data is taken from Mansfield and Outcalt [65]. Although GERG-2008 has been developed for nC_4 and nC_9 within this temperature range, it gives very large deviations up to around 130% at high mole fraction of nC_9 . Soave-BWR with 0 k_{ij} gives deviations no higher than around 10%. Figure 3.13 illustrates that GERG-2008 over predicts the bubble point pressures mainly at higher temperatures and high mole fraction of nC_9 , while Soave-BWR gives very accurate results for bubble point pressure at lower temperature and the whole composition range of nC_9 , and slightly over predicts this property at higher temperatures.

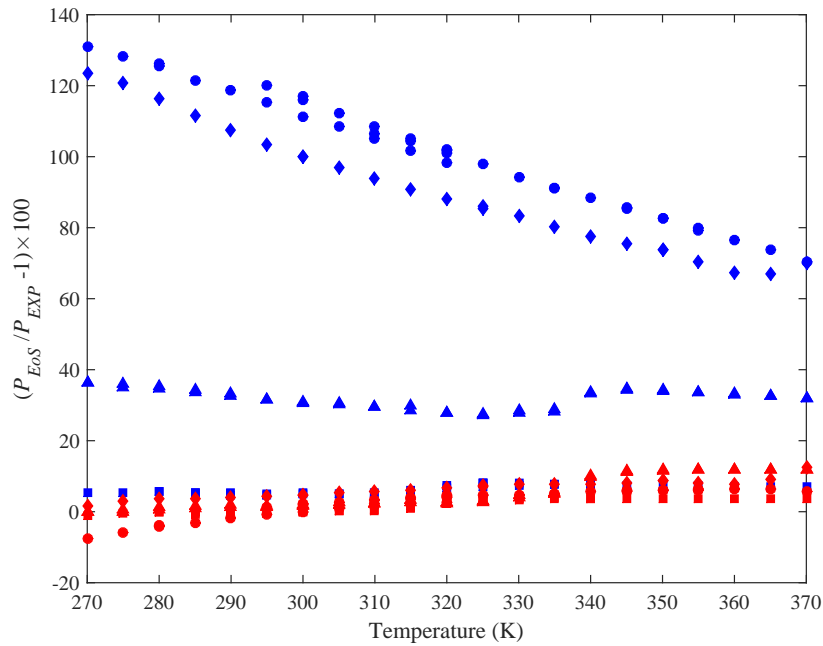


Figure 3.12 Deviations in bubble point pressure calculation as a function of temperature using GERG-2008 (blue markers) and Soave-BWR with 0 k_{ij} (red markers) for different binary mixtures of n-butane (1) + n-nonane (2). 74.9 mol% nC₄ (■), 50.2 mol% nC₄ (▲), 26.2 mol% nC₄ (◆), and 21.4 mol% nC₄ (●). The experimental data is taken from [65].

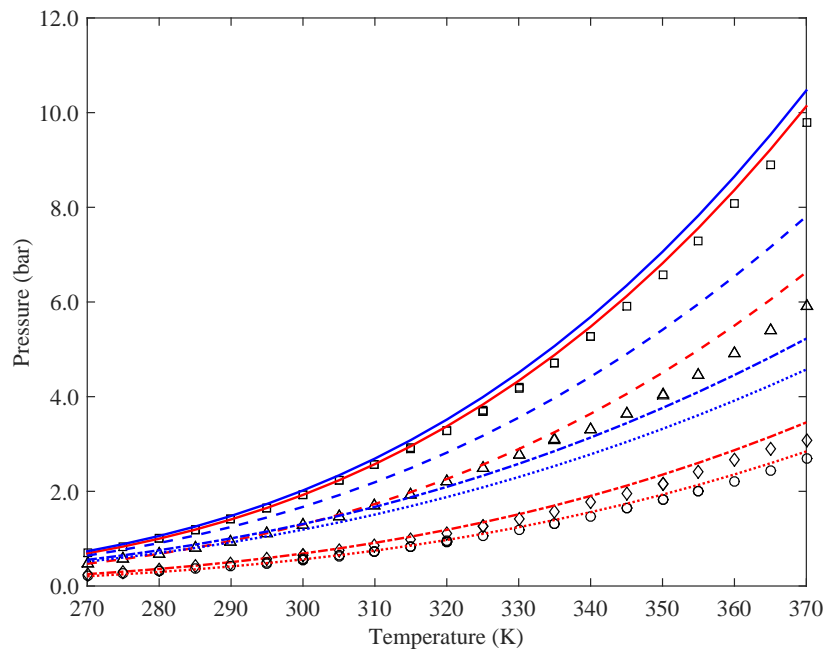


Figure 3.13 Bubble point pressures at different temperatures using GERG-2008 (blue lines) and Soave-BWR with 0 k_{ij} (red lines) for binary mixtures of nC₄ and nC₉. 74.9 mol% nC₄ (□, solid lines), 50.2 mol% nC₄ (△, dashed lines), 26.2 mol% nC₄ (◇, dash-dot lines), and 21.4 mol% nC₄ (○, dotted lines). The experimental data is taken from [65].

Table 3.13 presents some statistics of SRK, PR, PC-SAFT and Soave-BWR in binary VLE calculation. Two properties are investigated here, one is the average k_{ij} and the other is the sensitivity of the VLE results with respect to k_{ij} . The average k_{ij} is calculated by averaging the absolute values of the optimal k_{ij} 's for all the binary pairs. Its magnitude reflects how far the optimal interaction parameter is to the default value ($k_{ij} = 0$). If a model has a smaller average k_{ij} , it means that only a small adjustment is needed to tune it from its default state to its optimal state. Among the four models, SRK and PR give similar average k_{ij} values (around 0.08), PC-SAFT gives an obviously smaller value (around 0.05) and Soave-BWR gives the smallest (0.03). SRK and PR seem to be inferior to the other two models if this k_{ij} criterion is used. And Soave-BWR seems to be the best since the smallest tuning from its default value is needed. The sensitivity with respect to k_{ij} is calculated as follows: if we change k_{ij} from its default value ($k_{ij} = 0$) to its optimal value, the deviations in calculated bubble point pressure and vapor phase composition will decrease. The absolute values of these decreases divided by the change in k_{ij} are defined as the sensitivities, i.e.,

$$\text{Sensitivity in } DP/P = \left| \frac{(DP/P)_{optimal} - (DP/P)_{default}}{k_{ij,optimal} - k_{ij,default}} \right| \quad (3.2)$$

$$\text{Sensitivity in } DY_1 = \left| \frac{(DY_1)_{optimal} - (DY_1)_{default}}{k_{ij,optimal} - k_{ij,default}} \right| \quad (3.3)$$

Table 3.13 Statistics for the four EoS models in binary VLE calculation: sensitivities and average k_{ij} .

	SRK	PR	PC-SAFT	Soave-BWR
Average sensitivity in DP/P (%)	109	115	231	161
Average sensitivity in DY_1 (mol%)	11.4	12.6	22.5	17.2
$\overline{ k_{ij} }$	0.086	0.082	0.048	0.031

In Table 3.13, the sensitivities for DP/P (%) and DY_1 (mol%) averaged for all the binary pairs are reported. For both bubble point pressure and vapor phase composition, SRK and PR are less sensitive to k_{ij} than PC-SAFT and Soave-BWR. According to the average sensitivities, if we change k_{ij} by 0.01, SRK and PR will give around 1% change in DP/P (%), as compared with 2.3% for PC-SAFT and 1.6% for Soave-BWR. This indicates that PC-SAFT is roughly twice as sensitive as SRK and PR, and Soave-BWR is around 50% more sensitive than SRK and PR. It should be mentioned that the change of DP/P with k_{ij} is not linear and its slope is in principle different at different k_{ij} values. But these average sensitivities calculated using eqs. (3.2)–(3.3) still provide a

rough sensitivity index for these models. The relatively high sensitivities for PC-SAFT and Soave-BWR can become a disadvantage when applying them to ill-defined fluids since a more sensitive model is more vulnerable to the uncertainty in parameters, such as k_{ij} .

Finally, in order to apply the four models to PVT calculation (chapter 4), we need to generalize the k_{ij} values for components above C₇₊. Table 3.14 gives the generalized k_{ij} values for N₂-C₇₊, CO₂-C₇₊, H₂S-C₇₊, and CH₄-C₇₊. They are generated based on the optimal k_{ij} values with heavy components up to C₂₀ in Table 3.12. The k_{ij} values in Table 3.14 are either calculated by averaging the k_{ij} values from C₇ to C₂₀ or set to the value for a certain binary pair. There is some arbitrariness in this process. In principle, we can tune the k_{ij} values within a certain range through regression of PVT data. However, we would like to limit parameter tuning as much as possible in this comparative study and thus have not done that here.

Table 3.14 Interaction parameters for N₂-C₇₊, CO₂-C₇₊, H₂S-C₇₊, and CH₄-C₇₊ for SRK, PR, PC-SAFT and Soave-BWR.

EoS	N ₂ -C ₇₊	CO ₂ -C ₇₊	H ₂ S-C ₇₊	CH ₄ -C ₇₊
SRK	0.1079	0.1237	0.0447	0.0510
PR	0.1172	0.1115	0.0352	0.0522
PC-SAFT	0.0540	0.0662	0.0387	0.0103
Soave-BWR	-0.0414	0.0103	0.0000	-0.0441

3.3 Phase Envelopes of Multicomponent Mixtures

PC-SAFT, Soave-BWR and GERG-2008 are used to predict the phase envelopes of 30 synthetic natural gases from eleven different sources [72–82]. Table 3.15 lists the basic information about those gases. Only a few gases, such as Gases 26 and 27, have a significant amount of components heavier than n-pentane. A few gases are ternary systems, including Gases 10, 25, 26 and 27.

Prediction calculations are made both with zero k_{ij} 's and the optimal k_{ij} 's given in Table 3.12. Comparison with SRK and PR are also made. Some selected results are presented in Figures 3.14–3.26. In each figure, the prediction with zero k_{ij} 's is given in (a) and the one with the optimal k_{ij} 's in (b). As GERG-2008 only uses optimal k_{ij} values, it has been included only in part (b) of each figure. From the calculation results,

Table 3.15 An overview of the phase envelopes tested in this study.

Gas	Source	C ₁	C ₆₊	Remark
1	[72]	98.94	0.04	
2	[72]	90.42	0.01	
3	[72]	96.62	0.03	
4	[72]	88.19	0.16	
5	[72]	83.35	0.09	
6	[73]	89.96	0.00	
7	[73]	88.76	0.00	
8	[73]	86.48	0.00	
9	[73]	96.47	0.00	
10	[78]	89.00	0.00	C ₁ /C ₂ /C ₄ ternary system
11	[74]	91.00	0.00	
12	[74]	81.40	2.30	Large deviation in dew point branch
13	[74]	95.90	0.00	
14	[74]	95.00	0.00	
15	[74]	94.50	0.00	Large deviation in dew point branch
16	[74]	94.30	0.27	Large deviation in dew point branch
17	[75]	69.11	0.11	High CO ₂ concentration (26%)
18	[75]	84.45	0.05	
19	[76]	93.51	0.00	
20	[76]	84.28	0.00	
21	[76]	96.61	0.00	
22	[76]	94.09	0.00	
23	[76]	93.60	0.00	
24	[77]	81.18	0.00	N ₂ /C ₁ /C ₂ /C ₃ four-component system
25	[79]	85.13	0.00	C ₁ /C ₂ /C ₃ ternary system
26	[80]	81.40	5.10	C ₁ /C ₄ /C ₁₀ ternary system
27	[80]	60.00	9.00	C ₁ /C ₄ /C ₁₀ ternary system
28	[81]	90.99	0.00	
29	[82]	82.32	1.98	
30	[82]	82.05	1.99	

including Figures 3.14–3.26 and those not presented here, the following observations are obtained:

(1) The prediction results are generally satisfactory for systems containing components up to C₅, both for zero k_{ij} 's and the optimal k_{ij} 's. Using the optimal k_{ij} 's gives very little differences for systems with components only up to C₅ (see Figures 3.14–3.17, Figures 3.20–3.23, and Figure 3.26). For all these systems, GERG-2008 also gives satisfactory and similar prediction of the phase envelopes as the other EoSs.

(2) Gas 17 is the only system with a very high content of CO₂ (26 mol%). For that system, using non-zero k_{ij} 's is essential to get the correct phase envelope (Figure 3.19). PR seems to be a bit better than the others for Gas 17 while it is also a matter how k_{ij} is selected.

- (3) Predicting the bubble point branch is relatively easy, as can be seen for Gas 24 in Figure 3.22. Using non zero k_{ij} 's can still improve the prediction for this system. The difference in predictions from different EoSs usually happens in the dew point branch.
- (4) The EoS models seem to fall into two groups in terms of their predicted phase envelopes: SRK, PC-SAFT, Soave-BWR and GERG-2008 generally predict a bit larger phase envelope, whereas PR give a bit smaller phase envelope (Figures 3.14–3.16, Figures 3.20–3.21, Figure 3.23 and Figure 3.26). This seems to be the case both for zero k_{ij} 's and non-zero k_{ij} 's. In general, SRK, PC-SAFT, Soave-BWR and GERG-2008 give predictions closer to the experimental data than PR. This is in agreement with Alfradique and Castier's observation that PC-SAFT gives closer predictions of phase envelopes than PR [83]. But it should also be noted that PC-SAFT and GERG-2008 seem to be similar to another CEoS (SRK) in phase envelope prediction.
- (5) As shown in Figure 3.15 and Figure 3.21, for all the EoS models, large deviations are observed in the dew point pressure branch above the cricondenbar for experimental data from several sources where the dew points were measured by the chilled mirror method [72, 73, 78, 76]. The experimental measurements tend to show larger envelopes than the predicted ones. It is not clear whether it is due to some inherent deficiency in the thermodynamic models, or due to systematic errors in the experiments.
- (6) Predictions for Gases 12 and 16 from source [74] show very large deviations in the dew point branches, probably due to big errors in the experiment (Figure 3.18).
- (7) Gases 26 and 27, measured by Urlic et al. [80], are highly asymmetric ternary systems, maybe the most challenging ones among the tested systems. None of the EoSs gives satisfactory prediction over the whole temperature and pressure range (Figures 3.24–3.25). PR seems to give the best overall performance for this system. Interestingly, for Gas 26, PR with zero k_{ij} 's seems to give a better result - using non-zero k_{ij} 's improves the dew point prediction but significantly overshoots the bubble point branch. For this system, the EoS models cannot be divided into the two groups as mentioned in (4). Each EoS gives its unique prediction, especially for the low molecular gas, Gas 26. Compared with the other models, Soave-BWR and GERG-2008 give a very different prediction. If zero k_{ij} 's are used, Soave-BWR predicts much larger envelopes than the others, while GERG-2008 gives the largest phase envelope with the optimal k_{ij} 's. When non-zero k_{ij} 's are used, Soave-BWR predicts much flatter envelopes than with zero k_{ij} 's but still large deviations in the dew point branches.

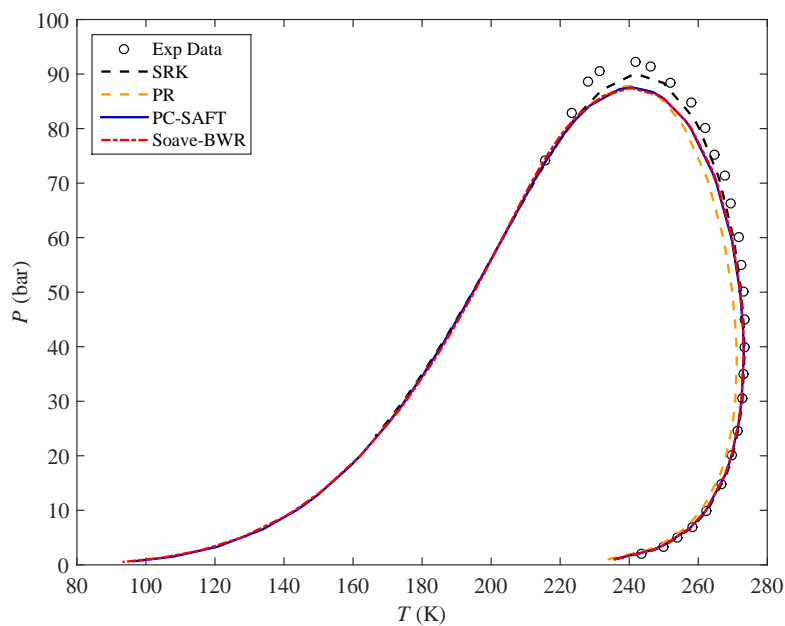
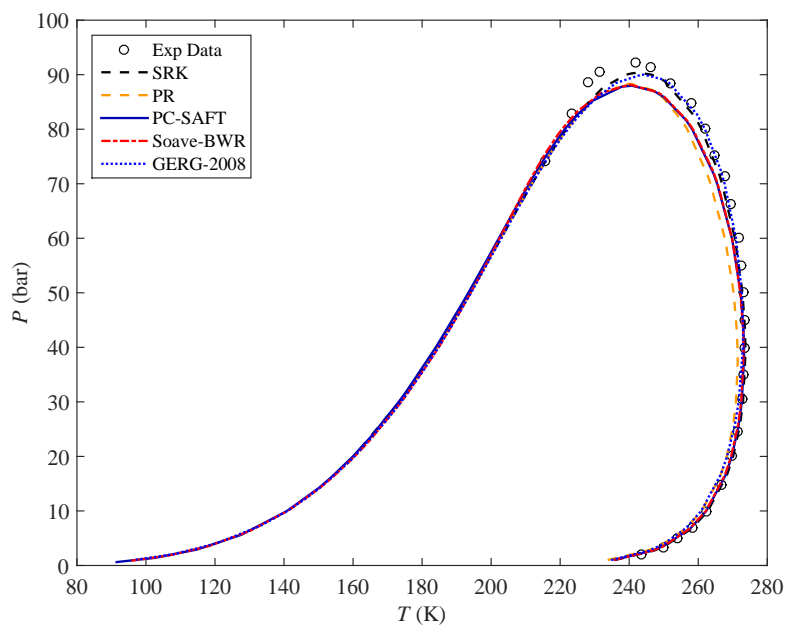
(a) 0 k_{ij} (b) Optimal k_{ij} 

Figure 3.14 Phase envelopes for Gas 5 with (a) zero k_{ij} 's and (b) the optimal k_{ij} 's.

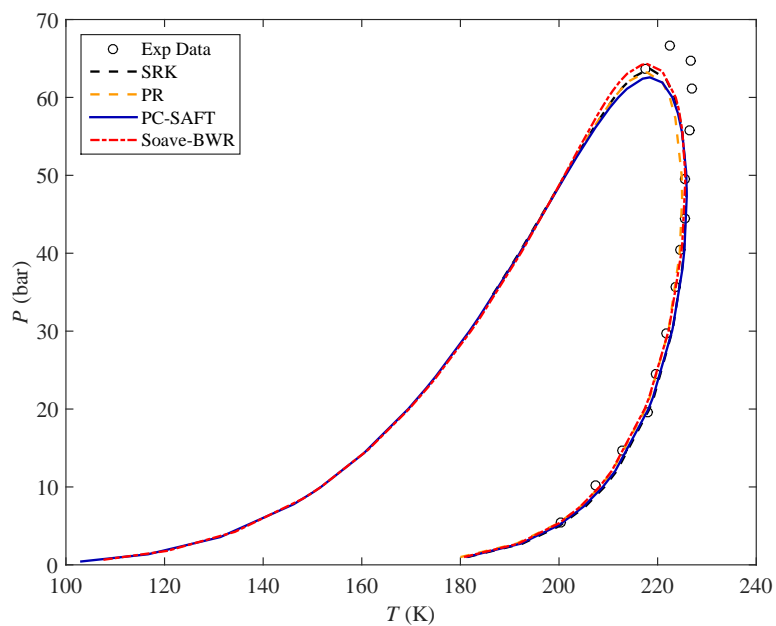
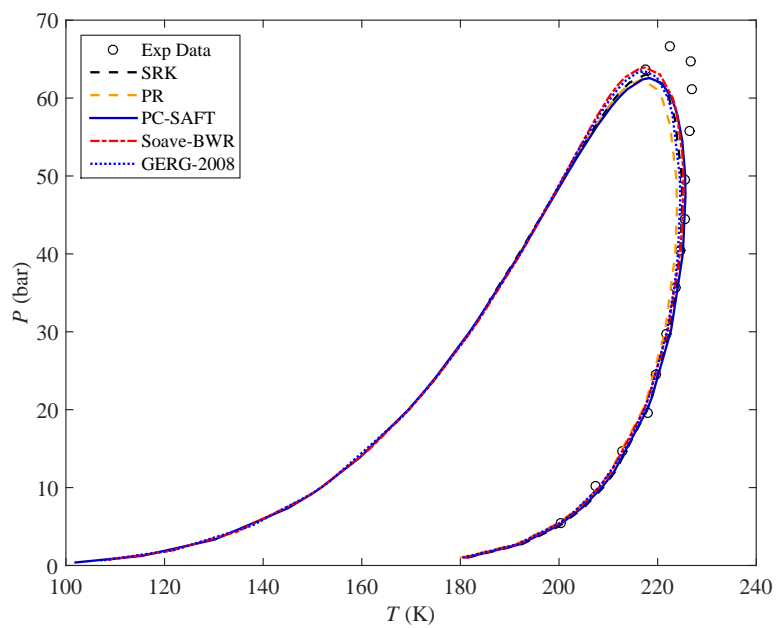
(a) 0 k_{ij} (b) Optimal k_{ij} 

Figure 3.15 Phase envelopes for Gas 6 with (a) zero k_{ij} 's and (b) the optimal k_{ij} 's.

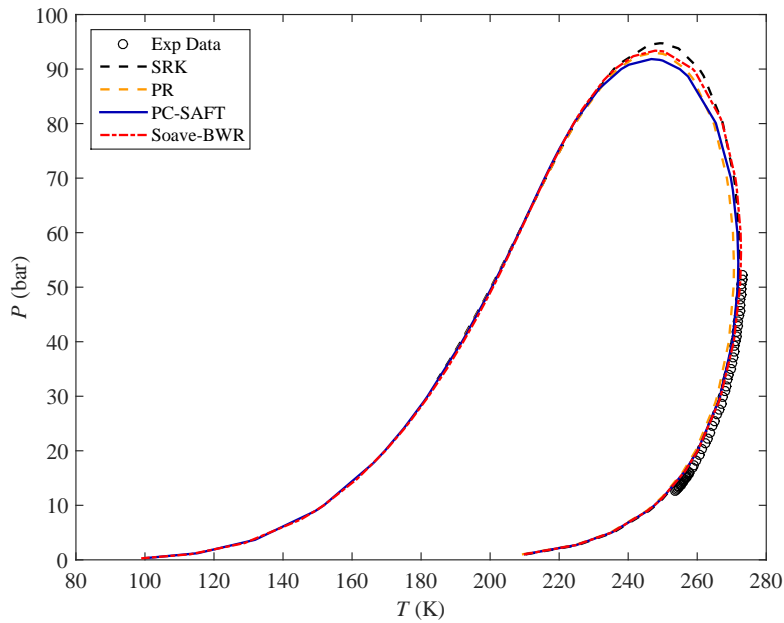
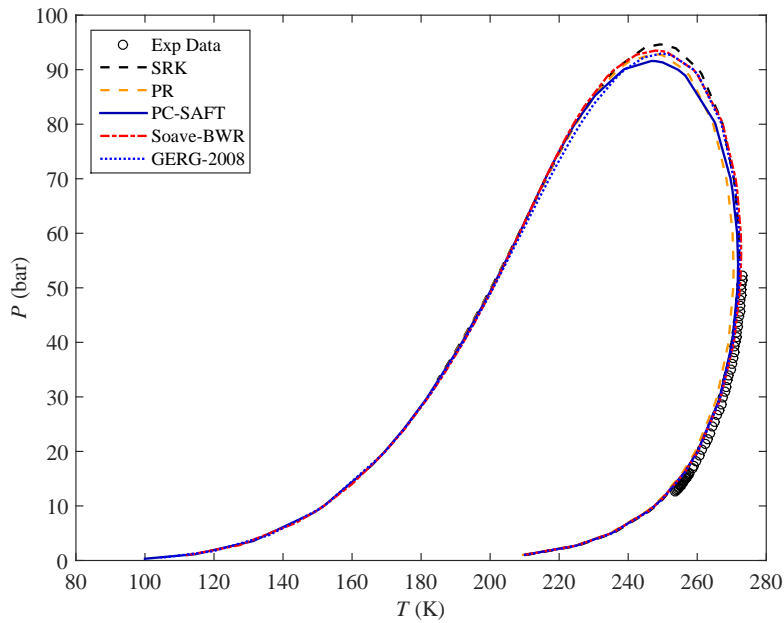
(a) 0 k_{ij} (b) Optimal k_{ij} 

Figure 3.16 Phase envelopes for Gas 10 with (a) zero k_{ij} 's and (b) the optimal k_{ij} 's.

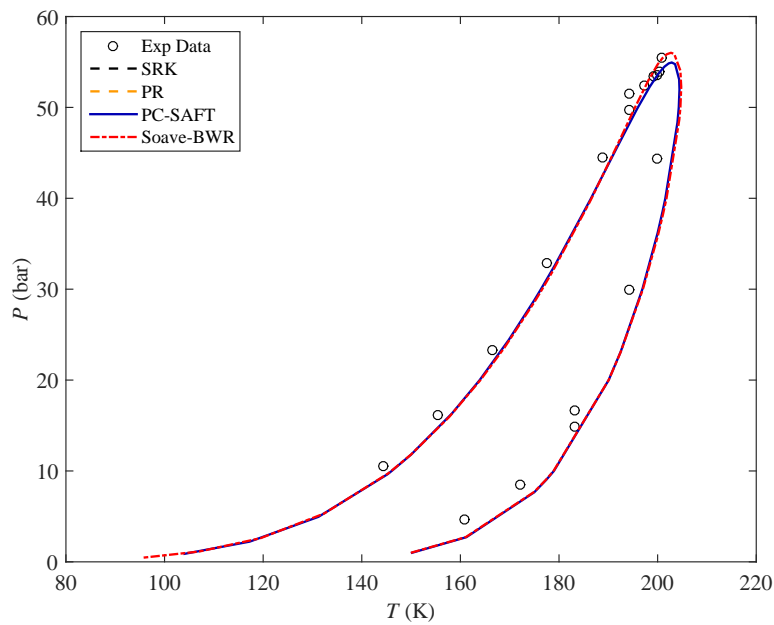
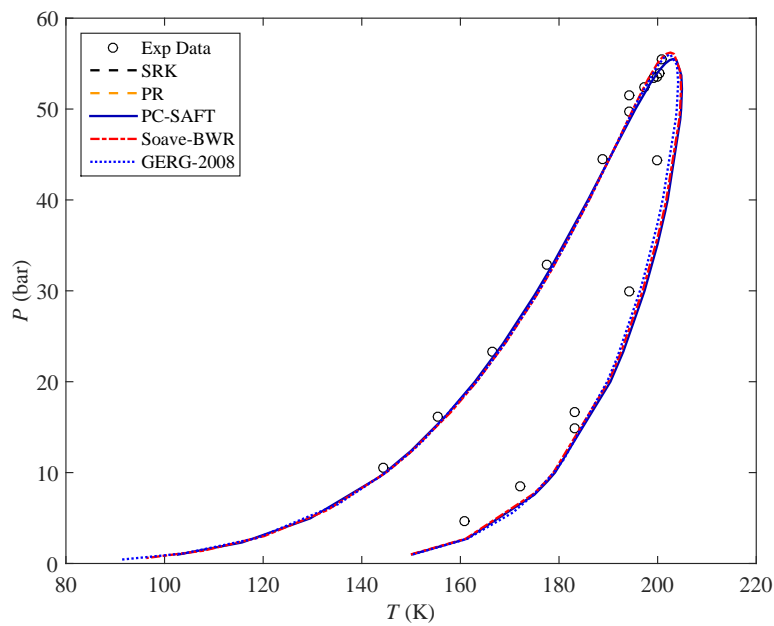
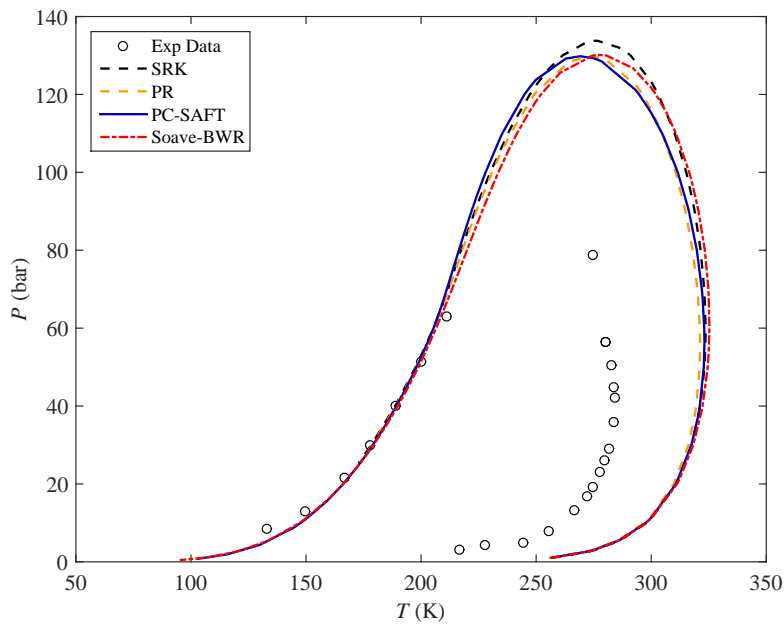
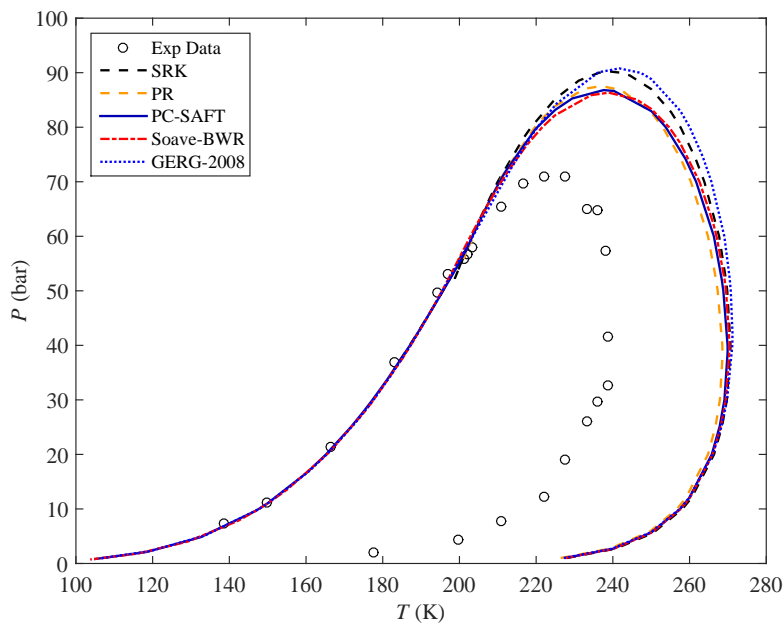
(a) 0 k_{ij} (b) Optimal k_{ij} 

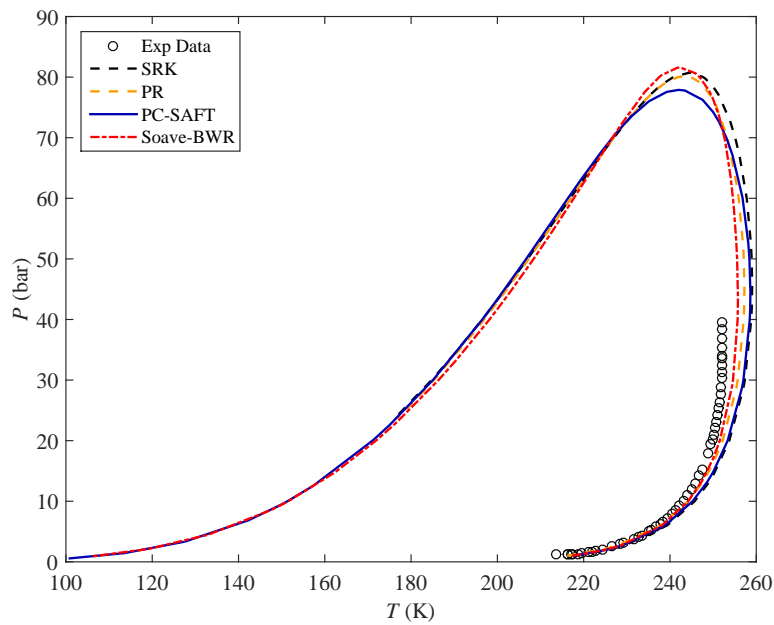
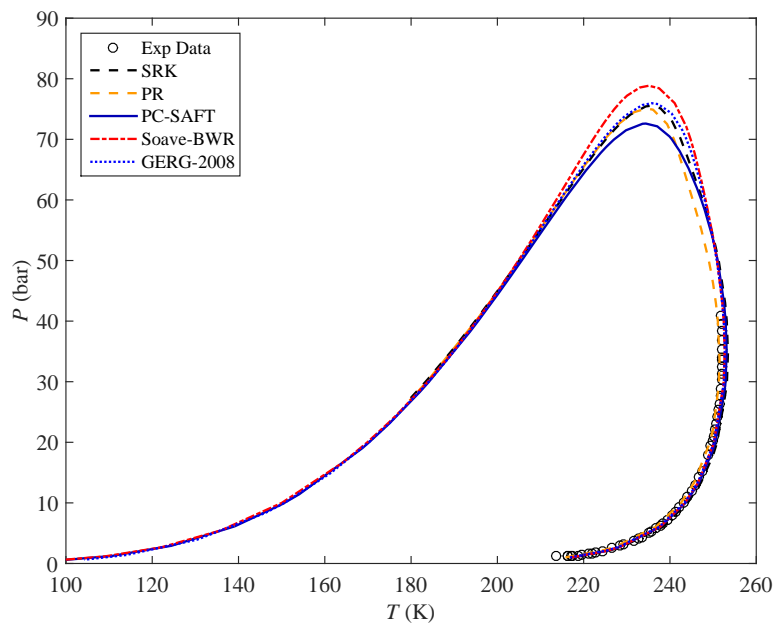
Figure 3.17 Phase envelopes for Gas 11 with (a) zero k_{ij} 's and (b) the optimal k_{ij} 's.

(a) Gas 12



(b) Gas 16

**Figure 3.18** Phase envelopes for (a) Gas 12, and (b) Gas 16 with optimal k_{ij} 's.

(a) 0 k_{ij} (b) Optimal k_{ij} **Figure 3.19** Phase envelopes for Gas 17 with (a) zero k_{ij} 's and (b) the optimal k_{ij} 's.

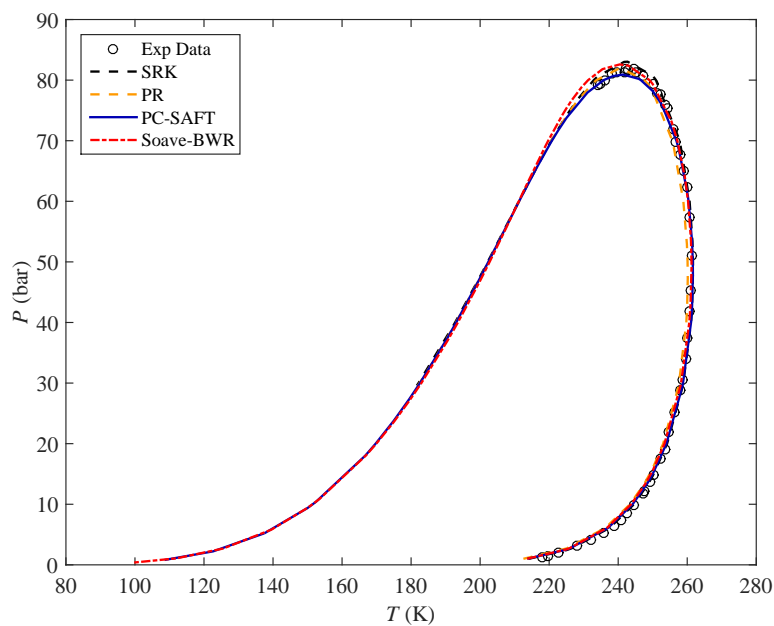
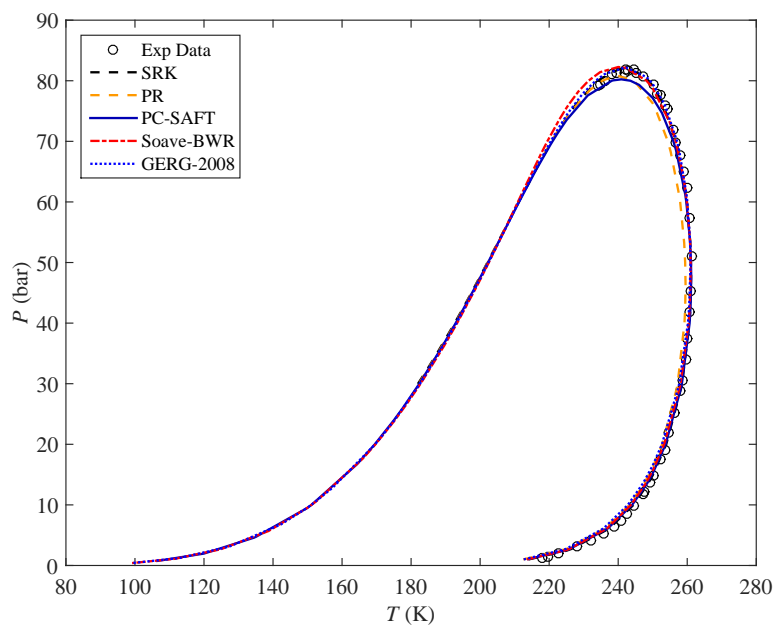
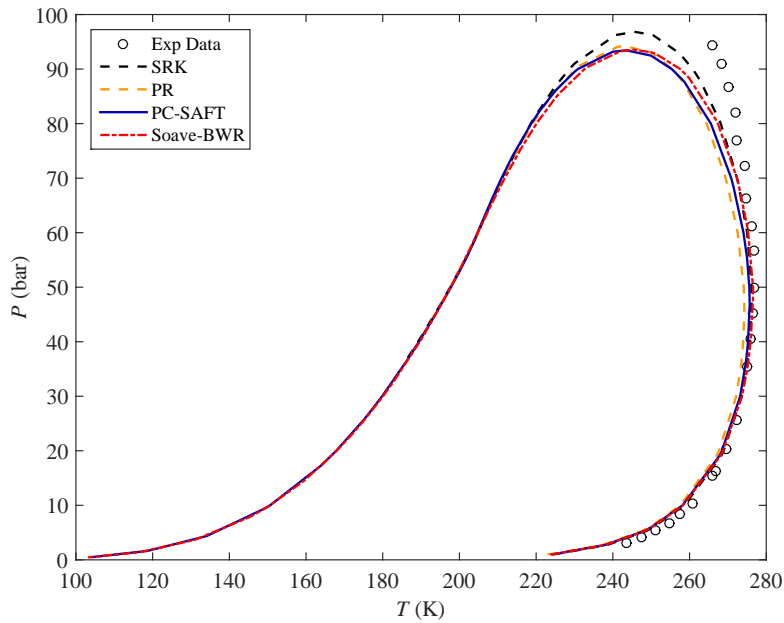
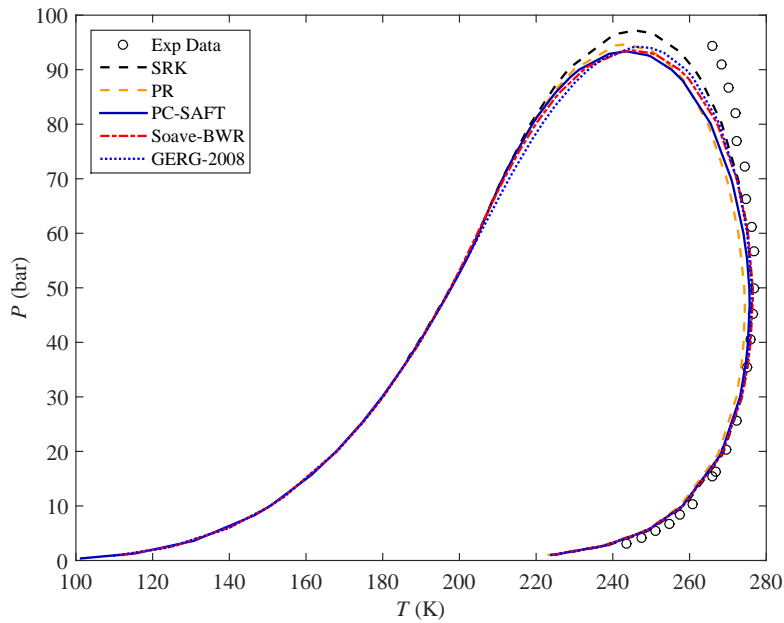
(a) 0 k_{ij} (b) Optimal k_{ij} 

Figure 3.20 Phase envelopes for Gas 18 with (a) zero k_{ij} 's and (b) the optimal k_{ij} 's.

(a) 0 k_{ij} (b) Optimal k_{ij} **Figure 3.21** Phase envelopes for Gas 22 with (a) zero k_{ij} 's and (b) the optimal k_{ij} 's.

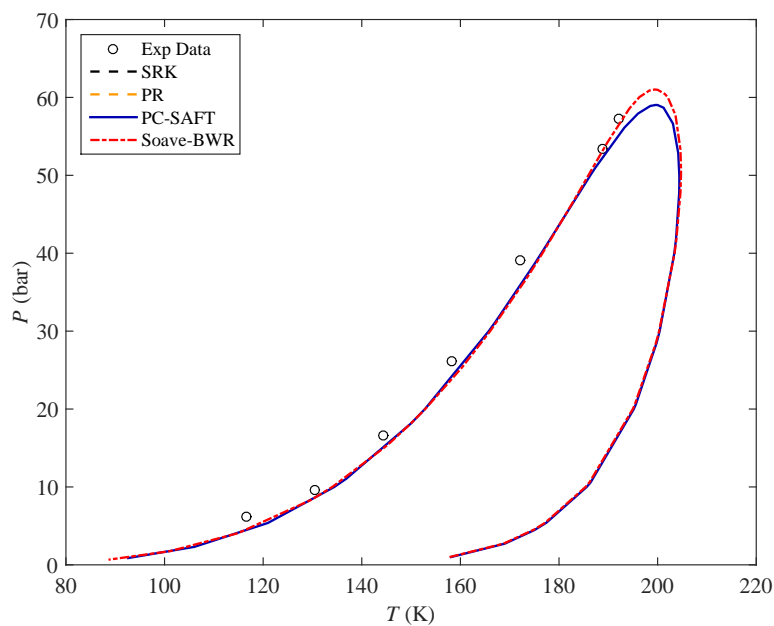
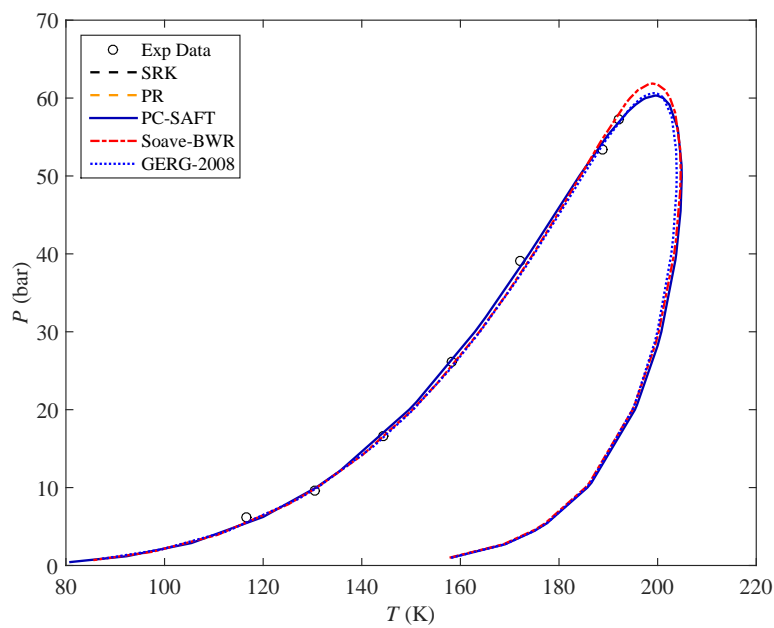
(a) 0 k_{ij} (b) Optimal k_{ij} 

Figure 3.22 Phase envelopes for Gas 24 with (a) zero k_{ij} 's and (b) the optimal k_{ij} 's.

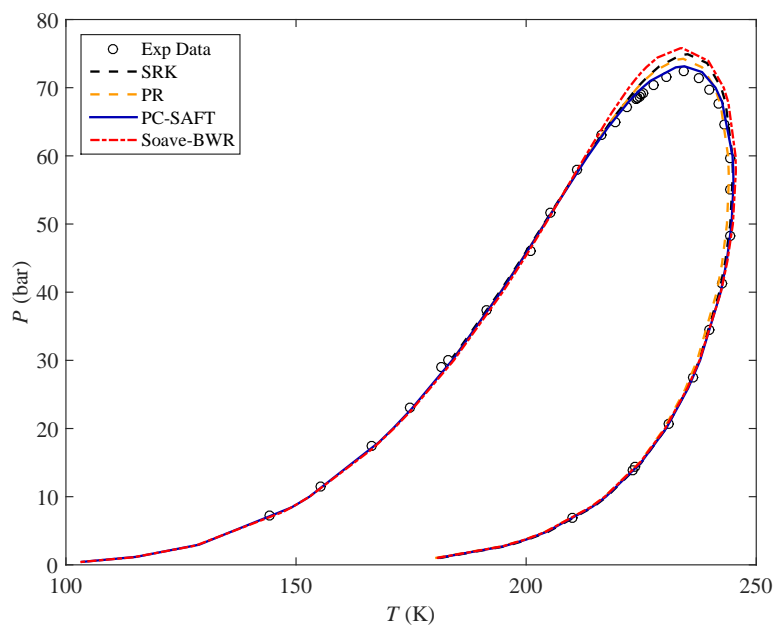
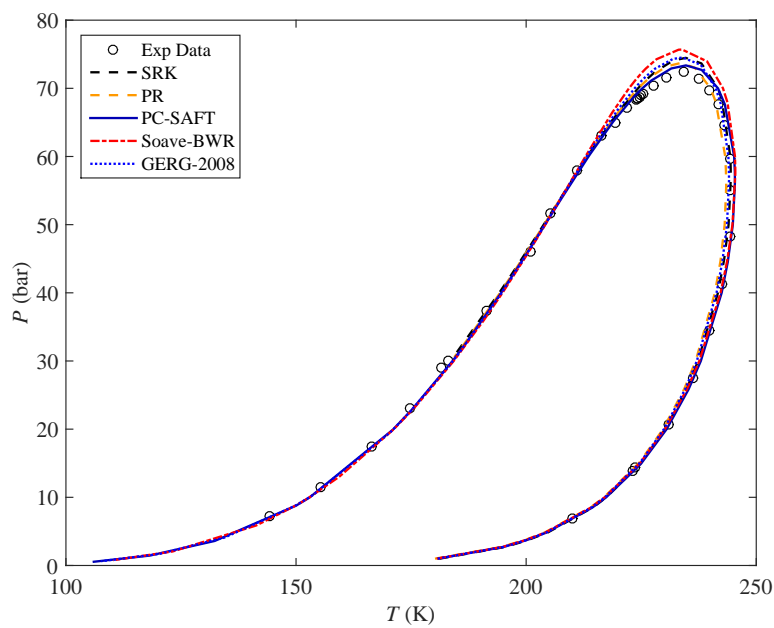
(a) 0 k_{ij} (b) Optimal k_{ij} 

Figure 3.23 Phase envelopes for Gas 25 with (a) zero k_{ij} 's and (b) the optimal k_{ij} 's.

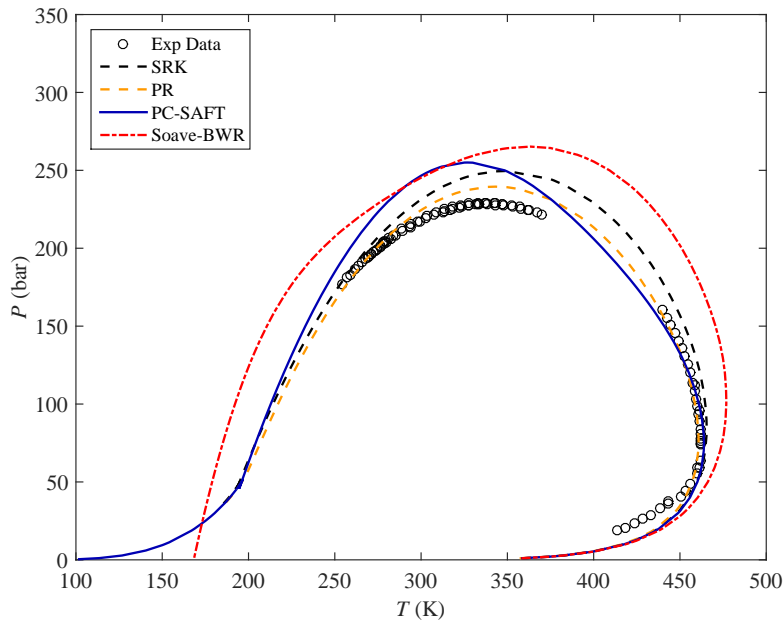
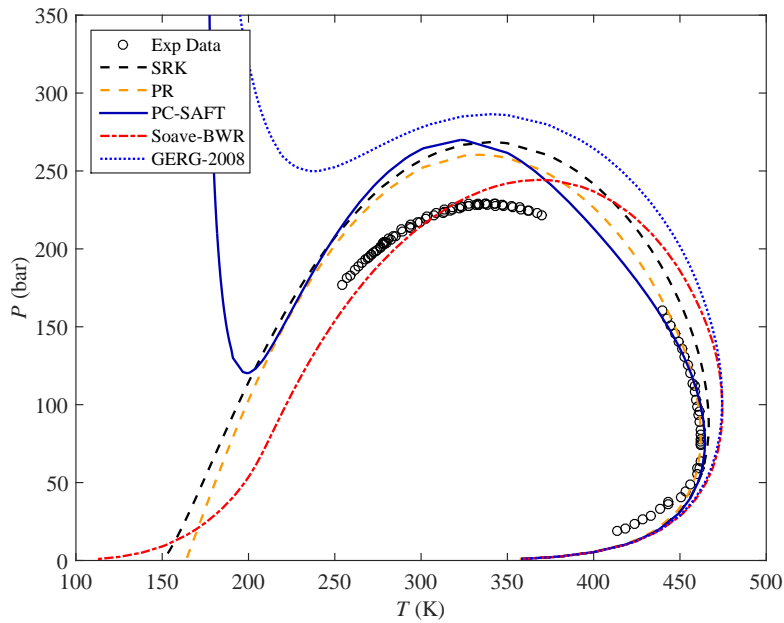
(a) 0 k_{ij} (b) Optimal k_{ij} 

Figure 3.24 Phase envelopes for Gas 26 with (a) zero k_{ij} 's and (b) the optimal k_{ij} 's.

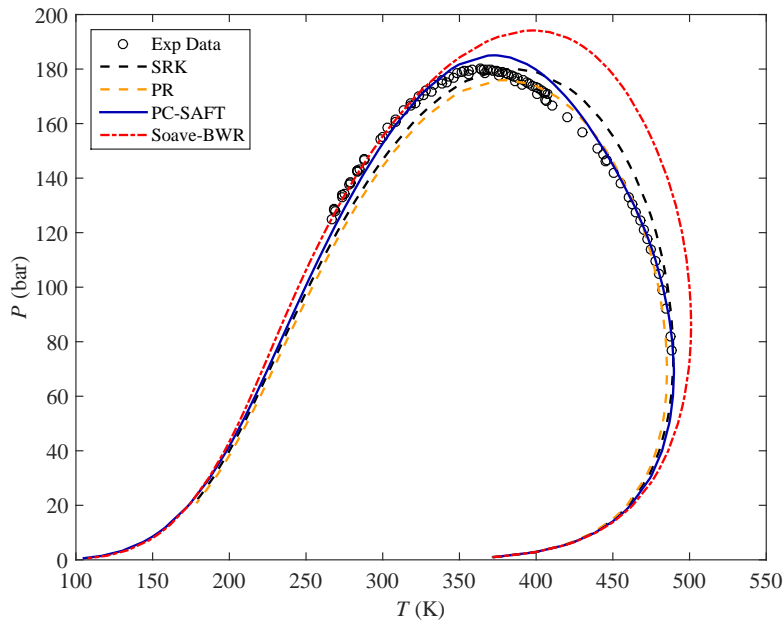
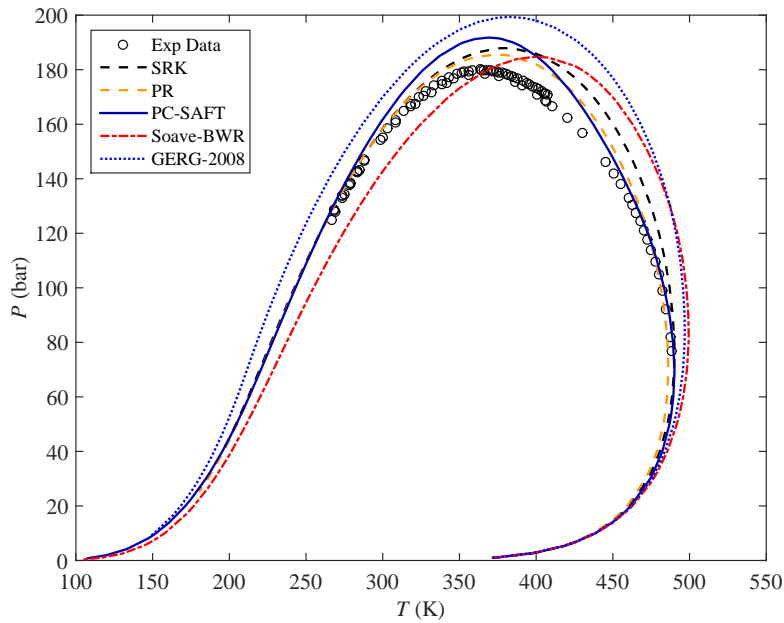
(a) 0 k_{ij} (b) Optimal k_{ij} 

Figure 3.25 Phase envelopes for Gas 27 with (a) zero k_{ij} 's and (b) the optimal k_{ij} 's.

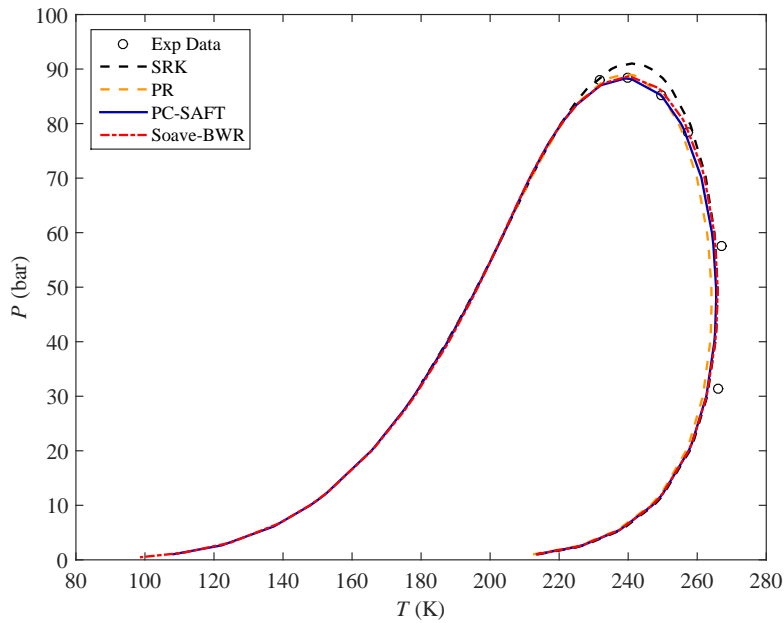
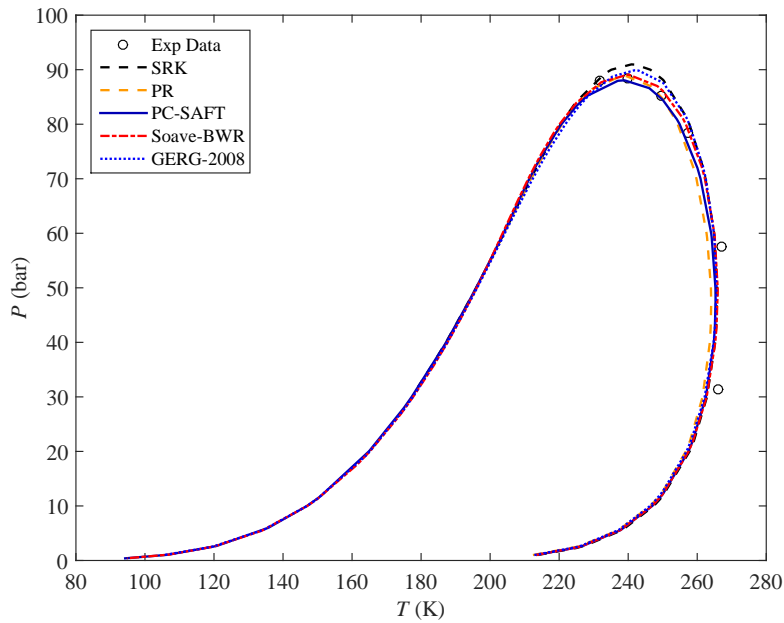
(a) 0 k_{ij} (b) Optimal k_{ij} 

Figure 3.26 Phase envelopes for Gas 28 with (a) zero k_{ij} 's and (b) the optimal k_{ij} 's.

Regueira et al. [61] compared the performance of SRK, PR, PC-SAFT and Soave-BWR in phase envelope calculation for three different mixtures of methane and n-decane binary system. They observed that the cubic EoSs give better predictions of the experimental data compared to the non-cubic models especially at lower composition of methane. At higher methane compositions, none of the models were able to predict the whole phase envelope correctly. Figures 3.27–3.29 show the phase envelope calculation results using all the four EoS models as well as GERG-2008 for three different compositions of methane in the binary mixture of methane and n-decane. GERG-2008 seems to under predict the phase envelope at $x_1 = 0.4031$ and over predict it at $x_1 = 0.8497$. Soave-BWR seems to give slightly better prediction of the phase envelope at $x_1 = 0.4031$ and $x_1 = 0.6021$, but also poor results at $x_1 = 0.8497$. As can be observed, it is not an easy task for complicated models like GERG-2008 to accurately model phase equilibrium for a highly asymmetric system as simple as methane and n-decane over a wide temperature, pressure and composition range; and for this system, the cubic models seem to have better performance than the non-cubic ones.

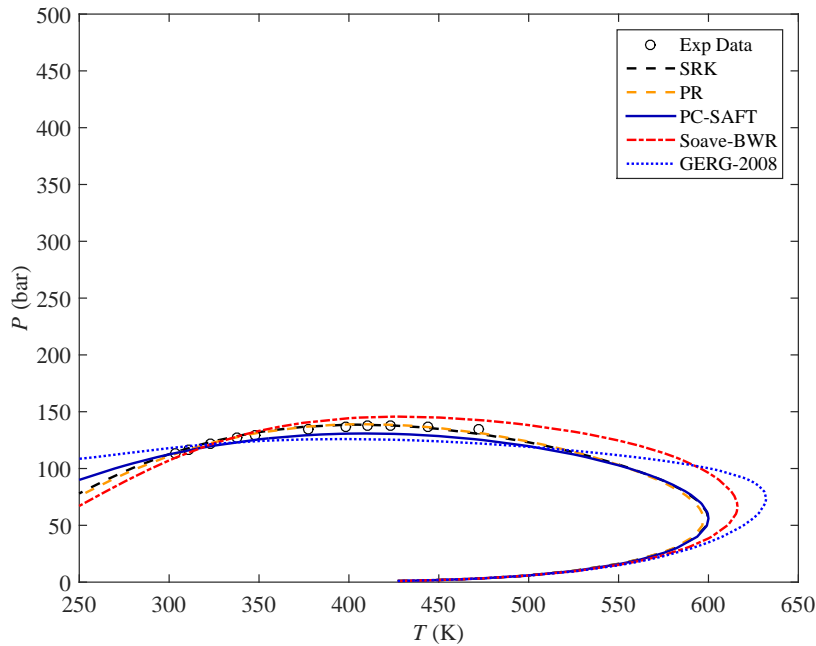


Figure 3.27 Phase envelope for binary mixtures of methane + n-decane (40.31 mol% C₁) using different EoSs with optimal k_{ij} 's. The experimental data is taken from [61].

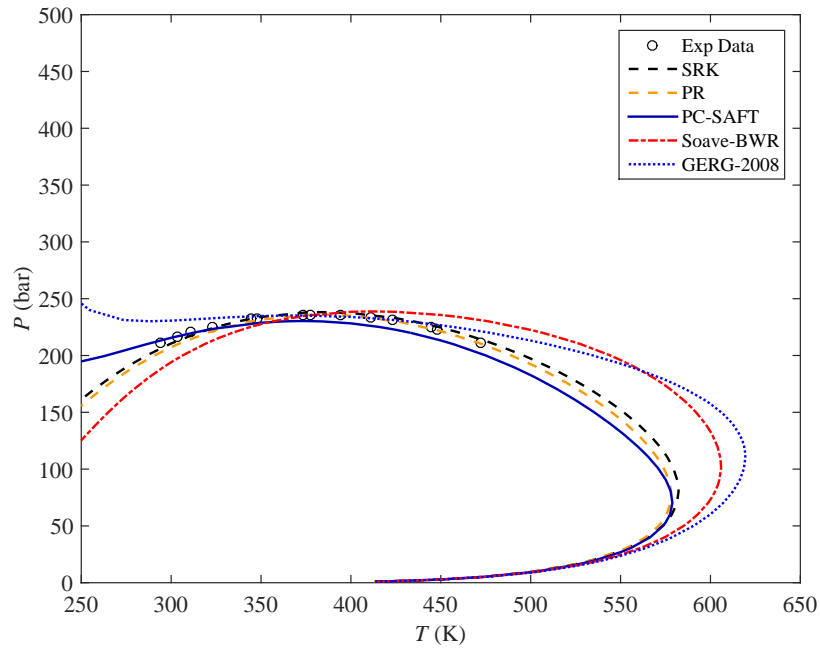


Figure 3.28 Phase envelope for binary mixtures of methane + n-decane (60.21 mol% C_1) using different EoSs with optimal k_{ij} 's. The experimental data is taken from [61].

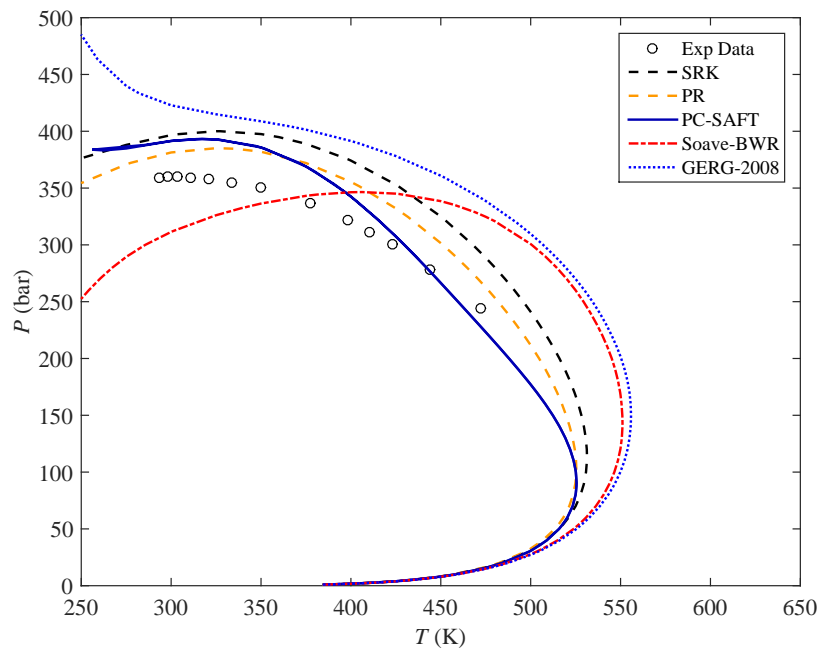


Figure 3.29 Phase envelope for binary mixtures of methane + n-decane (84.97 mol% C_1) using different EoSs with optimal k_{ij} 's. The experimental data is taken from [61].

3.4 Conclusions

A comprehensive evaluation of PC-SAFT, Soave-BWR and GERG-2008 in comparison with SRK and PR (with/without volume translation) has been made with regards to their potential in calculation of phase equilibrium and physical properties of different well defined systems. It was found that PC-SAFT, Soave-BWR and GERG-2008 are much better than SRK and PR in density and compressibility calculation of the well-defined light and heavy components in reservoir fluids over a wide temperature and pressure range, GERG-2008 being the best with the lowest deviation among all EoS models. The non-cubic models were also superior to the cubic models in prediction of gas compressibility factor of the multicomponent gas mixture tested here. This forms a major motivation for extending the non-cubic models to reservoir fluids. As it is not still possible to generalize GERG-2008 to reservoir fluids and ill-defined systems (due to lack of a proper characterization method for this EoS), we have only focused on PC-SAFT and Soave-BWR for the PVT modeling of reservoir fluids in the next chapter.

GERG-2008 has a clear advantage over SRK, PR, PC-SAFT and Soave-BWR in compressibility calculation for the pure components, while Soave-BWR with regressed binary interaction parameters seems to have better performance than GERG-2008 in bubble point pressure and vapor phase composition of binary mixtures up to nC₁₀. GERG-2008 gives very large deviations for bubble point pressure calculation of some heavy and asymmetric binary systems such as n-butane + n-nonane system. This suggests that this EoS and its binary interaction parameters could still be improved for some of the binary pairs.

The optimal k_{ij} values for SRK, PR, PC-SAFT and Soave-BWR have been regressed from extensive binary VLE data [63–65]. The binary VLE calculation also shows that PC-SAFT and Soave-BWR are similar to SRK and PR in correlating the important binary pairs in reservoir fluids. Although Soave-BWR gives a better prediction than the other three when zero k_{ij} values are used, its regression results for highly asymmetric systems seem to be poorer. Soave-BWR and PC-SAFT give smaller average k_{ij} values than SRK and PR. On the other hand, they are more sensitive to the change in k_{ij} .

Phase envelope prediction of synthetic gases shows that all the EoS models are similar for not too asymmetric synthetic gases, with or without the optimal k_{ij} values for SRK, PR, PC-SAFT and Soave-BWR. SRK, PC-SAFT and Soave-BWR seems to be slightly

better than PR. For highly asymmetric synthetic gases [80], the predictions from all the five models somewhat differ and Soave-BWR and GERG-2008 are usually very different from the others.

In summary, PC-SAFT and Soave-BWR have big potentials for applications related to reservoir fluids, including PVT modeling. Compared with SRK and PR, their advantages seem to lie in better density description rather than better VLE description. Obviously, there are challenges to be solved for both non-cubic models. For example, the characterization method for PC-SAFT is relatively immature compared to the cubic models. To provide a consistent basis in the comparison of PC-SAFT with SRK and PR, the characterization method for PC-SAFT should follow the framework widely used in the upstream industry for the cubic models. For Soave-BWR, its description for highly asymmetric systems is not satisfactory. This requires more study on its mixing rule as well as on how to parametrize the heavy components for this model. These challenges would be addressed in the next chapters.

Our main focus in this chapter was on the general aspects of PVT modeling and several particular problems with non-cubic models have not been addressed. In general, we need more precaution when using non-cubic models. One potential problem with non-cubic models is multiple liquid density roots at low temperatures. Such a problem for PC-SAFT has been analyzed by Privat et al. [84] and Polishuk et al. [85]. Polishuk et al. also pointed out that refitting the universal constants [49] could be a solution to the problem. For Soave-BWR, a similar problem at very low temperatures can also be observed. Another problem with PC-SAFT is that the model does not reproduce the critical properties of pure components exactly. This can cause deviations when the system conditions are close to the critical point of a major component in the system. This problem, however, does not exist for Soave-BWR which reproduces the critical properties exactly.

4 | Petroleum Fluid Characterization and PVT Modeling

Petroleum reservoir fluids are composed of many thousands of different components, hydrocarbons and hetero-compounds covering a wide range of boiling points and molecular weights. They are mainly mixtures of hydrocarbon compounds from methane to heavy hydrocarbons that are often divided into paraffinic (P), naphthenic (N) and aromatic (A) families. Paraffins consist of carbon atoms connected by single bonds without cyclic structures, Naphthenes contain one or more cyclic structures of which the segments are connected by single bonds, while Aromatics comprise compounds containing benzene rings. The density increases in the order of paraffin (P), naphthene (N), and aromatic (A), and is therefore a useful measure of the PNA distribution. Properties of hydrocarbon mixtures depend on the type of hydrocarbons in the mixture. Usually, paraffins are more identifiable in the light fractions and the heavy fractions are rich in molecules other than paraffins, such as aromatics.

In the oil and gas industry, normally a PVT study is performed on the reservoir fluid to define the fluid properties at reservoir conditions and at surface separation conditions. The PVT study also includes the compositional analysis of the reservoir fluid in terms of mole percent. Subsequently, the equations of state are used for description of PVT, including phase equilibrium and physical properties, over a wide temperature and pressure range. The EoS model parameters are tuned to match the reported experimental data, and once tuned, the EoS can be used to predict the reservoir fluid properties at different conditions and as an integral part of compositional reservoir simulators[86].

The primary input data to the EoS is the composition of the reservoir fluid in terms of mole percent and the measurable physical properties of the heavier Single Carbon Number (SCN) fractions together with those of the plus fraction. The measurable

physical properties normally required are MW and density. The quality of the input data set is of great importance as incomplete or inaccurate data can significantly affect the quality of the predictions provided by the EoS based simulators.

There are different ways to classify the constituents of the reservoir fluids. Normally the defined components consist of the main non-hydrocarbon constituents, such as H_2S , CO_2 and N_2 , and methane through normal pentane; hydrocarbons heavier than C_6 are expressed as Single Carbon Number (SCN) fractions and are usually grouped into one C_{7+} (heptane-plus) fraction [87]. Methane through propane exhibit unique molecular structures; butane can exist as two isomers and pentane as three isomers. For hexanes and heavier, the number of isomers rises exponentially. C_6 SCN fraction for example represents all hydrocarbons with a boiling point from $0.5\text{ }^\circ\text{C}$ above that of nC_5 to $0.5\text{ }^\circ\text{C}$ above that of nC_6 . Each SCN fraction contains paraffinic (P) and naphthenic (N) as well as aromatic (A) components, each of which should in principle have different model parameters. In practice, since the PNA distribution is not always available, people usually use only one set of model parameters to represent the whole SCN fraction. Analysis of petroleum composition in terms of SCN components can extend to a very high carbon number with modern chromatography, although their molecular weights and specific gravities are usually not experimentally determined. The compositional data are often reported to a certain carbon number with the remaining heavier constituents grouped to C_{n+} , where n is usually greater than 7, such as 30. The molar mass and specific gravity of the C_{7+} are experimentally determined and reported. The fractions heavier than C_6 need to be mathematically characterized in order to perform calculations for petroleum fluids with modern thermodynamic models.

Characterization of petroleum fractions involve methods that use measurable properties such as T_b , and SG to estimate mixtures critical properties or molecular weight needed in thermodynamic correlations [88]. Selection of characterization method has significant impact on calculated physical properties and choosing a right characterization method very much depends on the type of petroleum fluid. A generally valid characterization concept must be applicable to reservoir fluids with large PNA variations [89]. For the prediction of thermodynamic properties of ill-defined petroleum fractions, knowledge of the percentage contents of paraffinic, naphthenic and aromatic components of each C_{7+} fraction (PNA distribution) is usually helpful if they are available [87, 90]. In general, characterization for cubic EoS models are well established. For non-cubic EoS models like PC-SAFT, there are many methods in the recent literature but the characterization method for the non-cubic models is less matured and not well established.

In this chapter, we first review the current analytical techniques and the critical data from these techniques which can be used in compositional characterization. We will then present an overview of C_{7+} characterization procedure. A reservoir fluid characterization method for PC-SAFT is proposed by combining Pedersen's method with newly developed set of correlations for the PC-SAFT model parameters m , $m\varepsilon/k$ and $m\sigma^3$. In addition, we further improved the characterization method for PC-SAFT by adjusting the correlations with a large PVT database. We have further improved the correlations and more importantly, we have established a general approach to characterizing reservoir fluids for any EoS. The approach consists in developing correlations of model parameters first with a database for well-defined components and then adjusting the correlations with a large PVT database. The adjustment is made to minimize the deviation in key PVT properties like saturation pressures, densities at reservoir temperature and Stock Tank Oil (STO) densities, while keeping the n-alkane limit of the correlations unchanged. Apart from applying this general approach to PC-SAFT, we have also shown that the approach can be applied to classical cubic models like SRK and PR. In addition, we discussed how to develop a PNA based characterization for PC-SAFT and also utilize a large PVT database to further improve the characterization. To integrate more analytical information in characterization, we have modified the existing algorithms to account for the component distribution information from the compositional analysis data. In the end, we have made a comprehensive comparison in PVT calculation involving 17 EoS-characterization combinations and 260 reservoir fluids.

In section 4.9 and section 4.10.4, we also present our attempt to include more detailed analytical information in characterization and evaluate its impact on PVT modeling. Petroleum fluid characterization usually uses a subset of the available analytical data. Meanwhile, modern analytical techniques allow more detailed compositional data that can be potentially used in characterization. There is little discussion on how to utilize a more complete set of the analytical data and more detailed compositional information in characterization. We try to establish a procedure to utilize more analytical information from conventional analytical techniques including simulated distillation (SimDist) and true boiling point (TBP) distillation, and then apply the procedure to one low GOR system and one high GOR system to investigate the impact of compositional characterization.

4.1 Methods of Petroleum Hydrocarbon Analysis

4.1.1 Overview

In recent years, major advances have been made in the techniques for oil analysis. Various adsorbents (including silica gel, alumina, florisil, combination of silica and alumina and solid-phase extraction) and elution solvents have been used to separate oil into saturated, aromatic and polar groups. These fractions are analyzed using techniques that include gravimetric methods, gas chromatography (GC), gas chromatography–mass spectrometry (GC–MS), high-performance liquid chromatography (HPLC), infrared spectroscopy (IR), super critical fluid chromatography (SFC), ultraviolet (UV) and fluorescence spectroscopy, and nuclear magnetic resonance (NMR). Of all of these techniques, high-resolution capillary GC with flame ionization detection (FID) and combination of capillary GC with other techniques such as GC–MS are the most widely used [91].

Due to complexity of oil mixtures, there is no single method that can analyze the whole spectrum of oils and petroleum products and to measure the complete composition of a reservoir fluid. The analytical protocol for reservoir fluids generally accepted today includes flash of the live fluid into equilibrium gas and liquid phases at atmospheric conditions. These two phases are then analyzed separately and the overall composition of the original single-phase fluid is obtained by mathematically recombining the composition of the equilibrium gas and liquid [86].

The majority of the components in the equilibrium gaseous phase can be easily identified and analyzed by gas chromatography. Multidimensional chromatography using non-polar (capillary or packed) columns and multiple detection systems are the techniques used for the analysis of the equilibrium gaseous phase.

Unfortunately, for the analysis of the equilibrium liquid phase, no generally accepted standard procedure is available [92]. As the liquid contains many thousands of different components, a precise analysis of this phase is extremely complex. For simplification, the results are normally reported in terms of grouped SCN or pseudo-components including several SCNs and a plus fraction. The most common way for analyzing liquid petroleum samples is to use a gas chromatograph equipped with an FID and a non-polar capillary column [93–95]. Despite the high resolution of the available columns, quantification of many of the heavier hydrocarbons still remain unresolved.

The physical properties (MW and density) of the SCNs which are used as input data for the EOS cannot be determined directly from the results of the chromatographic analysis [96, 97]. The MW and density of each SCN is usually obtained either from the data proposed by Katz et al. [98] or from the normal alkanes properties. However, each crude oil is unique and the actual physical properties of its SCNs are dependent upon the NICA (Normal, Iso, Cyclo and Aromatic) distribution in the oil. As a result, it would be more realistic to use MW and density obtained from experimental measurements such as true boiling point distillation. In the following sections, we briefly introduce some of the analytical techniques for oil analysis.

4.1.2 True Boiling Point Distillation (TBP)

True Boiling Point (TBP) distillation has been a standard analytical tool in the industry for many years. According to ASTM D-2892 standard (also known as 15/5 distillation, which produces TBP of petroleum fuels using a distillation column with 15 theoretical plates and a reflux ratio of 5:1), TBP test method covers the procedure for the distillation of stabilized crude petroleum to a final cut temperature of 400 °C Atmospheric Equivalent Temperature (AET). As a result, it is possible to get the compositional distribution up to C_{24} - C_{25} fractions.

Despite advances in technology, the technique is still rather crude and governed by column efficiencies, boil up rates, carry-overs etc. The technique is very time consuming but does address all the shortcomings of the gas chromatographic methods for obtaining the overall composition of the flashed equilibrium liquid. The liquid is subjected to a TBP distillation with overhead cuts being taken corresponding to the boiling point of the respective n-alkanes. The distillation continues to the plus fraction. Molecular weight and density measurements are performed on each of the captured cuts together with the plus fraction. These information can be used as an effective input for the reservoir fluid characterization.

4.1.3 Simulated Distillation by Gas Chromatography (SimDist)

As mentioned in the previous section, despite the advantages of TBP distillation, there is a need for faster, more precise and automated methodologies. Oil chemists recognized the potential of GC, because of its similarities with distillation processes [99]. They saw the potential of a direct translation of GC results to distillation data. Simulated

distillation by gas chromatography (SimDist) was first reported by Eggerston et al. in 1960 [100]. It was based on the fact that hydrocarbons elute from a non-polar column during a temperature-programmed run in order of increasing boiling points.

The above approach first achieved formal status in 1973, as ASTM D2887. This test method is applicable to petroleum products and fractions (i.e. diesel, fuel oil, gas oil, and light lubricating oils), with final boiling points (FBPs) up to 538 °C (nC₄₄) which is higher than that of TBP method. It is however, limited to samples having a boiling range greater than 55 °C (nC₅), and having a vapor pressure sufficiently low to allow sampling at ambient temperature. Alkanes above C₆₀ cannot be distilled even under vacuum conditions. As a result, “virtual” boiling points are assigned to alkanes above C₆₀ by extrapolation of the curve correlating the boiling points of n-alkanes with their carbon numbers.

Most PVT laboratories only perform simulated distillation of oil samples in their routine PVT studies. The drawback, however, is that default molecular weights and densities, usually from the Katz-Firoozabadi table, have to be assumed for the SCN components which definitely introduces inaccuracies in the subsequent characterization of the oil.

For petroleum distillate fractions having an initial boiling point greater than 174 °C and a final boiling point of less than 700 °C (C₁₀ to C₉₀), ASTM D6352 test method is used. This method is also known as High Temperature Simulated Distillation (HT-SimDist).

Figure 4.1 presents raw SimDist results for an oil sample. The SCN fractions are not shown in this figure. The highlighted area in this figure is presented in Figure 4.2, where the retention times for each fraction has been illustrated up to C₁₀. The final retention time for each SCN fraction is found from the calibration table which is prepared before each run. The wt% of each SCN fraction can be calculated by finding the area under the curve divided by the total area.

To have an estimation of the Paraffinic (P) and Aromatic (A) distribution in each fraction, we have assumed that the highest peak in each fraction is representative of the n-alkanes in that fraction, while the rest of the fraction is made up of the aromatic compounds. Although we called them "aromatic" compounds, in the later property estimation, they are treated just as hydrocarbons other than n-alkanes. The amount of the Paraffinic group in each SCN can be calculated by finding the area under the highest peak (shown in red color in Figure 4.2) divided by the area of the SCN fraction.

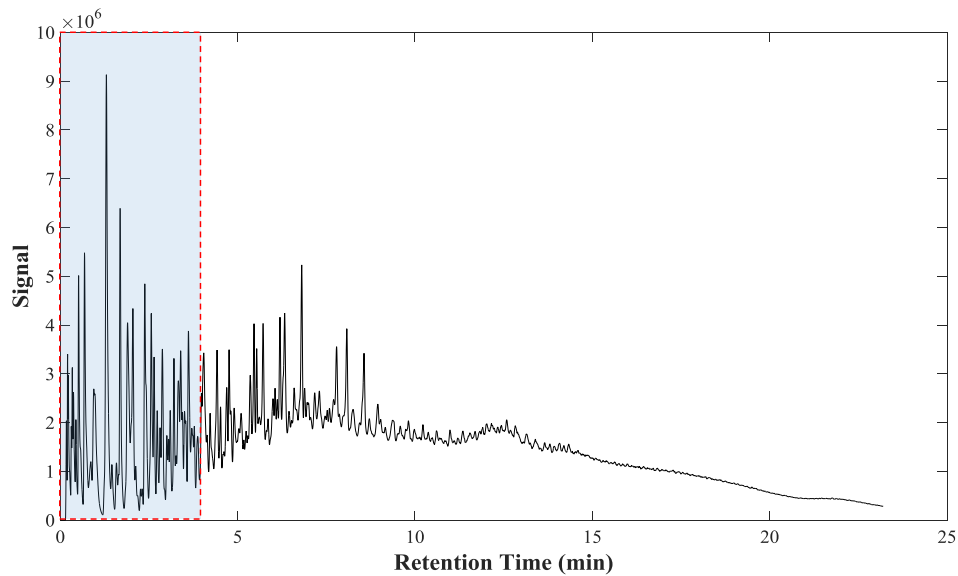


Figure 4.1 Sample SimDist results up to around C_{40} for an oil sample.

The wt% of the aromatic group can then be found by subtracting the wt% of the paraffinic group from 100. This additional information can be used in characterization as would be discussed in section 4.9. Dividing each fraction into P and A groups is a rough assumption, nevertheless it captures the main features of the SCN fraction and can always be improved, for example by more accurate quantification of P and A in the SCN group.

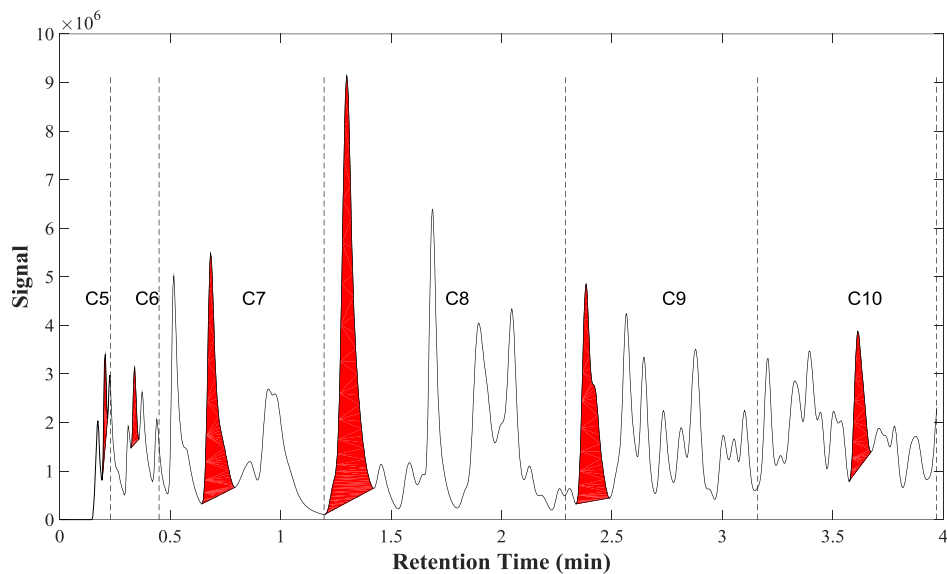


Figure 4.2 Isolating the paraffinic group within each SCN fraction for the oil sample in Figure 4.1.

4.1.4 Two-Dimensional Gas Chromatography (GC×GC)

Since its introduction in the 1990s, comprehensive two-dimensional gas chromatography (GC×GC) has demonstrated very promising perspectives for the analysis of complex mixtures. In this method, two independent GC separations are applied to an entire sample. The sample is first separated on a high-resolution capillary GC column in the programmed temperature mode. The effluent from the first column is then injected into a second capillary column which is short and narrow to allow very rapid, isothermal, separations. By selecting a non-polar column for the first dimension, this separation is based on the *volatility* of components. All components elute from the first column at different temperatures, but with very similar volatilities at the time of elution. The second separation, which is so fast as to be essentially isothermal at the elution temperature from the first-dimension column, is based on *polarity*, molecular geometry, size, etc. [101].

The resulting chromatogram can be represented as a two-dimensional plane from which the peaks emerge. One dimension of this plane represents the retention time on the first column, the second dimension represents the retention time on the second column, and the third dimension is the signal intensities. The most convenient way to represent a GC×GC chromatogram, however, is as a two-dimensional contour plot.

In Figure 4.3 a sample contour plot of a separated heavy gas oil from [102] is given. The first dimension retention times represent the boiling points (or better: vapor pressures) of the components. Since the second dimension separation is predominantly caused by the interaction of the compound and the (semi-polar) stationary phase, this dimension represents the chemical structure of the compounds. As a result a fast group-type separation originates from these analysis.

Figure 4.4 presents a detail of a 3D-plot derived from such a 3D-data set from the GC×GC separation of the heavy gas oil in Figure 4.3.

In the PIONA group type separation (standing for Paraffins, Isoparaffins, Olefins, Naphthenes and Aromatics), Isoparaffins elute slightly earlier than n-paraffin in each dimension. Isoparaffins are more volatile than n-paraffins due to lower van der Waals interactions and elute in the first dimension before n-paraffins. Furthermore, because of their reduced molecular area, the interaction of isoparaffins with the semi-polar second dimension stationary phase is slightly lower than that of n-paraffins. Olefins are separated from n-paraffins only in the first dimension, the selectivity of the second dimension is too low to improve this separation. On the contrary, diolefins are more

retained in the second dimension than n-paraffins. Most polar hydrocarbons, aromatics and di-aromatics, have the highest retention times and are located in the upper part of the chromatogram [103].

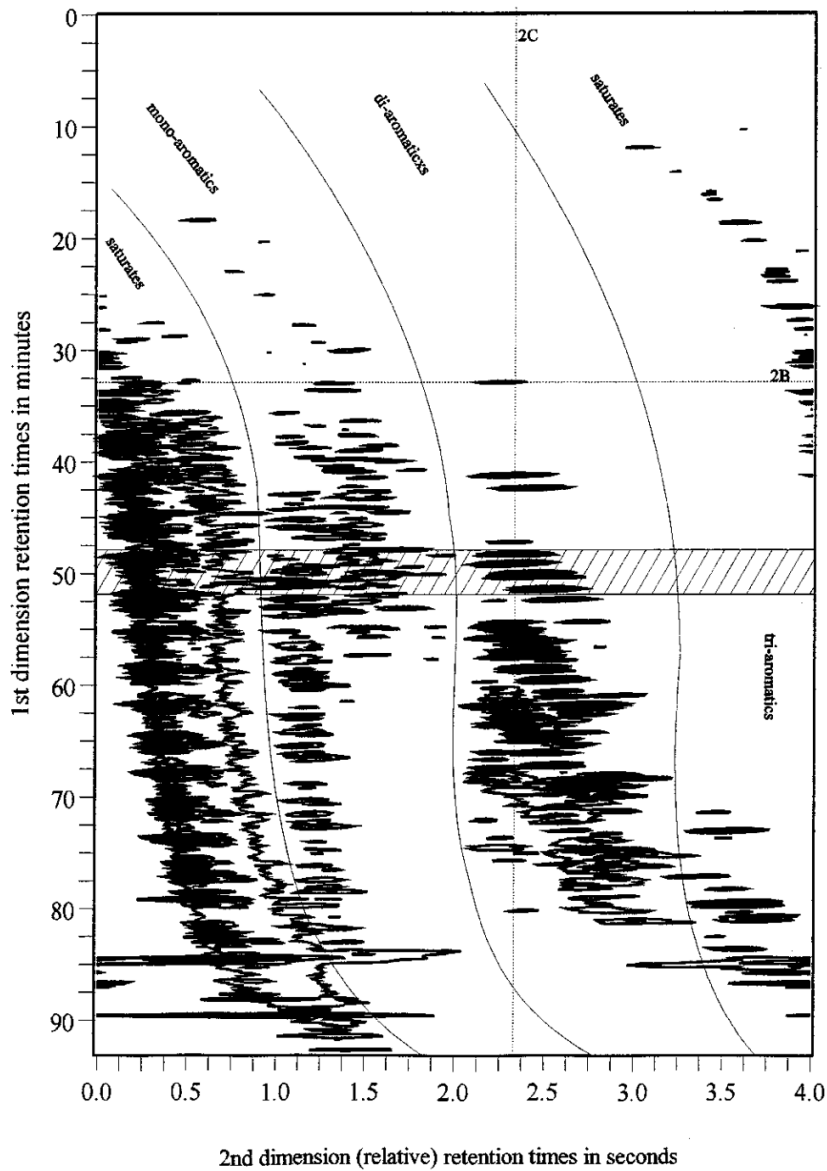


Figure 4.3 Contour plot of the GCxGC separation of a heavy gas oil from [102]. The shaded band is presented as a 3D-plot in Figure 4.4.

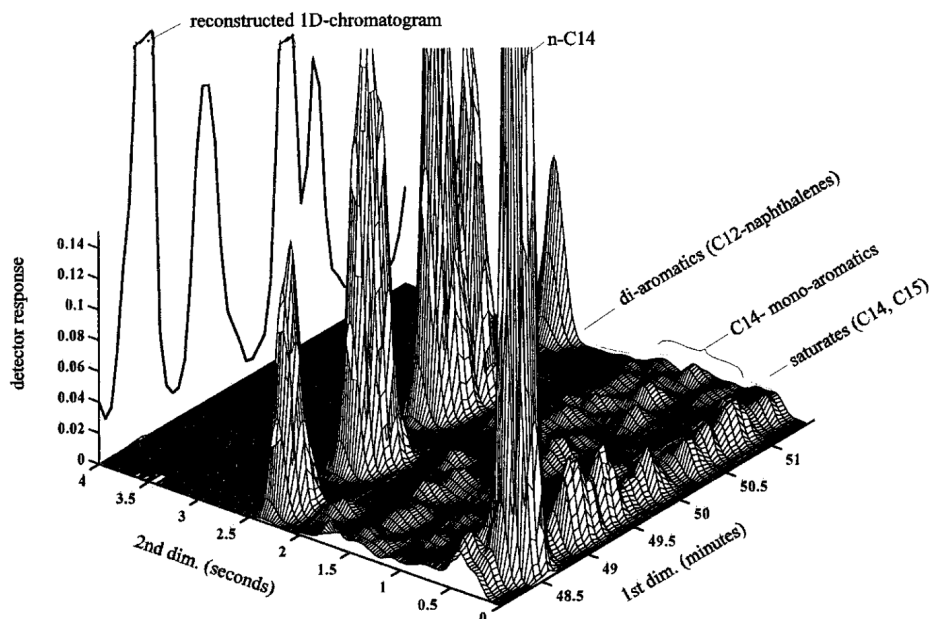


Figure 4.4 3D-plot of a part of the GC×GC separation of a heavy gas oil from [102] (the shaded part of Figure 4.3).

Potential and Limitations of GC×GC

There are four major advantages of GC×GC [102, 104]:

1. It provides highly detailed, readily interpretable images of very complex samples.
2. It allows a complex sample to be separated into individual peaks, which can be classified into groups, creating a viable alternative for group-type analysis.
3. It provides superior resolution and increased sensitivity relative to conventional GC. This allows the accurate determination of low concentrations of specified components in a complex mixture.
4. It may provide boiling-point distributions for many different classes of compounds (e.g., saturates, olefins, mono-aromatics, di-aromatics) simultaneously, thus massively increasing the amount of information generated per unit time.

Although GC×GC can characterize relatively volatile fractions in more detail and up to relatively high boiling-points, a GC×GC×GC system with a first-dimension separation according to volatility, a second-dimension separation according to “shape” and a third dimension separation according to polarity may complete the characterization of mixtures in the middle distillate range in the sense that all compounds present at relevant concentration levels in the mixture are essentially separated.

4.1.5 Critical Information Obtained from Various Analytical Methods

Table 4.1 summarizes the available information obtained from the analytical methods presented in the previous sections. TBP provides wt%, density, and *MW* for cuts up to and including C₂₄₊. SimDist gives detailed compositional distribution and wt% for nC₅ up to nC₄₄. This method however, does not provide the *MW* or density of the fractions. To find the compositional distribution up to higher SCNs (C₉₀) HT-SimDist is used. The resolution of the HT-SimDist however, might not be as high as SimDist for lower carbon number fractions. An additional SimDist for cuts obtained from TBP can always be done to get detailed information for each cut and have a more accurate understanding of PA distribution within the fraction. GC×GC provides more detailed information about the possible aromatic and non-aromatic groups in the oil sample and each fraction. Implementing these information in the reservoir fluid characterization could improve the accuracy of the calculations.

Table 4.1 Information provided by different analytical methods.

Analytical Method	Available Information
TBP (ASTM D2892)	Weight fraction of SCNs up to C ₂₄₊ (up to final cut temperature of 400 °C) <i>SG</i> and <i>MW</i> of each SCN as well as the plus fraction can also be measured.
SimDist (ASTM D2887)	Weight fraction of SCNs from nC ₅ up to around nC ₄₄ - no <i>MW</i> (Fractions having boiling point greater than 55 °C and up to 538 °C)
HT-SimDist (ASTM D6352)	Weight fraction of SCNs from C ₁₀ up to around C ₉₀ - no <i>MW</i> (Fractions having boiling point greater than 174 °C and up to 700 °C) * Modification of the method allows large CN range, with the lower CN also being covered.
GC×GC	Provides detailed component distribution, and more accurate information about the possible aromatic groups in the oil sample.

It should be noted that all the analytical methods, provide the compositional distribution in terms of weight fractions. To be able to use this information, the current algorithms should be modified to account for wt% (weight fractions). The benefit of using weight fractions instead of mole fractions is that the weight fractions are directly measured and are not dependent on the *MW*. As a result, one can use the Katz and Firoozabadi table or measured values of *MW* (if available), or a combination of the two, to find the mole fractions. This way, the resulting mole fractions would be representative of the real fluid sample and subject to smaller uncertainty. In section 4.9 we would present the modified characterization algorithms to account for wt% of the

components. We would also describe how to find the model parameters for the P and A groups when PA distribution is available from analyzing the SimDist results (mentioned in section 4.1.3). The same concept can be applied to the GC×GC results, however, it has not been tried in this study.

4.2 Overview of C₇₊ Characterization Procedure

To apply any cubic or non-cubic EoS model to PVT calculation of a reservoir fluid, we need to use reservoir fluid characterization which is to represent the reservoir fluid with an appropriate number of pseudo-components and assign appropriate model parameters to these components.

As mentioned in the beginning of this chapter, in characterization the components are normally classified into three categories: (1) Defined Components whose properties are well known, such as N₂, CO₂, H₂S, C₁, C₂, C₃, iC₄, nC₄, iC₅, nC₅ and C₆; (2) True Boiling Point (TBP) or Single Carbon Number (SCN) fractions, for which density and molecular weight are either measured or estimated within a given temperature interval as mentioned earlier; (3) The plus fraction which consists of the components that are too heavy to be separated into individual C₇₊ fractions, but its average molecular weight and density can be measured if a TBP analysis has been carried out [87].

Table 4.2 presents the typical input information used for the characterization of reservoir fluids. As can be seen, the only required information is the mole fraction of gas components as well as hydrocarbons up to the plus fraction together with the *SG* and *MW* of the plus fraction. The *SG* and *MW* of N₂, CO₂, H₂S, C₁-C₆ are known properties that can be taken from the DIPPR database [105], while for the other SCNs up to the plus fraction, these values are taken from Katz and Firoozabadi table [98] if the experimental values are not available. It should be noted that the current algorithms for fluid characterization are based on the mole fraction of the components. As the values of *MW*, with which the mole fractions are calculated, might not be always available in the PVT reports, using the Katz and Firoozabadi table or experimental values could be subjected to some uncertainties in the calculations.

Table 4.2 Typical input information for reservoir fluid characterization.

	Required Information
Typical Input	Mole fraction of N ₂ , CO ₂ , H ₂ S, C ₁ -C ₆ , C ₇₊ , as well as <i>SG</i> _{C₇₊} , <i>MW</i> _{C₇₊}
Typical Input (Extended)	Mole fraction of N ₂ , CO ₂ , H ₂ S, C ₁ up to C _{n+} (n>7), as well as <i>SG</i> _{C₇₊} , <i>MW</i> _{C₇₊}

Reservoir fluid characterization for cubic EoSs like SRK [5] and PR [6] is relatively mature. For example, the method of Pedersen et al. [15, 16] and that of Whitson et al. [17, 18] are amongst the widely used characterization methods in the upstream oil industry. The model parameters needed for SRK, PR and Soave-BWR are T_c , P_c , and ω , which can be generated by the methods of Pedersen et al. [15, 16] and that of Whitson et al. [17, 18]. For non-cubic models like PC-SAFT, their respective model parameters should be generated for the pseudo-components in the C₇₊ fractions but characterization for non-cubics is less mature.

Reservoir fluid characterization procedure normally involves the following steps:

1. Estimating the relation between molar composition distribution and carbon number or molecular weight or determining the characteristic parameters of a continuous molar composition distribution function.
2. Estimating the required properties or parameters of the chosen equation of state for each pseudo-component (carbon number fraction). As an example, T_c , P_c , and ω for cubic EoS and m , σ , and ε for PC-SAFT EoS. In addition, a binary interaction parameter (k_{ij}) is needed for each pair of components;
3. Lumping the fractions into a reasonable number of pseudo-components or creating these pseudo-components since it is time consuming to work with all the SCN fraction.

In what follows, different methods that have been suggested for each step of characterization are reviewed.

4.2.1 Molar Distribution

The most widely used characterization methods in the petroleum industry are those proposed by Pedersen et al. [15, 16] and Whiston et al. [17, 18] i.e., an exponential and a Gamma distribution models respectively, both of which were developed for cubic equations of state, mainly SRK and PR. Recently, Pedersen et al. [12, 106] have made some modifications on Pedersen's characterization method so that it can also be used with PC-SAFT EoS.

Pedersen Method - Exponential Distribution

Pedersen et al. [107–109] determined that the compositional distribution of SCNs in North Sea petroleum fractions, which were mainly gas condensate, is best described by an exponential function. They proposed that reservoir fluids for carbon numbers (C_i) above C_6 exhibit an approximate linear relationship between carbon number and the logarithm of the corresponding mole fraction, x_i

$$C_i = A + B \ln x_i \quad (4.1)$$

where coefficients A and B are determined from the plus fraction to an assumed highest carbon number component (usually C_{80}), by fulfilling the following mass balance equations:

$$x_{C_+} = \sum_{i=C_+}^{C_{\max}} x_i \quad (4.2)$$

$$MW_{C_+} = \frac{\sum_{i=C_+}^{C_{\max}} x_i MW_i}{\sum_{i=C_+}^{C_{\max}} x_i} \quad (4.3)$$

where MW_{C_+} is the molecular weight of the plus fraction. It is assumed that the molecular weight of a given single carbon number fraction, MW_i , can be determined from the equation

$$MW_i = 14C_i - 4 \quad (4.4)$$

The constant 14 expresses that approximately two hydrogen atoms accompany each extra carbon atom. The term 4 accounts for the presence of aromatic structures in the reservoir fluids, oil or gas condensate mixtures [87].

The densities of the plus fractions are assumed to be represented by a similar equation to eq. (4.1), where the carbon number is used as the independent variable. This is because the densities usually increase with the carbon number.

$$\rho_i = C + D \ln C_i \quad (4.5)$$

In this equation, C and D are constants determined from the overall density of the plus fraction, ρ_{C_+} , and that of the last defined SCN fraction.

$$\rho_{C_+} = \frac{\sum_{i=C_+}^{C_{\max}} x_i MW_i}{\sum_{i=C_+}^{C_{\max}} \frac{(x_i MW_i)}{\rho_i}} \quad (4.6)$$

With an analysis up to C₁₂₊ for example, the constants C and D must fit the density of the C₁₁ fraction. Equations (4.2)–(4.3), and eq. (4.6) guarantee that the mole fraction, molecular weight and density are consistent with the measured or estimated data for the plus fraction. Pedersen et al. [109] suggested C₈₀ to be the last SCN fraction to characterize the petroleum reservoir fluids, but recently Pedersen et al. [89] found that components as heavy as C₂₀₀ may influence the phase behavior for heavy oils, especially for highly aromatic ones. They also modified the coefficients in the correlations for T_c , P_c , and ω for SRK and PR EoS, based on the data for 28 high density oil samples. For the HPHT fluids, the new correlations are slightly superior to those of Pedersen et al. [109].

Whitson Method - Gamma Distribution

Whitson et al. [17, 18] proposed a Three-Parameter Gamma (TPG) distribution function to estimate the mole fraction of SCNs within the plus fraction. TPG is defined as a function of molecular weight by the following equation:

$$p(MW) = \frac{(MW - \eta)^{\alpha-1} \exp\left(-\frac{MW-\eta}{\beta}\right)}{\beta^\alpha \Gamma(\alpha)} \quad (4.7)$$

where η is the minimum molecular weight in the C₇₊ fraction, which is usually equal to that of C₆ fraction (Whitson [17] proposed $\eta = 92$ if C₇₊ is the plus fraction and for other plus fractions he suggested $\eta = 14n - 6$, where n is the carbon number), α is a measure of the form of the distribution and is used to fit the shape of the distribution and its value ranges from 0.5 to 2.5 for reservoir fluids, Γ is the gamma function, and β is given by the following formula:

$$\beta = \frac{MW_{C_{7+}} - \eta}{\alpha} \quad (4.8)$$

In this equation $MW_{C_{7+}}$ is the average molecular weight of the C₇₊ fraction. The North Sea oil can be described by $\alpha = 0.82$, $\eta = 93.2$, and $MW_{C_{7+}} = 227$ [90].

To find the mole fraction of the components with a molecular weight in the interval from MW_i to MW_{i-1} , the probability function (eq. (4.7)) must be integrated from MW_i to MW_{i-1} and multiplied by the total mole fraction of components with a molecular weight as follows:

$$P_0(MW) = \int_{\eta}^{MW} \frac{(MW - \eta)^{\alpha-1} \exp\left(-\frac{MW-\eta}{\beta}\right)}{\beta^{\alpha}\Gamma(\alpha)} \quad (4.9)$$

$$P_1(MW) = \int_{\eta}^{MW} \frac{MW \cdot (MW - \eta)^{\alpha-1} \exp\left(-\frac{MW-\eta}{\beta}\right)}{\beta^{\alpha}\Gamma(\alpha)} \quad (4.10)$$

$$x_i = x_{C_{7+}} \int_{MW_{i-1}}^{MW_i} P(MW) dMW = x_{C_{7+}} (P_0(MW_i) - P_0(MW_{i-1})) \quad (4.11)$$

$$MW_i = \frac{[P_1(MW_i) - P_1(MW_{i-1})]}{[P_0(MW_i) - P_0(MW_{i-1})]} \quad (4.12)$$

The three parameters α , β , η can be determined by fitting to experimental molar distribution data by use of a nonlinear least-squares algorithm to minimize the following objective function.

$$F(\alpha, \eta, \beta) = \sum_{i=1}^{N-1} \left(\frac{MW_i^{mod} - MW_i^{exp}}{MW_i^{exp}} \right)^2 \quad (4.13)$$

where superscript *mod* and *exp* represent the molecular weights from the gamma distribution model and experimental data respectively.

In 2010, Rodriguez and Hamouda [110] developed a characterization method based on a modification of Whitson's approach where they included a procedure to determine the value of the fitting parameter α and a new definition of the limits used to calculate the frequency of occurrence for each SCN. They based the developed method on the fact that molecular weight is not uniquely related to carbon numbers because of the hidden exponential increase of number of isomers/components with increasing the carbon numbers. In their study, the best trend fit for α was found when the molecular weight of the maximum mole fraction of the experimental data and the molecular weight of the maximum value of the TPG had the same value. Once the TPG has been generated, it is divided into SCNs with the new definition of the limits by the introduction of the

limiting molecular weight (*LMW*), which is the highest molecular weight included in the SCN. Equation (4.11) is then transformed to (*C*₇₊ is arbitrary):

$$x_i = x_{C_{7+}} \int_{MW_{\min}}^{LMW} P(MW) dMW \quad (4.14)$$

where *MW*_{min} is the minimum molecular weight present in the C₇₊ fraction as suggested by Whitson and *LMW* is calculated by an iterative process.

Riazi Method - Extension of Gamma Distribution

Riazi [111, 112] argued that the exponential distribution suggested by Pedersen et al. [107] was only suitable to characterize gas condensate systems and wet natural gases, and the gamma distribution could not model the very heavy oils and residues, and it was not also suitable for specific gravity predictions. As a result, he proposed a generalized distribution method which could be applied to all reservoir fluids and all the characterization parameters (*MW*, *T_b*, *SG* and refractive index parameter). The distribution function proposed by Riazi [111] has the following form:

$$P = P_0 \left(\left[\frac{A}{B} \ln \left(\frac{1}{1-x} \right) \right]^{1/B} + 1 \right) \quad (4.15)$$

This model has three parameters *A*, *B* and *P*₀, and *x* is the cumulative mole, volume or weight fraction and *P* is a property such as *T_b*, *MW* or *SG*. *P*₀ is the value of *P* at *x* = 0, which corresponds to the initial value. Parameter *B* for specific gravity of most C₇₊ samples is fixed at 3 and for the boiling point is 1.5. When *B* = 1 in the above model, it reduces to the exponential model. For light reservoir fluids such as gas condensates, value of *B* for molecular weight is one for most samples [111]. However, the best optimum value of *B* varies from one mixture to another and from one property to another. Generally *B* for heavier fluids has a higher value. Riazi has suggested the above model can be applied to any hydrocarbon plus fraction or crude oil sample.

In the proposed method, the mole fraction and property of each pseudo-component can be calculated from the following equations:

$$x_i = \exp \left(-\frac{B}{A} P_{i-1}^{*B} \right) - \exp \left(-\frac{B}{A} P_i^{*B} \right), \quad P^* = \frac{P - P_0}{P_0} \quad (4.16)$$

$$P_{i,av}^* = \frac{1}{x_i} \left(\frac{A}{B} \right)^{1/B} \left[\Gamma \left(1 + \frac{1}{B}, q_{i-1} \right) - \Gamma \left(1 + \frac{1}{B}, q_i \right) \right], \quad q_i = \frac{B}{A} P_i^{*B} \quad (4.17)$$

$$P_{i,av} = P_0 (1 + P_{i,av}^*) \quad (4.18)$$

In eq. (4.17), $\Gamma(1 + 1/B, q_i)$ is the incomplete gamma function and at $B = 1$ it would be:

$$\Gamma(2, q) = (1 + q) e^{-q} \quad (4.19)$$

Compared to eq. (4.7), this generalized distribution approach could be considered as an extended version of gamma distribution with varying exponent term, which it is always 1.0 in gamma distribution.

4.2.2 Parameter Estimation for Thermodynamic Models

It is a common practice to split a C₇₊ fraction into several SCN groups using the mentioned methods in Section 4.2.1, and then calculate the model parameters of each SCN group using available correlations. For most of the EoSs including SRK and PR, critical properties are the required parameters for PVT calculations, while the model parameters for PC-SAFT are m , ε and σ . The suggested correlations for the PC-SAFT parameters are presented in Section 4.4. The available correlations for acentric factor and critical properties such as T_c and P_c are summarized and compared in Appendix A.

It was found that Twu's method [113] with Lee-Kesler/Kesler-Lee correlations [114, 115] for ω seems to be the best set of correlations for calculation of critical properties for both n-alkanes and other hydrocarbons as also suggested by Whitson and Brule [90]. In our study, we use this set of correlations for calculation of the parameters for cubic EoSs (SRK and PR), and Soave-BWR.

4.2.3 Lumping

After finding the model parameters for all the SCN fractions, it would be more desirable to have a convenient number of pseudo-components to represent the crude oil before performing phase equilibrium calculations or other property estimations. The lumping procedure consists of grouping the SCN fractions into desirable number of pseudo-components and deciding the required properties or parameters for each

lumped group. This can be done in two ways as described below. Nasrifar and Bolland [116] recommended that C_{7+} fraction must be divided into at least 12 SCN groups so that the predictions can be improved and unchanged by any of the used EoSs.

Equal Mass Approach

As it is used by Pedersen et al. [108, 16] this procedure is to group the SCN fractions into user specified number of pseudo-components based on Equal Mass (fraction) of each pseudo-component. The properties of the pseudo-components are found as weight mean averages of the same property of the individual SCN fraction. For example, if the k^{th} pseudo-component contains the SCN fractions m to n ,

$$\Omega_k = \frac{\sum_{i=m}^n x_i MW_i \Omega_i}{\sum_{i=m}^n x_i MW_i} \quad (4.20)$$

where Ω could be any properties, such as T_c , P_c , and ω in cubic EoSs, or m , σ , and ε in SAFT models.

Gaussian Quadrature Approach

The Gaussian quadrature approach [90] is normally used to provide a discrete representation of continuous functions using different numbers of quadrature points. Here it is applied to define the user specified number of pseudo-components. The number of pseudo-components is the same as the number of quadrature points. The required properties are obtained directly for the pseudo-components, and the missing medium properties, like TBP and SG can be estimated from the molecular weight. One recommended estimation method of these properties was from the Søreide correlation [117].

4.3 Characterization for SRK, PR and Soave-BWR

The method proposed by Pedersen et al. [15, 16] is used here as the framework for C_{7+} characterization. As already mentioned in the previous sections, the method consists of three steps: (1) calculating the mole fraction of SCN components in the

last plus fraction using exponential decay; (2) estimating the critical properties T_c , P_c , and ω with a set of correlations developed by themselves [16]; (3) lumping the SCN components into a few pseudo-components with approximate equal mass, where the lumped components' properties are calculated as the mass average of the SCN components' properties. Another popular characterization method in PVT modeling is the method proposed by Whitson et al. [18]. It shares the same three steps although the detailed choices are different. A major difference is that Whitson et al. uses the gamma distribution for the molar distribution in C_{7+} . This seems to be superior to the method of Pedersen et al. However, it should be noted that the exponential distribution in the method of Pedersen et al. is applied to the last plus fraction instead of C_{7+} . Since many oil analysis can provide composition information to carbon number much higher than C_7 , e.g., the commonly employed simulated distillation using the ASTM 2887 protocol can cover boiling point range up to 1000 °F or around C_{43} , the molar distribution estimated by the method of Pedersen et al. is generally good enough unless the SCN components are over lumped.

In this study, the method of Pedersen et al. was employed for SRK, PR, and Soave-BWR with just one modification: its correlations for T_c , P_c , and ω are replaced by the Twu correlations [113] for T_c and P_c , and the Lee-Kesler/Kesler-Lee correlations [114, 115] for ω . The reason for not using the original correlations proposed by Pedersen et al. [16], which are developed by fitting PVT data directly, is that our calculation results, presented in Appendix A, show they are poor in reproducing the critical properties of individual heavy hydrocarbon components in C_{7+} . The Twu correlations and the Lee-Kesler/Kesler-Lee correlations, in contrast, give a much better estimation as mentioned earlier.

4.4 Characterization for PC-SAFT

Reservoir fluid characterization for PC-SAFT has been investigated mainly in connection with the recent research on asphaltene precipitation modeling with PC-SAFT [19, 20, 12, 21–27]. It is surely important that a specific EoS, such as PC-SAFT, can model phase behavior as complex as asphaltene precipitation with a proper characterization method. However, the main objective of a characterization method for any EoS should be a reasonable modeling of basic PVT properties. Once the basic PVT properties are satisfactorily described, specific adjustments of the characterization method can be introduced to model particular phase equilibrium phenomena like asphaltene

precipitation. Among several recent PC-SAFT characterization methods for basic PVT modeling [118–122], some follow Pedersen’s or Whitson’s method and only use a different set of correlations [118–120, 122], whereas the others use a completely different procedure in addition to a new set of correlations [121]. The correlations developed for PC-SAFT model parameters are usually expressed as a function of MW and/or T_b and SG for each SCN fraction [119–122], and some are developed for the PNA content in each fraction [12, 106, 118]. Leekumjorn and Krejbjerg [123] commented that reliable and generally applicable petroleum fluid characterization procedures are still to be developed for the PC-SAFT EoS.

Characterization for PC-SAFT also adopts the first and the third steps in the method of Pedersen et al. The second step, estimation of model parameters, has to be replaced by a set of newly developed correlations for the PC-SAFT model parameters m , σ and ε . Correlations for the PC-SAFT model parameters for n-alkanes or other hydrocarbons of a certain homologous series are available in the literature [34, 124]. Those correlations are usually expressed as functions of MW . However, estimating the PC-SAFT model parameters for a SCN component is a bit different.

There are several studies in the literature that use MW and SG for calculation of PC-SAFT parameters. Liang et al. [118] observed that using a linear correlation for $m\varepsilon/k$ against MW , has an overall good performance on the prediction of saturation pressure and density. In their recent study [120], they investigated the possibility of using the same principle for m and $m\sigma^3$, i.e. linear correlations against MW . They suggested the following set of correlations for the PC-SAFT parameters:

$$m = 0.023398MW + 0.94101 \quad (4.21)$$

$$m\sigma^3 = 1.4086MW + 52.6 \quad (4.22)$$

$$m\varepsilon/k = 6.8311MW + 124.42 \quad (4.23)$$

Assareh et al. [122] developed a set of correlations based on MW and SG for PC-SAFT parameters using a database of 840 pure components from three families (n-alkanes, cycloalkanes and alkylbenzenes). The pure component parameters were generated by the correlations of Tihic et al. [124] and Panuganti et al. [25] in the MW range of 70–350. Their correlations are linear functions of MW and quadratic functions of SG :

$$m = 33.58 + 0.08816MW - 90.75SG - 0.07727MW SG + 61.01SG^2 \quad (4.24)$$

$$m\sigma^3 = -75.14 + 2.848MW + 231.7SG - 1.288MW SG - 186.9SG^2 \quad (4.25)$$

$$m\varepsilon/k = 3372 + 11.24MW - 8955SG - 5.925MW SG + 6136SG^2 \quad (4.26)$$

A SCN component is a narrow boiling point range cut without a definite chemical composition or a fixed molecular weight. The component is therefore characterized by its average T_b and SG . The variation in SG for a SCN component of a certain T_b reflects the variation in aromaticity. Higher SG indicates a higher content of aromatic or cyclic hydrocarbons in the fraction. The developed correlations should be able to estimate m , σ and ε based on T_b and SG instead of MW .

To develop such a set of correlations, a database of m , σ and ε is needed for relevant hydrocarbons. 358 hydrocarbons in the DIPPR database [105], including 30 n-alkanes (up to nC₃₆), are used for this purpose. The values of m , σ and ε are regressed using the “synthetic” experimental vapor pressure and saturated liquid density data in the reduced temperature range from 0.5 to 0.9, which are calculated using the correlations in DIPPR. The regressed m , σ and ε for some compounds are excluded in the development of correlations, including (1) the compounds which are too light, such as methane; (2) the compounds without a vapor pressure correlation or a liquid density correlation valid over the required temperature range; (3) the compounds whose parameters are significantly off the trends. The final set of hydrocarbons includes 29 n-alkanes and 318 other hydrocarbons.

A two-step perturbation method, which is used by Twu [113] to develop the correlations for critical properties, is employed here to develop the correlations for the PC-SAFT model parameters. In the first step, the properties of the n-alkane at the T_b of the SCN component are calculated. The molecular weight of the n-alkane at this T_b , MW_p , can be estimated using Twu’s correlations [113]. The PC-SAFT model parameters for n-alkanes, m_p , σ_p and ε_p , are then calculated by the following linear correlations:

$$m_p = 0.02644MW_p + 0.83500 \quad (4.27)$$

$$m_p\varepsilon_p/k = 6.90845MW_p + 139.30870 \quad (4.28)$$

$$m_p\sigma_p^3 = 1.71638MW_p + 19.19189 \quad (4.29)$$

where m_p is dimensionless, ε_p/k is in Kelvin, and σ_p has the unit of Å.

The above equations differ slightly from those in [34, 124] due to the difference in the selected n-alkanes and temperature ranges. In the second step, the properties of the

SCN component is estimated by using the difference in specific gravity $SG - SG_p$ as the perturbation parameter, where SG_p is the specific gravity of the n-alkane calculated by Soave's correlation [125] as a function of T_b (in Kelvin):

$$SG_p = (1.8T_b)^{1/3} (11.7372 + 3.336 \times 10^{-3}T_b - 976.3T_b^{-1} + 3.257 \times 10^5 T_b^{-2})^{-1} \quad (4.30)$$

Establishing simple but accurate correlations between the difference in m , σ and ε and the difference in SG is far from a simple task. No general trends with sufficiently small scattering can be found between $m - m_p$, $(\varepsilon - \varepsilon_p)/k$ and $\sigma - \sigma_p$ and $\Delta SG = SG - SG_p$. However, it seems that σ/σ_p varies in a relatively narrow range, as indicated in Figure 4.5. Therefore, as a first approximation, it is assumed that:

$$\sigma = \sigma_p \quad (4.31)$$

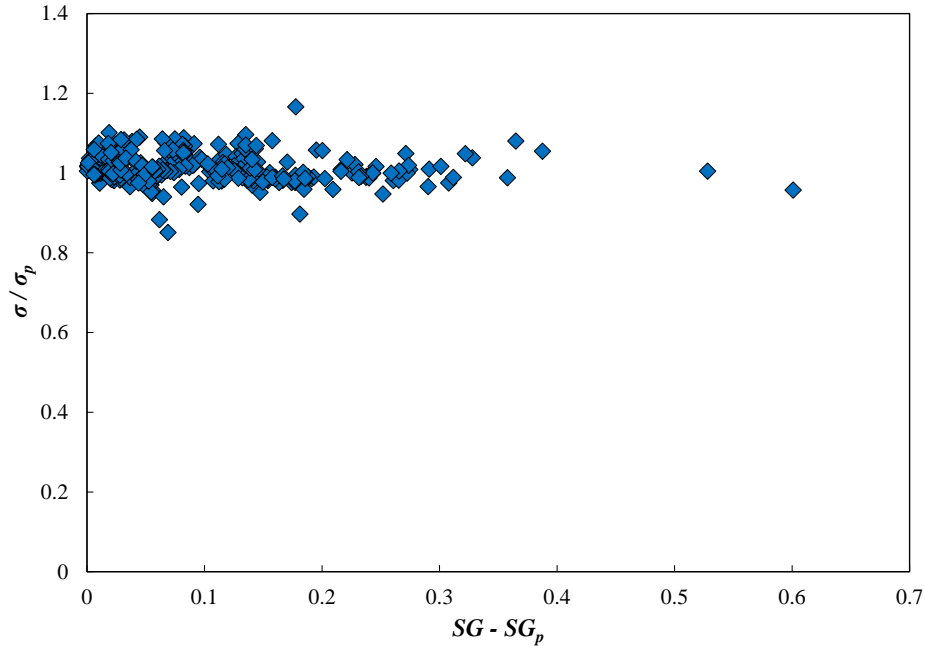


Figure 4.5 Change of σ for non n-alkanes with the relative difference in specific gravity SG . σ_p and SG_p are for the n-alkanes at the same boiling point temperatures.

By fixing σ equal to σ_p , the values of m and ε are regressed again and the following equation found to give the best fit for ε as shown in Figure 4.6.

$$\varepsilon = \varepsilon_p (1.2357\Delta SG + 1) \quad (4.32)$$

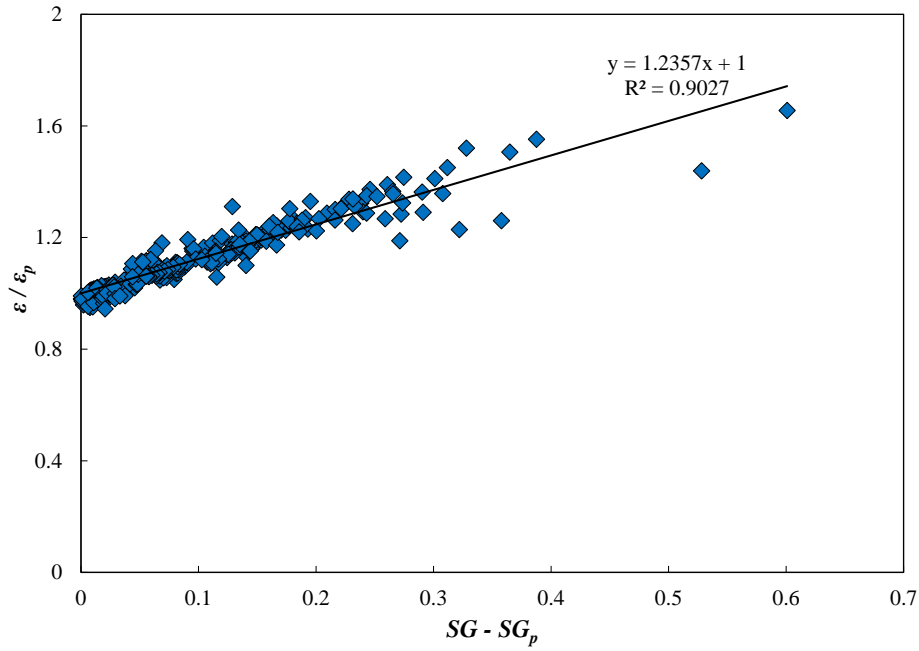


Figure 4.6 Change of ε for non n-alkanes with the relative difference in specific gravity SG . ε_p and SG_p are for the n-alkanes at the same boiling point temperatures.

With eqs. (4.31)–(4.32) as constraints, the m values for other hydrocarbons in DIPPR are refitted. The new m values are shown in Figure 4.7 and the following correlation is suggested:

$$m = m_p (1.3192\Delta SG^2 - 1.8218\Delta SG + 1) \quad (4.33)$$

Equations (4.32)–(4.33) provide the basis for determining the final correlations for m and ε . In the final step, the coefficients in these two expressions are further tuned to fit the vapor pressures and saturated liquid densities for all the 318 other hydrocarbons. Different weights have been assigned to different chemical classes in these hydrocarbons: cyclohydrocarbons and aromatics are set to 5, iso-alkanes to 2, and other unsaturated hydrocarbons to 1. The final correlations suggested for m and ε are:

$$\varepsilon = \varepsilon_p (1.1303391\Delta SG + 1) \quad (4.34)$$

$$m = m_p (1.0460471\Delta SG^2 - 1.6209973\Delta SG + 1) \quad (4.35)$$

and σ is still calculated by eq. (4.31). It should be noted that eq. (4.35) has a minimum value at $\Delta SG = 0.7748204$. To keep the monotonicity, the ratio of m/m_p will be fixed at this minimum for ΔSG larger than that. We can also assume that m and ε are

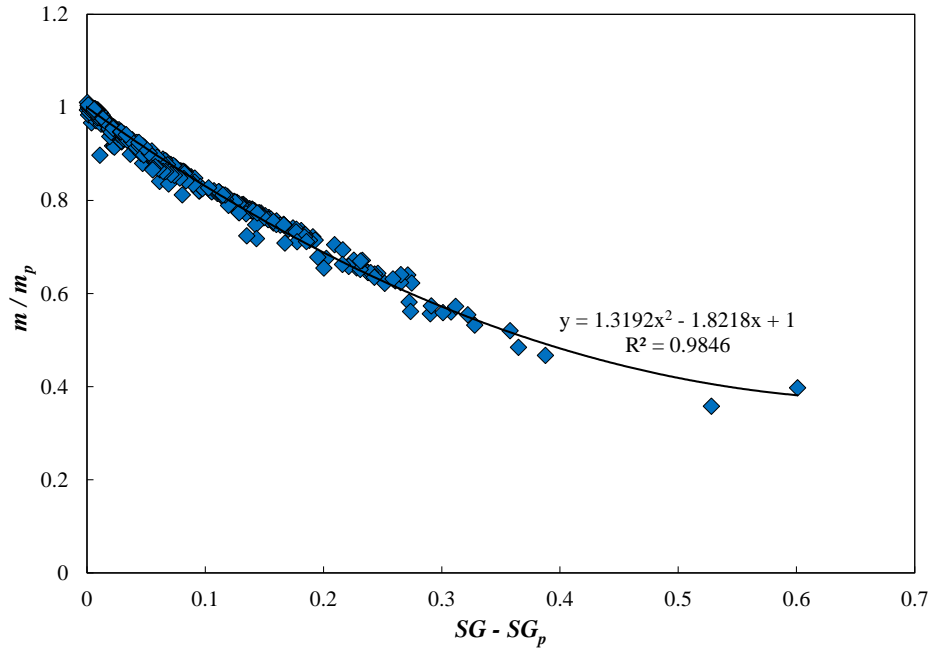


Figure 4.7 Change of m for non n-alkanes with the relative difference in specific gravity SG . m_p and SG_p are for the n-alkanes at the same boiling point temperatures.

functions of both ΔSG and SG and develop the following set of correlations:

$$\varepsilon = \varepsilon_p [(0.59822690 + 0.55100489/SG)\Delta SG + 1] \quad (4.36)$$

$$m = m_p/[1 + (2.6934054 - 0.57209122/SG)\Delta SG] \quad (4.37)$$

This set of correlations gives slightly better vapor pressures and saturated liquid densities in the final regression step. However, our test shows its PVT calculation results are not as good as the former simpler expressions. Therefore, the correlations eq. (4.31) and eqs. (4.34)–(4.35) are considered as the final set of correlations. In the following sections and for simplicity, we have called this set of correlations as Yan et al.'s [119] characterization method for PC-SAFT.

4.5 Considerations in a General Characterization Approach

From a pragmatic viewpoint, it is convenient to modify only the correlations of model parameters in step (2) of the characterization when developing a characterization

method for an EoS. Since the two other steps are kept unchanged, implementation into the existing codes is straightforward. This also facilitates evaluation of the new method since the existing PVT software needs little change, and a quicker acceptance of the new correlations can be expected if the evaluation results are positive. Modifications of the other two steps may also lead to a further improvement of the characterization results. But such modifications should in principle be effective to cubic models as well and it is better to study the necessity of such modifications in a more general context, not just limited to non-cubic models. For example, one can naturally ask whether those changes are needed for cubic models and whether the widely used procedures such as Pedersen’s method and Whitson’s method should be updated in the existing software. Those questions are interesting but not our focus in this research. Our major interest is non-cubic models where there is no “standard” characterization commonly accepted in the industry. We stick to the principle that the development should be mainly on the correlations for model parameters.

In this section we propose a general approach to developing the new correlations as illustrated by steps A and B in Figure 4.8. In the first step (A), a set of correlations for the model parameters is developed based on a large database for pure components, e.g., the DIPPR database. We prefer correlations developed in a two-step perturbation way because the properties of n-alkanes are expressed with high accuracy and the correction for the aromaticity is given in a separate set of equations. In the second step (B), the correlations accounting for the aromaticity will be adjusted using a large PVT database but the paraffinic limit should be kept unchanged. The general approach is applied to PC-SAFT in Section 4.6 and to SRK and PR in Section 4.7. In Section 4.8 where characterization using explicit PNA information is tried, we also use the general principles discussed above in the development.

4.6 General Characterization Approach for PC-SAFT

We use Pedersen’s characterization method as the framework and only modify the correlations in step (2) as discussed in Section 4.4. We first develop the correlations using the DIPPR database and then adjust them using a large PVT database. The adjustment is made to minimize the deviation in key PVT properties like saturation pressures, densities at reservoir temperature and Stock Tank Oil (STO) densities from single-stage separation.

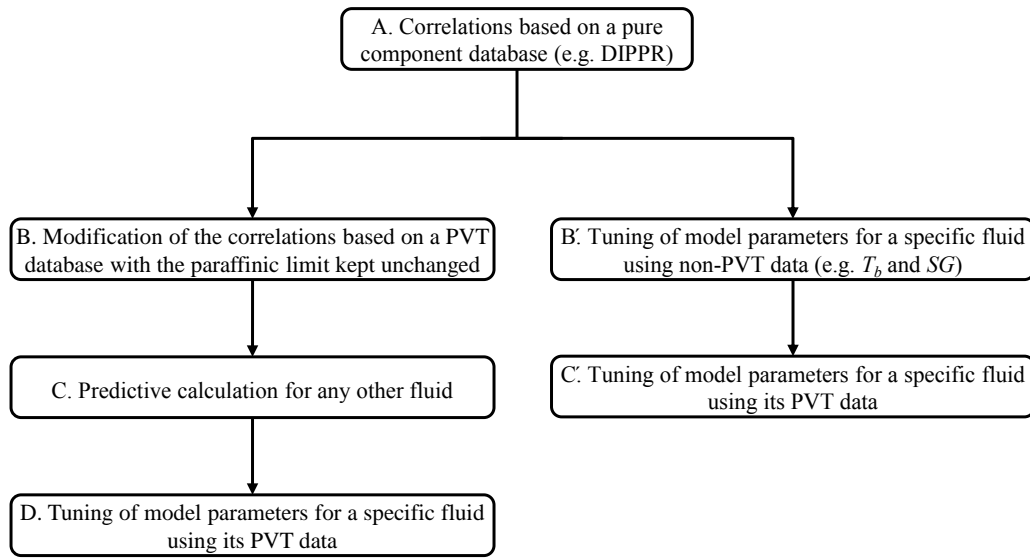


Figure 4.8 The recommended characterization procedure (steps A and B) and its application to PVT calculation.

The first step was presented in Section 4.4 where a set of correlations for the PC-SAFT model parameters m , σ , and ε were developed using a two-step perturbation method similar to that used by Twu [113] in the development of correlations of critical properties.

Equation (4.31) and eqs. (4.34)–(4.35), developed based on the DIPPR database, provide the optimal parameters that can calculate saturation pressure and density for the relevant hydrocarbon components in the DIPPR database. Despite a large number of components are involved, the heavy aromatic and naphthenic components are not well-represented. In the database, the heaviest n-alkane is nC_{36} with T_b equal to 770.15 K and the heaviest aromatic component is Tetraphenylethylene ($C_{25}H_{20}$) with T_b equal to 760 K. Only around 19% of the components in the database have T_b higher than 600 K and it decreases to around 5% for the components with T_b higher than 700 K. This shows that the majority of the components (around 81%) in the database are light and have T_b lower than 600 K. Furthermore, the naphthenic and aromatic components in the database do not necessarily represent the most probable population in the common reservoir fluids. Therefore, the developed correlations optimal for the database may not be optimal for common reservoir fluids. To address this problem, we suggest further tuning the correlations based on a large PVT database so that the resulting correlations can be representative for common reservoir fluid samples. The tuning is performed only for the eq. (4.31) and eqs. (4.34)–(4.35) in order to keep the

correct n-alkane limit (eqs. (4.27)–(4.29)). Development of the correlations for model parameters based on a PVT database was used before, e.g., by Pedersen et al. [15]. In their study, the correlations were developed without consideration for the n-alkane limit. As a result, the critical properties and acentric factors generated for n-alkanes by the correlations can be very different from the experimental values. We stress here the importance of keeping the n-alkane limit (eqs. (4.27)–(4.29)) since the parameters for paraffinic fluids will not be distorted. Besides, the tuning is only made for the coefficients in eq. (4.31) and eqs. (4.34)–(4.35) in order to keep the same functional forms for hydrocarbons other than n-alkanes.

Apparently, a larger database will give more representative results. We have included 260 reservoir fluids in our database (see Section 4.10.1). Three properties are used in the tuning of the coefficients:

1. Saturation pressure
2. Density at reservoir temperature
3. Stock Tank Oil (STO) density

The density at reservoir temperature includes liquid density of oils in both single-phase and two-phase regions, and density of gas condensates above dew point pressure. Selection of these properties is based on two considerations: first, these three properties are usually measured with the lowest uncertainty; second, each property has its particular importance. Saturation pressure is a crucial property for reservoir development since a second phase appears below the saturation pressure, and it is perhaps the most influential property in tuning of a PVT model in phase equilibrium calculation. Density at reservoir temperature is directly related to all the volume related engineering calculations in the reservoir. STO density reflects the volume calculation results at surface conditions and indirectly influences the calculation of formation volume factors and solution gas oil ratios.

There is no apparent way to modify eq. (4.31) and we only considered tuning of eqs. (4.34)–(4.35). In the tuning, we tried to use as few coefficients as possible and change them as little as possible. Two schemes were tested. In the first scheme, the only coefficient in the ε correlation (eq. (4.34)) was regressed to minimize the deviation in saturation pressure, density and STO density. In the second scheme, all the three coefficients in the correlations for m and ε (eqs. (4.34)–(4.35)) were tuned simultaneously. The tuning showed that the saturation pressure was the most influential data for the final values of the regressed coefficients whereas the influence of

density at reservoir temperature and STO density was moderate. The final correlations for the two schemes are as follows:

1. Regressing ε coefficient in eq. (4.34):

$$\varepsilon = \varepsilon_p(0.9533431\Delta SG + 1) \quad (4.38)$$

2. Regressing m and ε coefficients in eqs. (4.34)–(4.35) at the same time:

$$\varepsilon = \varepsilon_p(0.9550243\Delta SG + 1) \quad (4.39)$$

$$m = m_p(2.4516079\Delta SG^2 - 1.6710480\Delta SG + 1) \quad (4.40)$$

It should be noted that the above correlations are not proposed to be the ultimate correlations for the PC-SAFT characterization. Instead, they are used as an illustration how the correlations can be developed for an EoS. With a different PVT database, a different set of correlations can be developed by minimizing the deviations of the properties of interest for that database.

The characterization method developed using the general approach can be later applied to PVT calculation ($A \rightarrow B \rightarrow C \rightarrow D$ in Figure 4.8). The correlations developed in step B represent the average performance for the fluids in the database. For any other fluid sample not in the database, the calculation (step C) is still predictive. For the final PVT model for this specific fluid, final tuning in step D can be made. This procedure is compared in Figure 4.8 with another procedure ($A \rightarrow B' \rightarrow C'$) for improving the characterization results for a specific fluid sample. In step B', the model parameters can be tuned using boiling points and/or specific gravities of SCN fractions for a specific fluid, such as discussed in Yan et al. [119] and Liang et al. [118]. The boiling points and specific gravities are not final PVT data and the calculation based on the tuned model parameters is still predictive. However, since the tuning is directly used for the model parameters, the obtained parameters can only be used for this specific fluid. For the final PVT model, further tuning of model parameters in step C' can be made.

4.7 Application of The General Approach to SRK and PR

For cubic EoSs, we still use Pedersen's method as the framework for our development. But instead of using Pedersen's correlations [12], we would like to use a set of correlations similar to Twu's correlations for T_c and P_c [113] where their n-alkane limits are explicitly given. The Lee–Kesler correlations [114, 115] for ω is also used together with Twu's correlations as this combination gives good estimate of critical properties of hydrocarbons in C_{7+} and has also been recommended by Whitson [90].

Twu's method for calculation of T_c and P_c was already presented in Section A.2. Since the correlations in the second step of Twu's method (eq. (A.16)) are complex and difficult to update during the tuning process with a PVT database, we tried to replace them with simpler correlations. Figure 4.9 illustrates how T_c/T_{cp} and P_c/P_{cp} change with ΔSG for 318 hydrocarbons in the DIPPR database. Fitting a second order polynomial through the data points for T_c/T_{cp} and a linear function for P_c/P_{cp} give the following correlations for T_c and P_c where T_c is in Kelvin and P_c is in bar:

$$P_c = P_{cp}(3.56179\Delta SG + 1) \quad (4.41)$$

$$T_c = T_{cp}(-0.39220\Delta SG^2 + 0.50239\Delta SG + 1) \quad (4.42)$$

In eqs. (4.41)–(4.42), T_{cp} and P_{cp} are the critical temperature and pressure of n-alkanes calculated by eqs. (A.13)–(A.14) and are converted to Kelvin and bar respectively. The difference in the specific gravity $\Delta SG = SG - SG_p$ is calculated using SG_p from eq. (4.30). It should be noted that eq. (4.42) has a maximum around $\Delta SG = 0.62$, and we keep T_c/T_{cp} constant after its maximum value.

Figure 4.10 compares original Twu's method (eqs. (A.13)–(A.16)) with our simplified version (eqs. (A.13)–(A.14), eqs. (4.41)–(4.42)) in calculation of critical properties of 318 pure components in DIPPR. As can be seen in Figure 4.10, the simplified Twu's method gives very close results to that of original Twu's method. The percent average absolute deviations AAD% of the original Twu's method in T_c and P_c are 1.1% and 7.8%, respectively, while those of the simplified version are 1.0% and 7.5%, respectively. It shows that the simplified version of Twu's method (eqs. (A.13)–(A.14), eqs. (4.41)–(4.42)) can be used instead of the original Twu's method for calculation of critical properties.

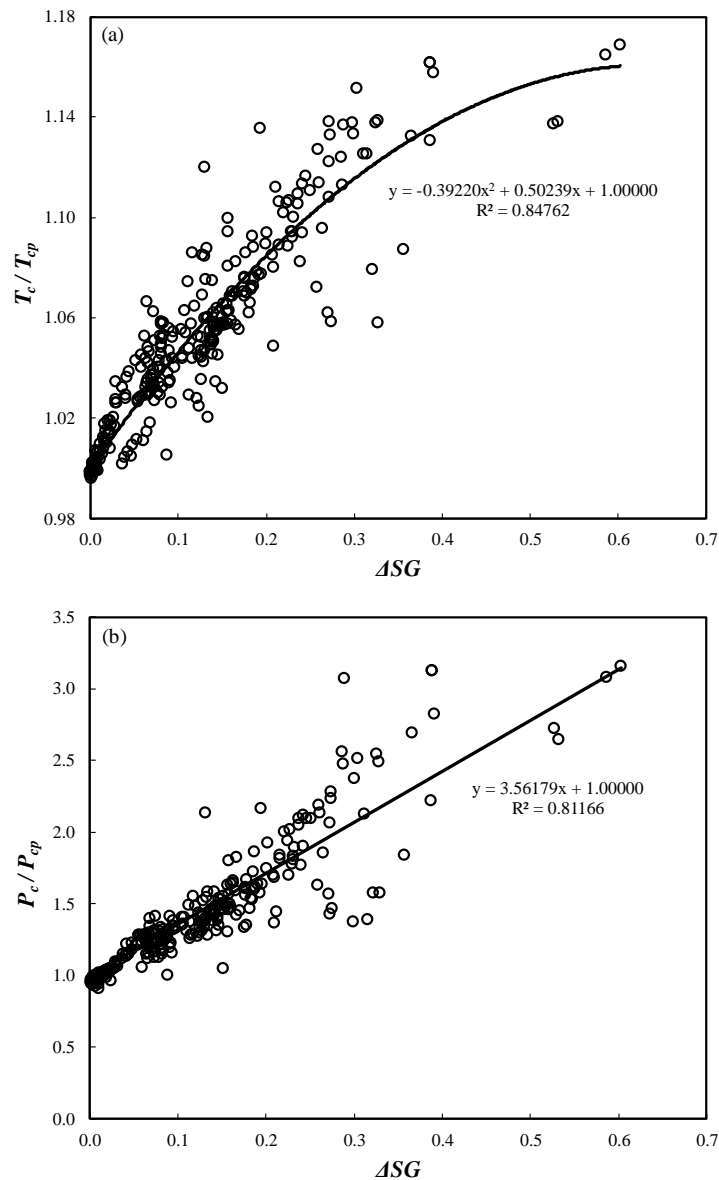


Figure 4.9 T_c and P_c correlations as a function of ΔSG for the pure components in DIPPR database.

The new correlations for T_c and P_c can be used together with the Lee-Kesler correlations for ω . For the tuning of eqs. (4.41)–(4.42) based on the PVT database, two schemes were tested for SRK and PR, similar to that used for PC-SAFT. In the first scheme, the only coefficient in the P_c correlation (eq. (4.41)) was regressed to minimize the deviation in saturation pressure, density and STO density. In the second scheme, all the three coefficients in the correlations for P_c and T_c (eqs. (4.41)–(4.42)) were tuned

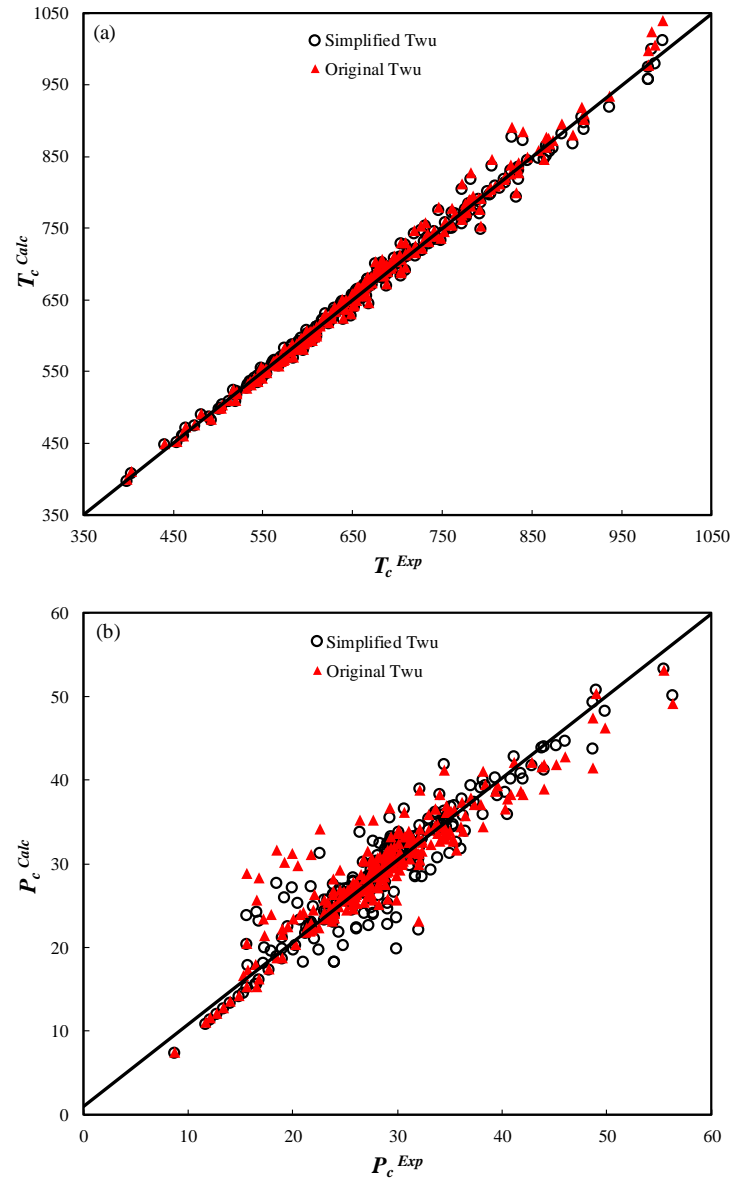


Figure 4.10 Comparison between original and simplified Twu's method in calculation of critical temperature and pressure vs. experimental data from DIPPR.

simultaneously. The final correlations for the two schemes are summarized below for SRK and PR:

1. Regressing P_c coefficient in eq. (4.41) for SRK:

$$P_c = P_{cp}(4.9242447\Delta SG + 1) \quad (4.43)$$

2. Regressing P_c and T_c coefficients in eqs. (4.41)–(4.42) at the same time for SRK:

$$P_c = P_{cp}(5.4974598\Delta SG + 1) \quad (4.44)$$

$$T_c = T_{cp}(-0.7220183\Delta SG^2 + 0.6604209\Delta SG + 1) \quad (4.45)$$

3. Regressing P_c coefficient in eq. (4.41) for PR:

$$P_c = P_{cp}(5.4536065\Delta SG + 1) \quad (4.46)$$

4. Regressing P_c and T_c coefficients in eqs. (4.41)–(4.42) at the same time for PR:

$$P_c = P_{cp}(5.5119793\Delta SG + 1) \quad (4.47)$$

$$T_c = T_{cp}(-0.7316782\Delta SG^2 + 0.6181465\Delta SG + 1) \quad (4.48)$$

Again, the above correlations are examples showing how the general approach can be applied to SRK and PR.

4.8 A PNA Based Characterization Method for PC-SAFT

The aromaticity of a SCN component is sometimes represented by use of the content of paraffinic (P), naphthenic (N) and aromatic (A) components in it. In both Pedersen's method and Whitson's method, PNA distribution is not used explicitly in the characterization. The aromatic content in each SCN component is reflected by the difference in SG . It can be advantageous sometimes to account for aromatic content explicitly. For example, when precipitation of asphaltene happens, it is reasonable to assume that the interaction between paraffinic compounds and asphaltenes and that between aromatic compounds and asphaltenes are different. Explicit expression of PNA components might also be useful in composition gradient modeling in petroleum reservoirs since it provides more flexibility.

In principle, if we can find representative chemical compounds to represent P, N and A, and somehow estimate the PNA distribution for each SCN fraction, then we can estimate the model parameters for P, N and A in each SCN fraction separately.

In practice, however, there are several challenges. The first challenge is that PNA distribution is usually unavailable. For heavy molecules, it is not easy to classify them into P, N or A, e.g. if they have aromatic rings, naphthenic rings and long paraffinic chains at the same time. There are some correlations for PNA estimation [126, 127] but their accuracy is difficult to evaluate for a wide range of SCN components. We present below a simple trial characterization method which avoids the first problem: Assuming that there are only P and A classes in each SCN fraction and their specific gravities are known, we can use volume additivity to get the composition of P and A directly from the SG for the SCN fraction:

$$\frac{1}{SG_{SCN}} = \sum \frac{w_i}{SG_i} = \frac{w_p}{SG_p} + \frac{w_{A_1}}{SG_{A_1}} + \frac{w_{A_2}}{SG_{A_2}} \quad (4.49)$$

In this equation w_p , w_{A_1} , w_{A_2} are the weight fraction of paraffinic, aromatic group 1 and aromatic group 2, respectively, SG_p , SG_{A_1} , and SG_{A_2} are the specific gravity of each group, and SG_{SCN} is the specific gravity of each SCN fraction. We assume here two possible aromatic groups: aromatics with one benzene ring A_1 , which are essentially linear alkylbenzenes and the aromatics with two benzene rings A_2 , which are mainly naphthalene derivatives with alkane chains. The heaviest aromatic component in A_1 group is n-octadecylbenzene ($C_{24}H_{42}$) with T_b equal to 673.15 K and the heaviest component in group A_2 is 1-n-decyl-naphthalene ($C_{20}H_{28}$) with T_b equal to 652.15 K. The A_1 group appears after 353.2 K and the A_2 group appears after 491.1 K. There are other possible aromatic compounds but it is difficult to classify them into classes with information as systematic and complete as for the A_1 and A_2 groups selected above. In addition, we assume that w_{A_1} is equal to w_{A_2} if all three groups exist in the SCN fraction. Hence, knowing the value of SG_{SCN} , we can solve eq. (4.49) to find the weight percent of each group.

The model parameters, MW and SG for P, A_1 and A_2 are readily available and their correlations can be easily developed. It seems that the characterization is straightforward but there is a second challenge. Figure 4.11 shows the distribution of SG with T_b for n-alkanes and 318 other hydrocarbons.

As can be seen, SG for the P group increases with T_b while SG for the A_1 and A_2 groups decreases with increasing T_b . But we know that the density of SCN fractions increases with the T_b (see Figure 4.11). The general perception is that the SG for aromatics should also increase with T_b . The opposite trends for A_1 and A_2 groups are because with increasing T_b , the complexity of the aromatics is expected to increase,

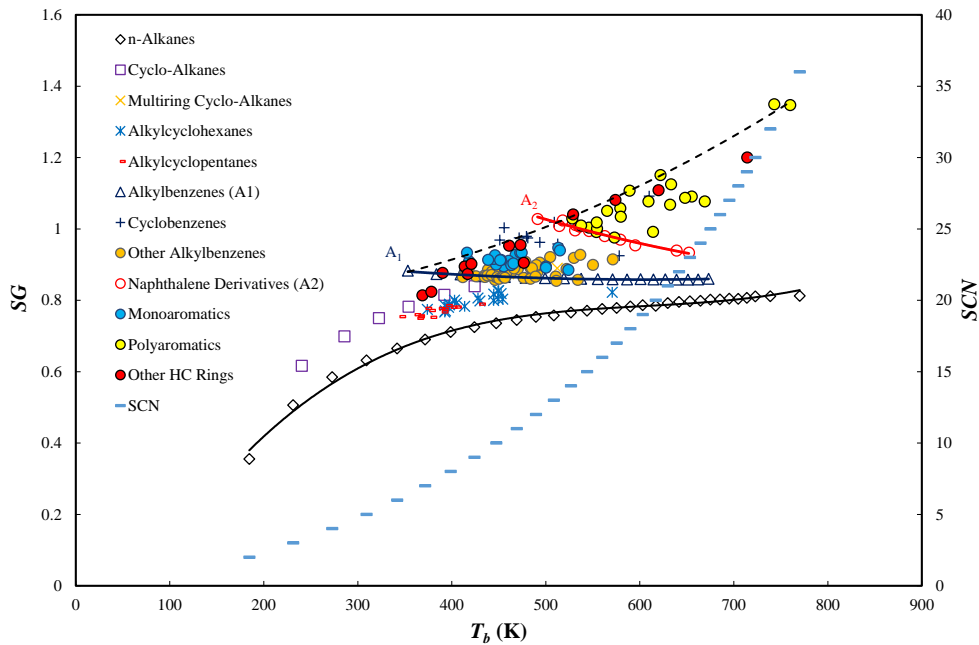


Figure 4.11 SG vs. T_b for n-alkanes and other hydrocarbons in DIPPR database. The black dashed line passes through the representative aromatic group listed in Table 4.3.

not just the length of the alkane chain. This is not reflected in the selected aromatic groups. In fact, it would be difficult to select a homologous aromatic family that shows an increase in SG with T_b . It should also be noted that the groups A_1 and A_2 are the aromatics groups that we have the most data for. For other groups of aromatics, it can be difficult to find a common trend in their model parameters. The difficulty of finding representative aromatic compounds is another challenge with PNA based characterization methods. Since SG for A_1 and A_2 can be far away from the SG for the actual aromatic group, it happens often that the density of a SCN fraction cannot be met by combining P, A_1 and A_2 groups. In such case, we have to assume the fraction is completely made up of A_2 .

Figure 4.12 illustrates the problem for the above test PNA characterization method. Compared with the characterization method for PC-SAFT (eq. (4.31) and eqs. (4.34)–(4.35)), the test PNA method gives a smaller phase envelope for Fluid 7 (31.28% methane and 36.78% C_{7+}) from Jaubert et al. [128]. It is caused by inadequate characterization of heavy fractions because for SCN components with large carbon numbers, their specific gravities can be larger than that of the A_2 group and we had to approximate these SCN components with A_2 . Even with this approximation, the obtained fraction will have properties lighter than it should have. This behavior was observed for most of the systems tested.

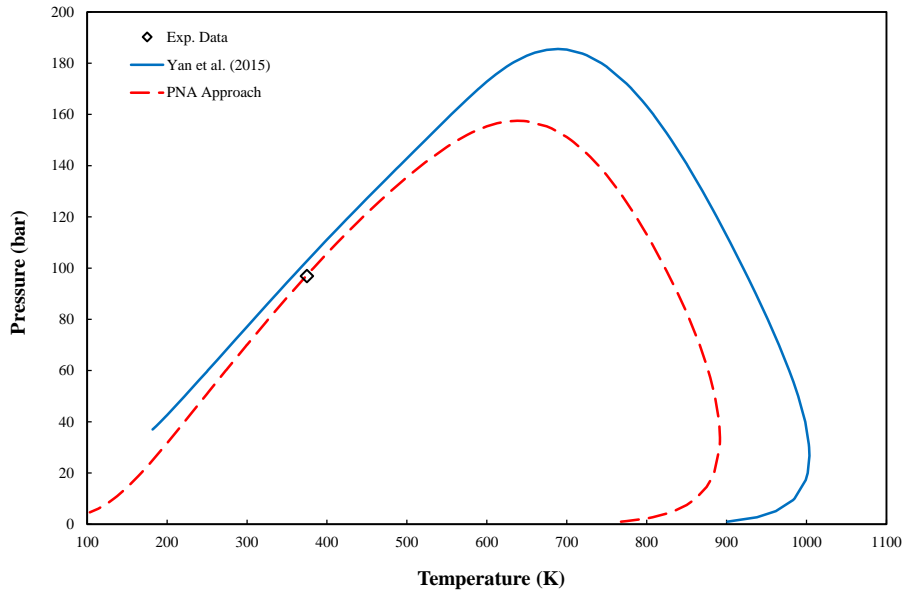


Figure 4.12 Phase envelope diagram for Fluid 7 from [128] using PC-SAFT and the “trial” PNA Approach.

In order to select the representative aromatic group that shows an increase in SG with T_b , we selected some aromatic compounds that capture the upper limit of SG in the aromatic compounds in the DIPPR database. The selection is somewhat arbitrary but we tried to consider the presence of single-ring, double-ring and multiple ring aromatics in the representative aromatic group. The black dashed line in Figure 4.11 passes through the representative components from different aromatic groups. The components and their properties are presented in Table 4.3. The lightest aromatic component in the A group is Benzene (C_6H_6) with T_b equal to 353.24 K which corresponds to C_7 fraction, and the heaviest aromatic component is Tetraphenylethylene ($C_{26}H_{20}$) with T_b equal to 760.0 K corresponding to C_{35} SCN fraction. The aromatic group appears after 353.24 K.

Table 4.3 Representative aromatic components and their parameters for the new PNA approach.

Component	Family	MW (g/mol)	T_b (K)	SG	m (-)	σ (Å)	ε/k (K)	$m.\varepsilon/k$ (K)	$m.\sigma^3$ (Å ³)
Benzene	n-Alkylbenzenes	78.112	353.24	0.883	2.487	3.626	286.104	711.635	118.603
Toluene	n-Alkylbenzenes	92.138	383.78	0.873	2.780	3.727	288.065	800.738	143.859
1,2,3-trimethylindene	Cyclobenzenes	158.240	509.00	1.019	3.893	3.870	311.764	1213.750	225.719
1-phenylindene	Cyclobenzenes	192.256	610.00	1.092	4.756	3.798	340.167	1617.830	260.654
Indane	Cyclobenzenes	118.176	451.12	0.969	3.079	3.839	318.609	980.873	174.230
Ethynylbenzene	Monoaromatics	102.133	416.00	0.934	2.683	3.869	318.811	855.488	155.378
Naphthalene	Naphthalenes	128.171	491.14	1.028	3.013	3.910	353.084	1063.758	180.100
Tetraphenylmethane	Polyaromatics	320.426	743.00	1.350	5.835	3.995	369.840	2158.003	372.009
Tetraphenylethylene	Polyaromatics	332.437	760.00	1.347	6.127	3.985	369.619	2264.786	387.795

The values of m , $m\varepsilon/k$, $m\sigma^3$ can be estimated as a function of T_b for the representative aromatic group using the following correlations. T_b in the following equations is in Kelvin:

$$m_A = 5.98957 \times 10^{-6} \times T_b^2 + 2.44045 \times 10^{-3} \times T_b + 0.807171 \quad (4.50)$$

$$(m\varepsilon/k)_A = 2.85713 \times 10^{-3} \times T_b^2 + 0.661777 \times T_b + 107.971 \quad (4.51)$$

$$(m\sigma^3)_A = 4.92174 \times 10^{-4} \times T_b^2 + 0.0938404 \times T_b + 30.1198 \quad (4.52)$$

Using the above correlations in a wide range of T_b (from 300 K to 1000 K), the molar density of the aromatic group ρ_A can be found using PC-SAFT. The correlation for ρ_A as a function of T_b can therefore be written as:

$$\rho_A = 2.03166 \times 10^{-5} \times T_b^2 - 3.93733 \times 10^{-2} \times T_b + 21.9838 \quad (4.53)$$

Assuming that there are only P and A classes in each SCN fraction, we can calculate the composition of P and A by solving the following equation:

$$\frac{MW_{SCN}}{SG_{SCN}} = \frac{x_p MW_p}{SG_p} + \frac{x_A}{\rho_A} \quad (4.54)$$

where x_p and x_A are the mole fractions of paraffinic and representative aromatic group, respectively. MW_p and MW_A are the molecular weights and SG_p is the specific gravity of the paraffinic group, while MW_{SCN} and SG_{SCN} are the molecular weight and specific gravity of each SCN fraction, the values of which are known from the first step of Pedersen's characterization. The specific gravity of the paraffinic group can be calculated by eq. (4.30) while MW_p is calculated by a few iterations using the following correlation as a starting value [113]:

$$MW_p^0 = \frac{T_b}{10.44 - 0.0052T_b} \quad (4.55)$$

In this correlation T_b is in °R. As all the necessary parameters in eq. (4.54) are known, this equation can be solved to find the composition of P and A groups ($x_p = 1 - x_A$). Given the composition of each group, MW_A can then be found using the following equation:

$$MW_{SCN} = x_p MW_p + x_A MW_A \quad (4.56)$$

which can later be used in calculation of the specific gravity of the aromatic group, SG_A .

In our calculations, instead of applying this methodology to each SCN group and lumping them together to find the final pseudo-components parameters, we used the weighted average T_b (eq. (4.57)) for each pseudo-component and found m , $m\varepsilon/k$, $m\sigma^3$ for the pseudo-components directly using $T_{b,pseudo}$ instead of T_b in the eqs. (4.50)–(4.53). In other words, we found the PC-SAFT parameters after lumping the SCN fractions into fewer pseudo-components.

$$T_{b,pseudo} = \frac{\sum_i x_i MW_i T_{b,i}}{\sum_i x_i MW_i} \quad (4.57)$$

In addition, we further regressed the coefficients in eq. (4.51) using the PVT database to minimize the deviation in saturation pressure, density and STO density. To reduce the number of tuned coefficients from three to two, we included T_b of benzene in eq. (4.51) and fixed the last coefficient to make sure the new correlation would reproduce the correct value of $m\varepsilon/k$ for benzene, which is the lightest aromatic compound in our representative aromatic group. As a result, we only tuned the first two coefficients in eq. (4.51). The final set of correlations for m , $m\varepsilon/k$, $m\sigma^3$ is given by

$$m_A = 5.98957 \times 10^{-6} \times T_b^2 + 2.44045 \times 10^{-3} \times T_b + 0.807171 \quad (4.58)$$

$$(m\varepsilon/k)_A = 1.7044 \times 10^{-3} \times (T_b - T_{b,benzene})^2 + 3.3024 \times (T_b - T_{b,benzene}) + 711.6350 \quad (4.59)$$

$$(m\sigma^3)_A = 4.92174 \times 10^{-4} \times T_b^2 + 0.0938404 \times T_b + 30.1198 \quad (4.60)$$

The calculation results using the new PNA approach with only two representative groups (P and A) together with other EoSs are presented in Table 4.4.

4.9 C₇₊ Characterization using More Detailed Analytical Information

The characterization methods discussed in sections 4.3–4.8 are based on the typical compositional input as outlined in Table 4.2. Modern analytical methods can provide more detailed analytical information (Table 4.1) which can be potentially utilized in characterization. Here we presents a preliminary attempt to utilize some of the additional information from the modern analytical data. The purpose is to establish a

simple procedure that can account for the uncertainty in molecular weights, specific gravities and the additional information on the proportion of paraffins in SCN components. The simple procedure can then be used to estimate the impact of the detailed compositional information on PVT modeling.

We have used the method proposed by Pedersen et al. [15, 16] as the framework for the characterization. All the steps are similar to what is presented in section 4.2 with this difference that the wt% (fractions) are used instead of the mole fractions in the initial input file which are converted to mole fractions using MW . In addition, the new algorithm allows for dividing each SCN into two subgroups of Paraffinic and Aromatic compounds. As a result, if the PA distribution for an oil sample is available (e.g. from analyzing the SimDist or GC×GC results), it is possible to include this information in the calculations. Furthermore, it is possible to either use MW and SG from Katz and Firoozabadi table or from experimental measurements (e.g. TBP distillation) if available.

The input information for the modified characterization method is as follows:

1. Wt% (fraction) of all non-hydrocarbon and hydrocarbons up to C₆. The MW and SG of these components are already known (e.g. from DIPPR database) and do not need to be entered.
2. Wt% (fraction) of SCNs from C₆ up to C_{*n*}. In case the MW and SG of the SCN groups are available through TBP distillation and experiments, they can be entered in this step. Otherwise, the information is taken from the Katz and Firoozabadi table automatically by the code.
 - *Notice*: If the PA distribution is available for each SCN (wt% of the paraffinic and aromatic compounds in each SCN fraction), the wt% (fraction) of P and A groups can be used instead of the wt% (fraction) of the SCN. The MW and SG of the P and A groups would be found as it is described below.
3. Wt% (fraction) of the C_{*n*+} together with $MW_{C_{n+}}$ and $SG_{C_{n+}}$.
4. The desired number of final pseudo-components should also be defined.

If the PA distribution is not available, we can proceed with the characterization steps. We just need to convert the weight fractions to mole fractions. The mole fraction of component i in an N-component mixture is calculated as follows:

$$z_i = \frac{\frac{w_i}{MW_i}}{\sum_{j=1}^N \frac{w_j}{MW_j}} \quad (4.61)$$

We need some modifications in the characterization algorithm if the weight fractions of P and A groups (w_P and w_A) are known within each SCN (e.g. by analyzing the SimDist results as in section 4.1.3). The MW of the P group, which is in fact n-alkane, can be either read from DIPPR database or calculated using its chemical formula (C_nH_{2n+2}) as follows:

$$MW_P = 12.0107 \times n + 1.00794 \times (2n + 2) \quad (4.62)$$

where n is the carbon number of the SCN fraction, 12.0107 is the MW of carbon atom and 1.00794 is the MW of Hydrogen.

SG of the P group is calculated using Soave's correlation (eq. (4.30)). As the MW_{SCN} and SG_{SCN} are known either from measurements or Katz and Firoozabadi table, we can calculate the MW and SG for the A group using the following equations. For SG_A we have:

$$\frac{w_{SCN}}{SG_{SCN}} = \sum \frac{w_i}{SG_i} = \frac{w_P}{SG_P} + \frac{w_A}{SG_A} \Rightarrow SG_A = w_A \left(\frac{w_{SCN}}{SG_{SCN}} - \frac{w_P}{SG_P} \right)^{-1} \quad (4.63)$$

where $w_{SCN} = w_P + w_A$ and SG_P is calculated using eq. (4.30). For MW_A :

$$\frac{w_{SCN}}{MW_{SCN}} = \sum \frac{w_i}{MW_i} = \frac{w_P}{MW_P} + \frac{w_A}{MW_A} \Rightarrow MW_A = w_A \left(\frac{w_{SCN}}{MW_{SCN}} - \frac{w_P}{MW_P} \right)^{-1} \quad (4.64)$$

and MW_P is calculated using eq. (4.62).

Having the MW for both P and A groups, we can calculate their mole fractions and proceed with the characterization steps. The only modification would be in the parameter estimation step (second step of the characterization) where we need to distinguish between the correlations used for the P and A groups. As we use correlations based on T_b and SG for calculation of model parameters for different EoSs, for the P group we need to use T_b of n-alkane from DIPPR database together with SG_P calculated from eq. (4.30), and for the A group we use T_b of the SCN fraction from Katz and Firoozabadi table together with SG_A calculated from eq. (4.63). The rest of the calculations are the same as before. The application of the new characterization algorithm for an oil sample is presented in section 4.10.4.

4.10 Results and Discussions

4.10.1 Petroleum Fluid Database

In order to investigate and compare the overall performance of different EoSs and different characterization methods in PVT modeling, a petroleum fluids database covering wide composition, temperature and pressure ranges is needed. In this work, 260 petroleum fluids have been collected from different sources in the literature [128, 129], as well as from an internal PVT database [130]. An overview of these fluids including their methane and C_{7+} contents is given in Table B.1 in Appendix B. There are different types of petroleum fluids, from gas condensate to quite heavy oil. The database covers a wide range of methane content from 2.26% to 74.71% while the C_{7+} content changes from 6.39% to 83.21%. The range for the SG of C_{7+} is from 0.7597 to 0.9747, and maximum reservoir temperature and saturation pressure are 469.15 K and 427.96 bar, respectively. There are some fluids for which only the saturation pressure data is available [129]. However, various experimental data from different measurements, such as constant mass expansion (CME), differential liberation (DL), and/or separator test, are available for most of the fluids in this database. It should be noted that systems showing deviations larger than 20% in saturation pressure, density and/or STO density using all the EoSs tested were excluded from the final database. The large deviations could be due to poor quality of the data or the uniqueness of the system (being too heavy or too asymmetric) which may be better treated separately.

4.10.2 Deviations in Saturation Pressure, Density and STO Density

The percent average absolute deviations AAD% of saturation pressure, density, and STO density for the 260 petroleum fluids are listed in Table B.2 in Appendix B, where we have compared the performance of PC-SAFT EoS with Yan et al.'s characterization method [119] (eq. (4.31) and eqs. (4.34)–(4.35)) with SRK, PR, and Soave-BWR EoSs. STO density is also included in the evaluations. The critical properties for SRK, PR and Soave-BWR were calculated by the original Twu's method [113] (eqs. (A.13)–(A.16)) and the acentric factor was calculated from the Lee–Kesler correlation [114, 115] (eqs. (A.2)–(A.3)).

In order to compare the performance of the new general characterization method and several recent methods suggested for PC-SAFT [119, 120, 122], the global deviations in saturation pressure, density and STO density for all 260 fluids were evaluated (Table 4.4). The results from SRK, PR and Soave-BWR are also presented as references. Since volume translation is commonly used to improve the density calculation by cubic EoSs, we also included SRK and PR with volume translation in the comparison. Furthermore, Table 4.4 summarizes the performance of the new general characterization method for SRK and PR with/without volume translation and the new PNA approach for PC-SAFT. The binary interaction parameters for all the cases are taken from Section 3.2 except for the characterization method suggested by Liang et al. [120] for which the k_{ij} values are taken from Liang et al. [118]. The detailed AAD% of saturation pressure, density and STO density using the new general characterization for PC-SAFT together with SRK and PR with volume translation are listed in Table B.3 in Appendix B.

Table 4.4 Summary of AAD% and maximum deviations in the calculated saturation pressures, reservoir fluid densities and STO densities using SRK, PR, Soave-BWR and PC-SAFT with different characterization methods.

EoS	Saturation Pressure		Density		STO Density	
	AAD%	Max. Dev.	AAD%	Max. Dev.	AAD%	Max. Dev.
SRK	6.35	21.84	12.62	25.60	16.49	27.11
PR	6.26	22.36	3.95	16.94	6.76	18.61
SRK-VT	6.35	21.84	1.63	7.70	0.66	2.67
PR-VT	6.26	22.36	1.55	7.42	0.80	2.83
Soave-BWR	6.72	31.27	4.46	26.20	6.45	23.52
PC-SAFT Yan et al. [119] ↔(eq. (4.31) and eqs. (4.34)–(4.35))	7.36	28.73	2.82	9.39	2.03	7.41
PC-SAFT Liang et al. [120]	7.84	42.84	2.71	9.11	2.67	15.57
PC-SAFT Assareh et al. [122]	7.45	37.54	2.00	8.25	1.87	4.16
SRK New Char. - eq. (4.43)	5.83	27.27	12.18	26.43	16.37	27.96
SRK New Char. - eqs. (4.44)–(4.45)	5.76	27.65	10.92	25.08	14.88	26.56
SRK New Char. - eqs. (4.44)–(4.45) – With VT	5.76	27.65	1.67	6.08	0.79	2.68
PR New Char. - eq. (4.46)	6.01	29.53	3.92	15.68	4.77	20.88
PR New Char. - eqs. (4.47)–(4.48)	5.75	27.33	3.92	16.02	5.01	20.65
PR New Char. - eqs. (4.47)–(4.48) – With VT	5.75	27.33	1.66	6.67	0.91	2.92
PC-SAFT New PNA Method - eqs. (4.58)–(4.60)	9.40	26.76	1.64	7.33	0.77	3.07
PC-SAFT New Char. - eq. (4.38)	6.50	23.99	2.36	7.92	1.75	6.79
PC-SAFT New Char. - eqs. (4.39)–(4.40)	6.51	24.08	1.73	7.73	0.86	2.98

Comparison between cubic EoSs without volume translation and non-cubic EoSs shows that all previous versions of PC-SAFT [119, 120, 122] have better performance than SRK, PR, and Soave-BWR in density and stock tank oil density while the cubic ones give slightly lower deviation in saturation pressure. Using volume translation for cubics improves the density and STO density predictions. The change in deviation of density calculation is more significant for SRK than for PR.

Among the existing characterization methods for PC-SAFT tested here, Yan et al.'s method [119] (eqs. (4.34)–(4.35)) gives the smallest AAD% and maximum deviation in saturation pressure while Assareh et al. [122] method has better performance in density and STO density calculations.

The application of the new general characterization method to SRK and PR (eqs. (4.43)–(4.48)) yields lower deviation in all three properties than SRK and PR with the classical characterization. Actually, the new characterization method for cubics gives the lowest deviation in saturation pressure among all the combinations of EoSs and characterization methods studied in Table 4.4. However, the deviation in density and STO density for SRK and PR with the new general characterization method is still higher than SRK and PR with the classical characterization and volume translation. Applying volume translation to SRK and PR with the new characterization method further reduces deviations in density and STO density.

Applying the new PNA characterization approach to PC-SAFT gives lower deviation in density and STO density than the previous characterization methods for this EoS. However, the deviation in saturation pressure is poorer than the other models.

Applying the new characterization method developed in this study to Yan et al.'s [119] correlations (eqs. (4.34)–(4.35)), yields lower deviations in all three properties. Regressing the coefficient in the equation for ε (eq. (4.38)) mainly influences the saturation pressure deviation while the deviations in density and STO density reduce slightly. Regressing all three coefficients at the same time (eqs. (4.39)–(4.40)) gives even lower deviations in density and STO density but the deviation in saturation pressure slightly increases. In both regression cases, the deviation in saturation pressure is the lowest among the deviations calculated by the previous characterization methods for PC-SAFT and is very close to that of cubic EoSs. For the case where all the three coefficients are regressed, both the average and maximum deviation in density and STO density are very close to that of SRK and PR with volume translation.

In terms of maximum deviation, PC-SAFT with the new characterization method has a slightly higher maximum deviation for saturation pressure than the cubic models. However, it gives the lowest deviation in saturation pressure, density and STO density calculation among other characterization methods for PC-SAFT.

The sensitivity of PC-SAFT to binary interaction parameters (k_{ij}) in calculation of saturation pressure and vapor phase composition was investigated in Section 3.2. It was shown that although PC-SAFT gives small absolute average k_{ij} values, it is more

sensitive to the change in k_{ij} . Sensitivity to k_{ij} is a possible reason for the large deviations of PC-SAFT when applied to PVT calculation. The general characterization method does not include k_{ij} in the tuning process. Including k_{ij} in the future tuning as an additional parameter could improve the PVT calculation results. Knowing the k_{ij} for the binary mixtures of $C_1/N_2/CO_2$ and C_{7+} is difficult and cannot be completely reflected by the binary VLE systems that we know so far. Use of a large PVT database can make up for this defect.

In summary, application of the proposed general characterization method to PC-SAFT makes this model superior to the previous PC-SAFT characterization methods and gives the smallest AAD% and maximum deviation for all three properties. Furthermore, application of the new characterization method to the cubic EoSs yields better performance in saturation pressure calculation in comparison to the original SRK and PR. Using volume translation together with the new characterization approach for SRK and PR gives comparable results for density and STO density to that of SRK and PR with volume translation.

4.10.3 Simulation of DL and CME Tests

The accuracy of the general characterization method for PC-SAFT is tested against the other three characterization methods for PC-SAFT in calculation of oil density, gas compressibility factor, oil formation volume factor, solution gas-oil ratio and compressibility of an oil sample from the book of Pedersen and Christensen [87]. The composition and experimental data for the Constant Mass Expansion (CME) and Differential Liberation (DL) tests can be found in Tables 3.7, 3.6 and 3.12 of Pedersen and Christensen's book [87]. This fluid was not used in our regression and the presented results are pure predictions.

Table 4.5 summarizes the AAD% in calculation of different properties for this oil mixture. It can be seen that PC-SAFT with the new general characterization approach gives the lowest deviation in saturation pressure and density while Soave-BWR gives the lowest deviation in STO density. Yan et al.'s [119] method has better performance in calculation of STO density among other PC-SAFT characterization methods.

For the gas compressibility factor, PR with volume translation gives the lowest deviation. Among non-cubic models, Soave-BWR has better performance and PC-SAFT gives the highest deviation for this property.

Table 4.5 AAD% in calculated saturation pressure, density, STO density and other properties of the oil from [87] using SRK, PR, Soave-BWR and PC-SAFT EoS with different characterization methods.

EoS	Saturation Pressure	Density	STO Density	Gas Z Factor	B_o	R_s	Compressibility	Relative Volume
SRK	8.07	16.50	21.40	2.63	3.15	14.49	25.56	2.73
PR	9.51	6.85	12.04	1.52	2.70	4.67	21.02	2.10
SRK-VT	8.07	1.18	1.51	1.93	3.45	8.14	9.33	1.95
PR-VT	9.51	1.37	1.74	0.50	3.70	8.73	15.44	2.01
Soave-BWR	3.23	3.47	0.33	1.36	7.70	7.43	9.14	1.41
PC-SAFT Yan et al. [119]	2.01	0.67	0.93	2.62	1.49	5.20	4.28	1.27
PC-SAFT Liang et al. [120]	3.53	0.62	2.41	2.68	2.70	6.48	2.65	1.35
PC-SAFT Assareh et al. [122]	2.94	1.18	3.12	2.43	0.75	3.05	3.69	1.18
PC-SAFT New Char. - eqs. (4.39)–(4.40)	1.69	0.35	1.85	2.57	2.12	6.60	3.21	1.13

PC-SAFT with Assareh et al.'s characterization method [122] seems to give the lowest deviation in calculation of Oil Formation Volume Factor (B_o) and solution gas-oil ratio (R_s), while Liang et al.'s method [120] gives the lowest deviation in calculation of compressibility. Our new characterization method for PC-SAFT gives slightly higher deviation in compressibility compared to Liang et al.'s method. For relative volume, the non-cubic models including Soave-BWR seem to have better performance in comparison to the cubic models.

Figures 4.13–4.18 show the simulated DL results for the oil mixture from Pedersen and Christensen's book [87] using SRK and PR with and without volume translation, as well as Soave-BWR, and PC-SAFT with different characterization methods. It can be seen from Figure 4.13 (a) that SRK and PR under predict the density over the whole pressure range while PC-SAFT with the new characterization method gives the lowest deviation and almost a good match of the experimental data at all pressures. Using volume translation, improves the density prediction of cubic models, however, the final results are not as good as the PC-SAFT prediction.

Figure 4.13 (b) illustrates the density prediction results using different characterization methods for PC-SAFT where our developed method gives the lowest deviation especially at higher pressures.

Figure 4.14 presents the results for the gas compressibility factor. In general, it seems all the models have some deficiencies in calculation of Z factor especially at higher pressures. PR with volume translation gives the closest predictions to the experimental data. All the characterization methods for PC-SAFT give more or less similar predictions, while Assareh et al.'s method is slightly better than the rest of PC-SAFT characterization methods.

The simulated Oil Formation Volume Factors (B_o) are compared with the experimental data in Figure 4.15. The results show that our characterization method for PC-SAFT

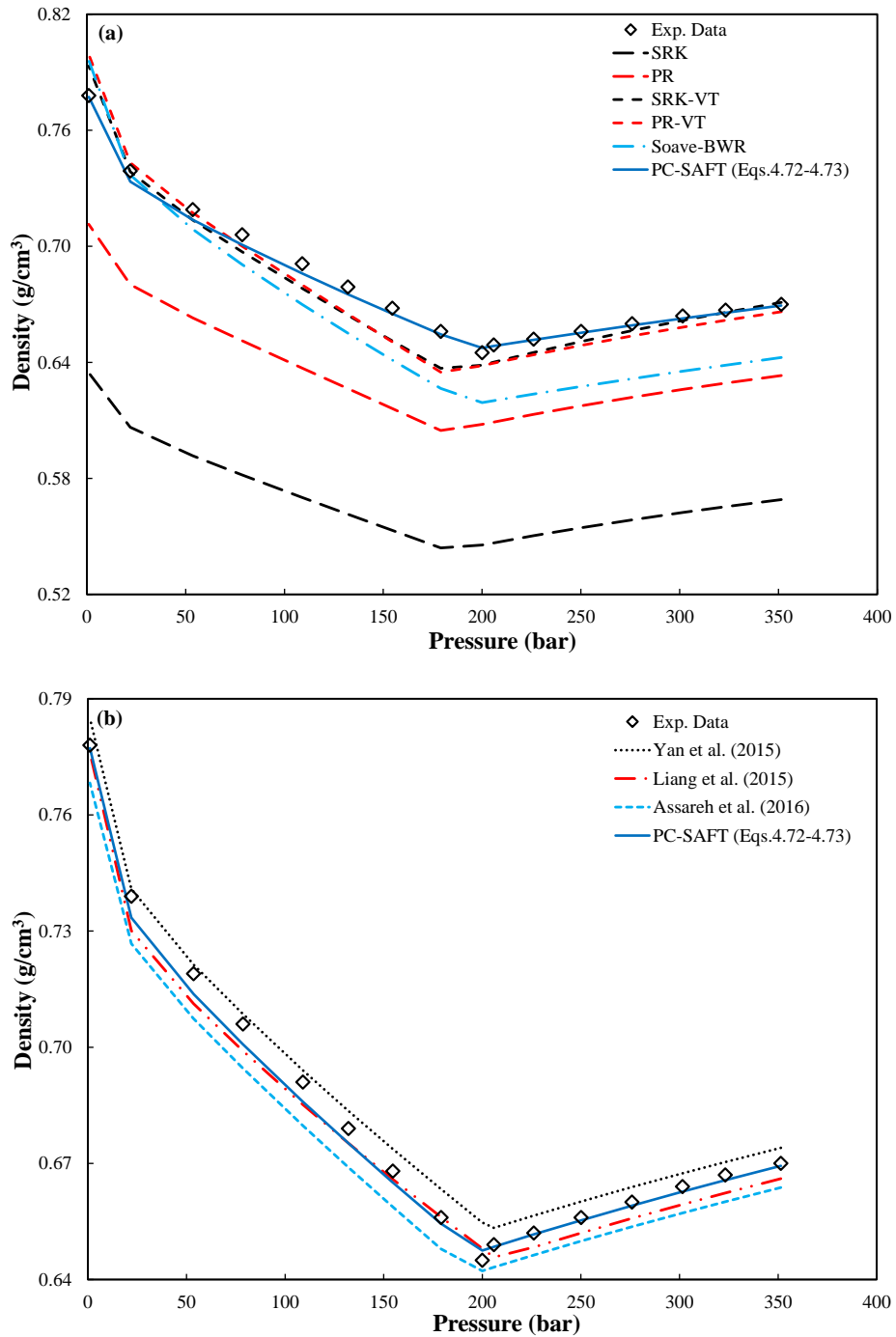


Figure 4.13 Density vs. pressure for the oil mixture from [87] - a) Comparison between cubics with and without volume translation and non-cubic models including PC-SAFT with the new general characterization method, b) Comparison between different characterization methods for PC-SAFT.

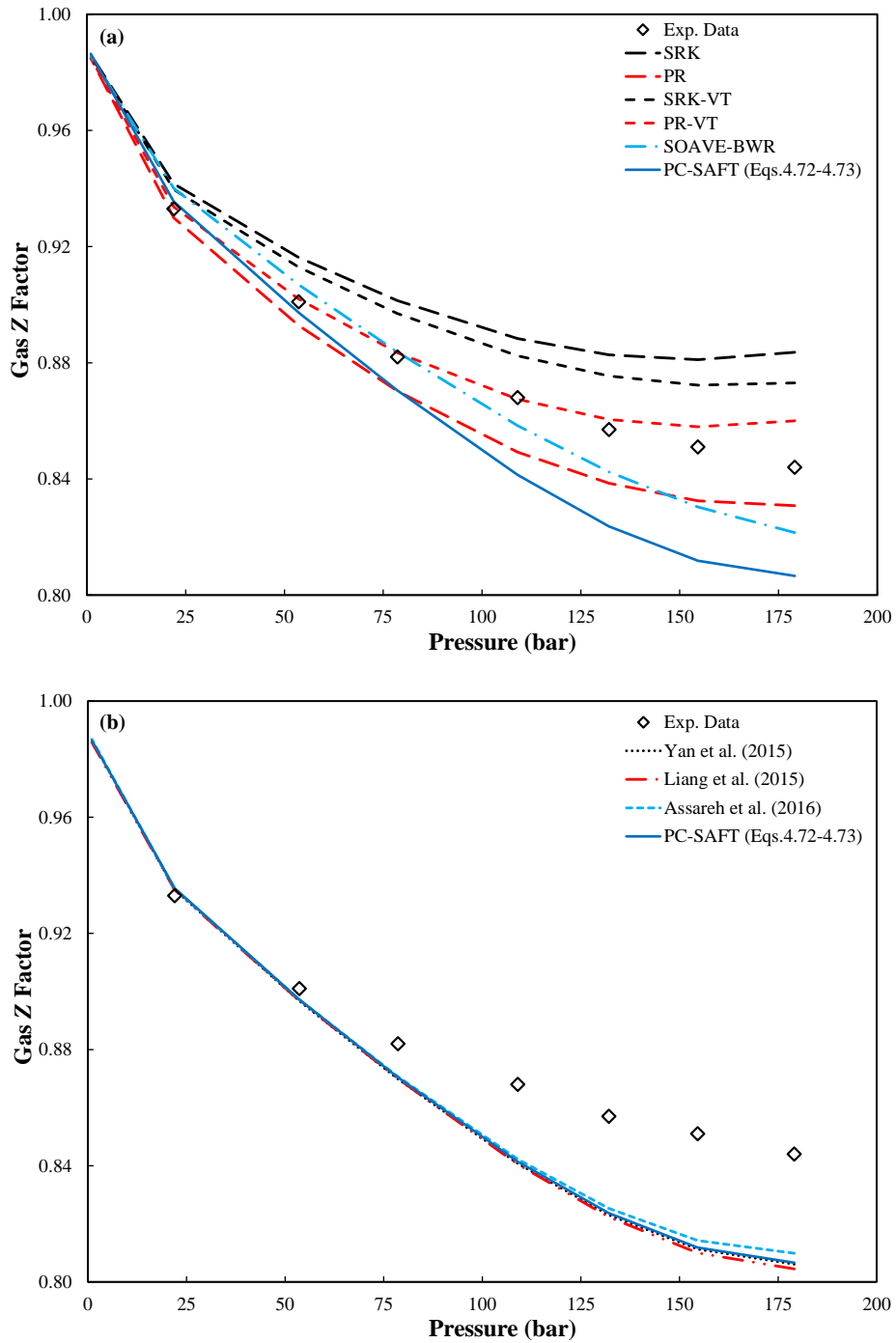


Figure 4.14 Gas compressibility factor vs. pressure for the oil mixture from [87] - a) Comparison between cubics with and without volume translation and non-cubic models including PC-SAFT with the new general characterization method, b) Comparison between different characterization methods for PC-SAFT.

gives better prediction of B_o than cubics and Soave-BWR in the whole pressure range. SRK and PR without volume translation under predict B_o especially at higher pressures, while using volume translation yields over prediction of the experimental data. PC-SAFT with Assareh et al.'s characterization method [122] seems to give the lowest deviation in calculation of Oil Formation Volume Factor (B_o) as can be seen in Figure 4.15 (b). This trend is also observed in Figure 4.16 where R_s is plotted against pressure. For most of the reservoir fluids in the database it was noticed that using volume translation for cubics might improve the prediction of B_o and R_s for pressures below the saturation pressure, however, it makes the predictions worse for higher pressures. In general, it would be difficult to get accurate prediction of B_o and R_s in the whole pressure range using cubic EoSs either with or without volume translation.

Oil compressibility is one of the important properties in HPHT reservoirs as expansion of the reservoir fluid is the main production mechanism from these types of reservoirs. Therefore, accurate prediction of this property is of great importance. Figure 4.17 shows the compressibility calculation above saturation pressure for the oil mixture from [87]. Our proposed characterization method for PC-SAFT gives slightly higher deviation in compressibility compared to Liang et al.'s method (Figure 4.17 (b)). In general, PC-SAFT gives the lowest deviation in compressibility compared to the cubic EoSs and Soave-BWR, and predicts this property almost accurately in the whole pressure range. The cubic models over predict the compressibility even after using volume translation while Soave-BWR seems to give the correct slope for the experimental data. Although, the deviation is larger at lower pressures, the cubics seem to give better prediction of compressibility at higher pressures.

As another example and for slightly heavier reservoir fluid, the compressibility calculation results for reservoir fluid 73 from the database are presented in Figure 4.18. The results show almost similar trend as in Figure 4.17.

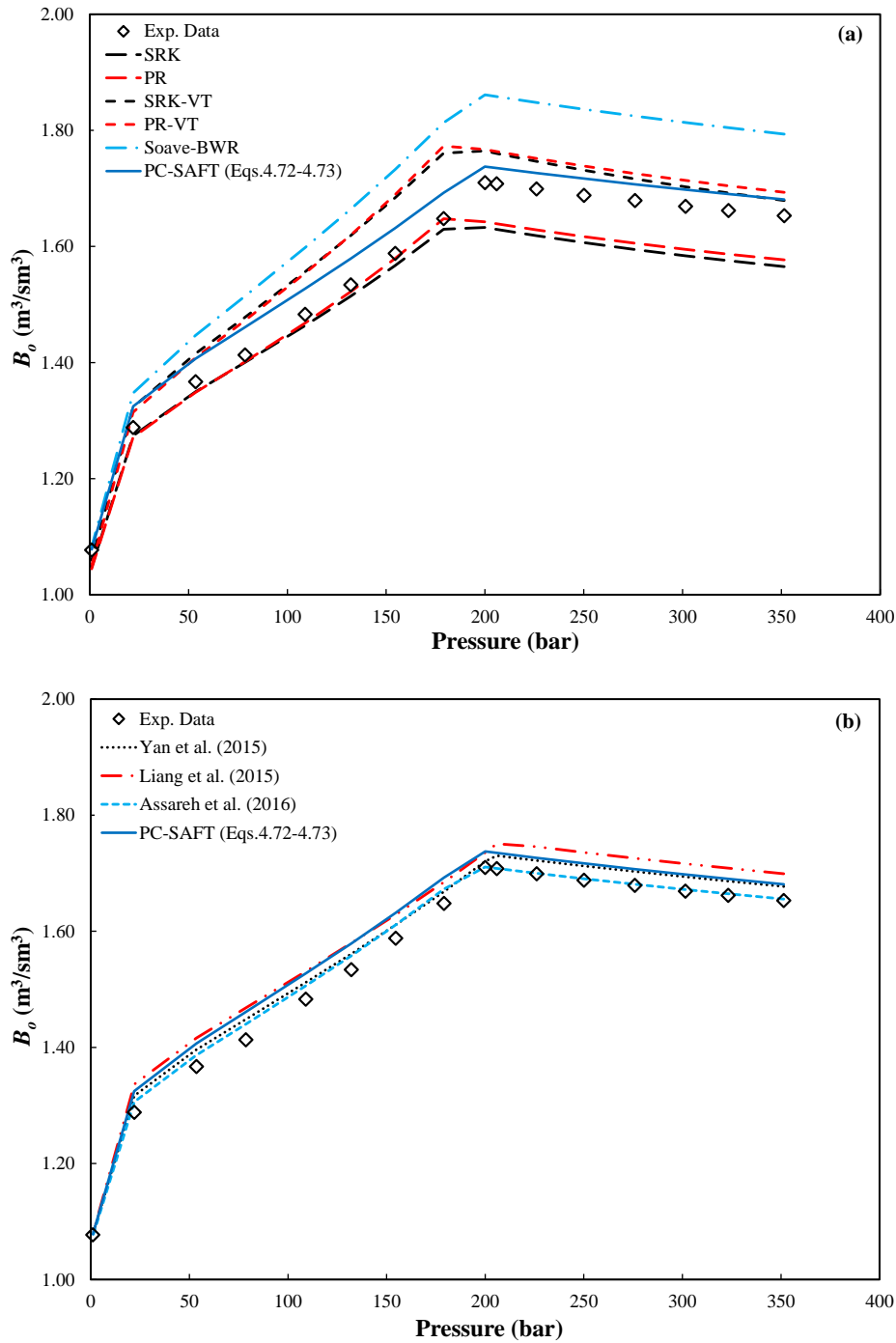


Figure 4.15 Oil formation volume factor vs. pressure for the oil mixture from [87] - a) Comparison between cubics with and without volume translation and non-cubic models including PC-SAFT with the new general characterization method, b) Comparison between different characterization methods for PC-SAFT.

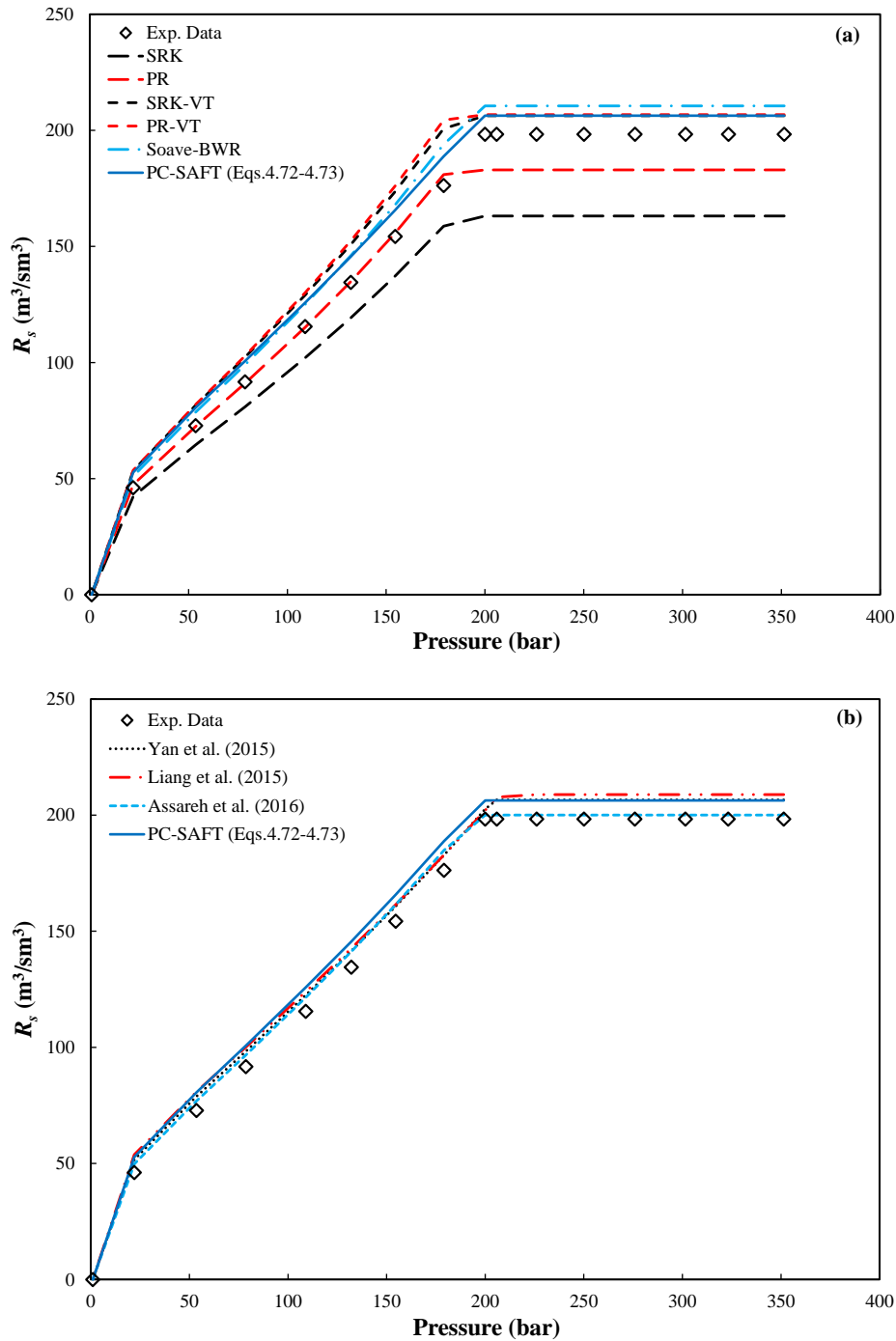


Figure 4.16 Solution gas-oil ratio vs. pressure for the oil mixture from [87] - a) Comparison between cubics with and without volume translation and non-cubic models including PC-SAFT with the new general characterization method, b) Comparison between different characterization methods for PC-SAFT.

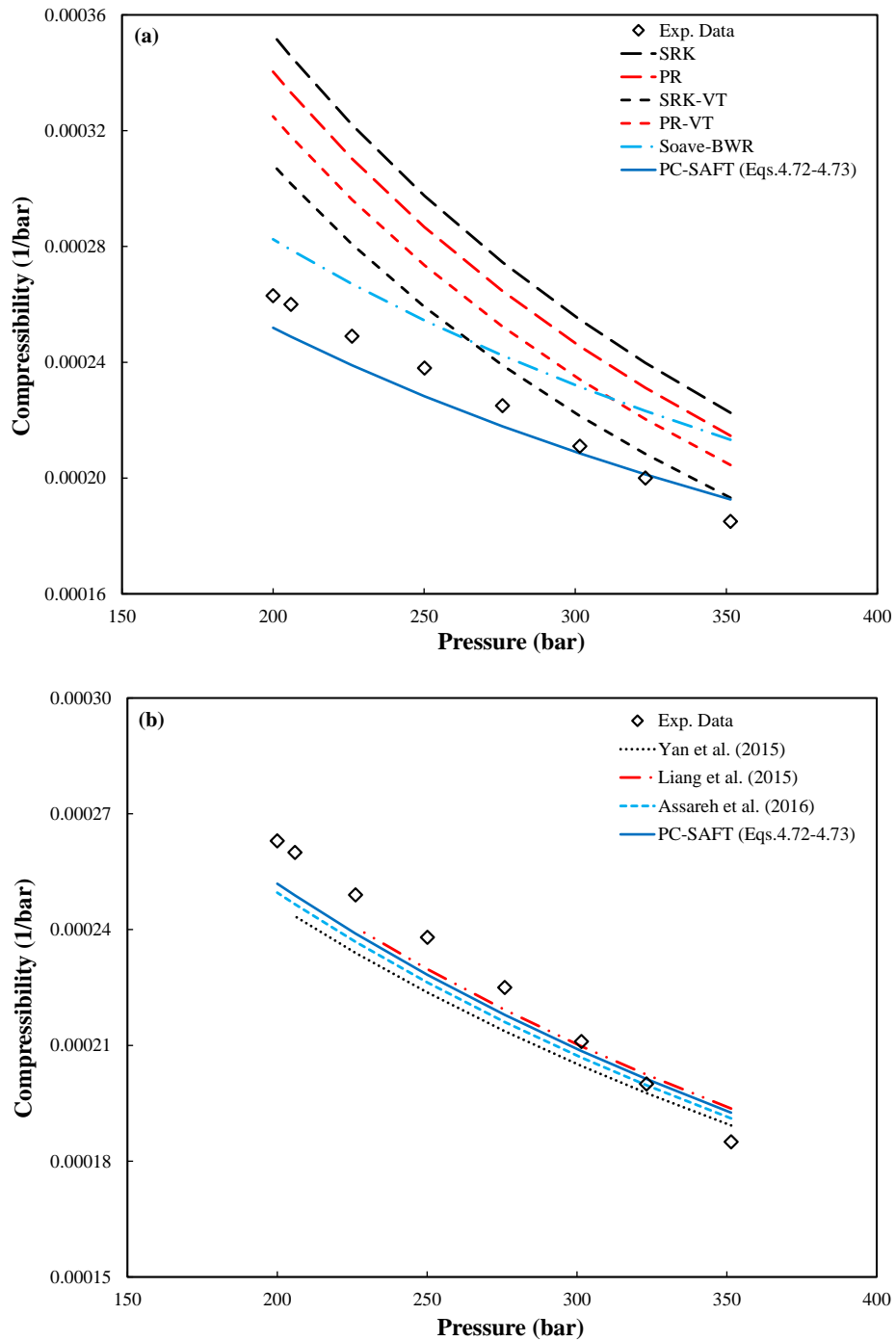


Figure 4.17 Oil compressibility vs. pressure for the oil mixture from [87] - a) Comparison between cubics with and without volume translation and non-cubic models including PC-SAFT with the new general characterization method, b) Comparison between different characterization methods for PC-SAFT.

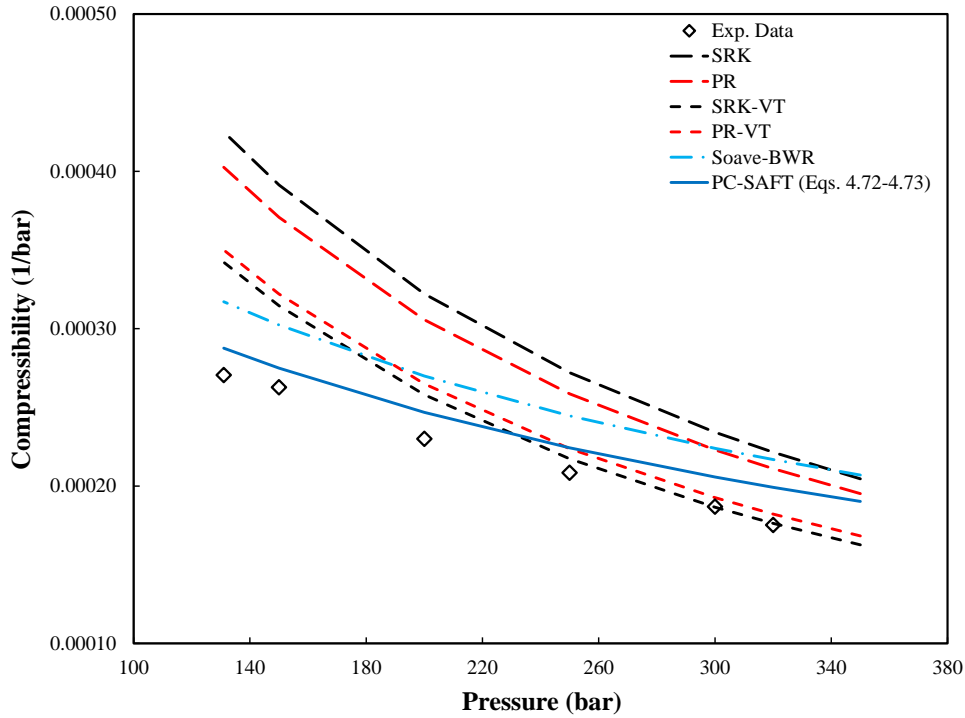


Figure 4.18 Oil compressibility vs. pressure for fluid 73 from the database - Comparison between cubics with and without volume translation and non-cubic models including PC-SAFT with the new general characterization method.

The experimental compressibility data was not available for most of the fluids in the database. As a result, to get a better overview of the performance of cubic and non-cubic models for calculation of compressibility, we calculated this property using the density data above saturation pressure. We used a polynomial to fit the density data in order to calculate its slope with pressure. The compressibility was then calculated using the following equation:

$$\beta = \frac{1}{\rho} \left(\frac{\partial \rho}{\partial P} \right)_T \quad (4.65)$$

Table 4.6 summarizes the AAD% in compressibility of all the 260 reservoir fluids in the database using SRK and PR (with/without volume translation), Soave-BWR and PC-SAFT with different characterization methods. The detailed calculation results can be found in Table B.4 in Appendix B. On average, SRK and PR give larger deviations than PC-SAFT and Soave-BWR, SRK being the poorest among all. However, using volume translation improves SRK and PR predictions and SRK with volume translation gives the lowest deviation. For the non-cubic models, Soave-BWR seems to be slightly better than PC-SAFT. Among different characterization methods for PC-SAFT, the method of Yan et al. [119] gives the lowest AAD% and maximum deviation.

Table 4.6 AAD% in calculated compressibility of all the reservoir fluids in the database using different EoSs.

EoS	Compressibility	
	AAD%	Max. Dev.
SRK	19.38	58.81
PR	16.28	48.30
SRK-VT	12.67	40.93
PR-VT	15.40	45.15
Soave-BWR	12.91	38.78
PC-SAFT Yan et al. [119]	12.97	40.77
PC-SAFT Liang et al. [120]	13.31	46.14
PC-SAFT Assareh et al. [122]	13.52	43.03
PC-SAFT New Char. - eqs. (4.39)–(4.40)	13.49	44.29

4.10.4 Impact of Compositional Characterization on PVT Modeling

Available Analytical Information for a Sample Crude Oil

To evaluate the impact of the compositional characterization, we used the available data for a light stock tank oil (high API gravity) from the Danish North Sea (DK oil sample) and investigated the effect of using analytical information in the characterization step on PVT modeling using SRK EoS. Both TBP distillation and SimDist results were available for this fluid. In addition, the *MW* and *SG* of each cut were measured during the TBP distillation test.

Figure 4.19 shows the simulated distillation results up to C_{40} for the DK oil sample. To get an estimation of the wt% of each SCN fraction, we need to know the retention time corresponding to the boiling point of each fraction. Figure 4.20 shows the simulated distillation results for the calibration mixture. From this figure we can find the retention (or elution) time for each fraction. For example, the retention time for C_5 fraction is 0.437 minutes, the retention time for the C_6 fraction is 0.689 minutes and so on so forth. The retention time for the missing n-alkanes (e.g. C_{13}) is found by interpolation. After analyzing the oil mixture under the same conditions as the calibration mixture, the resulting chromatogram is divided into discrete area slices using the information obtained from the calibration curve. The area under the curve for each fraction, divided by the total area under the curve gives an estimation of the wt% of that fraction in the oil sample. Sometimes it might be needed to shift the retention times slightly to get the desired peak for the n-alkane inside the corresponding SCN fraction.

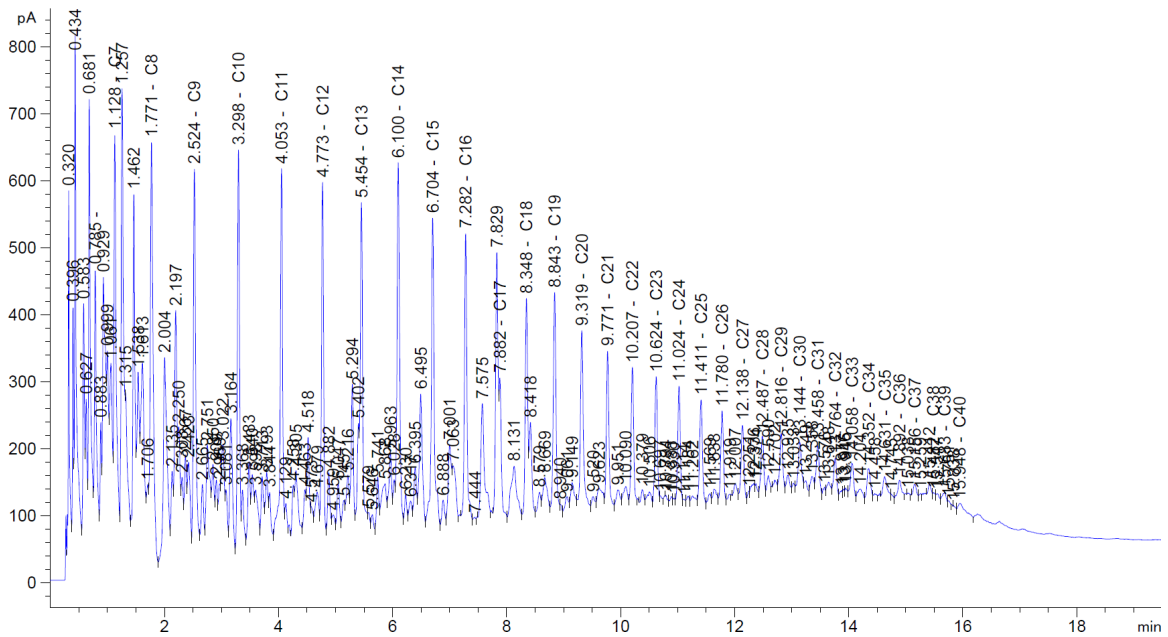


Figure 4.19 SimDist results for the light crude oil from the Danish North Sea (DK oil sample).

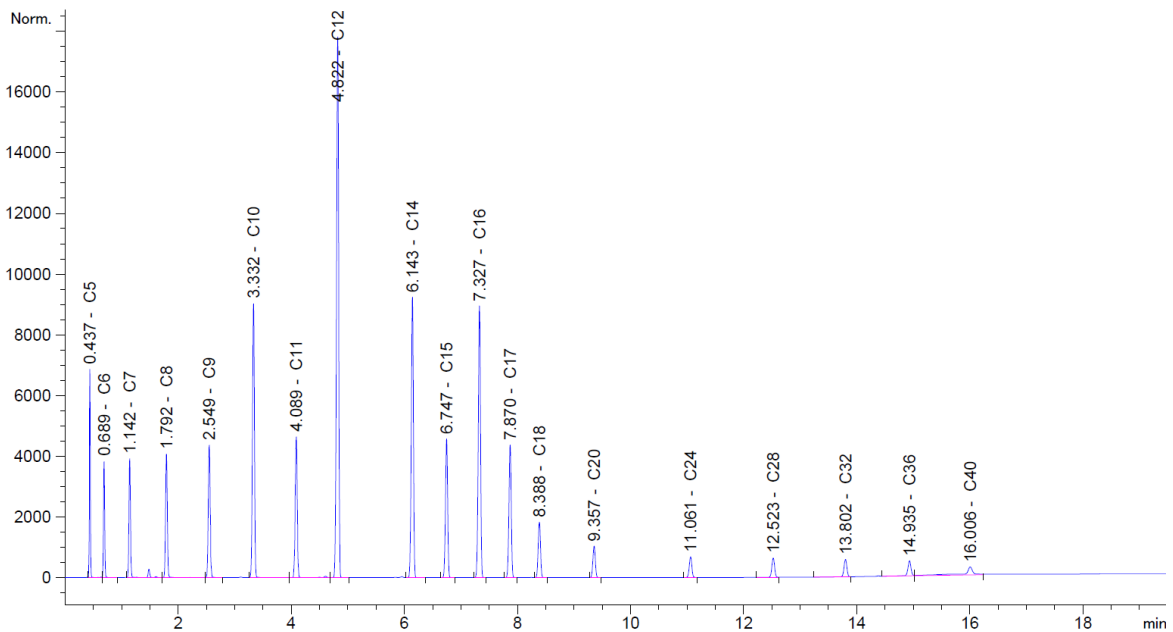


Figure 4.20 Simulated distillation calibration chromatogram.

Figure 4.21 shows how the SCN fractions are identified and separated based on the retention time of the n-alkane representative for the SCN fraction up to C₄₀, where the numbers between the dashed lines show the SCN number. The PA distribution can also be found from further analyzing the SimDist results. The wt% of the P group

in each fraction is found by calculating the area under the highest peak in each SCN fraction and dividing it by the total area of the fraction. The wt% of the A group is then calculated by subtracting the wt% of the P group from the wt% of the whole SCN. In other words, the area under the highest peak of each SCN is representative of the P group and the rest is assumed to be the A group. Figure 4.22 illustrates how the PA distribution is found for each of the SCN fractions of the DK oil sample. The area under the highest peak (amount of the P group) is highlighted with red color in this figure. It should be noted that for SCNs C_{13} , C_{17} and C_{18} the signals are modified slightly so that the highest peak is identified correctly. The PA distribution found using the proposed method is just an approximation of the real PA distribution. If the characterization results were sensitive to this additional information, other methods such as GC \times GC could be used for better estimation of the PIONA distribution in the oil sample.

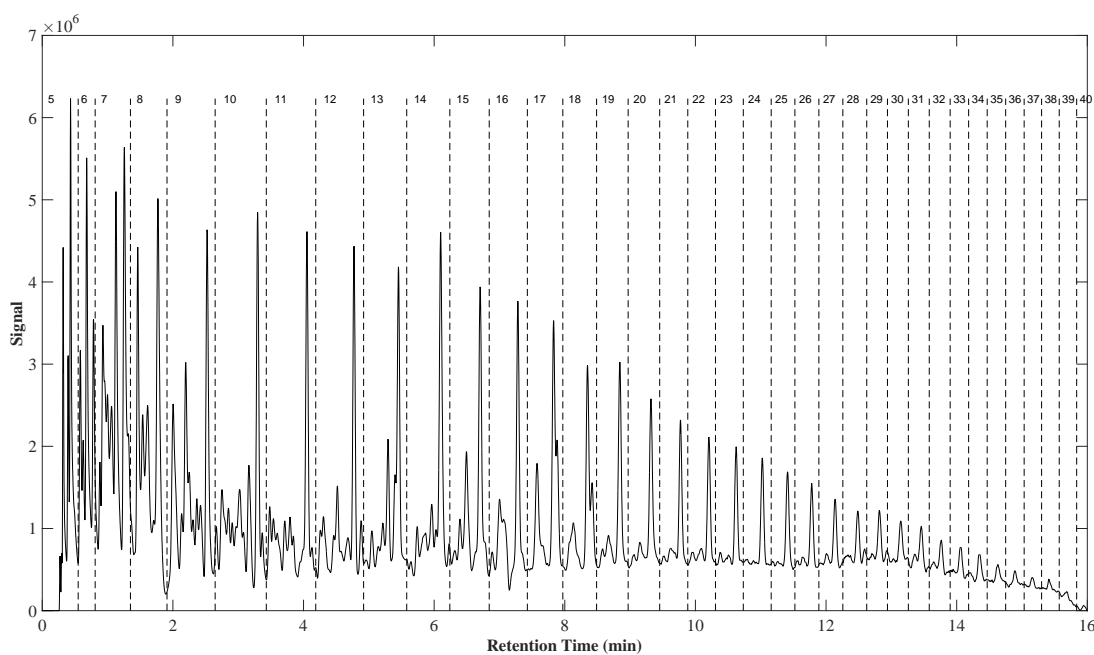


Figure 4.21 Simulated distillation for the DK oil sample up to C_{40} .

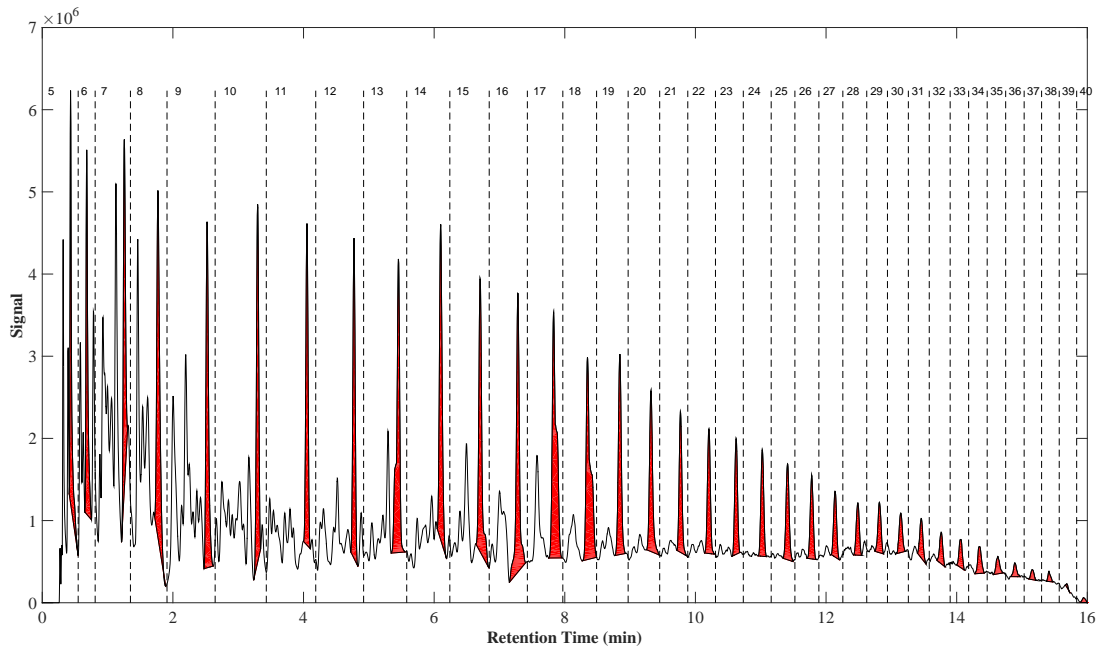


Figure 4.22 Isolating the paraffinic group within each SCN fraction for the DK oil sample.

Table 4.7 presents the wt% of the SCNs from C_6 up to C_{24+} using TBP distillation and SimDist analysis (with/without PA distribution). As can be seen, there is a slight difference between the results from TBP distillation and SimDist methods which is inevitable due to experimental limitations.

As the petroleum fluid sample tested was a dead oil, the compositional information for the lighter components (non-hydrocarbons and hydrocarbons up to C_5) was not available. In order to proceed with the characterization, we needed to assume the wt% of these light components. As a result, we considered two cases of low GOR and high GOR based on some typical black oil and gas condensate sample compositions and normalized the wt% of the SCN fractions to add up to 100. For the low GOR case, the summation of the wt% of the components up to nC_5 is considered to be around 20% and for the high GOR case, it is considered to be around 60%. The final composition of the components used in the characterization as well as the measured MW and SG of the SCNs and the plus fraction are presented in Table 4.8 and Table 4.9.

The MW and SG of the C_{24+} fraction were measured in the TBP distillation experiment, and found to be 362.39 g/gmol and 0.9250 respectively. However, these data are not usually available for the simulated distillation. In SimDist, we use the Katz and Firoozabadi table to have an estimation of MW and SG of SCN fractions and we need to back calculate the MW and SG of the plus fraction using the MW and SG of the

Table 4.7 Weight% of SCN fractions up to C₂₄₊ from TBP distillation and SimDist (with/without PA distribution) for the DK oil sample.

SCN	wt% (TBP)	wt% (SimDist)	wt% P in SCN (SimDist)	wt% A in SCN (SimDist)
C ₆	2.19	4.62	24.60	75.40
C ₇	3.68	5.02	12.73	87.27
C ₈	4.13	6.7	22.91	77.09
C ₉	4.21	4.99	19.85	80.15
C ₁₀	3.77	4.39	20.15	79.85
C ₁₁	3.31	3.87	21.42	78.58
C ₁₂	3.31	3.5	22.48	77.52
C ₁₃	3.63	3.98	28.21	71.79
C ₁₄	3.2	3.55	26.74	73.26
C ₁₅	3.52	3.55	27.55	72.45
C ₁₆	3.06	2.84	34.94	65.06
C ₁₇	3.31	3.19	36.04	63.96
C ₁₈	2.72	2.04	36.26	63.74
C ₁₉	1.13	2.94	28.95	71.05
C ₂₀	2.46	2.38	25.91	74.09
C ₂₁	2.23	1.96	23.24	76.76
C ₂₂	1.66	1.89	22.38	77.62
C ₂₃	2.04	1.74	21.03	78.97
C ₂₄₊	46.44	36.85	-	-
Sum	100	100	-	-

oil sample which is usually available. To find the MW and SG of the oil sample, we used the following equations where the wt% and experimental MW and SG of the SCNs heavier than C₆, measured in the TBP distillation, were used:

$$MW_{oil} = \frac{\sum_{i=C_6}^{C_{24+}} w_i}{\sum_{i=C_6}^{C_{24+}} \frac{w_i}{MW_i}}, \quad SG_{oil} = \frac{\sum_{i=C_6}^{C_{24+}} w_i}{\sum_{i=C_6}^{C_{24+}} \frac{w_i}{SG_i}} \quad (4.66)$$

MW_{oil} and SG_{oil} were then used in the following equations to back calculate the MW and SG of the C₂₄₊ fraction using MW and SG of the SCNs heavier than C₆ from Katz and Firoozabadi table. The calculated values for $MW_{C_{24+}}$ and $SG_{C_{24+}}$ together with the MW and SG from Katz and Firoozabadi table (MW^{KF} , SG^{KF}) are also presented in Table 4.8 and Table 4.9.

$$MW_{N+} = \frac{MW_{oil} w_{N+}}{1 - MW_{oil} \sum_{i=C_6}^{N-1} \frac{w_i}{MW_i}}, \quad SG_{N+} = \frac{SG_{oil} w_{N+}}{1 - SG_{oil} \sum_{i=C_6}^{N-1} \frac{w_i}{SG_i}}, \quad N = 24 \quad (4.67)$$

Table 4.8 Weight%, MW and SG of the components for the low GOR (Black Oil) case used in compositional characterization. For both TBP distillation and SimDist (with/without PA distribution).

Comp.	wt% (TBP)	wt% (SimDist)	wt% P in Oil (SimDist)	wt% A in Oil (SimDist)	MW^{Exp}	SG^{Exp}	MW^{KF}	SG^{KF}
N ₂	0.12	0.12	-	-	28.014	0.804	28.014	0.804
CO ₂	0.15	0.15	-	-	44.01	0.809	44.01	0.809
H ₂ S	0.00	0.00	-	-	-	-	-	-
C ₁	7.34	7.34	-	-	16.043	0.3	16.043	0.3
C ₂	2.60	2.60	-	-	30.07	0.356	30.07	0.356
C ₃	3.99	3.99	-	-	44.096	0.508	44.096	0.508
iC ₄	0.79	0.79	-	-	58.123	0.563	58.123	0.563
nC ₄	2.70	2.70	-	-	58.123	0.584	58.123	0.584
iC ₅	1.14	1.14	-	-	72.15	0.625	72.15	0.625
nC ₅	1.76	1.76	-	-	72.15	0.631	72.15	0.631
C ₆	1.74	3.67	0.90	2.77	86.18	0.6781	86.18	0.6850
C ₇	2.92	3.99	0.51	3.48	97.77	0.7360	96.00	0.7220
C ₈	3.28	5.32	1.22	4.10	105.10	0.7531	107.00	0.7450
C ₉	3.34	3.96	0.79	3.18	120.31	0.7722	121.00	0.7640
C ₁₀	2.99	3.49	0.70	2.78	130.47	0.7889	134.00	0.7780
C ₁₁	2.63	3.07	0.66	2.42	144.71	0.7951	147.00	0.7890
C ₁₂	2.63	2.78	0.62	2.15	157.51	0.8101	161.00	0.8000
C ₁₃	2.88	3.16	0.89	2.27	169.55	0.8185	175.00	0.8110
C ₁₄	2.54	2.82	0.75	2.07	175.31	0.8326	190.00	0.8220
C ₁₅	2.80	2.82	0.78	2.04	195.95	0.8340	206.00	0.8320
C ₁₆	2.43	2.26	0.79	1.47	215.86	0.8436	222.00	0.8390
C ₁₇	2.63	2.53	0.91	1.62	225.07	0.8437	237.00	0.8470
C ₁₈	2.16	1.62	0.59	1.03	245.64	0.8442	251.00	0.8520
C ₁₉	0.90	2.33	0.68	1.66	240.13	0.8591	263.00	0.8570
C ₂₀	1.95	1.89	0.49	1.40	258.43	0.8604	275.00	0.8620
C ₂₁	1.77	1.56	0.36	1.19	268.60	0.8611	291.00	0.8670
C ₂₂	1.32	1.50	0.34	1.17	274.00	0.8700	305.00	0.8720
C ₂₃	1.62	1.38	0.29	1.09	293.52	0.8811	318.00	0.8770
C ₂₄₊	36.88	29.26	-	-	362.39	0.9250	340.56	0.9324
Sum	100	100.00	-	-	-	-	-	-

A C₂₄₊ molecular weight of 765.5 was calculated from eq. (4.67), using the default molecular weights (MW^{KF}) and SimDist wt% in Table 4.8 for SCNs heavier than C₆. This plus molecular weight is more than 100% higher than the molecular weight of 362.39 directly measured on the TBP residue (or C₂₄₊ fraction). There is some

uncertainty on the calculated average molecular weight of the oil sample due to the uncertainty in the measured MW of the TBP residue. For a GC composition this uncertainty is transferred to the molecular weight of the plus fraction. The uncertainty on the molecular weight of the plus fraction of a composition determined by GC can be very high indeed and the reported plus molecular weight could be completely unrealistic.

Although wt% from SimDist should have been used for calculation of $MW_{C_{24+}}$ and $SG_{C_{24+}}$, due to the uncertainty in the MW of the TBP residue and as a result MW_{oil} , and somewhat large differences between wt% from TBP and wt% from SimDist for some of the SCN fractions, we used wt% of the components from TBP distillation to calculate $MW_{C_{24+}}$ and $SG_{C_{24+}}$ using Katz and Firoozabadi's MW and SG . Doing this, we found $MW_{C_{24+}}$ and $SG_{C_{24+}}$ to be close to the experimentally measured MW and SG for the plus fraction. However, it should be noticed that we may not necessarily get the same stock tank oil densities using experimental MW and SG , and default values (MW^{KF} and SG^{KG}).

A comparison of the C_7 – C_{23} molecular weights and densities from the TBP analysis with the default molecular weights and densities (Katz and Firoozabadi) reveals some differences especially for the molecular weights. As can be seen, the measured MW s are very close to the MW s from the Katz and Firoozabadi table for lighter SCNs and the difference becomes larger as the carbon number increases. For example the difference between the measured MW and Katz and Firoozabadi's MW is around 2–5 g/gmol for hydrocarbons up to C_{13} and the difference increases up to around 30 g/gmol for C_{22} . Despite the large differences in MW of the higher carbon number groups, the calculated mole percents do not seem to be very different when MW^{KF} or MW^{Exp} are used to convert wt% of TBP data to mole%, as can be seen in Figure 4.23 for the low GOR case. The largest deviation in the mole% is for the plus fraction where the difference between MW^{Exp} and MW^{KF} is relatively large. The mole% of the plus fraction using MW^{KF} is larger than the mole% calculated using MW^{Exp} , while it is not the case for SCNs from C_8 to C_{23} . The difference in the mole% of the heavier SCNs leads to the difference in the phase envelopes especially in the dew curve part as would be discussed later in this section.

Table 4.9 Weight%, *MW* and *SG* of the components for the high GOR (Gas Condensate) case used in compositional characterization. For both TBP distillation and SimDist (with/without PA distribution).

Comp.	wt% (TBP)	wt% (SimDist)	wt% P in Oil (SimDist)	wt% A in Oil (SimDist)	MW^{Exp}	SG^{Exp}	MW^{KF}	SG^{KF}
N ₂	0.37	0.37	-	-	28.014	0.804	28.014	0.804
CO ₂	0.45	0.45	-	-	44.01	0.809	44.01	0.809
H ₂ S	0.00	0.00	-	-	-	-	-	-
C ₁	22.00	22.00	-	-	16.043	0.3	16.043	0.3
C ₂	7.81	7.81	-	-	30.07	0.356	30.07	0.356
C ₃	11.21	11.21	-	-	44.096	0.508	44.096	0.508
iC ₄	2.38	2.38	-	-	58.123	0.563	58.123	0.563
nC ₄	7.09	7.09	-	-	58.123	0.584	58.123	0.584
iC ₅	3.42	3.42	-	-	72.15	0.625	72.15	0.625
nC ₅	5.29	5.29	-	-	72.15	0.631	72.15	0.631
C ₆	0.88	1.85	0.45	1.39	86.18	0.6781	86.18	0.6850
C ₇	1.47	2.01	0.26	1.75	97.77	0.7360	96.00	0.7220
C ₈	1.65	2.68	0.61	2.06	105.10	0.7531	107.00	0.7450
C ₉	1.68	2.00	0.40	1.60	120.31	0.7722	121.00	0.7640
C ₁₀	1.51	1.76	0.35	1.40	130.47	0.7889	134.00	0.7780
C ₁₁	1.32	1.55	0.33	1.22	144.71	0.7951	147.00	0.7890
C ₁₂	1.32	1.40	0.31	1.08	157.51	0.8101	161.00	0.8000
C ₁₃	1.45	1.59	0.45	1.14	169.55	0.8185	175.00	0.8110
C ₁₄	1.28	1.42	0.38	1.04	175.31	0.8326	190.00	0.8220
C ₁₅	1.41	1.42	0.39	1.03	195.95	0.8340	206.00	0.8320
C ₁₆	1.22	1.14	0.40	0.74	215.86	0.8436	222.00	0.8390
C ₁₇	1.32	1.28	0.46	0.82	225.07	0.8437	237.00	0.8470
C ₁₈	1.09	0.82	0.30	0.52	245.64	0.8442	251.00	0.8520
C ₁₉	0.45	1.18	0.34	0.84	240.13	0.8591	263.00	0.8570
C ₂₀	0.98	0.95	0.25	0.70	258.43	0.8604	275.00	0.8620
C ₂₁	0.89	0.78	0.18	0.60	268.60	0.8611	291.00	0.8670
C ₂₂	0.66	0.76	0.17	0.59	274.00	0.8700	305.00	0.8720
C ₂₃	0.82	0.70	0.15	0.55	293.52	0.8811	318.00	0.8770
C ₂₄₊	18.57	14.73	-	-	362.39	0.9250	340.56	0.9324
Sum	100	100.00	-	-	-	-	-	-

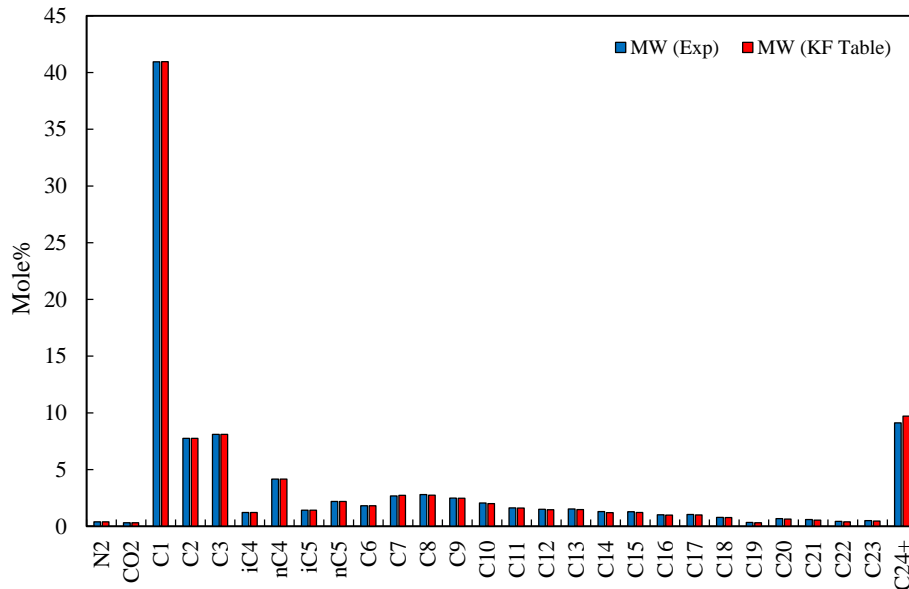


Figure 4.23 Mole% of the sample black oil calculated from wt% of TBP distillation using MW^{Exp} and MW^{KF} .

The Impact of Compositional Characterization on PVT Modeling

Using the information provided in Table 4.8 and Table 4.9, different scenarios were defined based on the following inputs:

1. TBP wt% with MW^{KF} and SG^{KF}
2. TBP wt% with MW^{Exp} and SG^{Exp}
3. SimDist wt% with MW^{KF} and SG^{KF}
4. SimDist wt% with MW^{Exp} and SG^{Exp}
5. SimDist (with PA) wt% with MW^{KF} and SG^{KF}
6. SimDist (with PA) wt% with MW^{Exp} and SG^{Exp}

For the above cases, the effect of compositional characterization on PVT modeling was studied using the SRK EoS and a comparison was made between the modeling results to investigate the effect of different parameters (e.g. experimental MW and MW from Katz and Firoozabadi table, PA distribution, etc.) on phase envelope and density calculations.

Figure 4.24 shows the phase envelope calculations for the black oil and gas condensate samples for cases 1 and 2, where TBP distillation data with MW^{Exp} (black lines)

and MW^{KF} (red lines) are used. As it was mentioned earlier, the difference between mole fractions calculated by MW^{Exp} and MW^{KF} was not significant for the light components and hydrocarbons up to C_7 , and it increased for the heavier SCNs. As the heavier components mainly control the dew curve part of the phase envelope, we see some deviations at higher temperatures for cases 1 and 2 for both the black oil and gas condensate samples. The phase envelopes obtained from the mole fractions calculated by MW^{KF} are smaller than those calculated with MW^{Exp} . The reason is mainly due to the smaller mole fractions of SCNs from C_8 to C_{23} calculated using MW^{KF} . The bubble point curve for both cases are almost similar.

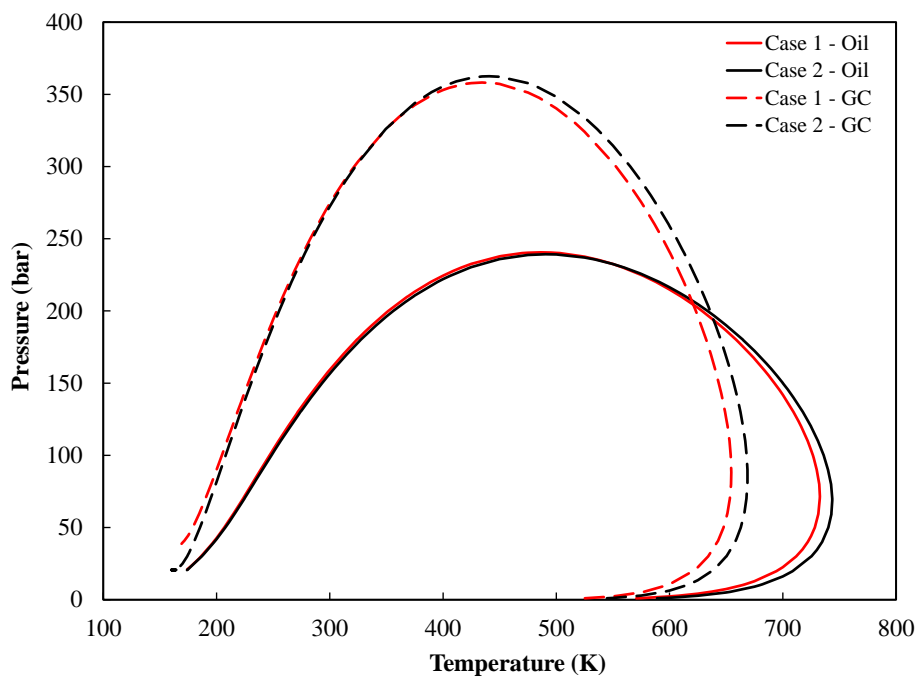


Figure 4.24 Phase envelopes of black oil and gas condensate samples using TBP distillation data.

Figure 4.25 presents the phase envelopes of the black oil and gas condensate samples for cases 3 to 6, which use SimDist data with MW^{Exp} (black lines) and MW^{KF} (red lines). For both samples, the phase envelopes are relatively similar in the bubble curve, while the difference between phase envelopes becomes more visible in the dew curve section for all the cases studied. Again, the phase envelopes obtained from the mole fractions calculated by MW^{KF} are smaller than those calculated with MW^{Exp} . It is expected that the difference between the phase envelopes calculated by experimental and default MW values would be more significant for the lighter gaseous systems (i.e. higher methane composition) with larger difference in MW^{Exp} and MW^{KF} . The

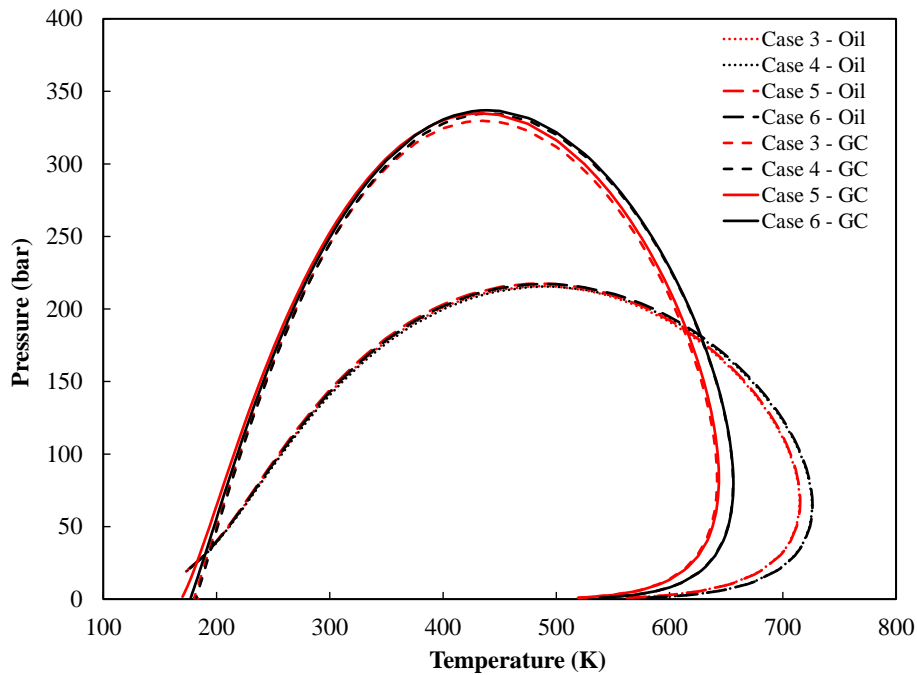


Figure 4.25 Phase envelopes of black oil and gas condensate samples using SimDist data.

difference between the measured MW and default MW would be larger if the amount of aromatic compounds are higher in each SCN fraction.

To investigate the effect of using measured MW and SG instead of the default values, we performed density calculations for the cases 1-6. Figures 4.26–4.29 illustrate the density calculation results using TBP and SimDist data for both the black oil and gas condensate samples. As can be seen in Figure 4.26, using experimental values of MW and SG gives lower prediction of density for cases 1 and 2 for the black oil sample. Similar behavior is observed in Figure 4.27, where the density calculation results are presented for the black oil sample using SimDist data. Using PA distribution in the calculations gives slightly different predictions of density compared to the case where the wt% of the SCNs are used. Similar behavior was observed for the gas condensate system as shown in Figures 4.28–4.29.

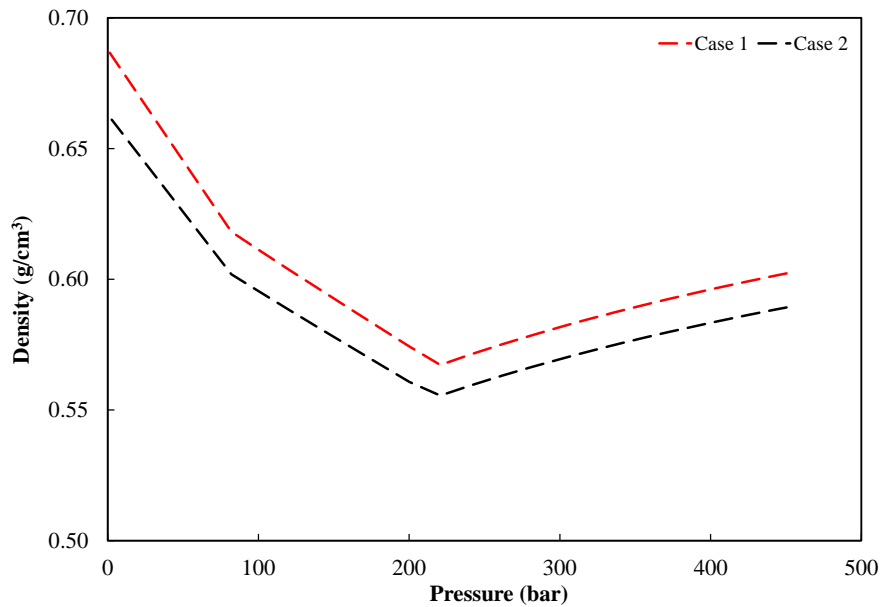


Figure 4.26 Density of black oil sample at 388.75 K using TBP distillation data with MW^{Exp} (black) and MW^{KF} (red).

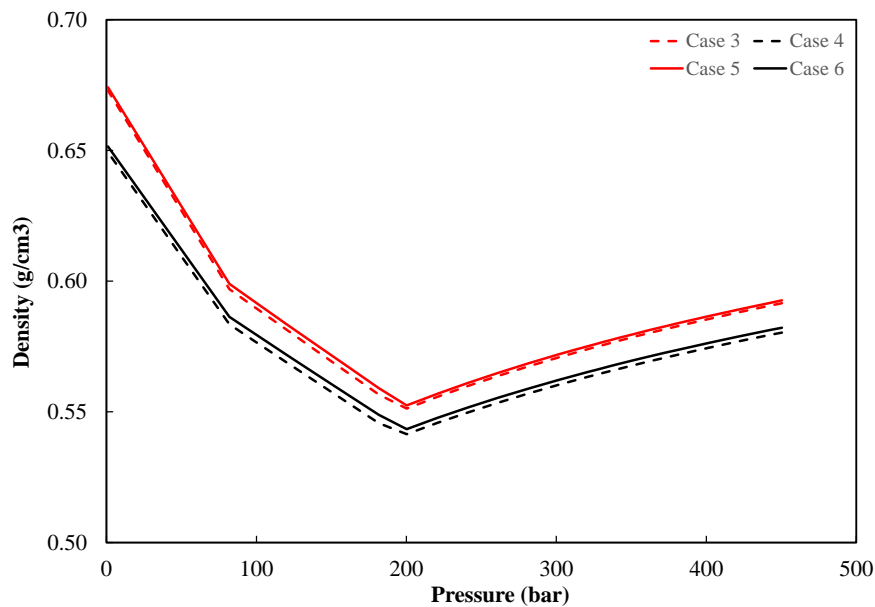


Figure 4.27 Density of black oil sample at 388.75 K using SimDist data with MW^{Exp} (black) and MW^{KF} (red).

The difference between the calculated density curves seems to be almost constant over the whole pressure range for the black oil sample. For the gas condensate system however, the difference between the density curves seems to be negligible for pressures higher than the saturation pressure, while for the pressures lower than the saturation

pressure, the deviation between the curves increases. In other words, for the high GOR sample, we can see the effect of using measured MW and SG instead of the default values, mainly at the pressures lower than the saturation pressure.

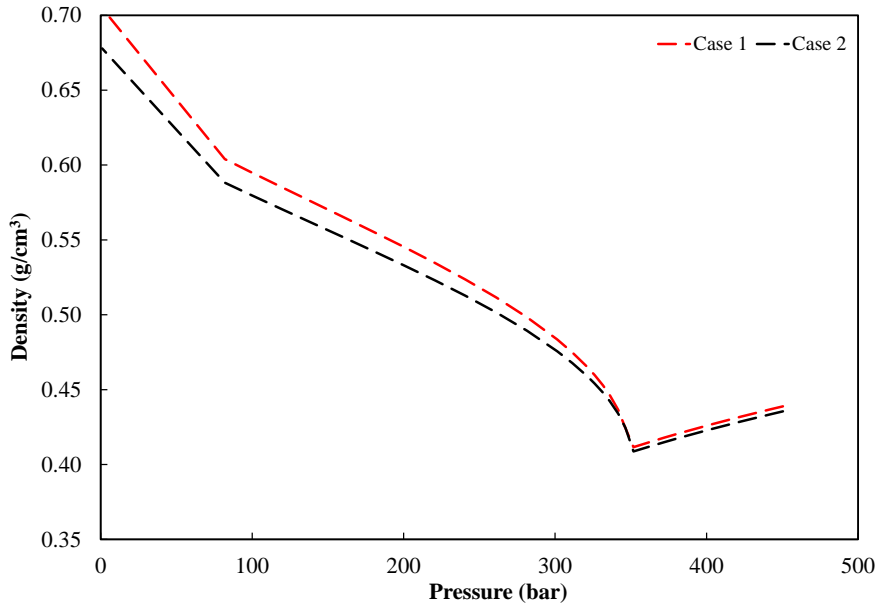


Figure 4.28 Density of gas condensate sample at 388.75 K using TBP distillation data with MW^{Exp} (black) and MW^{KF} (red).

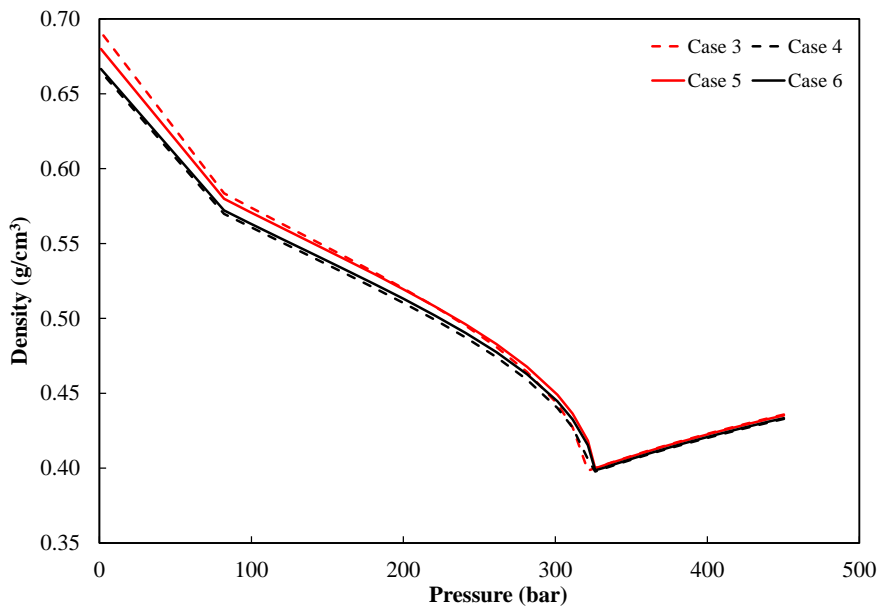


Figure 4.29 Density of gas condensate sample at 388.75 K using SimDist data with MW^{Exp} (black) and MW^{KF} (red).

4.11 Conclusions

The characterization method of Pedersen et al. is used as the framework for the developed characterization methods in this chapter, with specific modifications for different EoS models: for PC-SAFT, new correlations for estimating m , σ and ε have been developed; for Soave-BWR, SRK and PR, Twu's correlations for T_c and P_c , and the Lee-Kesler/Kesler-Lee correlations for ω are selected. A comprehensive evaluation of PC-SAFT and Soave-BWR in comparison with SRK and PR (with/without volume translation) has been made with regards to their potential in PVT modeling of reservoir fluids.

We presented a new characterization method for PC-SAFT. In order to improve the characterization method for PVT modeling of reservoir fluids, we developed a general approach to characterizing reservoir fluids based on a large PVT database and applied it to non-cubic PC-SAFT as well as cubic SRK and PR. In this approach, the correlations for the EoS model parameters were developed first based on a large pure component database such as DIPPR, and the coefficients in the obtained correlations were further adjusted using a large PVT database. We suggest keeping the n-alkane limit during the adjustment step, which can be readily realized for correlations developed in a two-step perturbation manner. Our final correlations were obtained using a PVT database of 260 reservoir fluids. The developed correlations are not meant to be an ultimate version. They can be constantly improved with a larger PVT database, or even customized to a certain type of reservoir fluid. Repeating the whole procedure for a set of improved correlations is rather straightforward. The obtained correlations can be easily implemented in PVT software.

PC-SAFT with the new general characterization method gives the lowest AAD% and maximum deviation in calculation of saturation pressure, density and STO density, and is superior to the previous characterization methods for PC-SAFT. Furthermore, application of the new characterization method to SRK and PR improves the saturation pressure calculation in comparison to the original characterization method for SRK and PR. Using volume translation together with the new characterization approach for SRK and PR gives comparable results for density and STO density to that of original characterization for SRK and PR with volume translation. Soave-BWR gives slightly higher deviation in saturation pressure than SRK and PR, however it gives the largest deviation in density and STO density compared to SRK and PR with volume translation and PC-SAFT with different characterization methods. The characterization method

based on PNA content for PC-SAFT gives accurate results for reservoir fluid density and STO density whereas the deviation in saturation pressure is not as low as those from the other characterization methods for PC-SAFT.

For the PVT database used in this study, cubic EoSs seem to have better performance than PC-SAFT in calculation of saturation pressure; PC-SAFT and cubics with volume translation show comparable results in calculation of density and STO density. For calculation of the derivative properties such as compressibility, PC-SAFT has shown to be superior to cubics for the two reservoir fluids tested. However, for the whole database and using the compressibility data calculated from the density data above the saturation pressure instead of measured compressibility, SRK with volume translation was shown to give the lowest deviation. Soave-BWR had slightly higher deviation than SRK with volume translation. The above observation contradicts with the observation for well-defined systems and the general expectation that non-cubics are better than cubics for compressibility modeling. The results must be interpreted with caution since the compressibility data, either calculated from density or reported directly in the PVT report, can be subject to large uncertainties. We also noticed some inconsistencies between the density data and reported compressibilities in some PVT reports. A more careful look at the experimental PVT data is recommended. In addition, our current test is based mainly on black oil, for lighter reservoir fluids like volatile oil and gas condensate, the conclusions can be different.

Furthermore, we investigated the possibility of incorporating more information from True Boiling Point (TBP) distillation and Simulated Distillation (SimDist) into characterization and PVT modeling. We used one dead oil sample with both TBP and SimDist analysis to generate a low gas oil ratio (GOR) fluid and a high GOR fluid and performed PVT calculations for six different characterization options (different compositions, molecular weights and specific gravities, and with or without PA information). For these two specific fluids, it was found that the selection of mass composition gives the largest impact on the calculation results, the selection of the MW and SG values are the second most influential factor, and the detailed PA information does not give significant effect on the final results.

5 | Heat Capacity and Joule-Thomson Coefficient

Accurate knowledge of heat capacity as a function of temperature and pressure is important to many industrial applications because this property is needed in energy balances, in entropy and enthalpy calculations or in the study of phase transitions. Heat capacity also provides information on the molecular structure, such as indicating structural changes [131–133]. As one of the second order derivative properties of Gibbs energy, heat capacity is difficult to describe accurately and modeling of this property is a demanding test for equations of state [132–135].

The Joule-Thomson coefficient (μ_{JT}) indicates the rate of temperature change with pressure during an isenthalpic (constant enthalpy) expansion. Knowledge of this derivative property is important in reservoir engineering, since it is often needed in describing the temperature change due to a large pressure drop. At low to moderate temperature and pressure, the μ_{JT} is usually positive, meaning a decrease in pressure results in a decrease in temperature. However, at high pressure and high temperature (HPHT) conditions, μ_{JT} is typically negative and the fluid warms up instead of cooling down after expansion. Isentropic expansion (constant entropy) of fluid that usually results in cooling (if Joule-Thomson coefficient is positive) may lead to wax formation in the well if the oil is around its cloud point near the wellbore [136]. The negative Joule-Thomson coefficient corresponds to the so-called reverse Joule-Thomson effect, i.e., temperature increase after depressurization. This can damage the surface production facilities and affect well integrity and safety [137, 138]. Accurate description of the Joule-Thomson coefficient allows better understanding of the reservoir fluid behavior and prediction of the unexpected behavior such as heating upon expansion. For high pressure-high temperature reservoirs, μ_{JT} is fundamental in the design and material selection, operation and maintenance of production operations [137, 139, 140]. This

coefficient is also needed as an input in the interpretation of temperature log data and prediction of the temperature profiles in the wells [141, 142].

In this chapter, we present a comprehensive comparison between cubic (SRK and PR) and non-cubic EoSs (Soave-BWR, PC-SAFT and GERG-2008) in calculation of thermal properties such as heat capacity and Joule-Thomson coefficient for pure components and multicomponent mixtures over a wide pressure and temperature range. The results are compared with available experimental data in the literature and special emphasis has been given to the reverse Joule-Thomson effects at high pressure high temperature (HPHT) conditions.

Normal alkanes are constituents of the reservoir fluids, and their heat capacity values are of importance for the oil and gas industry in order to develop and validate models which could be further applied to the real reservoir fluids in broad temperature and pressure ranges. The heat capacity and Joule-Thomson coefficients for different light and heavy n-alkanes (i.e. n-hexane, n-octane, n-decane, n-dodecane, n-tetradecane and n-hexadecane) are also calculated at both low and high pressures and temperatures up to 483.15 K using different EoS models (SRK, PR, PC-SAFT and Soave-BWR). The results are compared with the experimental measurements from [143] to evaluate the performance of the models at different pressure and temperature conditions.

In a $P - T$ diagram the locus where the Joule-Thomson coefficient is zero constitutes the inversion curve. The curve defines the border between heating (the Joule-Thomson coefficient smaller than zero) and cooling (the coefficient larger than zero) in Joule-Thomson processes. Experimental determination of this curve is complicated because it normally occurs at very extreme conditions which can represent up to 5 times the critical temperature and 12 times the critical pressure [144, 145]. There has been a literature focus on calculation of the inversion curve by means of EoSs such as cubics or Soft-SAFT EoS for n-alkanes, carbon dioxide, six different natural gas mixtures and gas condensates, among others [146–148]. Moreover the inversion curve has also been previously calculated by means of molecular simulation for carbon dioxide, methane, ethane, butane, nitrogen, argon, oxygen, ethylene, carbon monoxide, a model gas condensate mixture, six different natural gas mixtures and two natural gases, among others [137, 139, 140, 145, 147, 149–152]. In this chapter we also present results for the calculations of the Joule-Thomson inversion curve for the studied light and heavy n-alkanes through the four aforementioned EoSs.

5.1 Isobaric Heat Capacity Calculations

Isobaric heat capacity can be expressed by the following equation:

$$C_p = C_p^{id} + C_p^r \quad (5.1)$$

This property is evaluated from two independent steps: The ideal gas heat capacity, C_p^{id} which refers to the heat capacity of the free molecule at zero density, and the residual heat capacity, C_p^r which takes into account the intermolecular interactions. The ideal gas heat capacity term can be calculated by different specific equations and is dependent on temperature only. In this work, the ideal gas heat capacity is calculated from the correlations in DIPPR [105], and the residual part is calculated by means of equations of state. The temperature derivatives of the reduced Helmholtz energy are required in the calculation of the residual part [153]. The following equations show how C_p^r is calculated:

$$F = \frac{A^r(T, V, \mathbf{n})}{RT} \quad (5.2)$$

$$\frac{C_v^r(T, V, \mathbf{n})}{R} = -T^2 \left(\frac{\partial^2 F}{\partial T^2} \right)_{V, \mathbf{n}} - 2T \left(\frac{\partial F}{\partial T} \right)_{V, \mathbf{n}} \quad (5.3)$$

$$\frac{C_p^r}{R} = \frac{C_v^r(T, V, \mathbf{n})}{R} - \left(\frac{T}{R} \right) \frac{\left(\frac{\partial P}{\partial T} \right)_{V, \mathbf{n}}^2}{\left(\frac{\partial P}{\partial V} \right)_{T, \mathbf{n}}} - n \quad (5.4)$$

In these equations, V is the total volume, \mathbf{n} is the mole numbers vector, n is the total mole number, A^r is the residual Helmholtz energy, F is the reduced residual Helmholtz function, R is the universal gas constant, and C_v^r is the residual heat capacity at constant volume.

5.2 Joule-Thomson Coefficient Calculations

Joule-Thomson coefficients (μ_{JT}) can be expressed by

$$\mu_{JT}(T, P, \mathbf{n}) \equiv \left(\frac{\partial T}{\partial P} \right)_{H, \mathbf{n}} = -\frac{1}{C_p} \left[V + T \frac{\left(\frac{\partial P}{\partial T} \right)_{V, \mathbf{n}}}{\left(\frac{\partial P}{\partial V} \right)_{T, \mathbf{n}}} \right] = -\frac{1}{C_p} \left[V - T \left(\frac{\partial V}{\partial T} \right)_{P, \mathbf{n}} \right] \quad (5.5)$$

The last equation was used to calculate the Joule-Thomson coefficient through the different EoSs analyzed in this work. As concerns the calculation of the inversion curve, the pressure was obtained using the bisection method along isotherms until the calculated μ_{JT} was lower than 10^{-5} K.MPa⁻¹.

5.3 Results and Discussions

In this section the absolute average deviation (AAD) is employed to compare the calculation results with previously reported literature values. The following equation was used:

$$AAD/\% = \frac{100}{k} \sum_{i=1}^k \left| \frac{Y^{Calc.} - Y^{Exp.}}{Y^{Exp.}} \right| \quad (5.6)$$

where k is the number of experimental data points, Y stands for the analyzed property and *Calc.* and *Exp.* stand for calculated and experimental, respectively.

Critical pressure, critical temperature and acentric factor for SRK, PR, and Soave-BWR EoSs were taken from the DIPPR database [105], the model parameters for PC-SAFT were taken from Gross and Sadowski [7], and the model parameters for GERG-2008 were taken from Kunz and Wagner [10]. It should be mentioned that no volume translation was used for the cubic EoSs in this study and the calculation results are pure predictions of each model.

The NIST Reference Fluid Thermodynamic and Transport Properties Database (REFPROP, Version 9.1) uses high accuracy reference EoS models [7] to calculate different properties of pure components. This database uses GERG-2008 EoS for estimation of the properties for binary and multicomponent mixture. Figures 5.1–5.2 show the heat capacity and Joule-Thomson coefficient calculations for methane using the reference EoS models in REFPROP. As can be seen, the REFPROP results are very close to the experimental data at different temperatures taken from [154]. As a result, to evaluate the performance of different cubic and non-cubic EoSs including GERG-2008 in calculation of thermal properties such as heat capacity and Joule-Thomson coefficient of pure components in a wide temperature and pressure range, we used synthetic data from REFPROP for the 15 main components (Table 3.1) in the temperature range of 250-500 K and pressure range of 5-1500 bar.

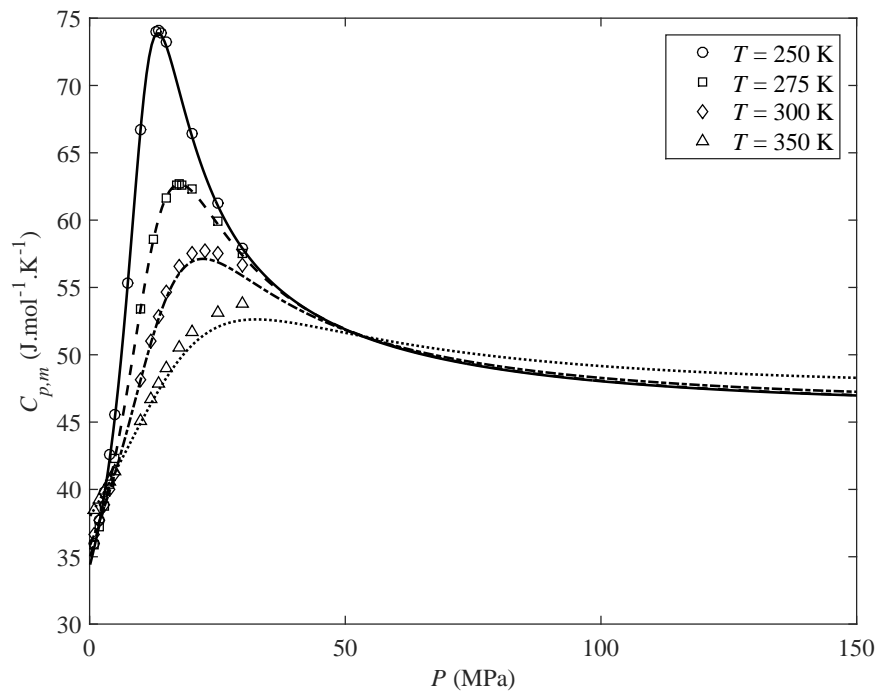


Figure 5.1 Heat capacity prediction for methane at different temperatures using REFPROP. The experimental data is taken from [154].

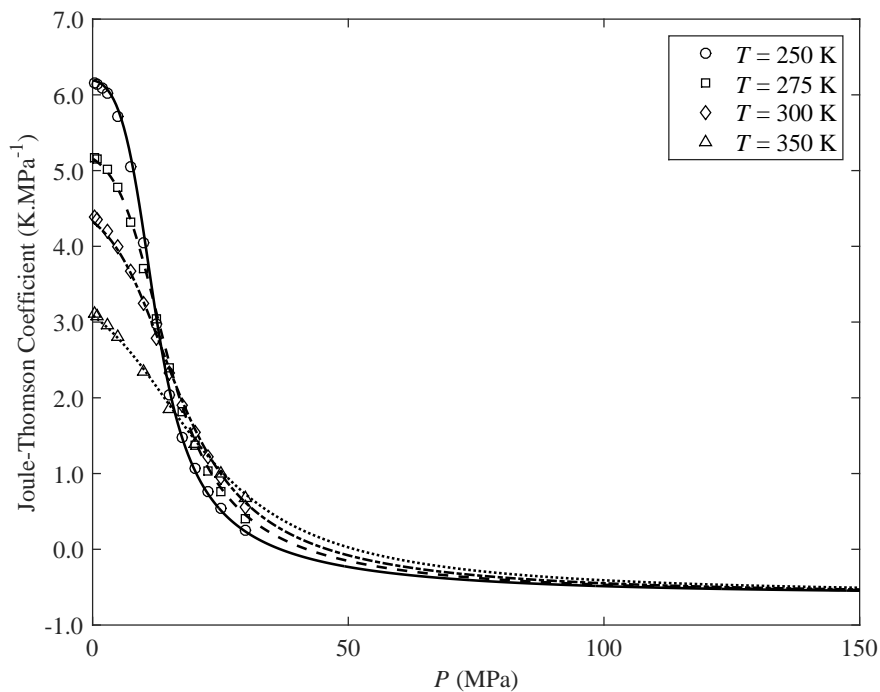


Figure 5.2 Joule-Thomson coefficient prediction for methane at different temperatures using REFPROP. The experimental data is taken from [154].

5.3.1 Systematic Comparison of Different EoSs for C_p and μ_{JT} of Pure and Multicomponent Systems

Figure 5.3 shows the AAD% in the calculated heat capacity using SRK, PR, PC-SAFT, Soave-BWR and GERG-2008 for the 15 main pure components from REFPROP. On average, the non-cubic models give lower deviation than the cubic ones, and GERG-2008 gives the lowest deviation. Soave-BWR gives the closest deviation to that of GERG-2008 among other EoSs. A similar trend is observed in Figure 5.4 where Mean Absolute Deviations (MAD) in the Joule-Thomson coefficient of the main components are reported. The reason for using MAD instead of AAD% was that the Joule-Thomson coefficient changes sign at high pressures. This means it would become zero at some pressures, which yields very large deviations if AAD% is used instead of MAD. The Mean Absolute Deviation for the Joule-Thomson coefficient was calculated using the following equation:

$$MAD = \frac{1}{n} \sum_{i=1}^n |\mu_{JT,i}^{Calc.} - \mu_{JT,i}^{Exp.}| \quad (5.7)$$

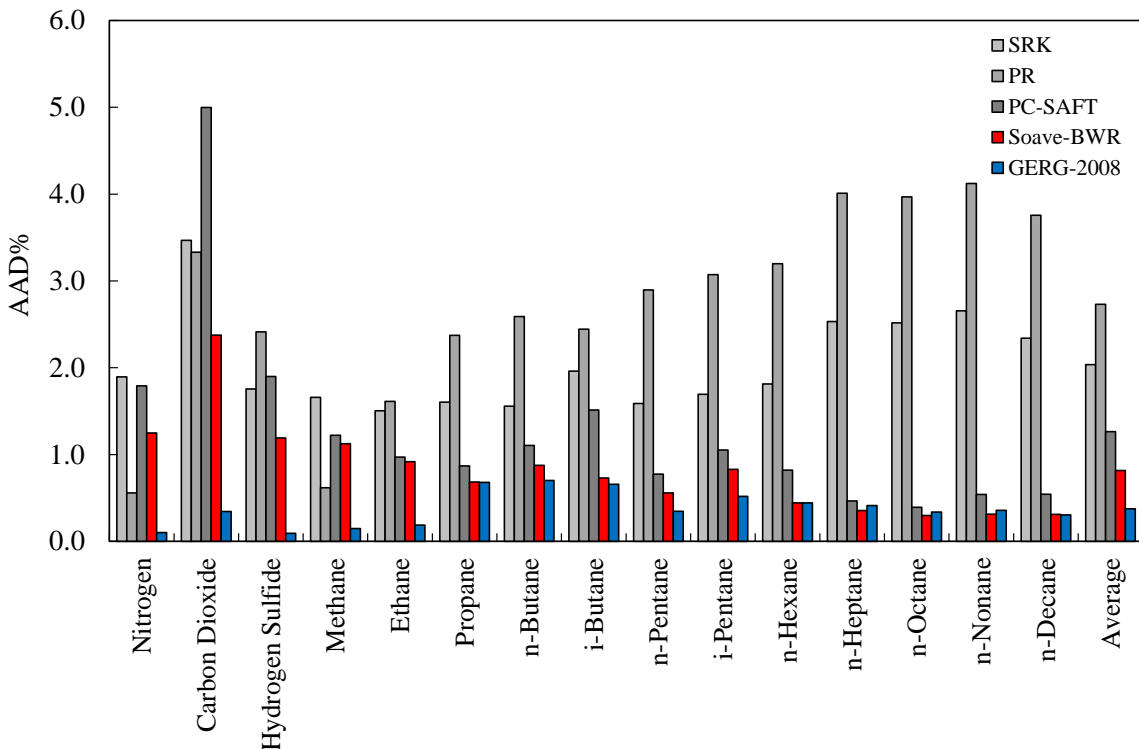


Figure 5.3 AAD% in the heat capacity of the “main components” within 250-500 K and 5-1500 bar using different EoSs. The model predictions are compared with REFPROP results.

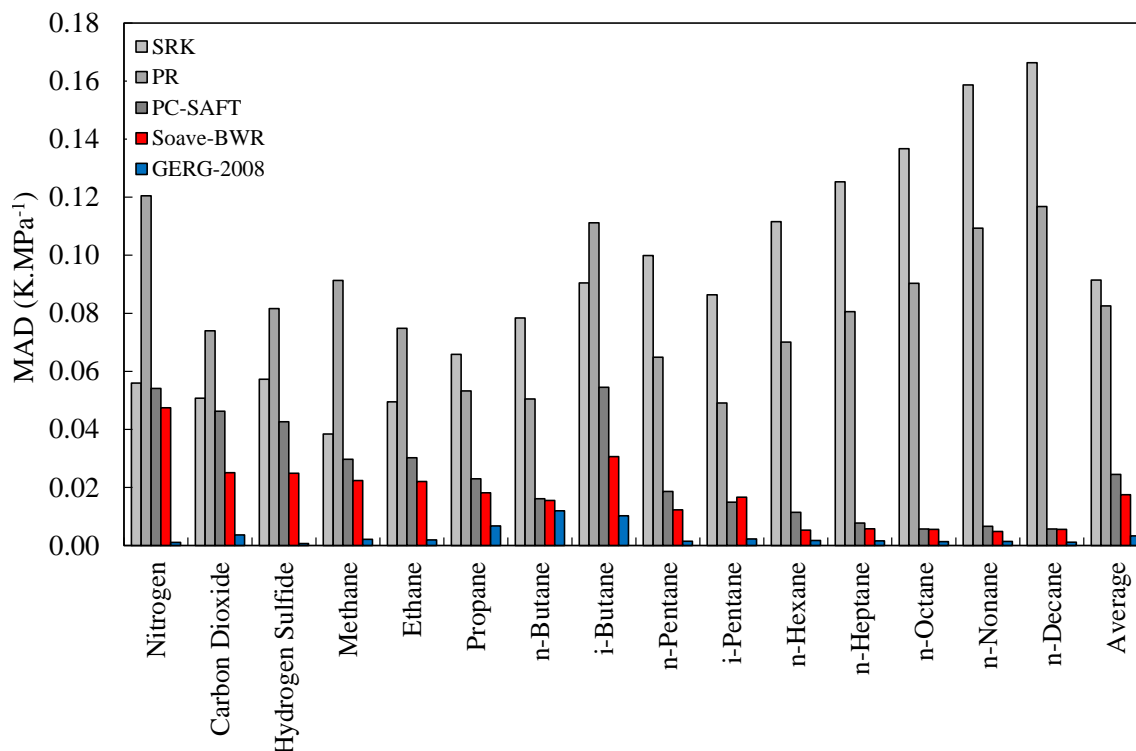
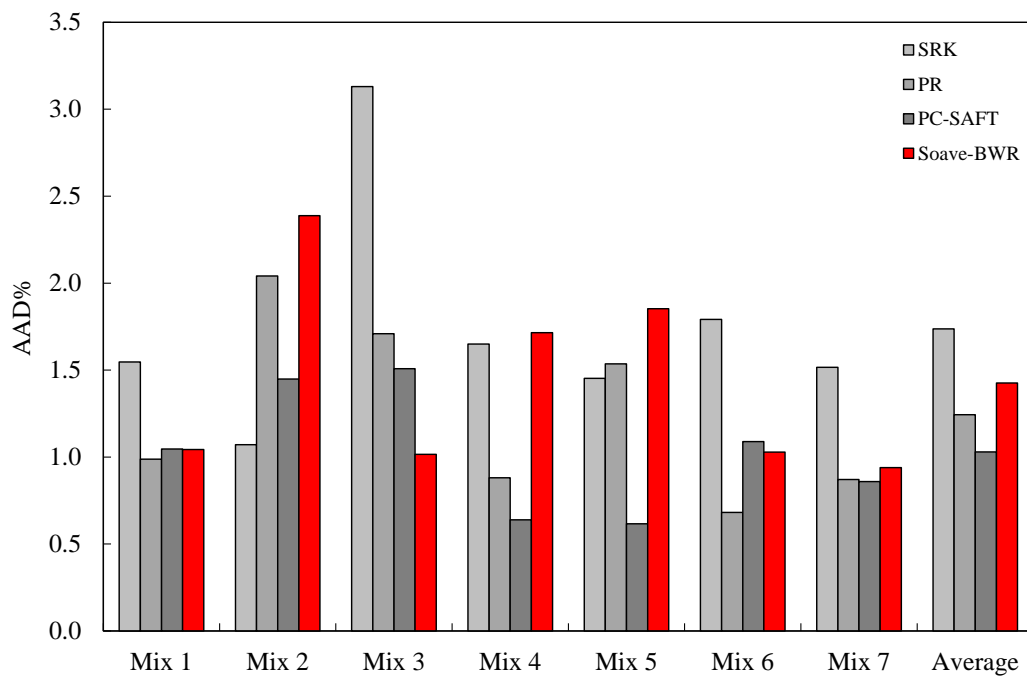


Figure 5.4 MAD in the Joule-Thomson coefficient of the “main components” within 250-500 K and 5-1500 bar using different EoS. The model predictions are compared with REFPROP results.

Table 5.1 presents the mole fraction of some sample binary and multicomponent mixtures. As it was mentioned earlier, REFPROP uses GERG-2008 for estimation of the properties of binary and multicomponent mixtures. We have used GERG-2008 to produce synthetic heat capacity and Joule-Thomson coefficient data in the temperature range of 250-500 K and pressure range of 5-1500 bar to see how accurate SRK, PR, PC-SAFT and Soave-BWR predict these thermal properties for multicomponent mixtures compared to GERG-2008. Figures 5.5–5.6 show AAD% in heat capacity and MAD in Joule-Thomson coefficient of binary and multicomponent mixtures within 250-500 K and 5-1500 bar. PC-SAFT gives the lowest deviation in heat capacity while Soave-BWR is superior in Joule-Thomson coefficient calculations. On average, PR gives slightly better prediction of heat capacity than Soave-BWR for the multicomponent mixtures. This is mainly due to its better performance for the systems with higher composition of methane (Mixtures No. 4 and 6).

Table 5.1 Mole fraction of different binary and multicomponent mixtures used for heat capacity and Joule-Thomson coefficient calculations.

Component	Mix 1	Mix 2	Mix 3	Mix 4	Mix 5	Mix 6	Mix 7
N ₂	-	-	-	-	-	0.1	-
CO ₂	-	-	0.5	-	-	0.02	-
CH ₄	0.5	0.5	0.5	0.81	0.6	0.8	0.7
C ₂ H ₆	0.5	-	-	-	-	0.05	0.13
C ₃ H ₈	-	-	-	-	-	0.03	0.11
nC ₄ H ₁₀	-	-	-	0.14	0.31	-	0.06
nC ₁₀ H ₂₂	-	0.5	-	0.05	0.09	-	-

**Figure 5.5** AAD% in the heat capacity of binary and multicomponent mixtures within 250-500 K and 5-1500 bar using different EoSs. The model predictions are compared with REFPROP results (REFPROP uses GERG-2008 for mixtures).

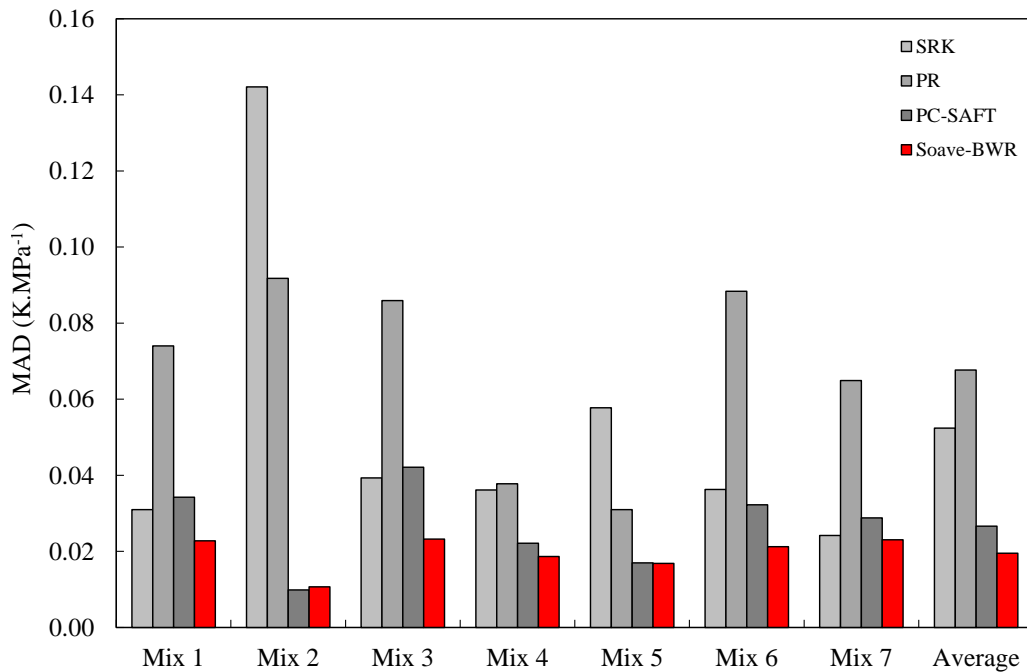


Figure 5.6 MAD in the Joule-Thomson coefficient of binary and multicomponent mixtures within 250-500 K and 5-1500 bar using different EoSs. The model predictions are compared with REFPROP results (REFPROP uses GERG-2008 for mixtures).

As Soave-BWR was superior to SRK, PR, and PC-SAFT in Joule-Thomson coefficient calculation of pure and multicomponent mixture and also heat capacity of pure components, we selected this EoS for comparison with GERG-2008 in the following calculations.

Figures 5.7–5.12 present the heat capacity and Joule-Thomson coefficient calculation results using GERG-2008 and Soave-BWR for methane, binary mixture of methane + ethane, and a multicomponent natural gas mixture. The experimental data for all these three systems is taken from Ernst et al.'s work [154]. In these figures the model predictions are presented up to very high pressures (1500 bar or 150 MPa) to see how the two models differ at HPHT conditions.

Figure 5.7 shows heat capacity calculations for pure methane. Both Soave-BWR and GERG-2008 give accurate prediction of heat capacity at lower temperatures and pressures, while GERG-2008 has slightly better performance at lower temperatures and higher pressures. At higher temperatures both models seem to under predict the heat capacity for methane, while Soave-BWR gives closer predictions to the experimental data. The same behavior is observed for the methane and ethane binary system and natural gas mixture (Figures 5.8–5.9).

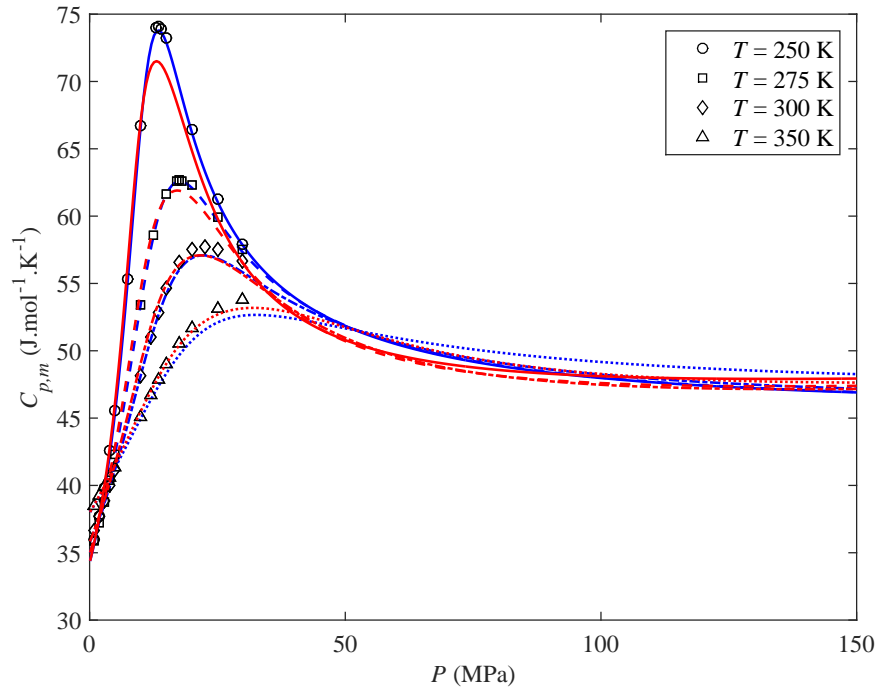


Figure 5.7 Heat capacity vs. pressure using GERG-2008 (blue lines) and Soave-BWR (red lines) for C_1 at different temperatures: 250 K (solid lines), 275 K (dashed lines), 300 K (dash-dot lines), 350 K (dotted lines). The experimental data is taken from [154].

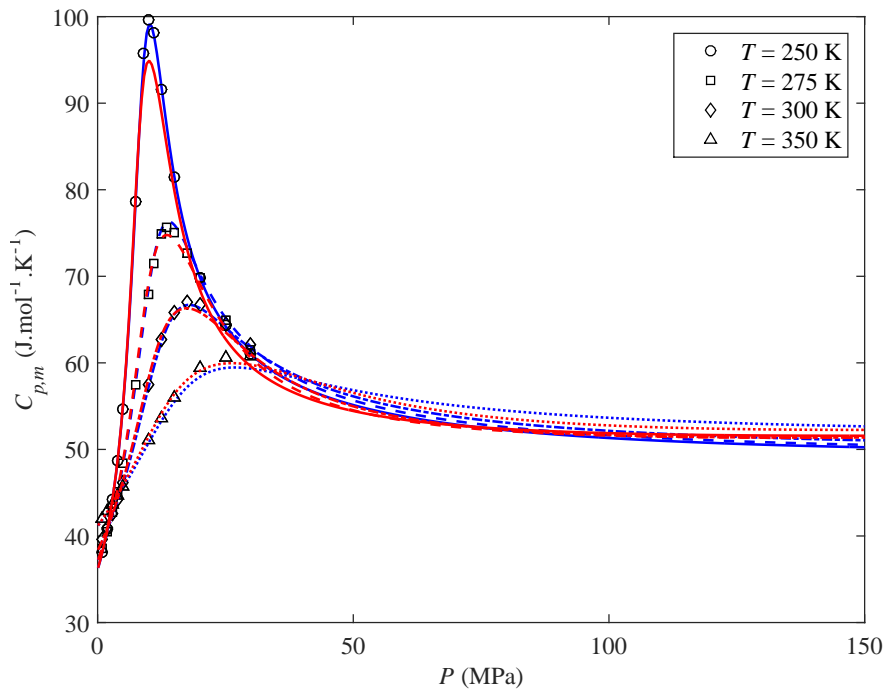


Figure 5.8 Heat capacity vs. pressure using GERG-2008 (blue lines) and Soave-BWR with regressed k_{ij} (red lines) for C_1 - C_2 mixture from [154] at different temperatures: 250 K (solid lines), 275 K (dashed lines), 300 K (dash-dot lines), 350 K (dotted lines).

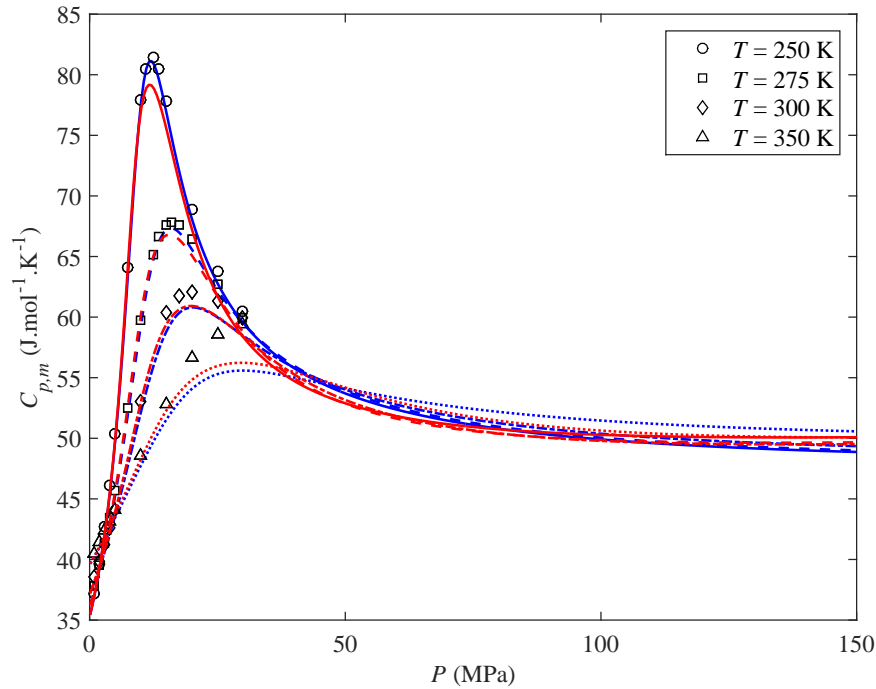


Figure 5.9 Heat capacity vs. pressure using GERG-2008 (blue lines) and Soave-BWR with regressed k_{ij} (red lines) for the natural gas mixture from [154] at different temperatures: 250 K (solid lines), 275 K (dashed lines), 300 K (dash-dot lines), 350 K (dotted lines).

The difference between two models is not significant for the Joule-Thomson coefficient calculations (Figures 5.10–5.12). GERG-2008 gives slightly better results than Soave-BWR, but in general both models give accurate predictions of Joule-Thomson coefficient over the whole pressure and temperature range. Although the experimental data is not available at high pressures, both models seem to predict a negative Joule-Thomson coefficient at 1500 bar and all temperatures. In fact, the value of Joule-Thomson coefficient seems to reach more or less a constant value at high pressures for the pure, binary and multicomponent systems. As the Joule-Thomson coefficient is negative at high pressures, the temperature of the fluid increases with the pressure drop. The temperature increase due to the pressure drop is known as the reverse Joule-Thomson effect. Although the temperature increase is not very significant (around 0.5 K/Mpa), it should be considered in the material selection for the tubing and surface facilities because the temperature increase can damage the surface production facilities and affect well integrity and safety.

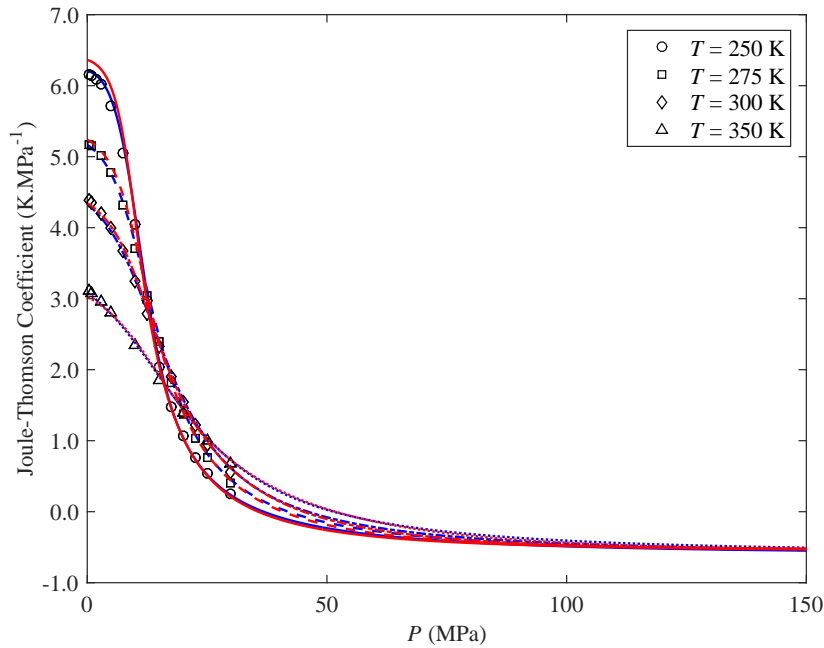


Figure 5.10 Joule-Thomson coefficient vs. pressure using GERG-2008 (blue lines) and Soave-BWR (red lines) for C_1 at different temperatures: 250 K (solid lines), 275 K (dashed lines), 300 K (dash-dot lines), 350 K (dotted lines). The experimental data is taken from [154].

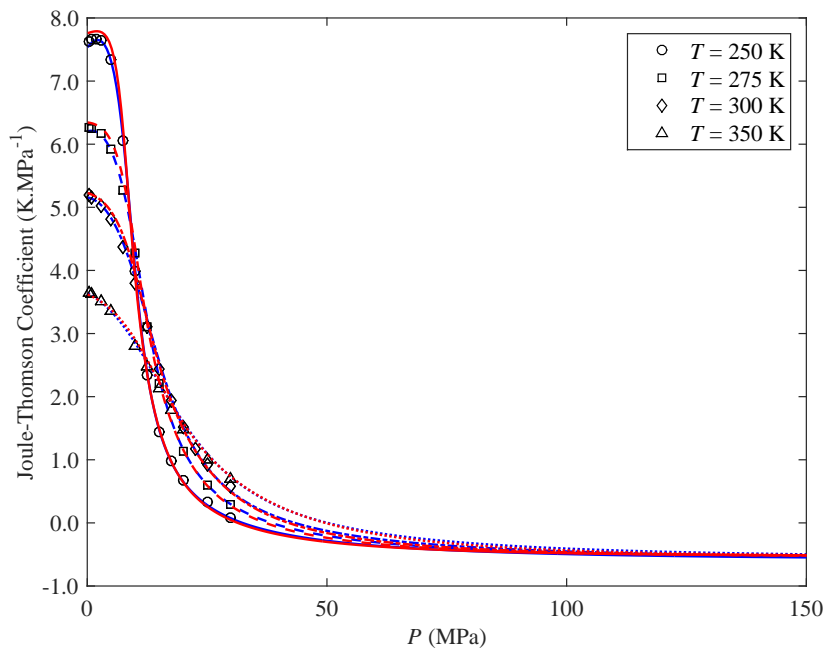


Figure 5.11 Joule-Thomson coefficient vs. pressure using GERG-2008 (blue lines) and Soave-BWR with regressed k_{ij} (red lines) for C_1 - C_2 mixture from [154] at different temperatures: 250 K (solid lines), 275 K (dashed lines), 300 K (dash-dot lines), 350 K (dotted lines).

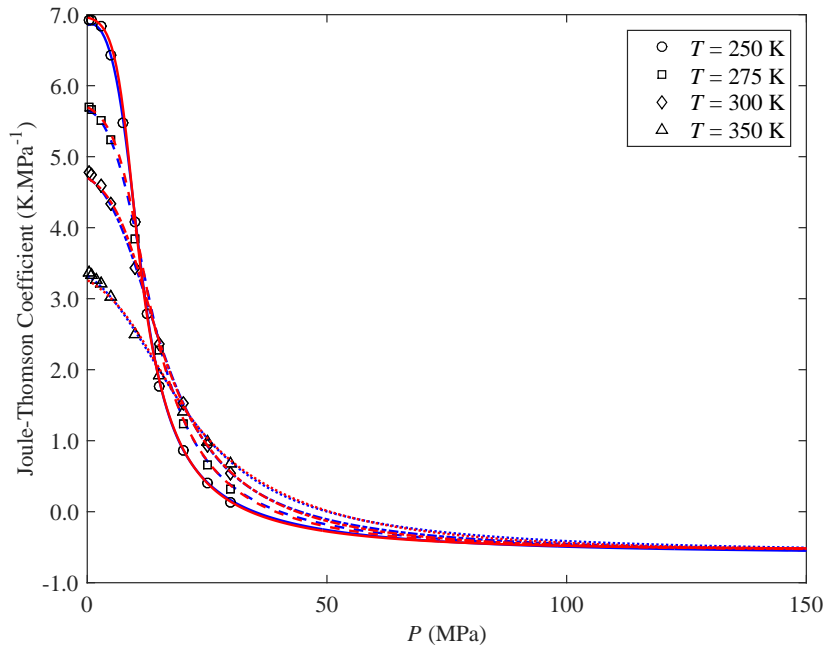


Figure 5.12 Joule-Thomson coefficient vs. pressure using GERG-2008 (blue lines) and Soave-BWR with regressed k_{ij} (red lines) for the natural gas mixture from [154] at different temperatures: 250 K (solid lines), 275 K (dashed lines), 300 K (dash-dot lines), 350 K (dotted lines).

5.3.2 Heat Capacity and Joule-Thomson Coefficient Calculations for Light and Heavy n-alkanes

In this section, the heat capacity and Joule-Thomson coefficients calculation results for some light and heavy n-alkanes (i.e. n-hexane, n-octane, n-decane, n-dodecane, n-tetradecane and n-hexadecane) are presented at both low and high pressures, and temperatures up to 483.15 K using different EoS models (SRK, PR, PC-SAFT and Soave-BWR). The results are compared with the experimental measurements to evaluate the performance of the models at different pressure and temperature conditions. The experimental measurements were performed internally at Center for Energy Resources Engineering (CERE) and the experimental values of heat capacity and Joule-Thomson coefficient used in our comparison are reported in Tables 5.2–5.3.

Table 5.2 Heat capacity values at constant pressure, C_p , of the n-alkanes studied in this work in $\text{Jg}^{-1}\text{K}^{-1}$.

T/K	P/MPa											
	0.14	10.09	0.1	10.13	0.12	10.17	0.1	10.18	0.12	10.12	0.13	10.09
	n-hexane		n-octane		n-decane		n-dodecane		n-tetradecane		n-hexadecane	
323.15	2.363	2.328	2.305	2.284	2.293	2.270	2.268	2.261	2.266	2.257	2.268	2.262
328.15	2.387	2.349	2.326	2.304	2.307	2.289	2.287	2.278	2.282	2.274	2.284	2.278
333.15	2.412	2.373	2.346	2.325	2.323	2.308	2.306	2.297	2.299	2.291	2.300	2.294
338.15	-	2.392	2.367	2.344	2.342	2.326	2.324	2.315	2.316	2.308	2.317	2.311
343.15	-	2.415	2.387	2.364	2.363	2.345	2.343	2.333	2.334	2.325	2.334	2.325
348.15	-	2.438	2.409	2.384	2.383	2.364	2.362	2.351	2.352	2.343	2.353	2.341
353.15	-	2.459	2.430	2.403	2.403	2.383	2.381	2.369	2.371	2.360	2.369	2.360
358.15	-	2.485	2.452	2.425	2.421	2.404	2.400	2.389	2.390	2.379	2.388	2.378
363.15	-	2.507	2.474	2.444	2.438	2.422	2.419	2.407	2.408	2.397	2.405	2.394
368.15	-	2.534	2.496	2.465	2.458	2.441	2.438	2.426	2.427	2.414	2.423	2.413
373.15	-	-	2.520	2.486	2.479	2.462	2.459	2.443	2.446	2.435	2.443	2.432
378.15	-	-	2.542	2.508	2.499	2.481	2.478	2.462	2.465	2.452	2.461	2.449
383.15	-	-	2.569	2.529	2.520	2.500	2.498	2.481	2.484	2.469	2.480	2.468
388.15	-	-	-	2.547	2.542	2.519	2.517	2.501	2.504	2.486	2.498	2.487
393.15	-	-	-	2.564	2.564	2.540	2.538	2.519	2.521	2.506	2.516	2.505
398.15	-	-	-	2.591	2.585	2.560	2.556	2.543	2.543	2.524	2.535	2.523
403.15	-	-	-	-	2.609	2.580	2.576	2.559	2.562	2.539	2.555	2.542
408.15	-	-	-	-	-	2.601	2.598	2.576	2.583	2.563	2.575	2.561
413.15	-	-	-	-	-	2.620	2.617	2.593	2.600	2.579	2.592	2.581
418.15	-	-	-	-	-	2.641	2.638	2.607	2.619	2.598	2.612	2.601
423.15	-	-	-	-	-	2.666	2.659	2.628	2.638	2.615	2.631	2.619
428.15	-	-	-	-	-	2.689	2.680	2.647	2.657	2.632	2.648	2.634
433.15	-	-	-	-	-	-	2.704	2.667	2.676	2.651	2.667	2.651
438.15	-	-	-	-	-	-	2.732	2.690	2.698	2.668	2.688	2.670
443.15	-	-	-	-	-	-	-	2.713	2.721	2.689	2.708	2.691
448.15	-	-	-	-	-	-	-	2.734	2.740	2.710	2.726	2.710
453.15	-	-	-	-	-	-	-	2.759	2.762	2.730	2.748	2.725
458.15	-	-	-	-	-	-	-	-	2.793	2.751	-	2.744
463.15	-	-	-	-	-	-	-	-	2.821	2.774	-	2.762
468.15	-	-	-	-	-	-	-	-	-	2.792	-	2.783
473.15	-	-	-	-	-	-	-	-	-	2.813	-	2.804
478.15	-	-	-	-	-	-	-	-	-	2.837	-	-
483.15	-	-	-	-	-	-	-	-	-	2.857	-	-

Table 5.3 Joule-Thomson coefficient of the studied n-alkanes, μ_{JT} , in K.MPa⁻¹.

T/K	P/MPa											
	0.14	10.09	0.1	10.13	0.12	10.17	0.1	10.18	0.12	10.12	0.13	10.09
	n-hexane		n-octane		n-decane		n-dodecane		n-tetradecane		n-hexadecane	
323.15	-0.341	-0.380	-0.390	-0.411	-0.397	-0.413	-0.407	-0.418	-0.412	-0.423	-0.410	-0.419
328.15	-0.329	-0.371	-0.382	-0.404	-0.392	-0.407	-0.402	-0.413	-0.406	-0.417	-0.405	-0.415
333.15	-0.317	-0.362	-0.374	-0.397	-0.386	-0.402	-0.396	-0.408	-0.401	-0.412	-0.399	-0.411
338.15	-	-0.353	-0.365	-0.391	-0.380	-0.397	-0.391	-0.404	-0.396	-0.407	-0.394	-0.407
343.15	-	-0.344	-0.357	-0.384	-0.373	-0.391	-0.385	-0.399	-0.390	-0.402	-0.388	-0.403
348.15	-	-0.334	-0.348	-0.378	-0.366	-0.386	-0.379	-0.394	-0.384	-0.397	-0.382	-0.399
353.15	-	-0.324	-0.339	-0.371	-0.359	-0.380	-0.373	-0.389	-0.379	-0.392	-0.377	-0.395
358.15	-	-0.314	-0.330	-0.364	-0.352	-0.374	-0.368	-0.384	-0.373	-0.386	-0.371	-0.390
363.15	-	-0.303	-0.320	-0.357	-0.346	-0.369	-0.361	-0.379	-0.367	-0.381	-0.366	-0.386
368.15	-	-0.292	-0.310	-0.350	-0.338	-0.363	-0.355	-0.374	-0.361	-0.376	-0.360	-0.382
373.15	-	-	-0.300	-0.342	-0.331	-0.357	-0.348	-0.369	-0.355	-0.371	-0.355	-0.377
378.15	-	-	-0.290	-0.334	-0.323	-0.351	-0.342	-0.363	-0.349	-0.366	-0.349	-0.373
383.15	-	-	-0.279	-0.327	-0.315	-0.345	-0.335	-0.358	-0.343	-0.361	-0.344	-0.368
388.15	-	-	-	-0.319	-0.307	-0.339	-0.328	-0.353	-0.337	-0.357	-0.338	-0.364
393.15	-	-	-	-0.312	-0.298	-0.333	-0.321	-0.347	-0.331	-0.352	-0.333	-0.359
398.15	-	-	-	-0.303	-0.290	-0.327	-0.314	-0.341	-0.325	-0.347	-0.328	-0.354
403.15	-	-	-	-	-0.281	-0.321	-0.307	-0.336	-0.319	-0.343	-0.322	-0.350
408.15	-	-	-	-	-	-0.314	-0.299	-0.331	-0.313	-0.338	-0.317	-0.345
413.15	-	-	-	-	-	-0.308	-0.291	-0.325	-0.307	-0.333	-0.312	-0.340
418.15	-	-	-	-	-	-0.301	-0.283	-0.320	-0.300	-0.329	-0.307	-0.335
423.15	-	-	-	-	-	-0.294	-0.275	-0.314	-0.294	-0.325	-0.302	-0.330
428.15	-	-	-	-	-	-0.287	-0.267	-0.308	-0.287	-0.321	-0.297	-0.325
433.15	-	-	-	-	-	-	-0.257	-0.302	-0.281	-0.316	-0.293	-0.320
438.15	-	-	-	-	-	-	-0.248	-0.295	-0.274	-0.312	-0.288	-0.315
443.15	-	-	-	-	-	-	-	-0.289	-0.267	-0.308	-0.283	-0.310
448.15	-	-	-	-	-	-	-	-0.282	-0.260	-0.304	-0.278	-0.304
453.15	-	-	-	-	-	-	-	-0.275	-0.253	-0.299	-0.274	-0.299
458.15	-	-	-	-	-	-	-	-	-0.245	-0.295	-	-0.294
463.15	-	-	-	-	-	-	-	-	-0.237	-0.291	-	-0.288
468.15	-	-	-	-	-	-	-	-	-	-0.287	-	-0.282
473.15	-	-	-	-	-	-	-	-	-	-0.283	-	-0.276
478.15	-	-	-	-	-	-	-	-	-	-0.279	-	-
483.15	-	-	-	-	-	-	-	-	-	-0.276	-	-

The calculation results for C_p using SRK, PR, PC-SAFT and Soave-BWR are presented in Tables C.1–C.4 in Appendix C. The Absolute Average Deviation (AAD) and maximum deviation obtained in the calculation of C_p of the n-alkanes at 0.1 and 10 MPa (1 and 100 bar) using the different EoSs are summarized in Table 5.4. The results show that both the AAD and maximum deviation are lower for the non-cubic EoSs than

for the cubic models. PR, with AAD around 3%, gives the largest deviation among all the four analyzed EoSs, while PC-SAFT has the lowest AAD (0.27%) for both low and high pressures. Soave-BWR gives almost similar average deviation as PC-SAFT for 0.1 MPa but a slightly higher deviation for 10 MPa. In general, the model performance at 10 MPa and 0.1 MPa are very similar. The maximum deviation for PR is 6.65% for n-hexadecane at 10 MPa, while for PC-SAFT the maximum deviation is 1.13% for n-tetradecane at 0.1 MPa. The overall AAD for all the n-alkanes tested is presented in Figure 5.13.

Table 5.4 Absolute Average Deviation (AAD) and maximum deviation (Max. Dev.) in the C_p calculation of the n-alkanes studied in this work at 0.1 and 10 MPa using different EoSs.

P/MPa	SRK		PR		PC-SAFT		Soave-BWR	
	0.1	10	0.1	10	0.1	10	0.1	10
n-hexane								
AAD / %	0.14	0.34	2.18	2.10	0.13	0.35	0.76	0.92
Max. Dev. / %	0.22	0.89	2.42	2.93	0.15	0.44	0.77	1.03
n-octane								
AAD / %	0.66	0.88	2.39	2.55	0.07	0.27	0.63	0.78
Max. Dev. / %	1.62	1.99	3.72	3.96	0.13	0.47	0.77	1.10
n-decane								
AAD / %	1.12	1.29	2.91	2.90	0.19	0.25	0.37	0.43
Max. Dev. / %	2.97	2.86	5.02	4.80	0.34	0.39	0.61	0.58
n-dodecane								
AAD / %	1.31	1.61	3.03	3.18	0.31	0.27	0.16	0.21
Max. Dev. / %	2.81	3.19	4.82	5.11	0.89	0.91	0.66	0.68
n-tetradecane								
AAD / %	1.37	1.51	3.02	3.01	0.29	0.19	0.18	0.32
Max. Dev. / %	3.84	4.04	5.81	5.94	1.13	0.87	0.88	0.60
n-hexadecane								
AAD / %	1.91	2.05	3.60	3.61	0.39	0.32	0.18	0.25
Max. Dev. / %	4.50	4.71	6.49	6.65	0.82	0.67	0.71	0.91
Overall								
AAD / %	1.33	1.46	3.05	3.04	0.27	0.27	0.27	0.40

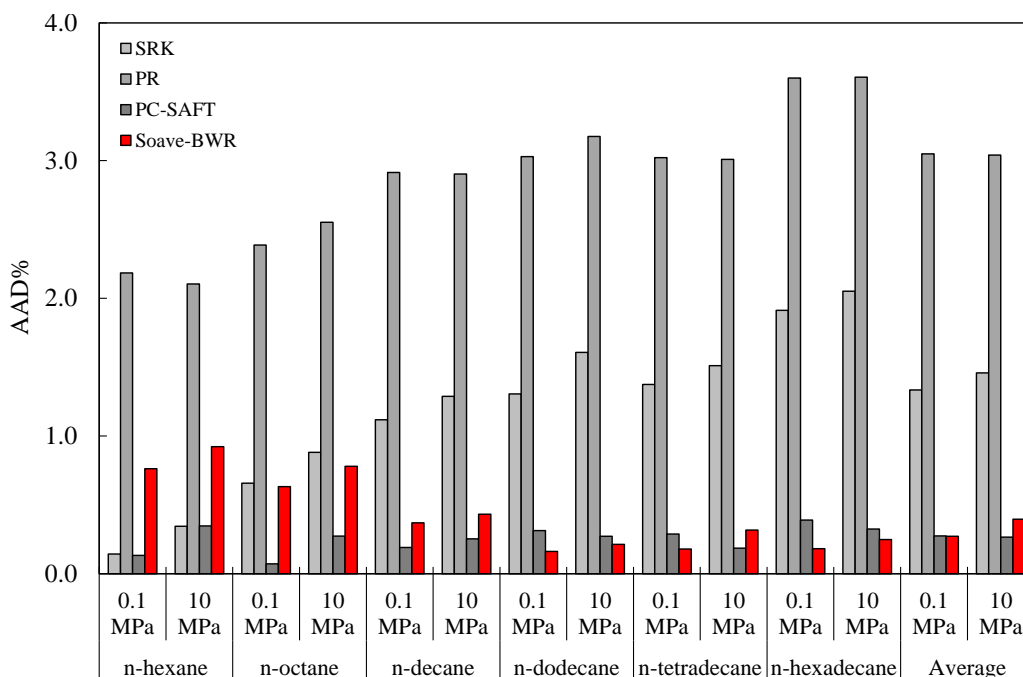


Figure 5.13 Absolute Average Deviation (AAD) in calculation of C_p of the n-alkanes studied in this work using different EoSs at 0.1 MPa and 10 MPa.

In order to see the trend of the specific C_p with the carbon number of the n-alkanes, we have plotted in Figure 5.14 the experimental C_p as well as the model predictions as a function of the carbon number at 0.1 and 10 MPa at four different temperatures. In general, it can be observed that the specific C_p decreases with carbon number until carbon number 10 or 12, and keeps almost constant for higher carbon numbers. This behavior has been already reported by Huang et al. [155]. Concerning model predictions, as it can be seen in Figure 5.14, SRK and PR under predict C_p values for all the n-alkanes and the deviation increases as the carbon number increases. PC-SAFT and Soave-BWR give better prediction of C_p as a function of carbon number at both 0.1 and 10 MPa.

In order to get a deeper understanding on how the models predict the values of C_p with carbon number, the model predictions using SRK, PR and PC-SAFT for heavier normal alkanes up to nC₃₆ are presented in Figure 5.15. The results show that these three EoSs tend to approach a constant value for the specific C_p as the carbon number increases. For Soave-BWR, on the other hand, the predictions for normal alkanes heavier than n-hexadecane seems to be unreliable as the values of specific heat capacities increase with carbon number.

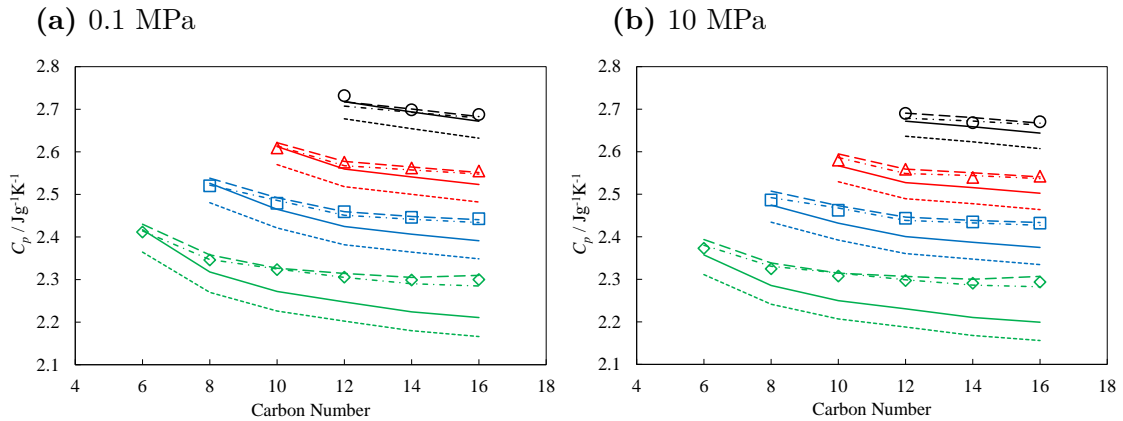


Figure 5.14 C_p of n-alkanes as a function of the carbon number at (a) 0.1 MPa and at (b) 10 MPa. 333.15 K (\diamond), 373.15 K (\square), 403.15 K (\triangle) and 438.15 K (\circ). SRK (solid line), PR (dashed line), PC-SAFT (dash-dot line) and Soave-BWR (long dashed line).

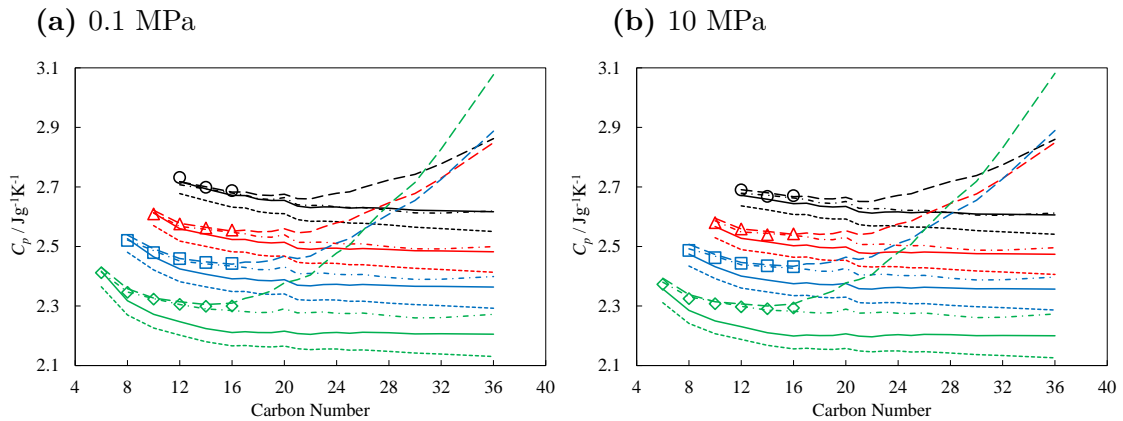


Figure 5.15 C_p of n-alkanes up to nC_{36} as a function of the carbon number at (a) 0.1 MPa and at (b) 10 MPa. 333.15 K (\diamond), 373.15 K (\square), 403.15 K (\triangle) and 438.15 K (\circ). SRK (solid line), PR (dashed line), PC-SAFT (dash-dot line) and Soave-BWR (long dashed line).

The calculation results for Joule-Thomson coefficient using all the four EoSs are presented in Tables C.5–C.8 in Appendix C. Table 5.5 summarizes the Absolute Average Deviation (AAD / %) and the maximum deviation in the calculation of the Joule-Thomson coefficient of the n-alkanes at different pressures using the different EoSs.

The results show that both the AAD and maximum deviation are significantly lower for the non-cubic EoSs in comparison to the cubic models for the n-alkanes tested in this study. SRK with around 46% deviation, gives the largest deviation among all the four EoSs while Soave-BWR gives the lowest deviation for both low and high pressures which is 3.24% and 2.70%, respectively. PC-SAFT gives slightly higher

Table 5.5 Absolute Average Deviation (AAD) and maximum deviation (Max. Dev.) in the Joule-Thomson coefficient calculation of the n-alkanes studied in this work at different pressures using different EoSs.

P/MPa	SRK		PR		PC-SAFT		Soave-BWR	
	0.1	10	0.1	10	0.1	10	0.1	10
	n-hexane							
AAD / %	9.11	16.65	3.30	6.97	4.65	3.90	3.09	3.26
Max. Dev. / %	11.30	20.82	5.14	11.35	4.83	4.33	3.29	3.69
	n-octane							
AAD / %	19.71	27.75	12.46	2.55	2.17	1.62	4.10	3.71
Max. Dev. / %	27.64	32.26	19.09	3.96	2.52	1.95	5.15	4.74
	n-decane							
AAD / %	34.37	39.55	25.38	27.95	2.59	2.22	1.49	1.30
Max. Dev. / %	41.87	44.33	31.70	32.85	2.97	2.50	1.82	1.84
	n-dodecane							
AAD / %	42.95	48.43	33.14	35.98	3.90	3.33	0.89	0.48
Max. Dev. / %	49.74	52.20	38.63	39.99	6.80	5.38	2.55	1.75
	n-tetradecane							
AAD / %	54.21	57.97	43.29	44.52	4.02	2.33	3.84	2.93
Max. Dev. / %	61.03	62.23	48.80	49.11	5.57	3.91	5.68	4.42
	n-hexadecane							
AAD / %	65.04	66.91	52.79	52.80	5.05	3.57	5.40	4.68
Max. Dev. / %	69.29	70.79	56.28	56.97	6.74	7.23	7.30	9.40
	Overall							
AAD / %	46.25	48.75	36.10	36.24	3.83	2.81	3.24	2.70

absolute average deviation than Soave-BWR for both 0.1 MPa and 10 MPa. The maximum AAD for SRK is 70.79% for n-hexadecane at 10 MPa, while for Soave-BWR the maximum AAD is 9.40% for n-hexadecane at 10 MPa. The maximum AAD for PC-SAFT is lower than the other three EoSs. The overall AAD for all the n-alkanes tested is presented in Figure 5.16.

Figure 5.17 illustrates the experimental Joule-Thomson coefficient as well as the model predictions as a function of the carbon number at 0.1 and 10 MPa. Both SRK and PR show large deviations and, for clarity, their results are only presented at 333.15 K. SRK and PR under predict the Joule-Thomson coefficient for all the n-alkanes and the deviation increases as the carbon number and pressure increase. PC-SAFT and Soave-BWR give better prediction of Joule-Thomson coefficient as a function of carbon number at both 0.1 and 10 MPa.

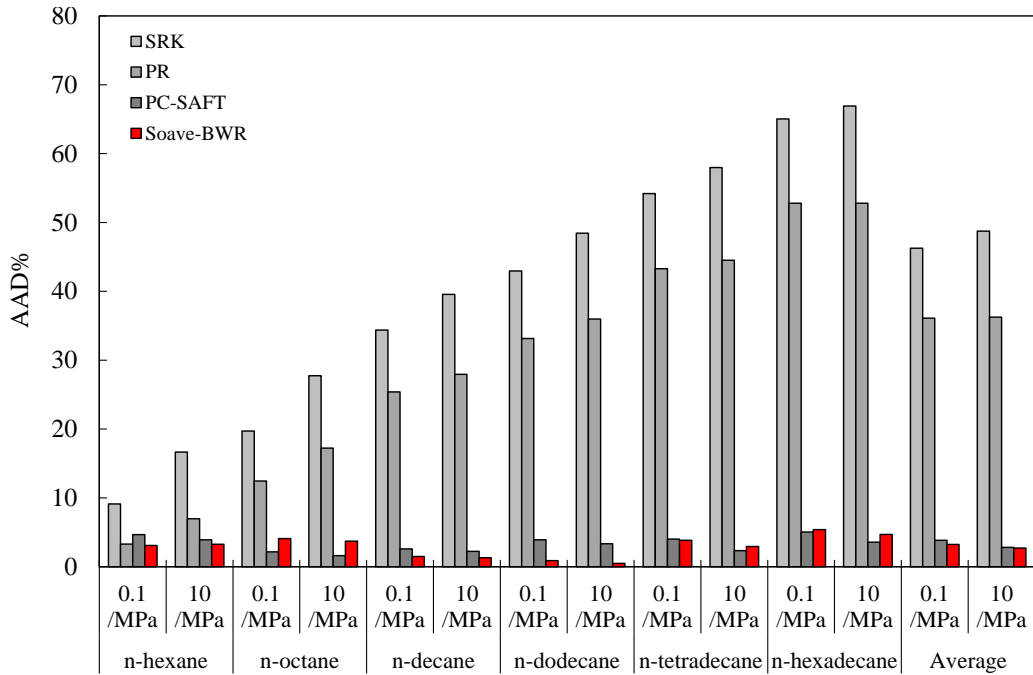


Figure 5.16 Absolute Average Deviation (AAD) in the calculation of the Joule-Thomson coefficient of the n-alkanes studied in this work using different EoS at 0.1 MPa and 10 MPa.

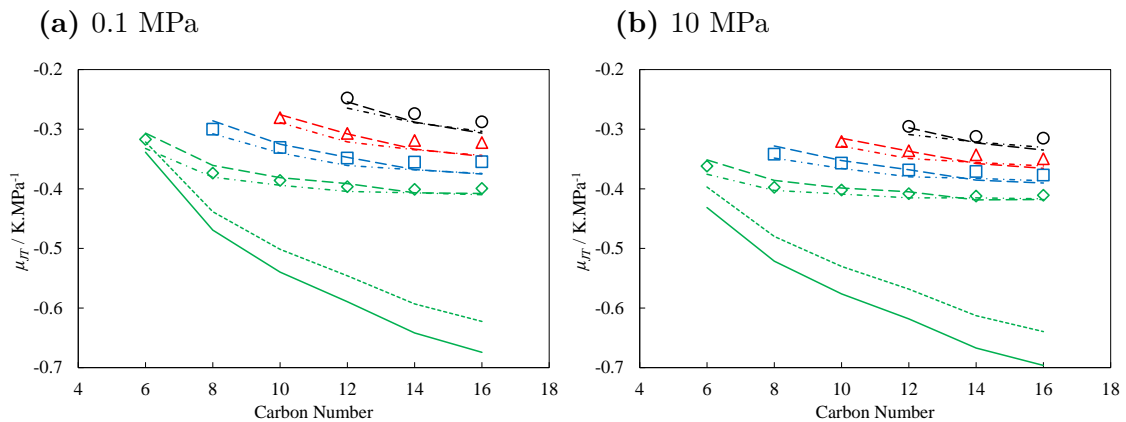


Figure 5.17 Joule-Thomson coefficient of n-alkanes as a function of the carbon number at (a) 0.1 MPa and at (b) 10 MPa. 333.15 K (\diamond), 373.15 K (\square), 403.15 K (\triangle) and 438.15 K (\circ). SRK (solid line), PR (dashed line), PC-SAFT (dash-dot line) and Soave-BWR (long dashed line).

Both for PC-SAFT and Soave-BWR we have further investigated the prediction capability of the Joule-Thomson coefficient of heavier n-alkanes, which is shown in Figure 5.18. It can be observed that both models give similar predictions at high temperatures. It is also interesting to note that both models predict an increase in μ_{JT} with carbon number, this increase happens for carbon numbers higher than nC_{32}

for PC-SAFT, whereas for Soave-BWR μ_{JT} increases for carbon numbers higher than n-C16 at low temperatures.

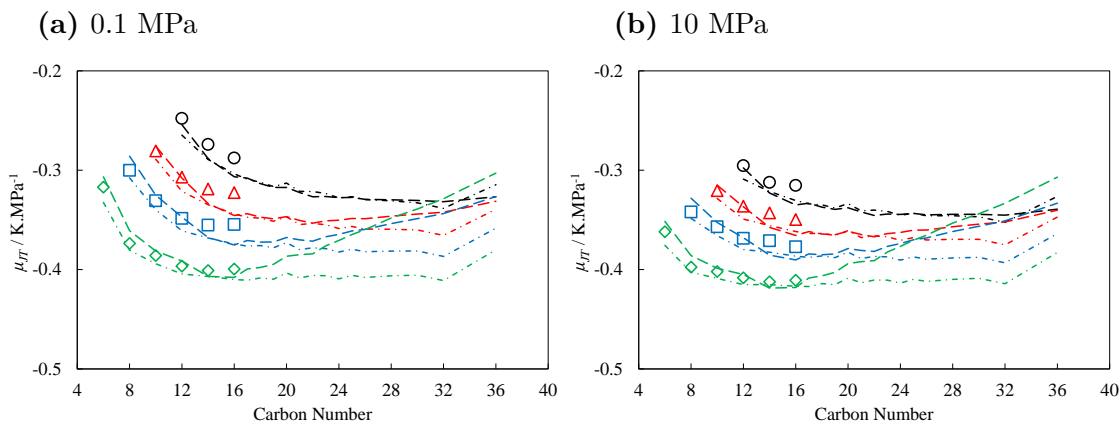


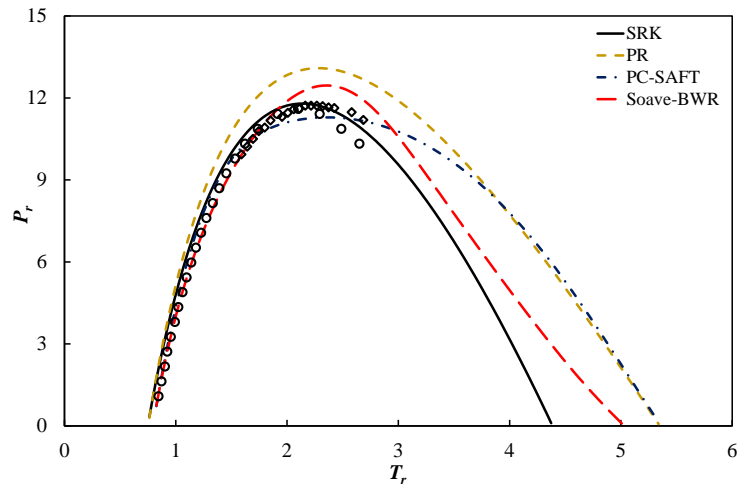
Figure 5.18 Joule-Thomson coefficient of n-alkanes up to nC₃₆ as a function of the carbon number at (a) 0.1 MPa and at (b) 10 MPa. 333.15 K (\diamond), 373.15 K (\square), 403.15 K (\triangle) and 438.15 K (\circ). PC-SAFT (dash-dot line) and Soave-BWR (long dashed line).

5.3.3 Joule-Thomson Inversion Curve

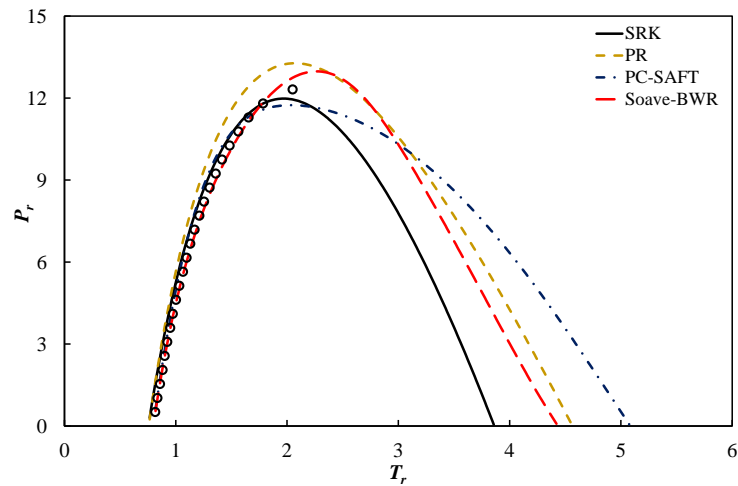
As concerns the calculation of the Joule-Thomson inversion curve through the four different EoSs studied in this work, the inversion curves of methane, ethane and propane were first calculated, as there are available experimental data [137, 156] for these light alkanes. The obtained results are presented in Figure 5.19, so that it is possible to see the performance of the different EoSs for the prediction of the experimental data. It can be observed that the best prediction for the inversion curve is obtained by Soave-BWR for ethane and propane, whereas SRK gives the best predictions for methane. Moreover, the studied models have a better agreement in the low-temperature branch, whereas noticeable differences occur in the high-temperature branch for these three n-alkanes. As previously stated by Colina et al. [139], this is because the Joule-Thomson coefficients are more sensitive to pressure and temperature in the high-temperature branch.

The calculation results of the Joule-Thomson inversion curve for the six n-alkanes studied in this work are presented in Figure 5.20. As for the light n-alkanes, the model predictions have a good agreement in the low-temperature branch but the pT regions with positive Joule-Thomson coefficients predicted by the cubic EoSs are smaller than those predicted by the non-cubic models.

(a) Methane



(b) Ethane



(c) Propane

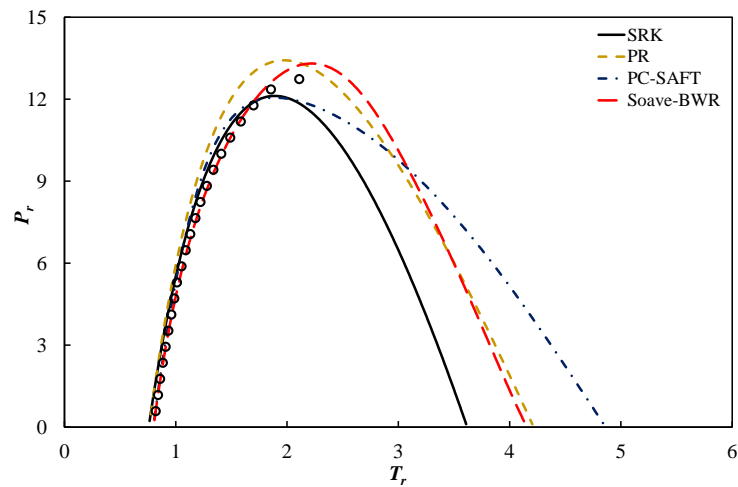


Figure 5.19 Calculated inversion curve for Joule-Thomson coefficient of (a) methane, (b) ethane and (c) propane through SRK, PR, PC-SAFT and Soave-BWR. Experimental data from Perry's handbook [156] (\circ) and Bessières et al. [137] (\diamond). P_r is the reduced pressure and T_r the reduced temperature.

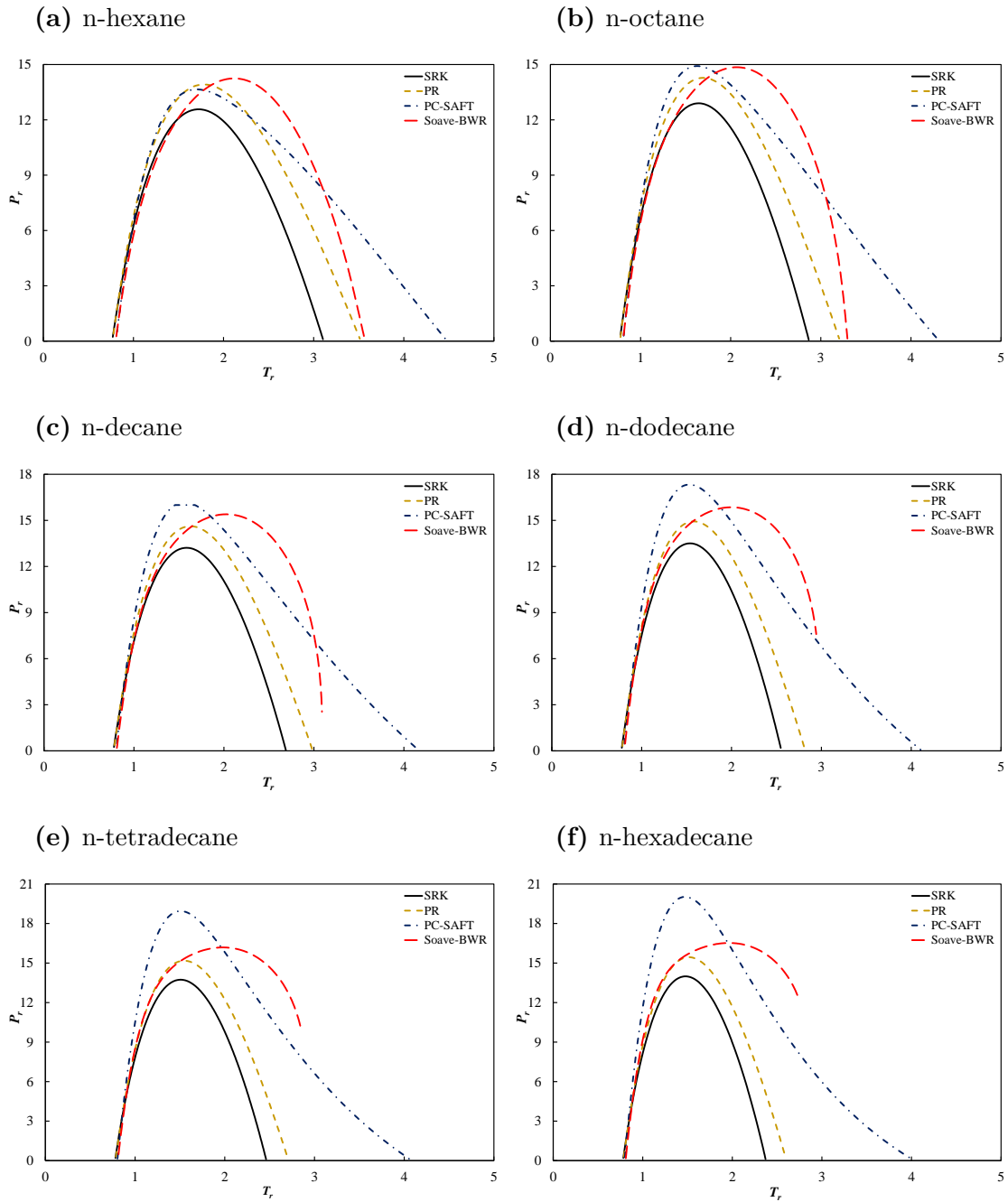


Figure 5.20 Predicted inversion curves for different n-alkanes using SRK, PR, PC-SAFT and Soave-BWR. P_r is the reduced pressure and T_r the reduced temperature.

Finally, in order to see how the Joule-Thomson inversion curves change with carbon number, the model predictions using PC-SAFT for the studied n-alkanes are presented in Figure 5.21. The calculation suggests that the peak of the inversion curve increases with the carbon number, while the maximum temperature decreases. This behavior is also noticed for the cubic EoSs.

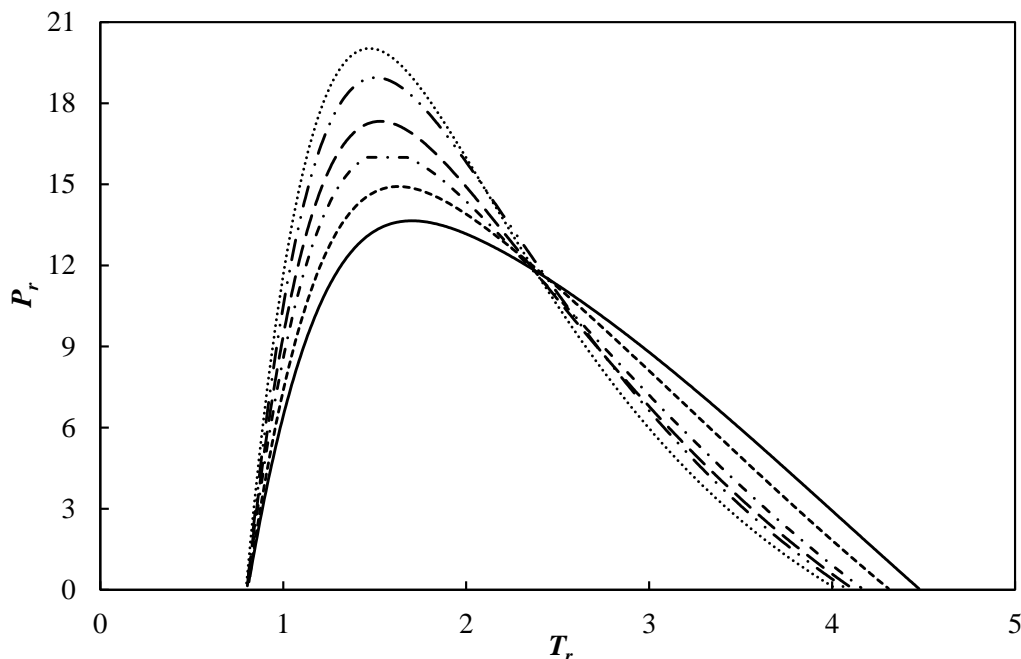


Figure 5.21 Predicted inversion curves for the n-alkanes studied in this work, obtained from the PC-SAFT EoS. n-hexane (solid line), n-octane (dashed line), n-decane (dash-dot line), n-dodecane (long dashed line), n-tetradecane (long dashed double dots line) and n-hexadecane (dotted line). p_r is the reduced pressure and T_r the reduced temperature.

5.4 Conclusions

A comprehensive comparison was made between cubic (SRK and PR) and non-cubic EoSs (Soave-BWR, PC-SAFT and GERG-2008) in calculation of heat capacity and Joule-Thomson coefficient for pure components and multicomponent mixtures over a wide pressure and temperature range. The results were compared with available experimental data in the literature and special emphasis was given to the reverse Joule-Thomson effects at high pressure high temperature (HPHT) conditions.

The calculation results showed that GERG-2008 have some advantages over other EoSs in calculation of heat capacity and Joule-Thomson coefficient of pure components over a wide temperature and pressure range. Soave-BWR gives the closest prediction of the thermal properties to that of GERG-2008 among other EoSs tested in this study. In general and for all the scenarios tested from pure components to multicomponent mixtures, the non-cubic models seem to be superior to the cubic models in calculation of derivative properties such as heat capacity and Joule-Thomson coefficient. For the

heat capacity of multicomponent mixtures, PC-SAFT gives the lowest deviation and PR seems to have slightly better performance than Soave-BWR.

It was observed that non-cubic models (i.e. Soave-BWR and GERG-2008) predict a negative Joule-Thomson coefficient at high pressures and all temperatures for pure, binary and multicomponent systems. In fact, the value of Joule-Thomson coefficient seems to reach more or less a constant value at high pressures for all the systems tested. The negative Joule-Thomson coefficient at high pressures causes the temperature of the fluid to increase with the pressure drop (reverse Joule-Thomson effect). Although the temperature increase is not very significant (around 0.5 K/Mpa), it should be considered in the material selection for the tubing and surface facilities because the temperature increase can damage the surface production facilities and affect well integrity and safety.

Values of C_p and μ_{JT} for n-hexane, n-octane, n-decane, n-dodecane, n-tetradecane and n-hexadecane at 0.1 and 10 MPa and temperatures up to 483.15 K was also calculated using SRK, PR, PC-SAFT and Soave-BWR and the results were compared with the experimental measurements. Again, non-cubic models were superior to the cubic ones and for C_p , the lowest AAD was obtained for PC-SAFT (0.27%) and the highest for PR (3.05%). For the Joule-Thomson coefficient calculations using the aforementioned models, a poorer performance was obtained with the cubic EoSs, thus the worst prediction was obtained for SRK with around 46% deviation, whereas the best prediction was obtained for Soave-BWR with around 3% deviation, closely followed by PC-SAFT. As regards the prediction of the Joule-Thomson inversion curve, it was found a reasonable agreement among the four models in the low-temperature branch and also that cubic EoSs yield a smaller $P-T$ region of positive Joule-Thomson coefficient.

6 | New Mixing Rules for Soave-BWR

In order to apply an EoS to multicomponent mixtures, we need to apply some mixing rules to calculate the model parameters for the mixtures. The functional form of any mixing rule always involves the mixture composition, the parameters of the constituting components and some interaction parameters characterizing the departure from some ideal interactions between molecules. Since it was found that the Soave-BWR EoS has problems in modeling petroleum fluids probably due to its mixing rules, we attempt to use some new mixing rules with Soave-BWR. In this chapter, we first review the classical mixing rules especially those used for non-cubic EoS models. We then describe several new mixing rules tested for Soave-BWR. Most mixing rules currently in use for EoS models are either semi-empirical or empirical and it is especially the case for non-cubic models including Soave-BWR. The mixing rules proposed for Soave-BWR here are based on some theoretical considerations as well as the previous mixing rules for non-cubic EoS models. In addition, we also tried to create some hybrid mixing rules to test their effects. A preliminary evaluation is used to screen out some of these mixing rules. Several selected ones are used in the final evaluation using more phase equilibrium and density data.

6.1 Equations of State Mixing Rules

The most common way to apply an EoS to fluid mixtures is to use the *one fluid* concept, where the same equation form is assumed to be valid for both pure components and mixtures as long as an appropriate way can be found to obtain the EoS parameters for mixtures. In the one fluid concept, the mixture's PVT behavior is assumed to have the same temperature and density dependence as pure components, and it is assumed

that there is no need to add mixture-only terms or modify the functional form of the EoS [157]. To use this approach and extend the use of equations of state developed for pure fluids to mixtures, we must find a way of calculating the EoS parameters for the mixture. For this purpose, we rely on mixing rules that express mixture EoS parameters as functions of three elements:

- Mixture composition
- Properties of the constituent pure components (such as critical properties or EoS parameters)
- Mixture-specific constants to characterize interactions between different components (such as binary interaction parameters)

The classical EoS mixing rules are firmly rooted in the one-fluid concept. They have a long history and most widely used in engineering calculations. They are suitable mainly for symmetric mixtures and can be applied to asymmetric ones with certain success by use of binary interaction parameters. For highly asymmetric mixtures or mixtures consisting of non-polar and polar or associating compounds, other types of mixing rules like excess free energy mixing rules and density dependent mixing rules [158] can usually provide better results. These mixing rules, however, usually result in either more interaction parameters, or more complicated equation form, or both. For hydrocarbon systems encountered in the oil industry or the chemical industry, it is still favorable to use the classical mixing rules or some similar forms if possible. This is because most binary pairs are rather symmetric and it can be an over complication to resort mixing rules with more than one interaction parameter. There is asymmetry in petroleum mixtures but for common PVT calculations, the extreme asymmetry between light hydrocarbons and the extreme heavy ends, say C_{100} , is usually not a major concern. Use of a reasonable interaction parameter to correct the classical mixing rules is a more pragmatic approach. For the above considerations, our focus here is on the classical mixing rules and their moderate modifications. The review below covers just the classical mixing rules and some typical mixing rules used for the virial type equations of state.

6.1.1 Classical Mixing Rules

It is convenient to distinguish two different ways how the classical mixing rules are constructed:

- The corresponding states approach where mixing rules are applied to critical properties or other similar physical parameters which are at the bottom level of the model calculations. These parameters are used to express the coefficients in the final functional form of the EoS. Usually for a mixture, the mixing rules calculate its pseudo-critical properties which play the same role as pure component critical properties for its constituting pure components.
- The van der Waals approach where mixing rules are directly applied to the coefficients in the final functional form of the EoS, such as the energy and co-volume parameters in most van der Waals-type EoS models.

The corresponding states approach is based on the corresponding state principle which assumes that at a given set of reduced specifications (for example reduced temperature and volume) that can determine the state of the system, the other reduced quantities (such as reduced pressure) should be the same. Since the reduced quantities are calculated using critical properties for pure components and pseudo-critical properties for the mixture, the central problem is therefore how to calculate pseudo-critical properties. It should be noted that the pseudo-critical properties calculated from the mixing rules are not the true critical properties for the mixture, and are actually quite far from them in general. The pseudo-critical properties are only meant to provide good corresponding states behavior. The simplest formulation for pseudo-critical properties is Kay's rules [159], which are simply mole fraction weighted sums of the individual pure component critical properties. According to Poling et al. [160], Kay's rules provide acceptable values for pseudo-critical temperature, volume, and compressibility, as well as acentric factor. For pseudo-critical pressure, they recommend using the rule of Prausnitz and Gunn [161, 162], in which pseudo-critical pressure is calculated using pseudo-critical compressibility, volume, and temperature from Kay's rules.

The van der Waals approach is quite common especially for cubic EoS models. For a parameter M in the final expression for an EoS, the mixing is made directly on M instead of the critical properties or other physical parameters used to calculate M . The mixing rules can be formulated in various ways but the linear and quadratic forms

seem to be the most common. The linear mixing rule assumes the following form:

$$M_{mix} = \sum_i x_i M_i \quad (6.1)$$

where x_i is the mole fraction of the i th pure component in the mixture. The linear mixing rule does not allow the incorporation of mixture-specific interaction parameters into the calculation. The quadratic mixing rule is slightly more complex and essentially expresses the mixture parameter as the sum of contributions from all possible binary pairs of pure components in the mixture, with each contribution weighted by the product of the mole fractions of the two components in the pair. The quadratic mixing rule can be written as:

$$M_{mix} = \sum_i \sum_j x_i x_j M_{ij} \quad (6.2)$$

where M_{ij} is referred to as the cross term for the pair consisting of the i th and j th components, or simply the combining rule. For $i = j$, the M_{ij} term is equal to the corresponding pure-component value.

One of the theoretical basis for the quadratic mixing rule is the quadratic composition dependence for the second virial coefficient required by the statistical mechanics [163]. There is, however, no precise requirement for the concrete form of the combining rule used for calculating M_{ij} . This creates some empirical flexibility in how the combining rule is defined. Among various forms proposed, the arithmetic mean and geometric mean are the most popular forms:

$$M_{ij} = \frac{M_i + M_j}{2} (1 - k_{ij}) \quad (6.3)$$

$$M_{ij} = \sqrt{M_i M_j} (1 - k_{ij}) \quad (6.4)$$

In eqs. (6.3)–(6.4), k_{ij} is a binary interaction parameter, essentially a correction factor specific to the binary pairing between components i and j . These two combining rules can be considered mathematically equivalent in the sense that for a specific M_{ij} calculated from eq. (6.3), one can in principle find a k_{ij} for eq. (6.4) to match it. There is however one constraint for eq. (6.4), namely M_i and M_j being the same sign. Equation (6.3) does not have such a constraint. It should also be noted that if zero k_{ij} is used for eq. (6.3), the quadratic mixing rule eq. (6.2) reduces to the linear form of eq. (6.1).

It should be noted that these two approaches are mathematically equivalent in the sense that the same value of M_{ij} can be calculated from either expression with the appropriate value of k_{ij} . Another important observation, however, is that with the geometric mean expression (eq. (6.4)), parameter M must have the same sign for both components to avoid a negative value under the square root sign. This restriction does not apply to the arithmetic mean expression in eq. (6.3).

The van der Waals one fluid mixing rules mentioned in section 2.1.2 are typical examples for the second approach. The mixing rules assume the following form:

$$a = \sum_i \sum_j x_i x_j a_{ij} \quad (6.5)$$

$$b = \sum_i \sum_j x_i x_j b_{ij} \quad (6.6)$$

with the following combining rules:

$$a_{ij} = \sqrt{a_i a_j} (1 - k_{ij}) \quad (6.7)$$

$$b_{ij} = \frac{b_i + b_j}{2} (1 - l_{ij}) \quad (6.8)$$

where k_{ij} and l_{ij} are the binary-interaction parameters obtained by fitting EoS predictions to measured phase-equilibrium and volumetric data. In these equations, arithmetic mean is used for the co-volume parameter b and geometric mean is used for the energy parameter a . Such a choice is often explained by following the Lorentz-Berthelot rules:

$$\sigma_{ij} = \frac{\sigma_i + \sigma_j}{2} \quad (6.9)$$

$$\varepsilon_{ij} = \sqrt{\varepsilon_i \varepsilon_j} \quad (6.10)$$

although it is arguable whether the analogy is completely correct [13]. Indeed, the theoretical basis for the mixing rules used in the engineering equations is not always strict. Multiple theoretical interpretations can sometimes be found and usually none has the sufficient rigor to prescribe a unique set of mixing and combining rules. The actual performance of a set of mixing rules must be evaluated by specific applications of interest, for instance, description of vapor-liquid equilibrium (VLE) data. For VLE of relatively ideal hydrocarbon mixtures, zero k_{ij} and l_{ij} are a good approximation. For non-ideal mixtures, nonzero k_{ij} 's will be needed that sometimes are temperature dependent [164].

6.1.2 Mixing Rules for The Virial Family of EoS

Most multi-parameter EoS models can be considered to be extension of the virial equations of state. We review here several typical mixing rules used for these virial family EoS.

Mixing Rules for the BWR EoS

One of the exact results from statistical mechanics is the virial equation of state:

$$Z = \frac{Pv}{RT} = 1 + \frac{B}{v} + \frac{C}{v^2} + \dots \quad (6.11)$$

where Z is the compressibility factor, P is the pressure, R is the gas constant, T is the temperature, v is the molar volume, and B and C are the second and third virial coefficients. The virial coefficients are related to the intermolecular force between molecules, and for pure fluids they are functions of temperature only. The second virial coefficient depends on interactions between pairs of molecules, while third virial coefficient depends on interactions between groups of three molecules, and so on. The mixing rules for the virial equation of state can be derived from statistical mechanics and are given by:

$$B = \sum_i \sum_j x_i x_j B_{ij}(T) \quad (6.12)$$

$$C = \sum_i \sum_j \sum_k x_i x_j x_k C_{ijk}(T), \text{ etc.} \quad (6.13)$$

As can be seen, the mixture second virial coefficients are quadratic in composition. As a result, B is the summation of contributions from all possible pairings of components in the mixture, and each contribution is proportional to the product of the mole fractions of the two substances in the pair. Similarly, third virial coefficients have a cubic composition dependence, and higher-order coefficients have higher-order composition dependencies. As will be seen, eq. (6.13) is used as the basis for mixing rules with extended virial EoSs. Although the composition dependence of the virial coefficients are determined by statistical mechanics, it is not clear from the theory how the combining rules for B_{ij} , C_{ij} , and higher-order coefficients can be calculated from pure component EoS parameters.

The virial equation is of limited use as it is only applicable to gases; however, the known composition dependence of the virial coefficients provides the basis for the mixing rule

for this family of equations of state. In 1940, Benedict, Webb, and Rubin developed the BWR EoS, which is a virial type EoS, by fitting the PVT data of n-alkanes from methane to n-butane [35], and later extended to include eight additional hydrocarbons up to n-heptane [165]. This equation is useful for the high-accuracy calculation of density and derived properties, such as enthalpy, fugacity, vapor pressure, and latent heat of vaporization. The BWR equation is a closed form of the virial EoS as it contains an exponential term that can be expanded into an infinite series in reciprocal molar volume representing all the remaining terms in the series. This exponential term makes a large contribution to the equation of state at high density and in the critical region. Expanding the BWR equation in virial form, we obtain:

$$Z = 1 + \frac{B_0 - \frac{A_0}{RT} - \frac{C_0}{RT^3}}{v} + \frac{b - \frac{a}{RT} + \frac{c}{RT^3}}{v^2} - \frac{\gamma c}{RT^3 v^4} + \dots \quad (6.14)$$

where B_0 , A_0 , C_0 , a , b , c , and γ are the EoS parameters.

The most common method of extending the BWR EoS to mixtures is based on the van der Waals one-fluid theory that the mixture and the pure fluids should satisfy the same equation of state. The method also attempts to ensure the correct composition dependence of as many virial coefficients as possible. Comparing eq. (6.14) with eq. (6.11) shows that the nominator of $\frac{1}{v}$ in the second term on the left hand side of eq. (6.14) is equivalent to the second virial coefficient. As a result, B_0 , A_0 , C_0 which are the parameters associated with the second virial coefficient should have a quadratic mixing rule. The following equations show the mixing rules used for BWR EoS (a linear mixing rule is used for B_0):

$$B_0 = \sum_i x_i B_{0i} \quad , \quad A_0 = \left[\sum_i x_i (A_{0i})^{1/2} \right]^2 \quad , \quad C_0 = \left[\sum_i x_i (C_{0i})^{1/2} \right]^2 \quad (6.15)$$

$$a = \left[\sum_i x_i (a_i)^{1/3} \right]^3 \quad (6.16)$$

$$b = \left[\sum_i x_i (b_i)^{1/3} \right]^3 \quad (6.17)$$

$$c = \left[\sum_i x_i (c_i)^{1/3} \right]^3 \quad (6.18)$$

$$\gamma = \left[\sum_i x_i (\gamma_i)^{1/2} \right]^2 \quad (6.19)$$

The shortcoming of these mixing rules was that their combining rules did not contain any adjustable parameters and binary interaction coefficients. As a result, although they may give satisfactory results for light hydrocarbon mixtures, they cannot provide accurate description of mixtures containing non-hydrocarbons or even heavy and asymmetric hydrocarbon systems [164].

Generalized Extended Virial Equations of State and Their Mixing Rules

Bishnoi and Robinson [166] proposed a different set of mixing rules that incorporated both higher-order composition dependence for the various parameters, as well as a binary interaction parameter for EoS constants associated with the second and third virial coefficients. For constants associated with the second virial coefficient, they proposed quadratic mixing rules, while for parameters associated with third and higher virial coefficients, cubic mixing rules were used. The cubic cross coefficient between a given group of three substances was defined as the products of the binary cross coefficients for the three possible pairings in the group (e.g. $b_{ijk} = (b_{ij}b_{ik}b_{jk})^{1/3}$). In this way, only binary interaction parameters were required, as opposed to interaction parameters specifically for ternary mixtures.

In 1973, and for this modification of the BWR equation, Starling [167] proposed a new set of mixing rules. For parameters associated with the second virial coefficient, he used the mixing rules proposed by Bishnoi and Robinson. For the higher-order terms, however, he used the same mixing rules as the original BWR equation—linear rules in varying powers of the EoS coefficients. The Starling modification of BWR (BWRS) EoS has the following form:

$$\begin{aligned}
 P = \rho_m RT + & \left(B_0 RT - A_0 - \frac{C_0}{T^2} + \frac{D_0}{T^3} - \frac{E_0}{T^4} \right) \rho_m^2 + \left(bRT - a - \frac{d}{T} \right) \rho_m^3 \\
 & + \alpha \left(a + \frac{d}{T} \right) \rho_m^6 + \frac{c\rho_m^3}{T^2} (1 + \gamma\rho_m^2) \exp(-\gamma\rho_m^2)
 \end{aligned} \tag{6.20}$$

and the following equations show the mixing rules suggested by Starling [167]:

$$B_0 = \sum_i x_i B_{0i} \quad (6.21)$$

$$A_0 = \sum_i \sum_j x_i x_j \sqrt{A_{0i} A_{0j}} (1 - k_{ij}) \quad (6.22)$$

$$C_0 = \sum_i \sum_j x_i x_j \sqrt{C_{0i} C_{0j}} (1 - k_{ij})^3 \quad (6.23)$$

$$D_0 = \sum_i \sum_j x_i x_j \sqrt{D_{0i} D_{0j}} (1 - k_{ij})^4 \quad (6.24)$$

$$E_0 = \sum_i \sum_j x_i x_j \sqrt{E_{0i} E_{0j}} (1 - k_{ij})^5 \quad (6.25)$$

$$a = \left[\sum_i x_i (a_i)^{1/3} \right]^3 \quad (6.26)$$

$$b = \left[\sum_i x_i (b_i)^{1/3} \right]^3 \quad (6.27)$$

$$c = \left[\sum_i x_i (c_i)^{1/3} \right]^3 \quad (6.28)$$

$$d = \left[\sum_i x_i (d_i)^{1/3} \right]^3 \quad (6.29)$$

$$\alpha = \left[\sum_i x_i (\alpha_i)^{1/3} \right]^3 \quad (6.30)$$

$$\gamma = \left[\sum_i x_i (\gamma_i)^{1/2} \right]^2 \quad (6.31)$$

It should be noted that the binary interaction parameters are defined only for parameters associated with the temperature dependence of the second virial coefficient (A_0 , C_0 , D_0 , and E_0). In each of the instances described above, a separate mixing rule is provided for each individual coefficient, even those within the temperature functions. As such, mixture values are first calculated for each individual parameter, and then inserted into the temperature functions to calculate the value of the mixture density coefficient at the temperature of interest.

Mixing Rules for the Lee-Kesler-Plocker (LKP) EoS

In 1978, Plocker et al. [47] developed a new set of mixing rules for the Lee and Kesler correlation [114]. Instead of defining the mixing rules directly for the EoS parameters,

they proposed the mixing rules for the pseudo-critical properties of the mixture as a function of pure-components' critical properties:

$$T_{cm} = \frac{1}{v_{cm}^\eta} \sum_i \sum_j x_i x_j v_{cij}^\eta \cdot T_{cij} \quad (6.32)$$

$$v_{cm} = \sum_i \sum_j x_i x_j v_{cij} \quad (6.33)$$

$$\omega_m = \sum_i x_i \omega_i \quad (6.34)$$

where v_c is the molar critical volume, T_c is the critical temperature, and ω is the acentric factor.

The combining rules are given by:

$$T_{cij} = \sqrt{T_{ci} T_{cj}} (1 - k_{ij}) \quad (6.35)$$

$$v_{cij} = \frac{1}{8} \left(v_{ci}^{1/3} + v_{cj}^{1/3} \right)^3 \quad (6.36)$$

and the pseudo-critical compressibility factor is found using the following correlation:

$$Z_{cm} = 0.2905 - 0.085\omega_m \quad (6.37)$$

They found that for the symmetric systems, the exponent η is of no importance and thus can be set equal to zero. For strongly asymmetric mixtures on the other hand, they noticed that while $\eta = 0$ could not take the effect of molecular size into proper account, setting $\eta = 1$ lead to overestimating that effect. The optimal value of η was empirically found to be 0.25.

Mixing Rules for the Soave-BWR EoS

To develop a new set of mixing rules for the BWR EoS, Soave suggested a new application of the pseudo-critical approach based on the analogy with the mixing rules for the cubic EoS [36]. He considered a typical two-parameter cubic equation:

$$a = \Omega_a R^2 \left(\frac{T_c^2}{P_c} \right) \alpha \quad (6.38)$$

$$b = \Omega_b R \left(\frac{T_c}{P_c} \right) \quad (6.39)$$

where a linear mixing rule for the co-volume parameter and a quadratic mixing rule for the attractive parameter of the EoS were used:

$$b = \sum_i x_i b_i \quad (6.40)$$

$$a = \sum_i \sum_j x_i x_j a_{ij} = \sum_i \sum_j x_i x_j (1 - k_{ij}) \sqrt{a_i a_j} \quad (6.41)$$

Combining eq. (6.39) and eq. (6.40) gave the following equation:

$$\frac{T_c}{P_c} = \sum_i x_i \frac{T_{ci}}{P_{ci}} \equiv S_3 \quad (6.42)$$

and from eq. (6.38) and eq. (6.41) he obtained:

$$\frac{T_c^2}{P_c} \alpha = \sum_i \sum_j x_i x_j (1 - k_{ij}) \frac{T_{ci} T_{cj}}{\sqrt{P_{ci} P_{cj}}} \sqrt{\alpha_i \alpha_j} \quad (6.43)$$

Using the definition for α (eq. (2.6)) in the above equation lead to the following set of equations that had to be valid at all temperatures:

$$\frac{T_c^2}{P_c} (1 + m)^2 = \sum_i \sum_j x_i x_j (1 - k_{ij}) \frac{T_{ci} T_{cj}}{\sqrt{P_{ci} P_{cj}}} (1 + m_i)(1 + m_j) \equiv S_1 \quad (6.44)$$

$$\frac{T_c}{P_c} m^2 = \sum_i \sum_j x_i x_j (1 - k_{ij}) \sqrt{\frac{T_{ci} T_{cj}}{P_{ci} P_{cj}}} m_i m_j \equiv S_2 \quad (6.45)$$

$$\begin{aligned} \frac{T_c^{3/2}}{P_c} m(1 + m) &= \sum_i \sum_j x_i x_j (1 - k_{ij}) \sqrt{\frac{T_{ci} T_{cj}}{P_{ci} P_{cj}}} \times \\ &[m_j(1 + m_i) \sqrt{T_{ci}} + m_i(1 + m_j) \sqrt{T_{cj}}] \end{aligned} \quad (6.46)$$

Since the left hand side of eq. (6.46) is the geometric mean of the left hand sides in eqs. (6.44)–(6.45), eq. (6.46) was neglected and the following set of mixing rules was proposed for the BWR EoS:

$$T_{cm} = S_1 / (\sqrt{S_2} + \sqrt{S_3})^2 \quad (6.47)$$

$$P_{cm} = T_{cm} / S_3 \quad (6.48)$$

$$m_m = \sqrt{S_2 / S_3} \quad (6.49)$$

m in eq. (6.49) is a function of ω and a simple proportionality relationship is used for it:

$$m = \mu\omega \quad (6.50)$$

with an empirical value 1.25 given to μ [9].

6.2 Development of New Mixing Rules for Soave-BWR

This section discusses the development and implementation of new mixing rules for Soave-BWR. We have developed two major sets of new mixing rules. The first set uses the van der Waals approach where the mixture EoS parameters are directly calculated from the pure component EoS parameters. This set is comparable to the mixing rules used by Starling [167]. The second set is the Lee-Kesler-Plöcker (LKP) mixing rules [47] where pseudo-critical properties are calculated from the pure component critical properties. We also tried some hybrid mixing rules by using the vdW approach for some EoS parameters and the original Soave mixing rules for the others. A preliminary evaluation was performed to screen the mixing rules.

6.2.1 Mixing Rules using the van der Waals (vdW) Approach

By expanding the Soave-BWR EoS (eq. (2.39)) and writing it in the form of the virial EoS we get:

$$Z = \frac{P}{\rho RT} = 1 + B\rho + D\rho^4 + E\rho^2 - \frac{EF^2\rho^6}{2} + \frac{EF^3\rho^8}{3} - \frac{EF^4\rho^{10}}{8} + \dots \quad (6.51)$$

Based on the statistical mechanics and to ensure the correct composition dependence of virial coefficients, the mixing rules for the EoS parameters should have the following

form:

$$B = \sum_i \sum_j x_i x_j B_{ij} \rightarrow \text{Quadratic} \quad (6.52)$$

$$D = \sum_i \sum_j \sum_k \sum_l \sum_m x_i x_j x_k x_l x_m D_{ijklm} \rightarrow \text{Quintic} \quad (6.53)$$

$$E = \sum_i \sum_j \sum_k x_i x_j x_k E_{ijk} \rightarrow \text{Cubic} \quad (6.54)$$

$$F = \sum_i \sum_j x_i x_j F_{ij} \rightarrow \text{Quadratic} \quad (6.55)$$

To make the equations simpler, we assumed the combining rules for the higher-order terms (D , E , and F) to be independent of binary interaction parameters. This assumption makes the mixing rules for D , E , and F parameters to be similar to the original BWR and Starling mixing rules for the higher-order terms [167] — linear rules in varying powers of the EoS coefficients.

For the B parameter, we used a mixing rule similar to Starling's mixing rule [167] for the second virial coefficient where the binary interaction parameter was defined only for the temperature dependent part of the second virial coefficient. To do that, we divided the B term into two parts, a temperature dependent part and a temperature independent part (namely the constant part as it is only a function of critical properties for each component). Hall et al. [168] showed that the virial expansion for the cubic EoSs leads to the following equation for the second virial coefficient:

$$B = b - \frac{a}{RT} \quad (6.56)$$

where b is the repulsive term parameter and a is the attraction term parameter of the equation of state. As can be seen, the b parameter in eq. (6.56) is considered as the temperature independent part. We calculated the b parameter using SRK EoS for different n-alkanes and compared the results with different ways of defining the temperature independent part of the B parameter. We found that we get closer results to the b parameter calculated using SRK EoS when the temperature independent part of the B parameter is defined as follows:

$$B_i^{Cons} = \left(\frac{RT_{ci}}{P_{ci}} \right) [\beta_{ci} + 0.422] \quad (6.57)$$

The temperature dependent part of the B parameter can then be written as:

$$B_i^{Tdep} = \left(\frac{RT_{ci}}{P_{ci}} \right) \left[0.422 \left(-\frac{1}{T_r^{1.6}} \right) + 0.234\omega_i \left(1 - \frac{1}{T_r^3} \right) \right] \quad (6.58)$$

The final set of mixing rules are presented below:

$$B = \sum_i \sum_j x_i x_j B_{ij}^{Cons} + \sum_i \sum_j x_i x_j B_{ij}^{Tdep} \quad (6.59)$$

$$D = \left(\sum_i x_i D_i^{1/5} \right)^5 \quad (6.60)$$

$$E = \left(\sum_i x_i E_i^{1/3} \right)^3 \quad (6.61)$$

$$F = \left(\sum_i x_i F_i^{1/2} \right)^2 \quad (6.62)$$

where the combining rules for the B parameter are defined as follows:

$$B_{ij}^{Cons} = \frac{B_i^{Cons} + B_j^{Cons}}{2} \quad (6.63)$$

$$B_{ij}^{Tdep} = \sqrt{B_i^{Tdep} B_j^{Tdep}} (1 - k_{ij}) \quad (6.64)$$

These mixing rules are very similar to that of Starling's mixing rules [167] used for the BWR EoS.

6.2.2 LKP Mixing Rules (LKP)

Since Soave-BWR uses critical properties and acentric factor to calculate its parameters, it is possible to use the LKP mixing rules directly for Soave-BWR. The only modification needed is that the correlation for Z_{cm} (eq. (6.37)) should be replaced by eq. (2.67) so as to make it consistent with its definition for the original Soave-BWR EoS.

6.2.3 Other Hybrid Mixing Rules

In addition to the above two sets vdW and LKP, we also tried to create several sets of hybrid mixing rules by combining the vdW mixing rules and the original Soave mixing rules for Soave-BWR. These hybrid mixing rules are as follows:

1. ***vdW-B***: We used the original mixing rules for Soave-BWR and only modified the mixing rule for the B term using eq. (6.59).
2. ***vdW-DEF***: We used the original mixing rules for Soave-BWR and modified the mixing rules for D , E , and F parameters using eqs. (6.60)–(6.62).
3. ***vdW-D***: We used the original mixing rules for Soave-BWR and modified the mixing rule for the D term using eq. (6.60).

There is no established guidelines on how to develop mixing rules for non-cubic models. For this reason, we experiment the above combinations to see their effects on the equilibrium and density calculation results. Such a trial is also helpful to understand the importance of various EoS parameters in the calculation.

6.2.4 Implementation of the New Mixing Rules

Implementation of these mixing rules require the modification of the Soave-BWR thermodynamic module to different extents. In principle, the equations for the pure components part are the same and the corresponding code can be kept the same. However, depending on whether the mixing rules are applied to critical properties or the EoS parameters (B , D , E and F), the calculation sequence may need to be changed. The original Soave mixing rules calculate mixture critical parameters first and then the EoS parameters. The LKP mixing rules follow the same procedure and can then use the original calculation sequence. However, the vdW mixing rules mix B , D , E and F directly and the calculation sequence is different, with B , D , E and F calculated for pure components first and then mixed for the mixture. The major modification required in the code is all the first and second order derivatives for B , D , E and F , including the composition, temperature, and pressure derivatives, their second order derivatives, and their second order mixed derivatives. All the derivatives are obtained analytically, and checked for their thermodynamic consistency, and compared with numerical derivatives. For the hybrid mixing rules, codes from two mixing rules must be combined so as to overwrite some parameters from one set of mixing rules by the counterparts from another set. The advantage of the current code structure is that once the thermodynamic properties and their derivatives are correctly programmed, the module can be plugged in and perform various phase equilibrium calculation in a robust manner. This has greatly facilitated the evaluation of new mixing rules.

6.2.5 Preliminary Evaluation of The New Mixing Rules

Binary VLE for C₁-C₂ and C₁-C₁₀ Systems

To get an impression about the performance of the Soave-BWR with the new mixing rules, we started with binary VLE calculations for a symmetric (C₁-C₂) and an asymmetric (C₁-C₁₀) system. Figures 6.1–6.2 present the binary VLE calculations for C₁-C₂ and C₁-C₁₀ systems using Soave-BWR EoS with different mixing rules. As can be seen in Figure 6.1, for C₁-C₂ which is a symmetric binary mixture, Soave, vdW, and vdW-D give the lowest deviation with 0 k_{ij} . Regressing the k_{ij} improves the model predictions for all the cases except for vdW-B, which still gives high deviations in the dew curve section of the VLE diagram. The improvement in the predictions is more noticeable for LKP and vdW-DEF. This shows the importance of using appropriate k_{ij} for these two models.

For the highly asymmetric binary system of C₁-C₁₀ as shown in Figure 6.2, LKP and vdW-DEF do not give any results with 0 k_{ij} . This confirms our earlier finding regarding the sensitivity of these two mixing rules to the k_{ij} values. Tuning the k_{ij} to minimize the deviation in bubble point pressure improves the model predictions for Soave, vdW and vdW-D. LKP provides acceptable predictions after using regressed k_{ij} , however the value of regressed k_{ij} for LKP is larger than the other mixing rules. vdW-B and vdW-DEF (and other combinations of the mixing rules that are not presented here) do not provide reasonable prediction of the binary VLE of asymmetric systems even after using regressed k_{ij} . This suggests some deficiency in the functional form of the mixing rules. As a result, we excluded these mixing rules from our further calculations and proceeded with vdW, LKP, and vdW-D mixing rules.

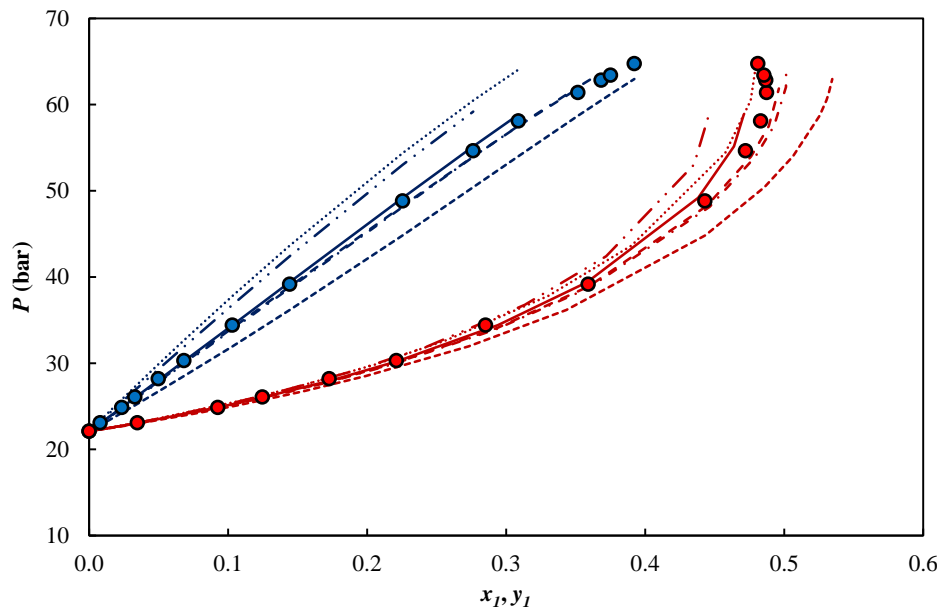
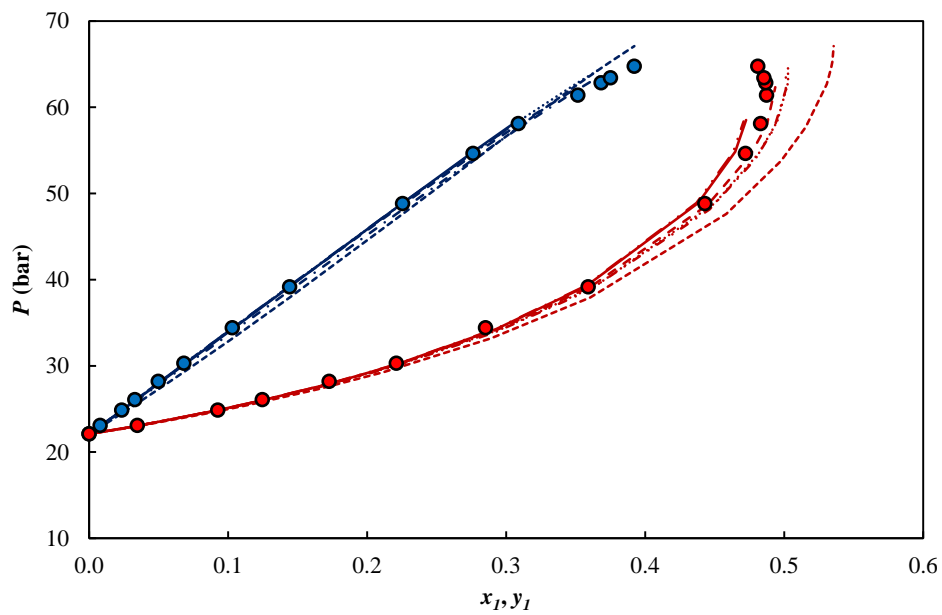
(a) 0 k_{ij} (b) Optimal k_{ij} 

Figure 6.1 $P - xy$ diagram for C_1-C_2 at 270 K with (a) zero k_{ij} and (b) the optimal k_{ij} . Soave ($-\cdot-$), vdW ($-$), LKP ($\cdot\cdot\cdot$), vdW-B ($- -$), vdW-DEF ($- \cdot \cdot -$), vdW-D ($- -$). The experimental data is taken from [169].

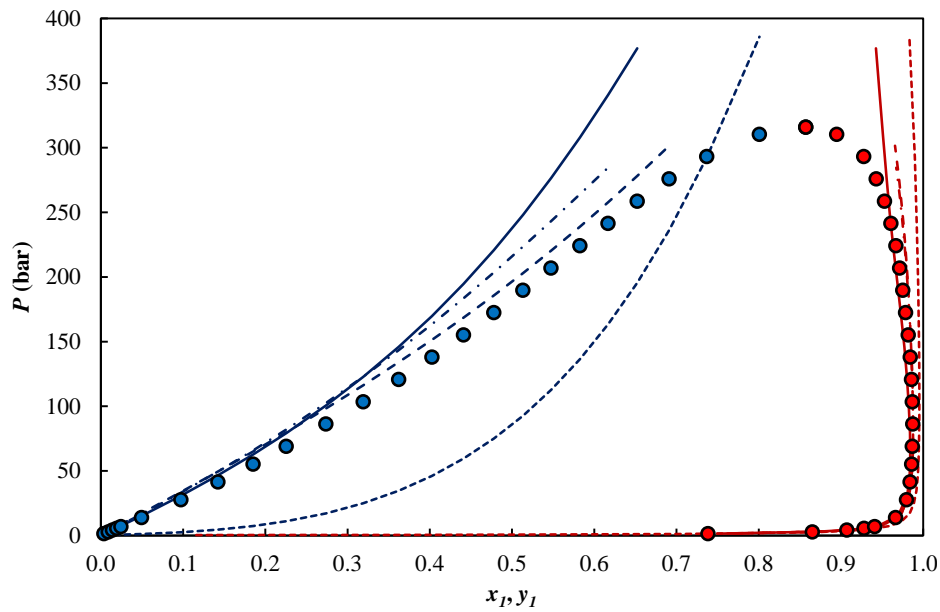
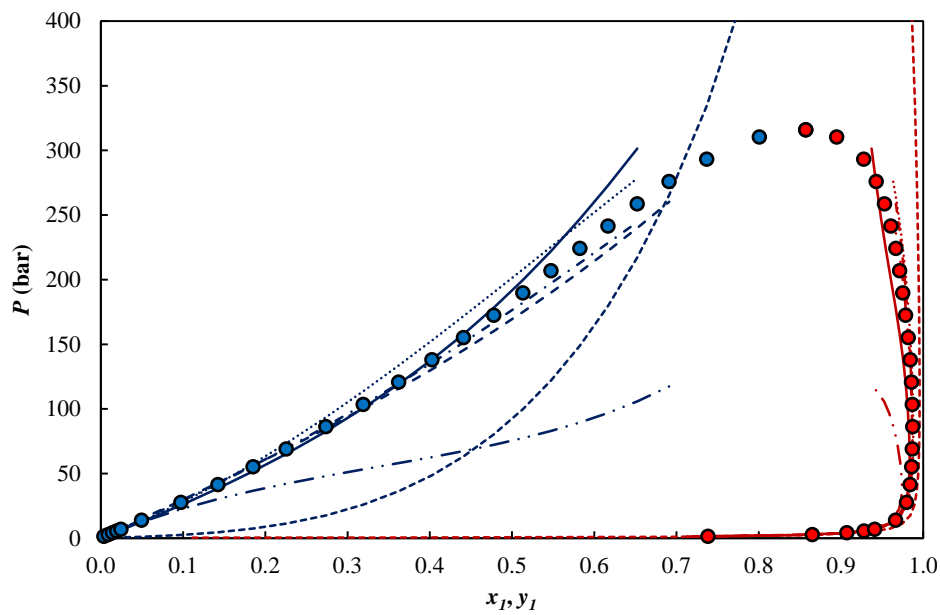
(a) 0 k_{ij} (b) Optimal k_{ij} 

Figure 6.2 P – xy diagram for C_1 – C_{10} at 410.9 K with (a) zero k_{ij} and (b) the optimal k_{ij} . Soave (– · –), vdW (—), LKP (· · ·), vdW-B (– –), vdW-DEF (– – –), vdW-D (– –). The experimental data is taken from [170].

Excess Molar Volume Calculations

The extent to which real liquid mixtures deviate from ideality is best expressed through the use of thermodynamic excess functions. Excess molar volume (V^E) is one of the most frequently used excess quantities. It is defined as the difference between the actual molar volume of a solution and the molar volume it would have as an ideal solution at the same temperature, pressure, and composition:

$$V^E = V^{mix} - V^{id} \quad (6.65)$$

where V^{mix} is the molar volume of the mixture calculated by the EoS, and V^{id} is the ideal molar volume calculated as follows:

$$V^{id} = \sum_i^n x_i V_i \quad (6.66)$$

where V_i is the molar volume of the pure component i in the mixture.

Regueira et al. [61] obtained the excess volumes of C₁-C₁₀ binary mixture from density measurements over a wide temperature and pressure range. The excess volumes were negative in the whole studied (P, T, x) range, becoming more negative as the pressure decreased or the temperature increased. They modeled the excess volumes using SRK, PR, PC-SAFT, and Soave-BWR EoSs and observed that SRK, PR, and PC-SAFT provide reasonable description for the measured excess volumes whereas the values calculated by Soave-BWR were inaccurate. In fact, Soave-BWR seemed to predict positive excess volumes at higher pressures.

As the second step in our preliminary evaluation of the new mixing rules for Soave-BWR, we calculated the excess volume for the C₁-C₁₀ binary mixture. We used 0 k_{ij} to treat all the different mixing rules for Soave-BWR EoS equally. We excluded LKP in this step as it was sensitive to the k_{ij} value. As illustrated in Figure 6.3, only the vdW mixing rules provide almost accurate prediction of excess volume especially at lower pressures. This shows an improvement over Soave mixing rules which, together with vdW-D, predicts positive values for V^E at elevated pressures. The similar behavior of vdW-D to that of Soave-BWR shows that the mixing rule for the D parameter in both equations may not be accurate enough, as the mixing rule for the D parameter is the only modification of the Soave-BWR's original mixing rules in the vdW-D. It is not an easy task to modify the mixing rule for a desired EoS parameters in the original Soave-BWR, without affecting the other EoS parameters, because the mixing rules in

Soave-BWR are defined for the critical properties and acentric factor, and all the EoS parameters are complicated functions of these properties.

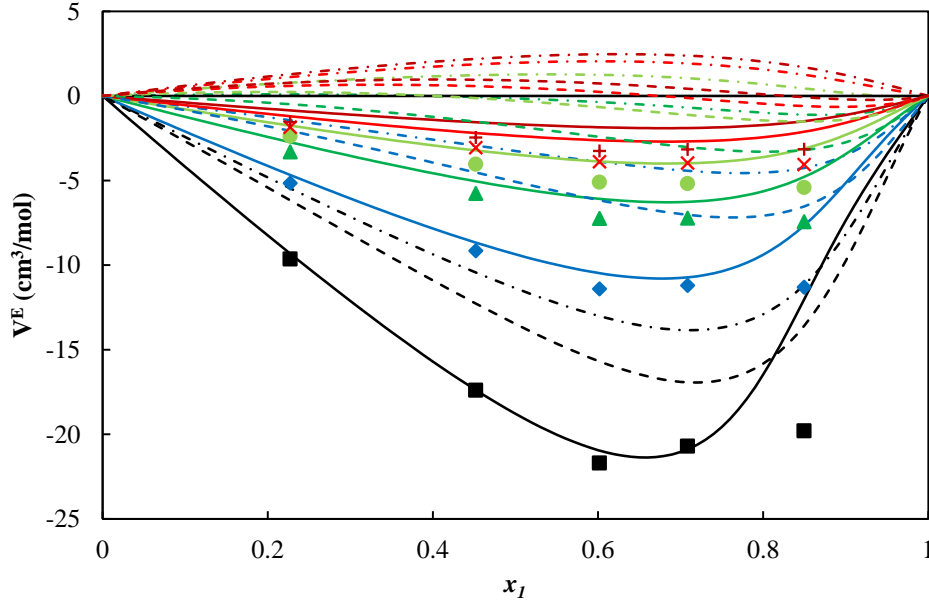


Figure 6.3 Excess volume for the binary system methane (1) + n-decane (2) at 463.15 K. (■) 40 MPa, (◆) 60 MPa, (▲) 80 MPa, (●) 100 MPa, (×) 120 MPa and (+) 140 MPa. Soave (− · −), vdW (—), vdW-D (− −), all with 0 k_{ij} . The experimental data is taken from [61].

For the vdW-D, we noticed that the shape of the V^E curves changes as the exponent of the mixing rule for the D parameter in eq. (6.60) changes. By increasing the exponent to values higher than 5.3, the vdW-D mixing rule provides negative V^E even at higher pressures, which shows an improvement over the original Soave-BWR. On the other hand, this modification slightly worsen the bubble point pressure calculations for the binary system of C_1 - C_{10} , especially at higher compositions of methane and near the critical region, where the model over-predicts the bubble point pressure and vapor phase composition. This however could be improved by using appropriate k_{ij} values. After evaluating different values for the exponent of the D parameter in eq. (6.60), we decided to set the exponent to 5.38. Therefore, the mixing rule for the D parameter in the vdW-D was changed to the following equation:

$$D = \left(\sum_i x_i D_i^{1/5.38} \right)^{5.38} \quad (6.67)$$

All the calculations from this point forward using vdW-D refers to eq. (6.67) as the mixing rule of the D parameter. Figure 6.4 presents the calculation results using

Soave-BWR with different mixing rules and 0 k_{ij} . As can be seen, the problem of positive excess volume calculation at elevated pressures is solved for the vdW-D using the new mixing rule for the D parameter (eq. (6.67)), and it gives very close results to that of vdW (Equations (6.59)–(6.60)).

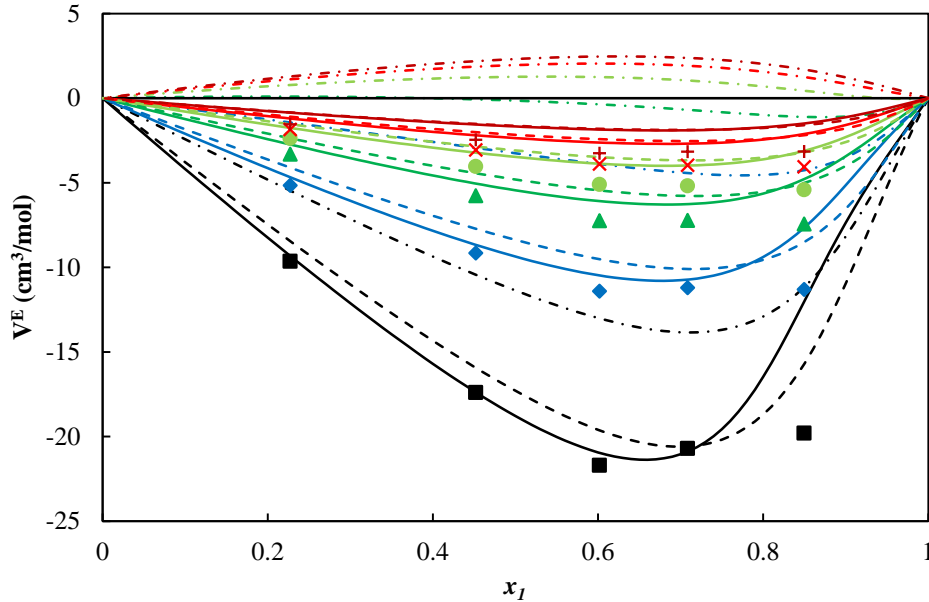


Figure 6.4 Excess volume for the binary system methane (1) + n-decane (2) at 463.15 K. (■) 40 MPa, (◆) 60 MPa, (▲) 80 MPa, (●) 100 MPa, (×) 120 MPa and (+) 140 MPa. Soave (– · –), vdW (—), vdW-D (eq. (6.67)) (– –), all with 0 k_{ij} . The experimental data is taken from [61].

Figure 6.5 presents the excess volume calculations using Soave-BWR with different mixing rules and regressed k_{ij} from Table 6.1. Soave-BWR with original mixing rules is the only model that gives positive excess volume at pressures higher than 80 MPa. vdW gives the best predictions compared to other models, while vdW-D (eq. (6.67)) gives slightly higher deviations. Although, LKP predicts negative excess volumes over the whole pressure range, it under-predicts the experimental values of V^E over the whole pressure and composition range. It should be mentioned that at a fixed pressure and temperature, some of the models predicted two phases for some values of x_1 . For those data points, the liquid volume was used in calculation of V^E .

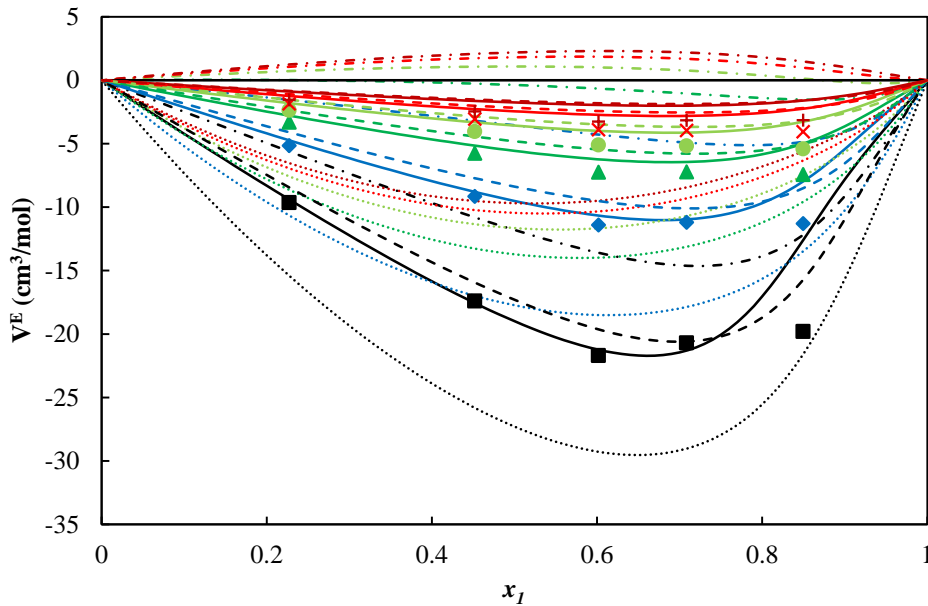


Figure 6.5 Excess volume for the binary system methane (1) + n-decane (2) at 463.15 K. (■) 40 MPa, (◆) 60 MPa, (▲) 80 MPa, (●) 100 MPa, (×) 120 MPa and (+) 140 MPa. Soave (− · −), vdW (—), vdW-D (eq. (6.67)) (− −), LKP (⋯), all with regressed k_{ij} . The experimental data is taken from [61].

6.3 Results and Discussions

6.3.1 Density Calculations

In section 3.1.3 we made a comparison between Soave-BWR, PC-SAFT and GERG-2008 in density calculation of different binary mixtures of methane and n-decane within 278.15-463.15 K and 1-1400 bar. We observed that Soave-BWR gives larger deviation as methane mole fraction increases in the binary mixture. Figure 6.6 presents the AAD% in the calculated density as a function of the methane mole fraction (x_1) in the binary mixture of methane and n-decane using Soave-BWR with different mixing rules. The regressed binary interaction parameters k_{ij} 's used for Soave, vdW, LKP, and vdW-D were -0.0311, -0.0182, -0.5311, and -0.0003 respectively. LKP gives the poorest results among other mixing rules. vdW gives the lowest deviation in density especially at $x_1 = 0.6017$, and $x_1 = 0.7085$ where its predictions are even more accurate than that of GERG-2008 (Figure 3.8). vdW-D gives slightly higher deviation than vdW, but still gives better estimation of density than the original Soave-BWR. As mentioned earlier, the deviation in density seems to increase at higher methane composition. It is more noticeable for the vdW where the deviation increases from less than 1% to around

4%. This behavior might be due to the shortcoming of the Soave-BWR EoS at higher methane composition. Figure 6.7 shows how the density predictions differ for Soave and vdW for two mixtures of methane and n-decane at different temperatures. Soave under predicts the density especially at higher temperatures, and vdW gives accurate prediction of density at higher temperatures and up to very high pressures.

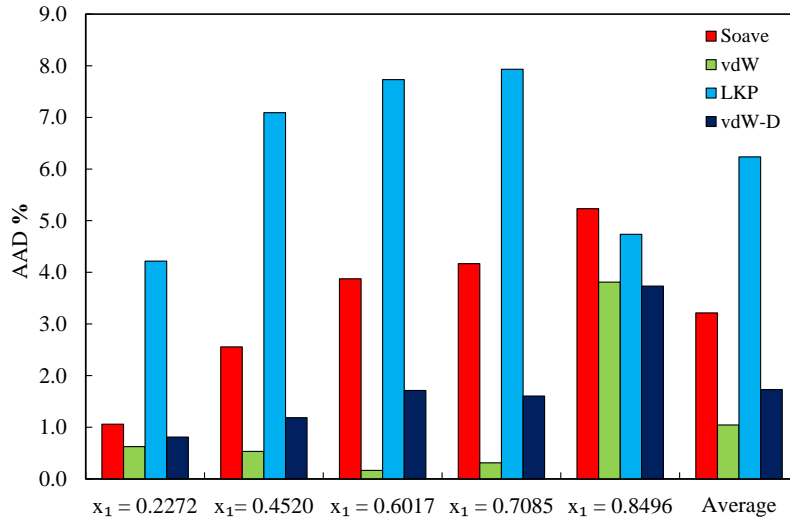


Figure 6.6 AAD% in the calculated densities of the binary system methane (1) + n-decane (2) using Soave, vdW, LKP, vdW-D (eq. (6.67)) with regressed k_{ij} within 278.15-463.15 K and 1-1400 bar. The experimental data is taken from [61].

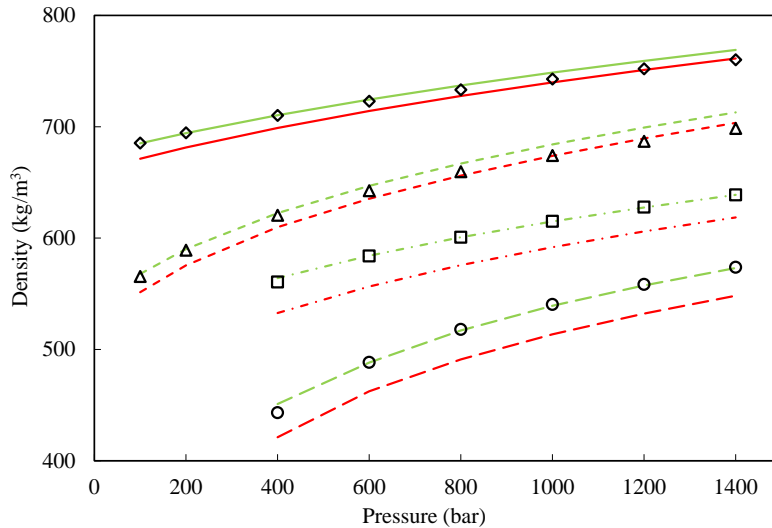


Figure 6.7 Density vs. pressure using vdW (green lines) and Soave (red lines) both with regressed k_{ij} for two mixtures of methane and n-decane at different temperatures. 22.27 mol% C₁ and 323.2 K (\diamond , solid lines), 22.27 mol% C₁ and 463.2 K (Δ , dashed lines), 70.85 mol% C₁ and 323.2 K (\square , dash-dot lines), and 70.85 mol% C₁ and 463.2 K (\circ , long-dashed lines). The experimental data is taken from [61].

6.3.2 Binary VLE and Regression of Binary Interaction Parameters

Similar to the calculations performed in section 3.2, we found the deviation in bubble point pressure and vapor phase composition for the binary pairs of N₂, CO₂, H₂S, CH₄ and hydrocarbons up to nC₁₀ using Soave-BWR with different mixing rules. The temperature ranges for these binary data can be found in Table 3.11.

Table 6.1 provides the regression results including the regressed k_{ij} 's. We tuned the binary interaction parameters to minimize the deviation in bubble point pressures. The results for Soave-BWR have also been presented in this table for comparison. The comparison between all the four mixing rules for Soave-BWR with regressed k_{ij} shows that Soave gives better prediction of bubble point pressures and vapor phase compositions. Figure 6.8 summarizes the comparison results. Although vdW was better than the other mixing rules for Soave-BWR in the density and excess volume calculations, it gives the poorest results both for the bubble point pressure and vapor phase composition. Among the new mixing rules for Soave-BWR, vdW-D seems to give the lowest deviation in bubble point pressure and vapor composition, but it still gives around 1% larger deviation than Soave. Comparing the k_{ij} values shows that LKP needs relatively larger k_{ij} 's than other models, and it would not provide reasonable results if the k_{ij} values are very different from the regressed k_{ij} . The large k_{ij} for LKP suggests that some inherent problems with the mixing rules require a large non-zero value as the default k_{ij} .

Table 6.1 Regressed k_{ij} values for the four EoS models and their deviations in calculated bubble point pressures and vapor phase compositions (experimental data from [63, 64]).

System		Soave			vdW			LKP			vdW-D (eq. (6.67))		
COMP1	COMP2	k_{ij}	DP/P (%)	DY_1 (mol%)	k_{ij}	DP/P (%)	DY_1 (mol%)	k_{ij}	DP/P (%)	DY_1 (mol%)	k_{ij}	DP/P (%)	DY_1 (mol%)
C ₁	CO ₂	0.0804	1.97	0.84	0.0791	2.26	1.05	0.0189	2.53	0.97	0.0732	1.77	0.76
	H ₂ S	0.0692	3.93	1.66	0.0821	5.41	1.65	0.0282	3.52	1.68	0.0537	5.37	1.70
	C ₂	0.0002	1.41	0.36	0.0107	2.63	0.41	-0.0519	1.68	0.44	-0.0067	2.12	0.42
	C ₃	0.0024	2.99	0.65	0.0233	5.30	0.56	-0.1167	3.92	0.84	-0.0071	4.60	0.73
	iC ₄	-0.0079	2.62	1.01	0.0147	5.53	1.08	-0.1629	2.71	1.46	-0.0128	4.11	1.23
	nC ₄	-0.0044	4.19	0.78	0.0186	7.05	0.85	-0.1830	5.13	1.16	-0.0093	6.55	1.01
	iC ₅	-0.0142	8.72	3.16	-0.0216	10.00	3.77	-0.2213	8.73	3.39	-0.0036	8.51	3.35
	nC ₅	-0.0076	3.05	1.25	0.0083	5.84	0.78	-0.2447	2.57	1.60	-0.0076	3.29	1.48
	nC ₆	-0.0048	5.71	0.43	0.0181	9.63	0.87	-0.3081	4.89	0.63	-0.0064	7.03	0.70
	nC ₇	-0.0149	9.25	0.58	0.0017	12.59	0.54	-0.3760	8.38	0.92	-0.0154	9.58	0.83
N ₂	nC ₈	-0.0149	5.17	0.26	0.0093	10.11	0.34	-0.4271	9.31	0.30	-0.0071	8.24	0.31
	nC ₉	-0.0184	6.64	0.24	0.0008	9.36	0.60	-0.4882	9.41	0.30	-0.0016	5.20	0.27
	nC ₁₀	-0.0311	7.06	0.82	-0.0182	12.37	0.54	-0.5311	10.54	1.20	-0.0003	8.60	1.22
	CO ₂	0.0163	2.55	1.61	-0.0312	7.42	1.33	-0.1043	1.50	1.65	-0.0023	1.30	1.06
	H ₂ S	0.1041	9.07	1.48	0.0989	11.07	1.76	0.0275	5.83	1.92	0.0793	9.73	1.64
	C ₁	0.0246	2.09	1.14	0.0324	1.79	1.18	0.0242	1.72	1.21	0.0148	2.34	1.26
	C ₂	0.0333	2.69	0.84	0.0391	6.27	0.86	-0.0778	2.99	1.09	0.0128	3.49	0.87
	C ₃	0.0447	7.86	0.81	0.0318	7.50	0.88	-0.1740	6.74	0.99	0.0228	5.79	1.47
	iC ₄	0.0361	3.47	1.44	0.0219	6.06	1.62	-0.2462	5.49	1.71	0.0174	5.40	1.40
	nC ₄	0.0341	3.90	3.14	-0.0029	9.36	1.76	-0.2750	5.29	3.31	0.0199	6.38	3.10
CO ₂	iC ₅	0.0148	3.16	1.08	-0.0164	6.13	1.86	-0.3429	6.47	1.03	0.0003	5.50	1.10
	nC ₅	0.0145	4.30	0.98	-0.0212	8.06	1.16	-0.3795	5.16	0.64	-0.0025	5.59	0.92
	nC ₆	0.0280	5.26	1.74	-0.0160	5.62	0.75	-0.4432	8.89	1.47	0.0280	7.96	2.11
	nC ₇	0.0086	5.85	1.92	-0.0195	9.06	1.67	-0.5260	9.99	2.35	0.0153	6.25	2.15
	nC ₁₀	-0.0414	4.64	0.08	-0.0885	9.69	0.20	-0.7661	7.77	0.11	-0.0002	8.65	0.12
	H ₂ S	0.0733	1.53	0.88	0.0759	1.41	1.07	0.0787	1.54	0.96	0.0662	1.17	0.93
	C ₂	0.0937	2.48	2.11	0.0946	2.81	2.30	0.0957	2.46	2.13	0.0894	2.53	2.16
	C ₃	0.0802	3.07	0.53	0.1038	3.56	0.97	0.0891	4.41	1.15	0.0902	3.17	0.65
	iC ₄	0.0602	1.90	0.76	0.0972	3.26	1.21	0.0705	5.76	1.73	0.0752	2.52	1.10
	nC ₄	0.0675	2.52	1.14	0.1031	3.99	1.28	0.0828	12.04	3.31	0.0802	2.66	1.40
H ₂ S	iC ₅	0.0550	1.53	0.57	0.1052	4.08	1.41	0.0512	11.35	1.72	0.0708	2.35	0.83
	nC ₅	0.0541	3.64	0.67	0.0984	4.89	1.79	0.0120	6.68	0.71	0.0697	3.51	0.74
	nC ₆	0.0538	3.18	0.50	0.0995	6.97	0.83	-0.0133	8.70	0.69	0.0725	3.08	0.65
	nC ₇	0.0209	6.57	0.68	0.0834	7.72	1.04	-0.0708	8.20	1.08	0.0539	6.09	0.85
	nC ₈	0.0389	5.52	0.16	0.0807	9.36	0.26	-0.0264	9.06	0.40	0.0617	6.59	0.26
	nC ₉	0.0205	2.43	0.03	0.0706	13.65	0.50	-0.0422	11.58	0.46	0.0569	6.46	0.11
	nC ₁₀	0.0177	5.45	0.53	0.0683	11.51	0.82	-0.0414	9.67	0.71	0.0494	9.90	0.86
	C ₂	0.0605	1.51	1.62	0.0730	1.22	1.57	0.0876	1.03	1.49	0.0551	1.98	1.58
	C ₃	0.0486	1.95	1.73	0.0730	1.72	1.81	0.0802	1.79	1.80	0.0553	1.94	1.74
	iC ₄	0.0160	1.97	1.29	0.0702	2.14	1.32	0.0586	1.25	0.82	0.0397	2.25	0.93
Average	nC ₄	0.0364	1.84	0.87	0.0728	2.26	1.27	0.0493	1.24	0.76	0.0438	2.49	0.90
	iC ₅	0.0182	3.38	1.47	0.0710	3.72	2.09	0.0269	4.00	1.02	0.0385	3.52	1.40
	nC ₅	0.0152	1.50	1.22	0.0646	1.78	1.51	0.0179	4.92	1.34	0.0378	1.89	1.28
	nC ₆	0.0016	2.73	0.44	0.0600	4.00	0.69	-0.0141	5.94	0.81	0.0317	4.86	0.72
	nC ₇	0.0043	3.65	0.90	0.0625	7.49	1.28	-0.0272	6.42	1.06	0.0387	7.67	1.11
	nC ₁₀	-0.0336	4.31	0.13	0.0478	7.25	0.23	-0.0881	8.55	0.20	0.0053	8.75	0.21
Average			3.93	1.01		6.32	1.16		5.82	1.23		4.97	1.12

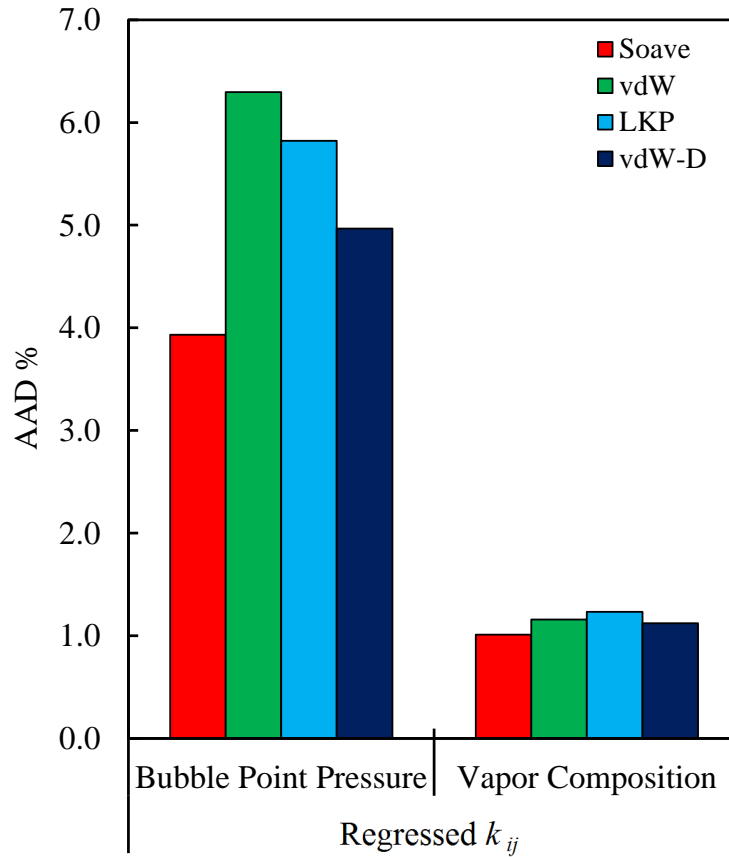


Figure 6.8 AAD% in bubble point pressure and vapor phase composition for binary pairs of N_2 , CO_2 , H_2S and C_1 using Soave-BWR with different mixing rules with regressed k_{ij} .

6.3.3 Phase Envelopes of Multicomponent Mixtures

We tested Soave-BWR with different mixing rules for prediction of the phase envelopes of 30 synthetic natural gases listed in Table 3.15. The calculations are made with the optimal k_{ij} 's given in Table 6.1. Some of the results are presented in Figures 6.9–6.16 where the prediction results using SRK are also presented for comparison. From the calculation results, including those not presented here, we observed that LKP and vdW-D generally give satisfactory results and close predictions to that of Soave-BWR and SRK for systems containing components up to C_5 (see Figures 6.9–6.14). vdW on the other hand, seems to give a bit smaller phase envelopes than the other mixing rules.

For the highly asymmetric systems however, none of the mixing rules for Soave-BWR provide satisfactory predictions over the whole temperature and pressure range. For gases 26 and 27 (which are highly asymmetric ternary systems), LKP gives the closest

prediction to that of Soave and the experimental data (Figures 6.15–6.16). Updating the k_{ij} for LKP would improve the prediction results noticeably. For gas 27 for example, which has higher methane composition, changing the k_{ij} for C₁-C₁₀ binary pair from -0.5311 to -0.2511 improves the predictions results using LKP (Figure 6.17). Tuning the k_{ij} 's has not been tried for other systems as we wanted to treat all the mixing rules equally in our comparisons. In contrast to the small phase envelopes for the majority of the systems tested, vdW gives very large phase envelopes for the highly asymmetric systems, especially in the liquid region. This mixing rule set however gives good predictions of the dew curve at higher temperatures for the asymmetric systems.

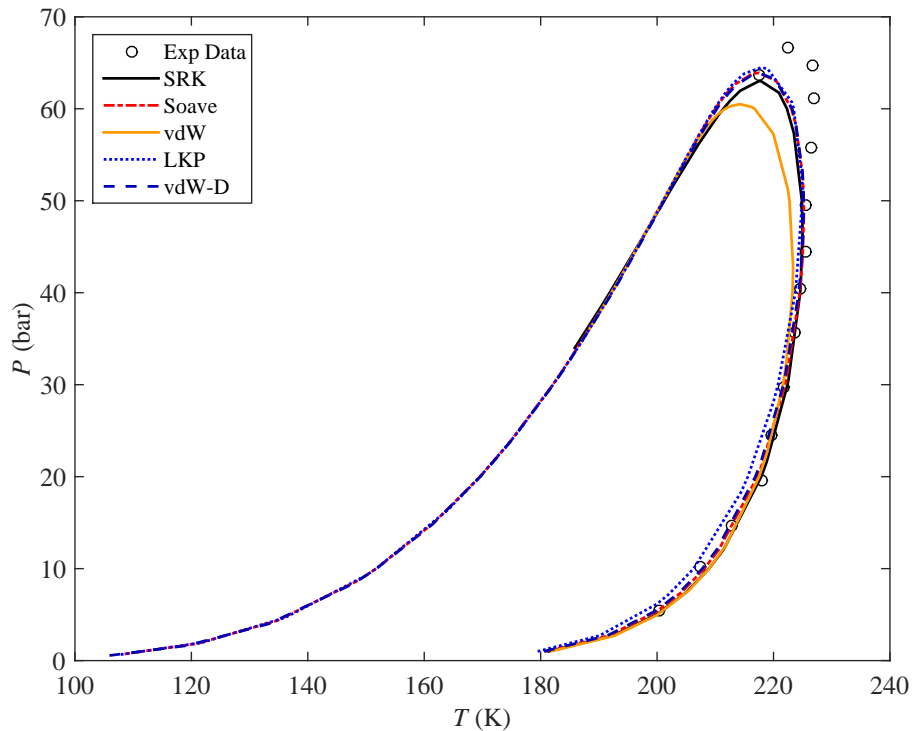


Figure 6.9 Phase envelopes for Gas 6 with the optimal k_{ij} 's.

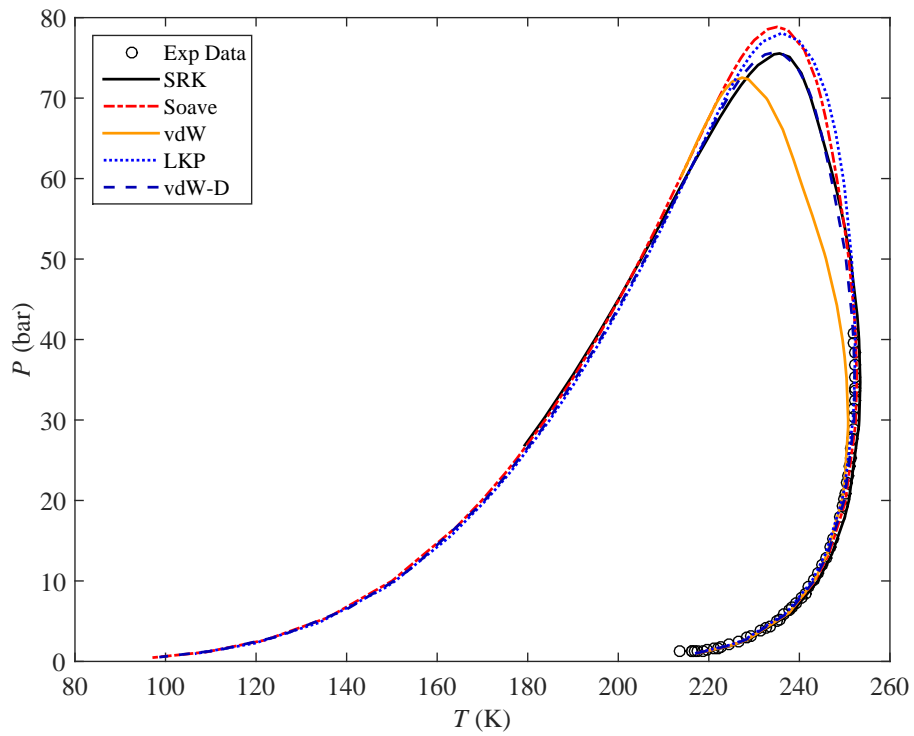


Figure 6.10 Phase envelopes for Gas 17 with the optimal k_{ij} 's.

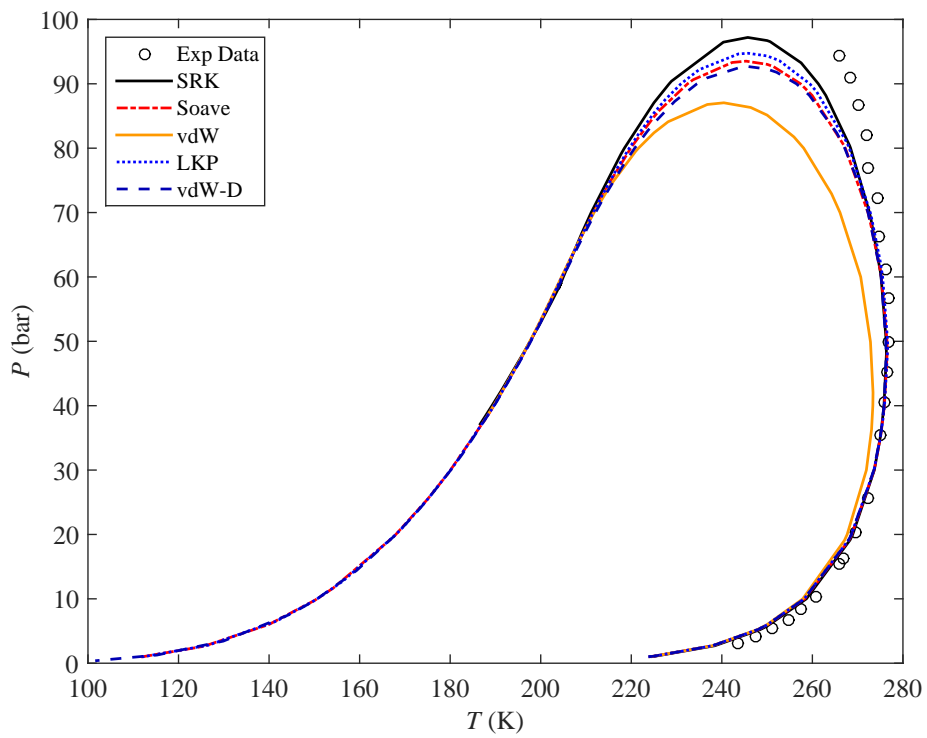


Figure 6.11 Phase envelopes for Gas 22 with the optimal k_{ij} 's.

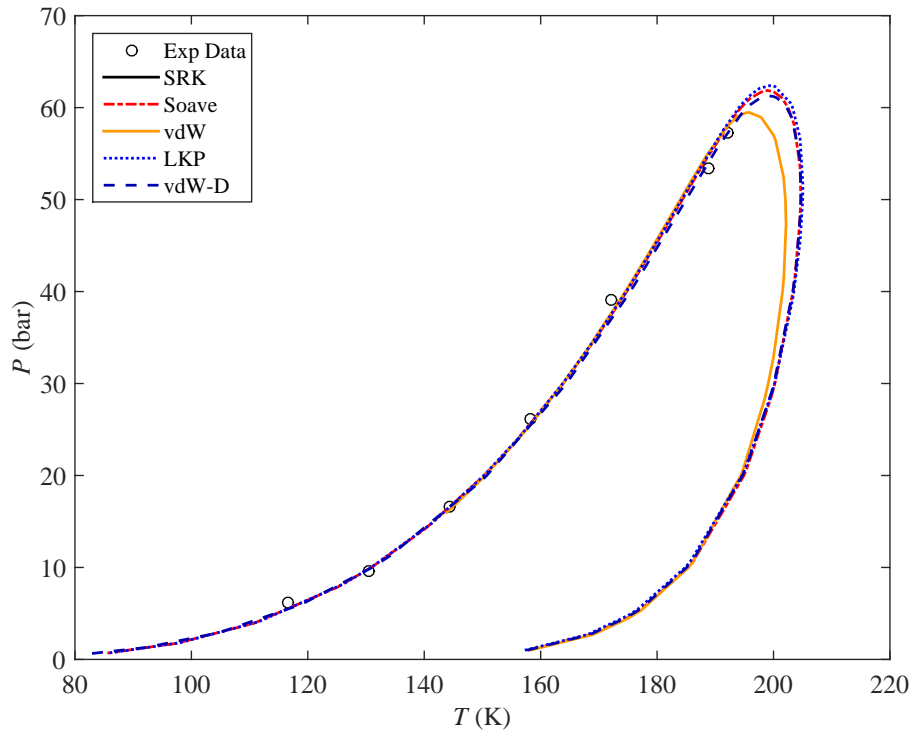


Figure 6.12 Phase envelopes for Gas 24 with the optimal k_{ij} 's.

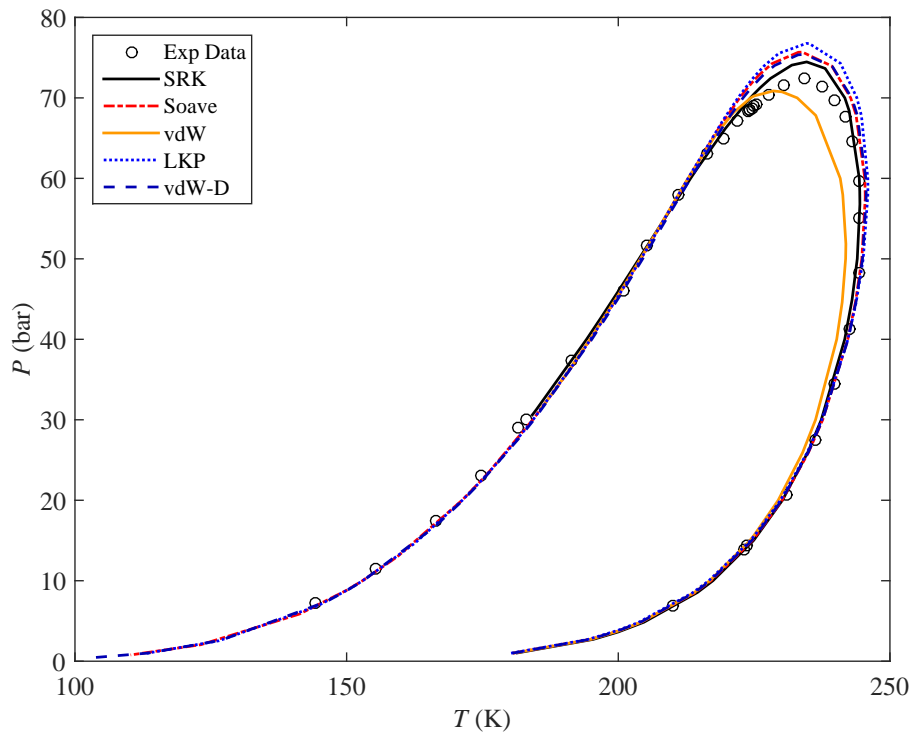


Figure 6.13 Phase envelopes for Gas 25 with the optimal k_{ij} 's.

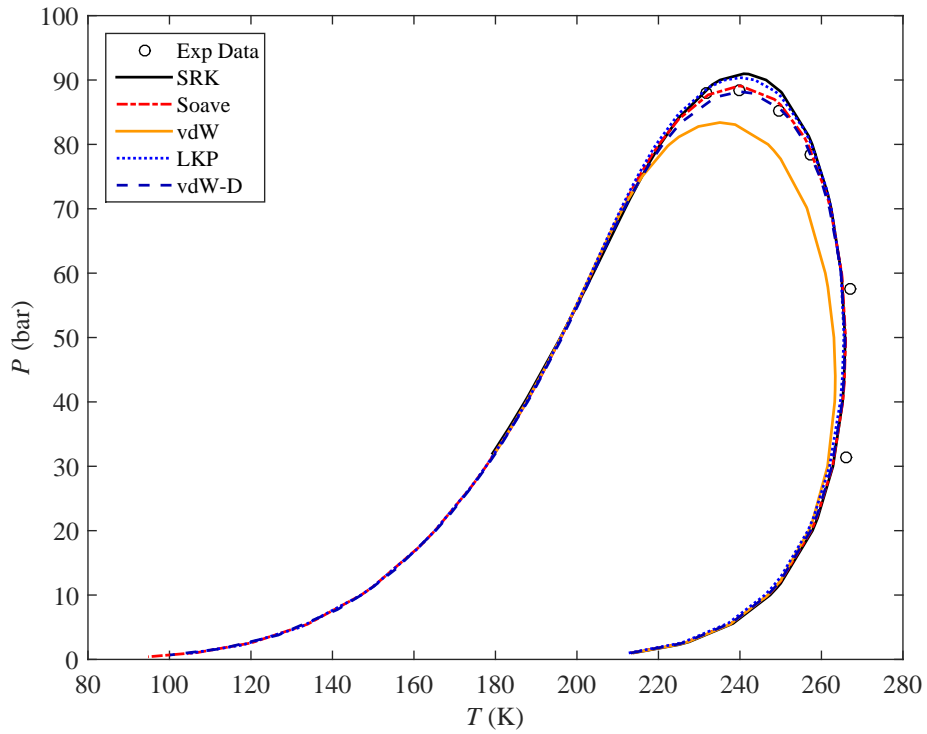


Figure 6.14 Phase envelopes for Gas 28 with the optimal k_{ij} 's.

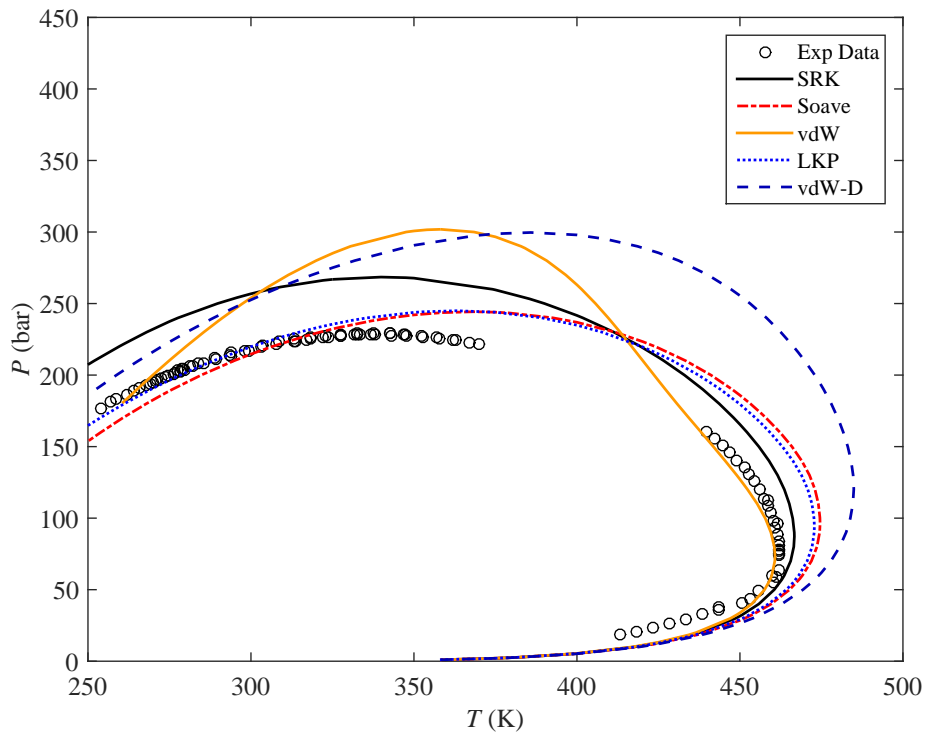


Figure 6.15 Phase envelopes for Gas 26 with the optimal k_{ij} 's.

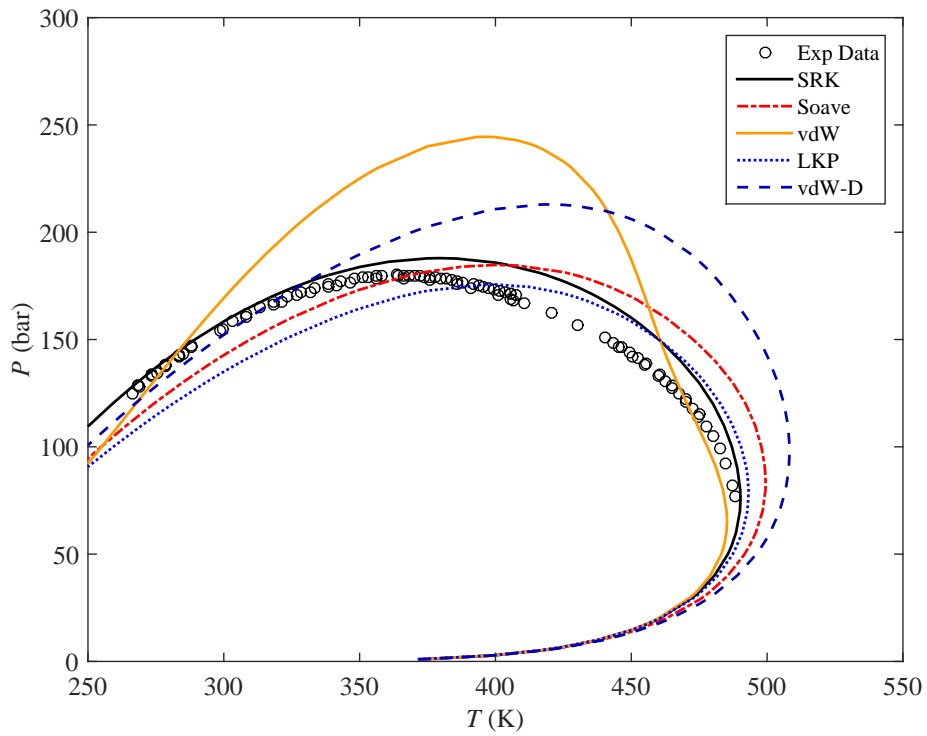


Figure 6.16 Phase envelopes for Gas 27 with the optimal k_{ij} 's.

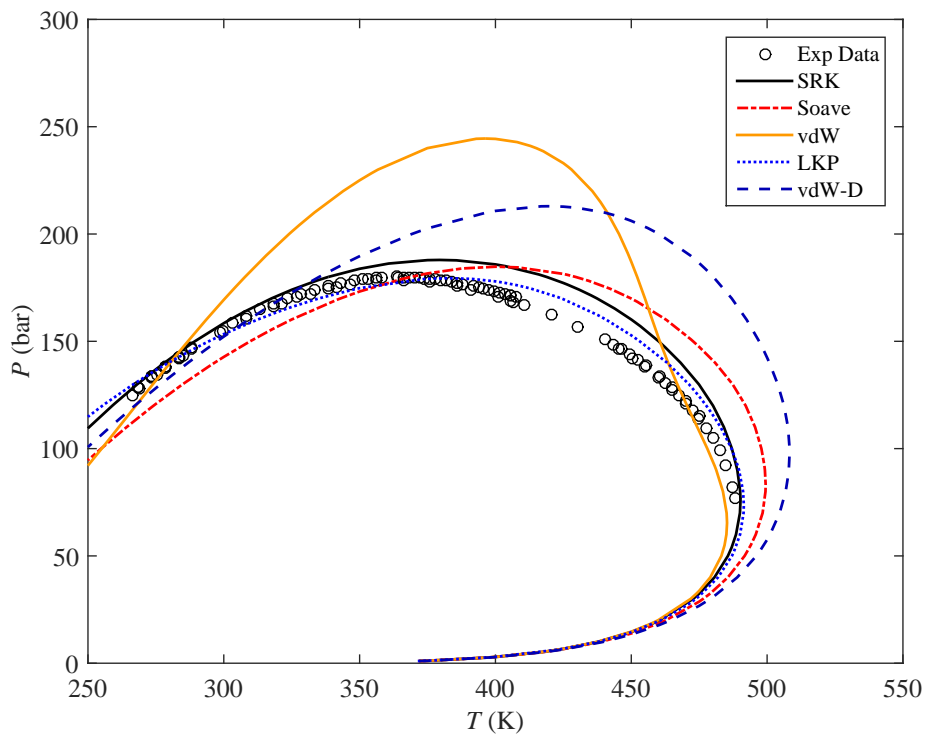


Figure 6.17 Phase envelopes for Gas 27 with the optimal k_{ij} 's - New k_{ij} is used for LKP.

For the binary mixtures of methane and n-decane, we noticed that again at the higher methane compositions, none of the models were able to predict the whole phase envelope correctly. vdW-D and vdW give the largest deviation for at $x_1 = 0.8497$, while vdW-D seems to give slightly better prediction of the phase envelope at $x_1 = 0.4031$ and $x_1 = 0.6021$. As can be observed, describing the phase equilibrium of a highly asymmetric system accurately over a wide temperature, pressure and composition range is not an easy task with any of the models tested.

Figures 3.27–3.29 show the phase envelope calculation results using all the four EoS models as well as GERG-2008 for three different compositions of methane in the binary mixture of methane and n-decane. GERG-2008 seems to under predict the phase envelope at $x_1 = 0.4031$ and over predict it at $x_1 = 0.8497$.

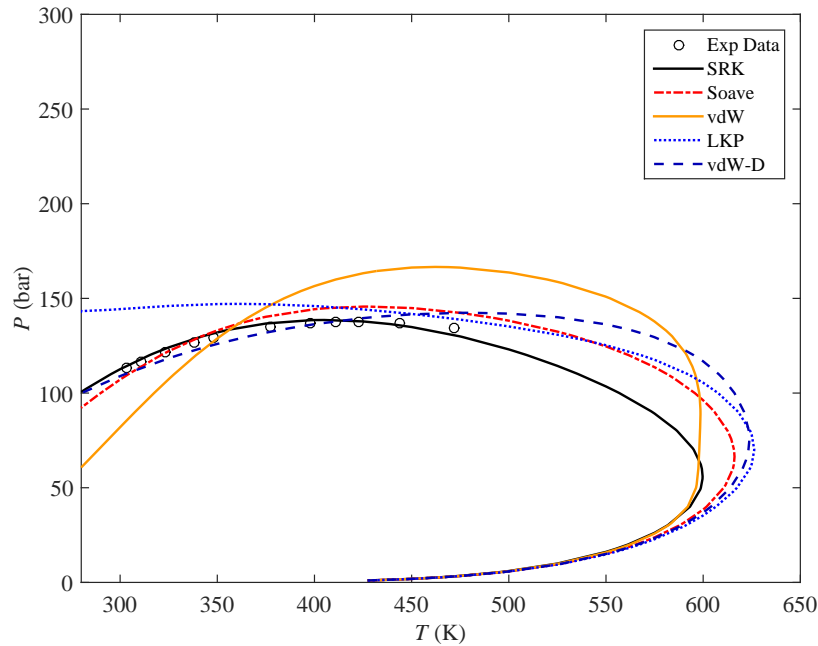


Figure 6.18 Phase envelope for binary mixtures of methane + n-decane (40.31 mol% C_1) using Soave-BWR with different mixing rules with optimal k_{ij} 's. The experimental data is taken from [61].

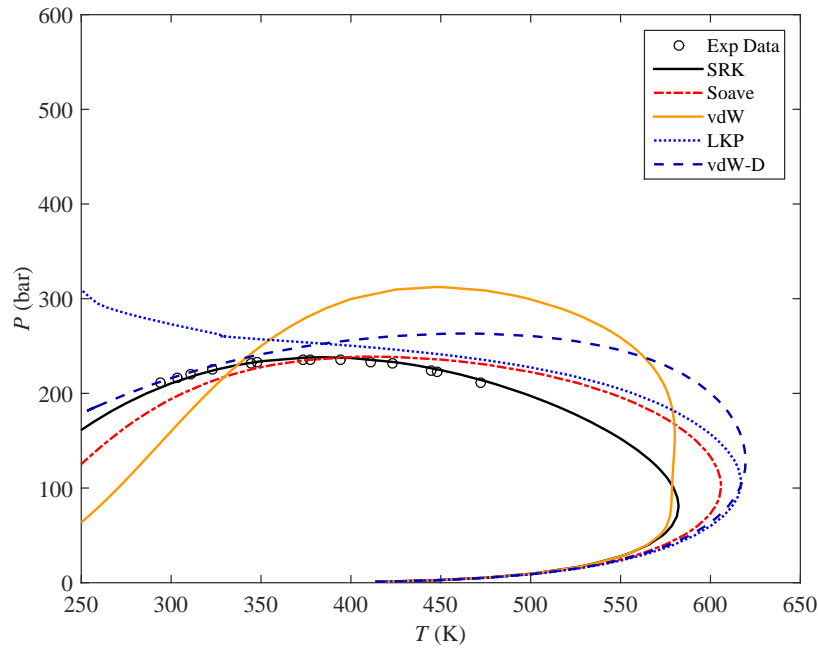


Figure 6.19 Phase envelope for binary mixtures of methane + n-decane (60.21 mol% C_1) using Soave-BWR with different mixing rules with optimal k_{ij} 's. The experimental data is taken from [61].

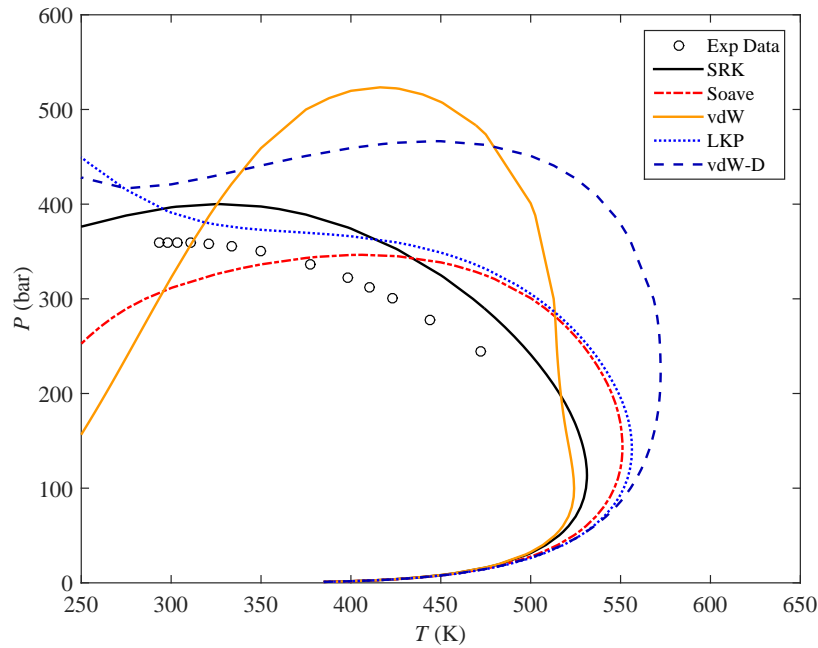


Figure 6.20 Phase envelope for binary mixtures of methane + n-decane (84.97 mol% C_1) using Soave-BWR with different mixing rules with optimal k_{ij} 's. The experimental data is taken from [61].

6.4 Conclusions

Soave-BWR with original mixing rules is one of the most successful extensions of the BWR EoS. It uses a set of mixing rules for the critical properties instead of the EoS parameters. The mixing rules are rather complicated in terms of derivation and implementation. However, the study in early chapters show that Soave-BWR has problems in phase equilibrium and density calculation which may be caused by its mixing rules.

In this chapter, we proposed two major sets of mixing rules to replace the original mixing rules for Soave-BWR. The first set (vdW), similar to those used by Starling [167], calculates the EoS parameters directly from the pure component EoS parameters; The second set is the LKP mixing rules [47], where pseudo-critical properties are calculated for the mixture. Furthermore, several hybrid mixing rules by combining vdW and the original Soave-BWR mixing rule were also tested. Among them, the vdW-D mixing rules use Soave mixing rules for all the EoS parameters except for D , where the vdW mixing rules are used instead. The vdW-D mixing rules, after modification of the exponent in the mixing rule for the D parameter, can overcome one of the shortcomings of the original Soave-BWR by providing the correct trend of excess volume at higher pressures. The vdW-D mixing rules were selected in the final evaluation together with the original Soave-BWR mixing rule (Soave), vdW and LKP.

We observed major improvements in calculation of excess volume over the whole composition range of methane in the binary mixture of methane + n-decane, and up to very high pressures. All the new mixing rules for Soave-BWR predicted negative excess volume in the studied temperature, pressure and composition range, while vdW and vdW-D ((eq. (6.67))) had the lowest deviation in calculation of V^E . For the density calculation of asymmetric binary system of methane + n-decane, vdW had better performance than other mixing rules for Soave-BWR, especially at lower methane compositions. vdW-D gave slightly higher deviations than vdW, but still lower than that of Soave. Based on these findings, vdW and vdW-D seem to be very promising for PVT modeling of the reservoir fluids and description of density and compressibility.

For the majority of the phase envelopes studied, LKP and vdW-D generally gave satisfactory results and close predictions to that of Soave, while vdW predicted smaller phase envelopes.

Although some of the new mixing rules improved the density calculation and fixed the problem in the excess volume calculation of asymmetric systems, they are not much better, and sometimes worse, than the original mixing rule in phase equilibrium calculation of highly asymmetric systems. The improvement can be observed for some individual examples for some mixing rules but it is far from a final solution. There is so far neither established procedure nor solid theoretical basis for development of mixing rules for non-cubic EoS models. The development of new mixing rules relies somehow on a trial-and-error procedure. Fortunately, we have developed the code in a structured manner and the new mixing rules can be quickly tested. If this procedure is further streamlined and improved, it is possible to test a large number of mixing rules and select a better set for Soave-BWR. Meanwhile, it is worth further investigating various theories for constructing mixing rules so that the selection is not a purely mathematical exercise. Finally, it should be pointed out that no attempt has been made here to improve Soave-BWR for pure components. The functional form of Soave-BWR for pure components and the parametrization of the EoS for pure components can also influence the mixture calculation. This should be taken into account in the future.

7 | Conclusions and Future Work

7.1 Conclusions

7.1.1 Phase Behavior Study of Well-Defined Components

To evaluate the performance of different thermodynamic models capable of more accurate description of the phase equilibrium and physical properties calculations for HPHT reservoir fluids, we focused on three non-cubic EoSs in this research: The Perturbed Chain Statistical Associating Fluid Theory (PC-SAFT) EoS [7, 8], Soave's modification of the Benedict-Webb-Rubin (Soave-BWR) EoS [9], and GERG-2008 [10]. We made a comprehensive comparison between cubic (SRK and PR with/without volume translation) and non-cubic EoSs with regards to their performance in calculation of phase equilibrium and physical properties of different well defined systems. It was found that PC-SAFT, Soave-BWR and GERG-2008 are much better than SRK and PR in density and compressibility calculation of the well-defined light and heavy components in reservoir fluids over a wide temperature and pressure range, with GERG-2008 being the best with the lowest deviation among all EoS models. The non-cubic models were also superior to the cubic models in prediction of gas compressibility factor of the multicomponent gas mixture tested in this study. GERG-2008 shows a clear advantage over SRK, PR, PC-SAFT and Soave-BWR in compressibility calculation for the pure components, while Soave-BWR with regressed binary interaction parameters shows better performance than GERG-2008 in bubble point pressure and vapor phase composition of binary mixtures up to nC_{10} . GERG-2008 gives very large deviations for bubble point pressure calculation of some heavy and asymmetric binary systems such as n-butane + n-nonane system, which suggests that this EoS and its binary interaction parameters could still be improved for some of the binary pairs.

The optimal k_{ij} values for SRK, PR, PC-SAFT and Soave-BWR have been regressed from extensive binary VLE data [63–65]. The binary VLE calculation also showed that PC-SAFT and Soave-BWR are similar to SRK and PR in correlating the important binary pairs in reservoir fluids. Although Soave-BWR gives a better prediction than the other three when zero k_{ij} values are used, its regression results for highly asymmetric systems seem to be poorer. Soave-BWR and PC-SAFT give smaller average k_{ij} values than SRK and PR. On the other hand, they are more sensitive to the change in k_{ij} .

Phase envelope prediction of synthetic gases showed that all the EoS models were similar for not too asymmetric synthetic gases, with or without the optimal k_{ij} values for SRK, PR, PC-SAFT and Soave-BWR. SRK, PC-SAFT and Soave-BWR seem to be slightly better than PR but in general, it is difficult to differentiate the performances of the tested models for synthetic gases representative for natural gases. For highly asymmetric synthetic mixtures [80], the predictions from all the five models somewhat differ and Soave-BWR and GERG-2008 are usually very different from the others; none of the test models can satisfactorily predict all the phase envelopes for these highly asymmetric mixtures.

In summary, PC-SAFT and Soave-BWR have big potentials for applications related to reservoir fluids, including PVT modeling. Compared with SRK and PR, their advantages seem to lie in better density description rather than better VLE description. This formed a major motivation for extending the non-cubic models to reservoir fluids.

7.1.2 Reservoir Fluid Characterization and PVT Modeling

The characterization method of Pedersen et al. was used as the framework for the developed characterization methods in this study, with specific modifications for different EoS models: for PC-SAFT, new correlations for estimating m , σ and ε have been developed; for Soave-BWR, SRK and PR, Twu's correlations for T_c and P_c , and the Lee-Kesler/Kesler-Lee correlations for ω were selected. A comprehensive evaluation of PC-SAFT and Soave-BWR in comparison with SRK and PR (with/without volume translation) was made with regards to their potential in PVT modeling of reservoir fluids.

We presented a new characterization method for PC-SAFT. In order to improve the characterization method for PVT modeling of reservoir fluids, we developed a general

approach to characterizing reservoir fluids based on a large PVT database and applied it to non-cubic PC-SAFT as well as cubic SRK and PR. In this approach, the correlations for the EoS model parameters were developed first based on a large pure component database such as DIPPR, and the coefficients in the obtained correlations were further adjusted using a large PVT database. We suggest keeping the n-alkane limit during the adjustment step, which can be readily realized for correlations developed in a two-step perturbation manner. Our final correlations were obtained using a PVT database of 260 reservoir fluids. The developed correlations are not meant to be an ultimate version. They can be constantly improved with a larger PVT database, or even customized to a certain type of reservoir fluid. Repeating the whole procedure for a set of improved correlations is rather straightforward. The obtained correlations can be easily implemented in PVT software.

PC-SAFT with the new general characterization method gives the lowest AAD% and maximum deviation in calculation of saturation pressure, density and STO density, among all the tested characterization methods for PC-SAFT. Application of the new characterization method to SRK and PR improved the saturation pressure calculation in comparison with the original characterization method for SRK and PR. Using volume translation together with the new characterization approach for SRK and PR gives comparable results for density and STO density to that of original characterization for SRK and PR with volume translation. Soave-BWR gives slightly higher deviation in saturation pressure than SRK and PR, however it gives the largest deviation in density and STO density compared to SRK and PR with volume translation and PC-SAFT with different characterization methods. The characterization method based on PNA content for PC-SAFT gives accurate results for reservoir fluid density and STO density whereas the deviation in saturation pressure is not as low as those from the other characterization methods for PC-SAFT.

For the PVT database used in this study, cubic EoSs seem to have better performance than PC-SAFT in calculation of saturation pressure; PC-SAFT and cubics with volume translation show comparable results in calculation of density and STO density. For calculation of the derivative properties such as compressibility, PC-SAFT has shown to be superior to cubics for the two reservoir fluids tested. However, for the whole database and using the compressibility data calculated from the density data above the saturation pressure instead of measured compressibility, SRK with volume translation was shown to give the lowest deviation. Soave-BWR had slightly higher deviation than SRK with volume translation. The above observation contradicts with the observation

for well-defined systems and the general expectation that non-cubics are better than cubics for compressibility modeling. The results must be interpreted with caution since the compressibility data, either calculated from density or reported directly in the PVT report, can be subject to large uncertainties. We also noticed some inconsistencies between the density data and reported compressibilities in some PVT reports. A more careful look at the experimental PVT data is recommended. In addition, our current test is based mainly on black oil, for lighter reservoir fluids like volatile oil and gas condensate, the conclusions can be different.

Furthermore, we investigated the possibility of incorporating more information from True Boiling Point (TBP) distillation and Simulated Distillation (SimDist) into characterization and PVT modeling. Instead of incorporating all the available composition information, we focused on the difference in mass compositions from different analytical techniques, the deviations between the experimental molecular weights and specific gravities and the default ones, and the utilization of the paraffinics and aromatics (PA) information from SimDist. We modified the existing fluid characterization code to express the component distribution in terms of weight fractions which allows using different sets of molecular weights to generate the corresponding mole fractions. We also developed a procedure to extract the PA information from the SimDist chromatogram.

For the two fluids studied, it was found that the selection of mass composition gives the largest impact on the calculation results, the selection of the MW and SG values are the second most influential factor, and the detailed PA information does not give significant effect on the final results. In particular, the MW values for the heavier fractions have a significant effect on the dew point branch of the phase envelopes for both the low GOR (black oil) and high GOR (gas condensate) fluids. Even at temperatures where the calculated saturation pressures are similar, the selection of MW and SG can give very different density results in constant mass expansion calculations. This is especially for the low GOR fluid and in the two-phase region. For the high GOR fluid, the density difference in the two-phase region is obvious but in the single-phase region is not significant.

7.1.3 Heat Capacities and Joule-Thomson Coefficients

Due to the importance of thermo-physical properties, a comprehensive comparison was made between cubic (SRK and PR) and non-cubic EoSs (Soave-BWR, PC-SAFT and

GERG-2008) in calculation of heat capacity and Joule-Thomson coefficient for pure components and multicomponent mixtures over a wide pressure and temperature range. The calculation results showed that GERG-2008 have some advantages over other EoSs in calculation of heat capacity and Joule-Thomson coefficient of pure components over a wide temperature and pressure range. Soave-BWR gives the closest prediction of the thermal properties to that of GERG-2008 among other EoSs tested in this study. In general and for all the scenarios tested from pure components to multicomponent mixtures, the non-cubic models seem to be superior to the cubic models in calculation of derivative properties such as heat capacity and Joule-Thomson coefficient. For the heat capacity of multicomponent mixtures, PC-SAFT gives the lowest deviation and PR seems to have slightly better performance than Soave-BWR.

It was observed that non-cubic models (i.e. Soave-BWR and GERG-2008) predict a negative Joule-Thomson coefficient at high pressures and all temperatures for pure, binary and multicomponent systems. In fact, the value of Joule-Thomson coefficient seems to reach more or less a constant value at high pressures for all the systems tested. The negative Joule-Thomson coefficient at high pressures causes the temperature of the fluid to increase with the pressure drop (reverse Joule-Thomson effect). Although the temperature increase is not very significant (around 0.5 K/Mpa), it should be considered in the material selection for the tubing and surface facilities because the temperature increase can damage the surface production facilities and affect well integrity and safety.

7.1.4 New Mixing Rules for Soave-BWR

In order to fix the problems in phase equilibrium and density calculation caused by the original Soave-BWR mixing rules, we proposed two new sets of mixing rules for Soave-BWR. The first set (vdW), similar to those used by Starling [167], calculates the EoS parameters directly from the pure component EoS parameters; The second set is the LKP mixing rules [47], where pseudo-critical properties are calculated for the mixture. Furthermore, several hybrid mixing rules by combining vdW and the original Soave-BWR mixing rule were also tested.

We observed major improvements in calculation of excess volume over the whole composition range of methane in the binary mixture of methane + n-decane, and up to very high pressures. All the new mixing rules for Soave-BWR predicted negative excess volume in the studied temperature, pressure and composition range, while vdW and

vdW-D ((eq. (6.67))) had the lowest deviation in calculation of V^E . For the density calculation of asymmetric binary system of methane + n-decane, vdW had better performance than other mixing rules for Soave-BWR, especially at lower methane compositions. vdW-D gave slightly higher deviations than vdW, but still lower than that of Soave. Based on these findings, vdW and vdW-D seem to be very promising for PVT modeling of the reservoir fluids and description of density and compressibility. For the majority of the phase envelopes studied, LKP and vdW-D generally gave satisfactory results and close predictions to that of Soave, while vdW predicted smaller phase envelopes.

Although some of the new mixing rules improved the density calculation and fixed the problem in the excess volume calculation of asymmetric systems, they were not much better, and sometimes worse, than the original mixing rule in phase equilibrium calculation of highly asymmetric systems. The improvement was observed for some individual examples for some mixing rules but it is far from a final solution.

7.2 Future Work

7.2.1 Further Development of Soave-BWR EoS

The comparison shows the potential of Soave-BWR as a light-weight alternative to GERG-2008 especially in PVT modeling and Joule-Thomson coefficient calculations. There is apparently room for improvement of Soave-BWR in order to reach an accuracy comparable to that of GERG-2008 in description of some physical properties and to give better phase equilibrium calculation. Soave-BWR was developed mainly based on hydrocarbons. It should be pointed out that no attempt has been made here to improve Soave-BWR for pure components. The functional form of Soave-BWR for pure components and the parametrization of the EoS for pure components can influence the mixture calculation. Other components common in industrial applications should definitely be included in its further development. It is relatively easy to apply Soave-BWR to systems containing ill-defined heptanes plus fractions with the existing characterization methods. Such a characterization procedure can be applied to the Soave-BWR with the new mixing rules.

There is so far neither established procedure nor solid theoretical basis for development of mixing rules for non-cubic EoS models. The development of new mixing rules relies

somehow on a trial-and-error procedure. Fortunately, we have developed the code in a structured manner and the new mixing rules can be quickly tested. If this procedure is further streamlined and improved, it is possible to test a large number of mixing rules and select a better set for Soave-BWR. Meanwhile, it is worth further investigating various theories for constructing mixing rules so that the selection is not a purely mathematical exercise.

It should be mentioned that we have through this project established large databases for well-defined components and reservoir fluids, developed a general characterization procedure for EoS models, improved the software for comprehensive evaluation of phase equilibrium and thermodynamic properties involving many EoS models. Such a platform will shorten the cycle of EoS development and evaluation, and facilitate improvement of the EoS models in terms of their functional form instead of just their parameters.

7.2.2 Fluid Characterization using More Detailed Analytical Information

Our preliminary study on the influence of analytical information on PVT calculation can also be further pursued in the future. Some of the possibilities are:

1. This study was based on one dead oil sample where both SimDist and TBP data were available. It is desirable to extend the analysis to more samples especially those with actual PVT data. The study will be more systematic if the samples cover a large range of composition and aromaticity and represent the typical fluids in the fields of interest (e.g. the Danish North Sea). It is more beneficial if the PVT data can be used for comparison so that the study is not merely an evaluation of sensitivity but also a test for different characterization methods.
2. The developed characterization method uses more consistent weight fractions instead of mole fractions which are influenced by the MW values. It also allows utilizing the PA information obtained from SimDist. It should be noted that the current extraction of the PA information is empirical and can be surely improved by a more detailed look at the retention times of various paraffinic compounds. Besides, the GC×GC data can provide a more detailed picture of the components in each SCN fraction. This extra information could be integrated into the characterization in the future.

Bibliography

- [1] W. a. Burgess, D. Tapriyal, B. D. Morreale, Y. Wu, M. a. McHugh, H. Baled, and R. M. Enick. Prediction of fluid density at extreme conditions using the perturbed-chain SAFT equation correlated to high temperature, high pressure density data. *Fluid Phase Equilibria*, 319:55–66, 2012.
- [2] R. Greenaway, Mi. Parris, and F. Mueller. High-Pressure, High-Temperature Technologies. *Oilfield Review*, 20(3):46–60, 2008.
- [3] R. Bland, G. Mullen, Y. Gonzalez, Fl. Harvey, M. Pless, and B. Hughes. HP/HT Drilling Fluids Challenges. *IADC/SPE 103731 HP/HT*, pages 1–11, 2006.
- [4] D. Tapriyal, R. Enick, M. McHugh, I. Gamwo, and B. Morreale. High Temperature , High Pressure Equation of State Density Correlations and Viscosity Correlations. *National Energy Technology Laboratory*, (July):1–98, 2012.
- [5] G. S. Soave. Equilibrium constants from a modified Redlich-Kwong equation of state. *Chemical Engineering Science*, 27(6):1197–1203, 1972.
- [6] D. Y. Peng and D. B. Robinson. A New Two-Constant Equation of State. *Industrial & Engineering Chemistry Fundamentals*, 15(1):59–64, feb 1976.
- [7] J. Gross and G. Sadowski. Perturbed-Chain SAFT: An Equation of State Based on a Perturbation Theory for Chain Molecules. *Industrial & Engineering Chemistry Research*, 40(4):1244–1260, feb 2001.
- [8] J. Gross and G. Sadowski. Application of the Perturbed-Chain SAFT Equation of State to Associating Systems Application of the Perturbed-Chain SAFT Equation of State to. *Ind. Eng. Chem. Res.*, 41:5510–5515, 2002.
- [9] G. S. Soave. An effective modification of the Benedict-Webb-Rubin equation of state. *Fluid Phase Equilibria*, 164(2):157–172, oct 1999.
- [10] O. Kunz and W. Wagner. The GERG-2008 wide-range equation of state for natural gases and other mixtures: An expansion of GERG-2004. *Journal of Chemical and Engineering Data*, 57(11):3032–3091, nov 2012.
- [11] N. Von Solms, I. A. Kouskoumvekaki, M. L. Michelsen, and G. M. Kontogeorgis. Capabilities, limitations and challenges of a simplified PC-SAFT equation of state. *Fluid Phase Equilibria*, 241(1-2):344–353, mar 2006.

- [12] K. S. Pedersen and C. H. Sørensen. PC-SAFT Equation of State Applied to Petroleum Reservoir Fluids. In *SPE Annual Technical Conference and Exhibition*, volume 1, pages 1–10, 2007.
- [13] G. M. Kontogeorgis and G. K. Folas. *Thermodynamic models for industrial applications – from classical and advanced mixing rules to association theories*. John Wiley and Sons, Inc., New York, 2010.
- [14] A. J. De Villiers. *Evaluation and improvement of the sPC-SAFT equation of state for complex mixtures*. Phd dissertation, Stellenbosch University, 2011.
- [15] K. S. Pedersen, Aa. Fredenslund, and P. Thomassen. *Propertises of Oils and Natural gases*. Gulf Publishing Inc., Houston, 1989.
- [16] K. S. Pedersen, P. Thomassen, and Aa. Fredenslund. Characterization of Gas Condensate Mixtures. *Advances in Thermodynamics*, 1:137–152, 1989.
- [17] C. H. Whitson. Characterizing Hydrocarbon Plus Fractions. *Society of Petroleum Engineers Journal*, 23(4):683–694, 1983.
- [18] C. H. Whitson, T. F. Andersen, and I. Søreide. C7+ characterization of related equilibrium fluids using the gamma distribution. *Advances in Thermodynamics*, 1:35–36, 1989.
- [19] P. D. Ting, P. C. Joyce, P. K. Jog, W. G. Chapman, and M. C. Thies. Phase equilibrium modeling of mixtures of long-chain and short-chain alkanes using Peng-Robinson and SAFT. *Fluid Phase Equilibria*, 206(1-2):267–286, apr 2003.
- [20] D. L. Gonzalez, P. D. Ting, G. J. Hirasaki, and W. G. Chapman. Prediction of asphaltene instability under gas injection with the PC-SAFT equation of state. *Energy and Fuels*, 19(4):1230–1234, jul 2005.
- [21] D. L. Gonzalez, G. J. Hirasaki, J. Creek, and W. G. Chapman. Modeling of asphaltene precipitation due to changes in composition using the perturbed chain statistical associating fluid theory equation of state. *Energy and Fuels*, 21(3):1231–1242, may 2007.
- [22] D. L. Gonzalez, F. M. Vargas, G. J. Hirasaki, and W. G. Chapman. Modeling Study of CO₂-Induced Asphaltene Precipitation. *Energy and Fuels*, 22(6):757–762, 2008.
- [23] F. M. Vargas, D. L. Gonzalez, J. L. Creek, J. Wang, J. Buckley, G. J. Hirasaki, and W. G. Chapman. Development of a General Method for Modeling Asphaltene Stability. *Energy and Fuels*, 23(3):1147–1154, 2009.
- [24] F. M. Vargas, D. L. Gonzalez, G. J. Hirasaki, and W. G. Chapman. Modeling asphaltene phase behavior in crude oil systems using the perturbed chain form of the statistical associating fluid theory (PC-SAFT) equation of state. *Energy and Fuels*, 23(3):1140–1146, 2009.

- [25] S. R. Panuganti, F. M. Vargas, D. L. Gonzalez, A. S. Kurup, and W. G. Chapman. PC-SAFT characterization of crude oils and modeling of asphaltene phase behavior. *Fuel*, 93:658–669, mar 2012.
- [26] S. R. Panuganti, M. Tavakkoli, F. M. Vargas, D. L. Gonzalez, and W. G. Chapman. SAFT model for upstream asphaltene applications. *Fluid Phase Equilibria*, 359:2–16, dec 2013.
- [27] S. Punnapala and F. M. Vargas. Revisiting the PC-SAFT characterization procedure for an improved asphaltene precipitation prediction. *Fuel*, 108:417–429, jun 2013.
- [28] J. D. van der Waals. *On the continuity of the gas and liquid state*. Doctoral dissertation, Universiteit Leiden, 1873.
- [29] O. Redlich and J. N. S. Kwong. On the Thermodynamics of Solutions. *Chemical Review*, 44:233–244, 1948.
- [30] A. Péneloux, E. Rauzy, and R. Fréze. A consistent correction for Redlich-Kwong-Soave volumes. *Fluid Phase Equilibria*, 8(1):7–23, 1982.
- [31] B. S. Jhaveri and G. K. Youngren. Three-Parameter Modification of the Peng-Robinson Equation of State To Improve Volumetric Predictions. *SPE Reservoir Engineering*, 3(03):1033–1040, 1988.
- [32] W. G. Chapman, K. E. Gubbins, G. Jackson, and M. Radosz. New reference equation of state for associating liquids. *Industrial & Engineering Chemistry Research*, 29(8):1709–1721, 1990.
- [33] W. G. Chapman, G. Jackson, and K. E. Gubbins. Phase equilibria of associating fluids. *Molecular Physics*, 65(5):1057–1079, dec 1988.
- [34] N. von Solms, M. L. Michelsen, and G. M. Kontogeorgis. Computational and Physical Performance of a Modified PC-SAFT Equation of State for Highly Asymmetric and Associating Mixtures. *Ind. Eng. Chem. Res.*, 42:1098–1105, 2003.
- [35] M. Benedict, G. B. Webb, and L. C. Rubin. An Empirical Equation for Thermodynamic Properties of Light Hydrocarbons and Their Mixtures I. Methane, Ethane, Propane and n-Butane. *The Journal of Chemical Physics*, 8(4):334–345, 1940.
- [36] G. S. Soave. A Noncubic Equation of State for the Treatment of Hydrocarbon Fluids at Reservoir Conditions. *Industrial & Engineering Chemistry Research*, 34(11):3981–3994, 1995.
- [37] O. Kunz, R. Klimeck, W. Wagner, and M. Jaeschke. *The GERG-2004 Wide-Range Equation of State for Natural Gases and Other Mixtures*. 2007.
- [38] M. Jaeschke. and A. E. Humphreys. *The GERG Databank of High Accuracy Compressibility Factor Measurements*. 1990.

- [39] M. Jaeschke and A. E. Humphreys. Standard GERG virial equation for field use. *GERG Technical Monograph 5*, 1991.
- [40] M. Jaeschke., H. M. Hinze, and A. E. Humphreys. Supplement to the GERG databank of high-accuracy compression factor measurements. *GERG Technical Monograph 7*, 1996.
- [41] M. L. Michelsen and H. Kistenmacher. On composition-dependent interaction coefficients. *Fluid Phase Equilibria*, 58(1-2):229–230, 1990.
- [42] F. Dauber and R. Span. Achieving higher accuracies for process simulations by implementing the new reference equation for natural gases. *Computers and Chemical Engineering*, 37:15–21, 2012.
- [43] F. Dauber and R. Span. Modelling liquefied-natural-gas processes using highly accurate property models. *Applied Energy*, 97:822–827, 2012.
- [44] F. J. Pérez-Sanz, M. C. Martín, C. R. Chamorro, T. Fernández-Vicente, and J. J. Segovia. Heat capacities and acoustic virial coefficients for a synthetic coal mine methane mixture by speed of sound measurements at $T = (273.16 \text{ and } 250.00) \text{ K}$. *Journal of Chemical Thermodynamics*, 97:137–141, 2016.
- [45] Z. Yuan, M. Cui, R. Song, and Y. Xie. Evaluation of prediction models for the physical parameters in natural gas liquefaction processes. *Journal of Natural Gas Science and Engineering*, 27:876–886, 2015.
- [46] Aspen Technology, Inc, 2013.
- [47] U. Plocker, H. Knapp, and J. Prausnitz. Calculation of High-pressure Vapor-Liquid Equilibria from a Corresponding-States Correlation with Emphasis on Asymmetric Mixtures. *Ind. Eng. Chem. Process Des. Dev.*, 17(3):324–332, 1978.
- [48] A. J. de Villiers, C. E. Schwarz, A. J. Burger, and G. M. Kontogeorgis. Evaluation of the PC-SAFT, SAFT and CPA equations of state in predicting derivative properties of selected non-polar and hydrogen-bonding compounds. *Fluid Phase Equilibria*, 338:1–15, 2013.
- [49] X. Liang, B. Maribo-Mogensen, K. Thomsen, W. Yan, and G. M. Kontogeorgis. Approach to improve speed of sound calculation within PC-SAFT framework. *Industrial and Engineering Chemistry Research*, 51(45):14903–14914, nov 2012.
- [50] I. Polishuk. Semi-theoretical versus entirely empirical: Comparing SAFT + Cubic and Soave-Benedict-Webb-Rubin (SBWR) equations of state. *Industrial and Engineering Chemistry Research*, 50:11422–11431, 2011.
- [51] I. Polishuk. Hybridizing SAFT and cubic EOS: What can be achieved? *Industrial and Engineering Chemistry Research*, 50(7):4183–4198, 2011.
- [52] I. Polishuk. Implementation of SAFT + Cubic, PC-SAFT, and Soave-Benedict-Webb-Rubin Equations of State for Comprehensive Description of Thermodynamic Properties in Binary and Ternary Mixtures of CH_4 , CO_2 , and $n\text{-C}_{16}\text{H}_{34}$. *Industrial & Engineering Chemistry Research*, 50(24):14175–14185, 2011.

- [53] I. Polishuk. Till which pressures the fluid phase EOS models might stay reliable? *Journal of Supercritical Fluids*, 58(2):204–215, 2011.
- [54] G. Jackson, W. G. Chapman, and K. E. Gubbins. Phase equilibria of associating fluids Spherical molecules with multiple bonding sites. *Molecular Physics*, 65(1):1–31, 1988.
- [55] Paul H. Salim and Mark A. Trebble. A modified trebble—bishnoi equation of state: thermodynamic consistency revisited. *Fluid Phase Equilibria*, 65:59 – 71, 1991.
- [56] O. Pfohl. Evaluation of an improved volume translation for the prediction of hydrocarbon volumetric properties. *Fluid Phase Equilibria*, 163(1):157–159, 1999. cited By 39.
- [57] Georgios M. Kontogeorgis, Epaminondas C. Voutsas, Iakovos V. Yakoumis, and Dimitrios P. Tassios. An equation of state for associating fluids. *Industrial & Engineering Chemistry Research*, 35(11):4310–4318, 1996.
- [58] Georgios M Kontogeorgis, Iakovos V. Yakoumis, Henk Meijer, Eric Hendriks, and Tony Moorwood. Multicomponent phase equilibrium calculations for water–methanol–alkane mixtures. *Fluid Phase Equilibria*, 158–160:201 – 209, 1999.
- [59] The Cubic-Plus-Association EoS: Parameters for Pure Compounds and Interaction Parameters. Technical University of Denmark. Technical report, 2012.
- [60] A. K. Doolittle. Specific Volumes of n-Alkanes. *J. Chem. Eng. Data*, 9:275–279, 1964.
- [61] T. Regueira, G. Pantelide, W. Yan, and E. H. Stenby. Density and phase equilibrium of the binary system methane + n-decane under high temperatures and pressures. *Fluid Phase Equilibria*, 428:48–61, nov 2016.
- [62] J. Mollerup and P. Angelo. Measurement and correlation of the volumetric properties of a synthetic natural gas mixture. *Fluid Phase Equilibria*, 19:259–271, 1985.
- [63] H. Knapp, R. Doring, L. Oellrich, U. Plocker, and J.M. Prausnitz. Vapor–Liquid Equilibria for Mixtures of Low Boiling Substances. *Chemistry data series*, vol. VI, 1982.
- [64] A. Mączyński and A. Skrzecz. *TRC Data Bases for Chemistry and Engineering Floppy Book on Vapor-Liquid Equilibrium Data*. Binary Systems Version 1998- 1, Thermodynamics Data Center, Institute of Physical Chemistry and Institute of Coal Chemistry of the Polish Academy of Sciences.
- [65] E. Mansfield and S. L. Outcalt. Bubble-Point Measurements of n-Butane + n-Octane and n-Butane + n-Nonane Binary Mixtures. *Journal of Chemical & Engineering Data*, 60(8):2447–2453, 2015.

- [66] J. N. Jaubert and F. Mutelet. VLE predictions with the Peng–Robinson equation of state and temperature dependent k_{ij} calculated through a group contribution method. *Fluid Phase Equilibria*, 224(2):285–304, 2004.
- [67] E. Voutsas, K. Magoulas, and D. Tassios. Universal Mixing Rule for Cubic Equations of State Applicable to Symmetric and Asymmetric Systems: Results with the Peng–Robinson Equation of State. *Industrial & Engineering Chemistry Research*, 43(19):6238–6246, 2004.
- [68] Epaminondas Voutsas, Vasiliki Louli, Christos Boukouvalas, Kostis Magoulas, and Dimitrios Tassios. Thermodynamic property calculations with the universal mixing rule for eos/ge models: Results with the peng–robinson eos and a {UNIFAC} model. *Fluid Phase Equilibria*, 241(1–2):216 – 228, 2006. A Festschrift in Honor of John M. Prausnitz.
- [69] Stephane Vitu, Romain Privat, Jean-Noel Jaubert, and Fabrice Mutelet. Predicting the phase equilibria of {CO₂} + hydrocarbon systems with the {PPR78} model (pr {EOS} and k_{ij} calculated through a group contribution method). *The Journal of Supercritical Fluids*, 45(1):1 – 26, 2008.
- [70] Jean-Noël Jaubert, Romain Privat, and Fabrice Mutelet. Predicting the phase equilibria of synthetic petroleum fluids with the ppr78 approach. *AIChE Journal*, 56(12):3225–3235, 2010.
- [71] Vasiliki Louli, Georgia Pappa, Christos Boukouvalas, Stathis Skouras, Even Solbraa, Kjersti O. Christensen, and Epaminondas Voutsas. Measurement and prediction of dew point curves of natural gas mixtures. *Fluid Phase Equilibria*, 334:1 – 9, 2012.
- [72] S. Avila, S. T. Blanco, I. Velasco, E. Rauzy, and S. Otín. Thermodynamic Properties of Synthetic Natural Gases . 1 . Dew-Point Curves of Synthetic Natural Gases and Their Mixtures with Water and Methanol . Measurement and Correlation. *Ind. Eng. Chem. Res.*, 41:3714–3721, 2002.
- [73] Susana Avila, Sofía T Blanco, Inmaculada Velasco, Evelyne Rauzy, and Santos Otín. Thermodynamic Properties of Synthetic Natural Gases. 2. Dew Point Curves of Synthetic Natural Gases and Their Mixtures with Water and Methanol. Measurement and Correlation. *Energy & Fuels*, 16(4):928–934, jul 2002.
- [74] Mario H Gonzalez and Anthony L Lee. Dew and bubble points of simulated natural gases. *Journal of Chemical & Engineering Data*, 13(2):172–176, apr 1968.
- [75] C Jarne, S Avila, S T Blanco, E Rauzy, S Otín, and I Velasco. Thermodynamic Properties of Synthetic Natural Gases. 5. Dew Point Curves of Synthetic Natural Gases and Their Mixtures with Water and with Water and Methanol: Measurement and Correlation. *Industrial & Engineering Chemistry Research*, 43(1):209–217, jan 2004.
- [76] Ø Mørch, Kh. Nasrifar, O Bolland, E Solbraa, A O Fredheim, and L H Gjertsen. Measurement and modeling of hydrocarbon dew points for five synthetic natural gas mixtures. *Fluid Phase Equilibria*, 239(2):138–145, jan 2006.

- [77] JL Oscarson and B Saxey. Measurement of total fraction condensed and phase boundary for a simulated natural gas. research report. Technical report, Gas Processors Association, Tulsa, OK (USA), 1982.
- [78] Sofía T Blanco, Susana Avila, Inmaculada Velasco, Evelyne Rauzy, and Santos Otín. Dew points of ternary methane+ethane+butane and quaternary methane+ethane+butane+water mixtures: measurement and correlation. *Fluid Phase Equilibria*, 171(1-2):233–242, may 2000.
- [79] Jayendra S Parikh, Richard F Bukacek, Lois Graham, and Stuart Leipziger. Dew and bubble point measurements for a methane-ethane-propane mixture. *Journal of Chemical & Engineering Data*, 29(3):301–303, jul 1984.
- [80] L. E. Urlic, L. J. Florusse, E. J. M. Straver, S. Degrange, and C. J. Peters. Phase and Interfacial Tension Behavior of Certain Model Gas Condensates : Measurements and Modeling. *Transport in Porous Media*, 52:141–157, 2003.
- [81] J. Zhou, P. Patil, S. Ejaz, M. Atilhan, J. C. Holste, and K. R. Hall. (p, Vm, T) and phase equilibrium measurements for a natural gas-like mixture using an automated isochoric apparatus. *Journal of Chemical Thermodynamics*, 38(11):1489–1494, nov 2006.
- [82] F Gozalpour, A Danesh, A C Todd, D.-H Tehrani, and B Tohidi. Vapour–liquid equilibrium volume and density measurements of a five-component gas condensate at 278.15–383.15 K. *Fluid Phase Equilibria*, 206(1-2):95–104, apr 2003.
- [83] M. F. Alfradique and M. Castier. Calculation of phase equilibrium of natural gases with the Peng-Robinson and PC-SAFT equations of state. *Oil and Gas Science and Technology*, 62(5):707–714, 2007.
- [84] Romain Privat, Rafiqul Gani, and Jean-Noël Jaubert. Are safe results obtained when the pc-saft equation of state is applied to ordinary pure chemicals? *Fluid Phase Equilibria*, 295(1):76 – 92, 2010.
- [85] Ilya Polishuk, Romain Privat, and Jean-Noël Jaubert. Novel methodology for analysis and evaluation of saft-type equations of state. *Industrial & Engineering Chemistry Research*, 52(38):13875–13885, 2013.
- [86] T.J. Broad, N Varotsis, and N Pasadakis. The Compositional Characterization of Gas Condensate Fluids - A Review Featuring the Impact of the Analysis Data Quality on the Accuracy of Equation of State Based PVT Predictions. *SPE Middle East Oil Show*, 2001.
- [87] K. S. Pedersen and P. Christensen. *Phase Behavior of Petroleum Reservoir Fluids*. CRC Press, Taylor & Francis Group, Boca Raton, FL, second ed. edition, 2007.
- [88] H. A. Aladwani and M. R. Riazi. Some Guidelines for Choosing a Characterization. *Chemical Engineering Research and Design*, 83(February):160–166, 2005.

- [89] K. S. Pedersen, A. S. Calsep, J. Milter, and H. Sørensen. Cubic Equations of State Applied to HT / HP and Highly Aromatic Fluids. *SPE 77385*, (October 2003):186–192, 2004.
- [90] C. H. Whitson and M. R. Brule. *Phase Behavior*, volume 20. 2000.
- [91] Zhendi Wang and Merv Fingas. Developments in the analysis of petroleum hydrocarbons in oils, petroleum products and oil-spill-related environmental samples by gas chromatography. *Journal of Chromatography A*, 774(1-2):51–78, 1997.
- [92] A. Y. Dandekar, S. I. Andersen, and E. H. Stenby. COMPOSITIONAL ANALYSIS OF NORTH SEA OILS. *Petroleum Science and Technology*, 18(7-8):975–988, aug 2000.
- [93] H. P. Roenningsen, I. Skjevraak, and E. Osjord. Characterization of North Sea petroleum fractions: hydrocarbon group types, density and molecular weight. *Energy & Fuels*, 3(6):744–755, nov 1989.
- [94] Z. Wang, M. Fingas, and K. Li. Fractionation of a light crude oil and identification and quantitation of aliphatic, aromatic, and biomarker compounds by gc-fid and gc-ms, part I. *Journal of Chromatographic Science*, 32(9):361–366, 1994.
- [95] J. Beens and U. A.T. Brinkman. The role of gas chromatography in compositional analyses in the petroleum industry. *Trends in Analytical Chemistry*, 19(4):260–275, apr 2000.
- [96] E. H. Osjord, H. P. Rønningsen, and L. Tau. Distribution of weight, density, and molecular weight in crude oil derived from computerized capillary gc analysis. *Journal of High Resolution Chromatography*, 8(10):683–690, 1985.
- [97] J. P. Durand, A. Fafet, and A. Barreau. Direct and automatic capillary gc analysis for molecular weight determination and distribution in crude oils and condensates up to c20. *Journal of High Resolution Chromatography*, 12(4):230–233, 1989.
- [98] D. L. Katz and A. Firoozabadi. Predicting Phase Behavior of Condensate/Crude-Oil Systems Using Methane Interaction Coefficients. *Journal of Petroleum Technology*, 30(11):1649–1655, 1978.
- [99] J. Blomberg, P. J. Schoenmakers, and U. A Th Brinkman. Gas chromatographic methods for oil analysis. *Journal of Chromatography A*, 972(2):137–173, 2002.
- [100] F. T. Eggertsen, Sigurd. Groennings, and J. J. Holst. Analytical distillation by gas chromatography. programmed temperature operation. *Analytical Chemistry*, 32(8):904–909, 1960.
- [101] J. Beens, R. Tijssen, and J. Blomberg. Prediction of comprehensive two-dimensional gas chromatographic separations: A theoretical and practical exercise. *Journal of Chromatography A*, 822(2):233 – 251, 1998.

- [102] Jan Beens, Hans Boelens, Robert Tijssen, and Jan Blomberg. Quantitative aspects of comprehensive two-dimensional gas chromatography (gc x gc). *Journal of High Resolution Chromatography*, 21(1):47–54, 1998.
- [103] Bhajendra N. Barman, Vicente L. Cebolla, and Luis Membrado. Chromatographic Techniques for Petroleum and Related Products. *Critical Reviews in Analytical Chemistry*, 30(2-3):75–120, 2000.
- [104] Philip J Marriott and Russell M Kinghorn. New operational modes for multidimensional and comprehensive gas chromatography by using cryogenic modulation. *Journal of Chromatography A*, 866(2):203–212, 2000.
- [105] T. E. Daubert and R. P. Danner. *Physical and Thermodynamic Properties of Pure Compounds: Data Compilation Title*. Hemisphere, New York, 1998.
- [106] K. S. Pedersen, S. Leekumjorn, K. Krejbjerg, and J. Azeem. Modeling of EOR PVT data using PC-SAFT equation. *Abu Dhabi International Petroleum Conference and Exhibition, 11-14 November, Abu Dhabi, UAE*, page 11, 2012.
- [107] K. S. Pedersen, P. Thomassen, and Aa. Fredenslund. SRK-EOS calculation for crude oils. *Fluid Phase Equilibria*, 14(C):209–218, 1983.
- [108] K. S. Pedersen, P. Thomassen, and Aa. Fredenslund. Thermodynamics of Petroleum Mixtures Containing Heavy Hydrocarbons. 1. Phase Envelope Calculations by Use of the Soave-Redlich-Kwong Equation of State. *Ind. Eng. Chem. Process*, 23:163–170, 1984.
- [109] K. S. Pedersen, A. L. Blilie, and K. K. Meisingset. PVT Calculations on Petroleum Reservoir Fluids Using Measured and Estimated Compositional Data for the Plus Fraction cm. *Industrial & Engineering Chemistry Research*, 31:1378–1384, 1992.
- [110] I. Rodriguez and A. A. Hamouda. An Approach for Characterization and Lumping of Plus Fractions of Heavy Oil. *SPE 117446*, (April):283–295, 2010.
- [111] M. R. Riazi. Distribution Model for Properties of Hydrocarbon-Plus Fractions. *Industrial & Engineering Chemistry Research*, 28:1731–1735, 1989.
- [112] M. R. Riazi. *Characterization and properties of petroleum fractions*. ASTM International, 2005.
- [113] C. H. Twu. An internally consistent correlation for predicting the critical properties and molecular weights of petroleum and coal-tar liquids. *Fluid Phase Equilibria*, 16(2):137–150, 1984.
- [114] B. I. Lee and M. G. Kesler. A Generalized Thermodynamic Correlation Based on Three-Parameter Corresponding States. *AIChE Journal*, 21(3):510–527, 1975.
- [115] M. G. Kesler and B. I. Lee. Improve Prediction of Enthalpy of Fractions. *Hydrocarbon Processing*, 55(3):153–158, 1976.

- [116] Kh. Nasrifar and O. Bolland. Prediction of thermodynamic properties of natural gas mixtures using 10 equations of state including a new cubic two-constant equation of state. *Journal of Petroleum Science and Engineering*, 51(3-4):253–266, may 2006.
- [117] I. Søreide. *Improved Phase Behavior Predictions of Petroleum Reservoir Fluids from a Cubic Equation of State*. PhD thesis, NTNU, 1989.
- [118] X. Liang, W. Yan, K. Thomsen, and G. M. Kontogeorgis. On petroleum fluid characterization with the PC-SAFT equation of state. *Fluid Phase Equilibria*, 375:254–268, aug 2014.
- [119] Wei Yan, Farhad Varzandeh, and Erling H Stenby. PVT modeling of reservoir fluids using PC-SAFT EoS and Soave-BWR EoS. *Fluid Phase Equilibria*, 386:96–124, 2015.
- [120] X. Liang, W. Yan, K. Thomsen, and G. M. Kontogeorgis. Modeling the liquid-liquid equilibrium of petroleum fluid and polar compounds containing systems with the PC-SAFT equation of state. *Fluid Phase Equilibria*, 406:147–155, 2015.
- [121] P. Hosseinifar, M. Assareh, and C. Ghotbi. Developing a new model for the determination of petroleum fraction PC-SAFT parameters to model reservoir fluids. *Fluid Phase Equilibria*, 412:145–157, 2016.
- [122] M. Assareh, C. Ghotbi, M. Tavakkoli, and G. Bashiri. PC-SAFT modeling of petroleum reservoir fluid phase behavior using new correlations for petroleum cuts and plus fractions. *Fluid Phase Equilibria*, 408:273–283, 2016.
- [123] S. Leekumjorn and K. Krejbjerg. Phase behavior of reservoir fluids: Comparisons of PC-SAFT and cubic EOS simulations. *Fluid Phase Equilibria*, 359:17–23, dec 2013.
- [124] A. Tihic, G. M. Kontogeorgis, Ni. von Solms, and M. L. Michelsen. Applications of the simplified perturbed-chain SAFT equation of state using an extended parameter table. *Fluid Phase Equilibria*, 248(1):29–43, oct 2006.
- [125] G. S. Soave. treatment by the Soave – Redlich – Kwong equation of state. *Fluid Phase Equilibria*, pages 29–39, 1998.
- [126] K. Van Nes and H. A. Van Westen. *Aspects of the constitution of mineral oils*. Elsevier Pub. Co., Houston-Amsterdam, 1951.
- [127] M. R Riazi and T. E. Daubert. Prediction of Molecular-Type Analysis of Petroleum Fractions and Coal Liquids. *Ind. Eng. Chem. Process*, 25:1009–1015, 1986.
- [128] J. N. Jaubert, L. Avaullee, and J. F. Souvay. A crude oil data bank containing more than 5000 PVT and gas injection data. *Journal of Petroleum Science and Engineering*, 34(1-4):65–107, jun 2002.

- [129] A. M. Elsharkawy. An empirical model for estimating the saturation pressures of crude oils. *Journal of Petroleum Science and Engineering*, 38(1-2):55–77, may 2003.
- [130] DTU. Internal PVT Database at Center for Energy Resources Engineering, Technical University of Denmark. Technical report, 2014.
- [131] D. González-Salgado, J. L. Valencia, J. Troncoso, E. Carballo, J. Peleteiro, L. Romani, and D. Bessières. Highly precise experimental device for determining the heat capacity of liquids under pressure. *Review of Scientific Instruments*, 78(5):55103, 2007.
- [132] R. Páramo, M. Zouine, and C. Casanova. New batch cells adapted to measure saturated heat capacities of liquids. *Journal of Chemical and Engineering Data*, 47:441–448, 2002.
- [133] Amr Henni. Heat capacity of non-electrolyte solutions. In E. Wilhelm and T. M. Letcher, editors, *Heat capacities: liquids, solutions and vapours*, pages 86–111. Royal Society of Chemistry, Cambridge, 2010.
- [134] D. Bessières, H. Saint-Guirons, and J. L. Daridon. High pressure measurement of n-dodecane heat capacity up to 100 MPa. Calculation from equations of state. *High Pressure Research*, 18:279–284, 2000.
- [135] E. Wilhelm and R. Battino. Partial molar heat capacity changes of gases dissolved in liquids. In E Wilhelm and T M Letcher, editors, *Heat capacities: liquids, solutions and vapours*, pages 457–471. Royal Society of Chemistry, Cambridge, 2010.
- [136] D. V. Nichita, J. Pauly, and J. L. Daridon. Joule–Thomson inversion in vapor–liquid–solid solution systems. *International Journal of Thermophysics*, 30(4):1130–1143, 2009.
- [137] D. Bessières, S. L. Randzio, M. M. Piñeiro, Th. Lafitte, and J. L. Daridon. A combined pressure-controlled scanning calorimetry and monte carlo determination of the Joule-Thomson inversion curve. Application to methane. *The Journal of Physical Chemistry B*, 110(11):5659–5664, 2006.
- [138] A. C. Baker and M. Price. Modelling the performance of high-pressure high-temperature wells, 1990.
- [139] C. M. Colina, L. F. Turrens, K. E. Gubbins, C. Olivera-Fuentes, and L. F. Vega. Predictions of the Joule-Thomson inversion curve for the n-alkane series and carbon dioxide from the Soft-SAFT Equation of State. *Industrial & Engineering Chemistry Research*, 41(5):1069–1075, 2002.
- [140] M. Lagache, P. Ungerer, A. Boutin, and A. H. Fuchs. Prediction of thermodynamic derivative properties of fluids by Monte Carlo simulation. *Physical Chemistry Chemical Physics*, 3(19):4333–4339, 2001.

- [141] Mario C Pinto, Chaitanya Karale, and Prasanta Das. A simple and reliable approach for the estimation of the Joule-Thomson coefficient of reservoir gas at bottomhole conditions. *SPE Journal*, 18:960–968, 2013.
- [142] Jeffrey F App. Field cases: Nonisothermal behavior due to Joule-Thomson and transient fluid expansion/compression effects, 2009.
- [143] Teresa Regueira, Farhad Varzandeh, Erling H. Stenby, and Wei Yan. Heat capacity and joule-thomson coefficient of selected n-alkanes at 0.1 and 10mpa in broad temperature ranges. *The Journal of Chemical Thermodynamics*, 111:250 – 264, 2017.
- [144] Rima Abbas, Christian Ihmels, Sabine Enders, and Jürgen Gmehling. Joule–Thomson coefficients and Joule–Thomson inversion curves for pure compounds and binary systems predicted with the group contribution equation of state VTPR. *Fluid Phase Equilibria*, 306(2):181–189, 2011.
- [145] A Chacín, J M Vázquez, and E A Müller. Molecular simulation of the Joule-Thomson inversion curve of carbon dioxide. *Fluid Phase Equilibria*, 165(2):147–155, 1999.
- [146] Naser Seyed Matin and Behzad Haghighi. Calculation of the Joule–Thomson inversion curves from cubic equations of state. *Fluid Phase Equilibria*, 175(1–2):273–284, 2000.
- [147] Jadran Vrabec, Ashish Kumar, and Hans Hasse. Joule–Thomson inversion curves of mixtures by molecular simulation in comparison to advanced equations of state: Natural gas as an example. *Fluid Phase Equilibria*, 258(1):34–40, 2007.
- [148] W G Kortekaas, C J Peters, and J de Swaan Arons. Joule-Thomson expansion of high-pressure-high-temperature gas condensates. *Fluid Phase Equilibria*, 139(1):205–218, 1997.
- [149] Fernando A Escobedo and Zhong Chen. Simulation of isoenthalps and Joule-Thomson inversion curves of pure fluids and mixtures. *Molecular Simulation*, 26(6):395–416, 2001.
- [150] C M Colina and E A Müller. Molecular simulation of Joule–Thomson inversion curves. *International Journal of Thermophysics*, 20(1):229–235, 1999.
- [151] Jadran Vrabec, Gaurav Kumar Kedia, and Hans Hasse. Prediction of Joule–Thomson inversion curves for pure fluids and one mixture by molecular simulation. *Cryogenics*, 45(4):253–258, 2005.
- [152] M. H. Lagache, Ph. Ungerer, and A. Boutin. Prediction of thermodynamic derivative properties of natural condensate gases at high pressure by Monte Carlo simulation. *Fluid Phase Equilibria*, 220(2):211–223, 2004.
- [153] J M Mollerup and M L Michelsen. Calculation of thermodynamic equilibrium properties. *Fluid Phase Equilibria*, 74:1–15, 1992.

- [154] G. Ernst, B. Keil, H. Wirbser, and M. Jaeschke. Flow-calorimetric results for the massic heat capacity and the Joule–Thomson coefficient of CH₄, of (0.85CH₄+0.15C₂H₆), and of a mixture similar to natural gas. *The Journal of Chemical Thermodynamics*, 33(6):601–613, 2001.
- [155] Dinghai Huang, Sindee L Simon, and Gregory B McKenna. Chain length dependence of the thermodynamic properties of linear and cyclic alkanes and polymers. *The Journal of Chemical Physics*, 122(8):84907, 2005.
- [156] R H Perry and D W Green. *Perry's Chemical Engineers' Handbook*. McGraw-Hill, 7th edition, 1998.
- [157] C.J Kedge and M.a Trebble. Development of a new empirical non-cubic equation of state. *Fluid Phase Equilibria*, 158-160:219–228, jun 1999.
- [158] Bruce E Poling, John M Prausnitz, John P O'connell, et al. *The properties of gases and liquids*, volume 5. Mcgraw-hill New York, 2001.
- [159] W. B. Kay. Density of hydrocarbon gases and vapours at high temperature and pressure. *Ind. Eng. Chem.*, 28:1014–1019, 1936.
- [160] Bruce E Poling, John M Prausnitz, John P O'connell, et al. *The properties of gases and liquids*, volume 5. Mcgraw-hill New York, 2001.
- [161] JM Prausnitz and RD Gunn. Volumetric properties of nonpolar gaseous mixtures. *AIChE Journal*, 4(4):430–435, 1958.
- [162] JM Prausnitz and RD Gunn. Pseudocritical constants from volumetric data for gas mixtures. *AIChE Journal*, 4(4):494–494, 1958.
- [163] Edward Allen Mason and Thomas H Spurling. *The virial equation of state*, volume 2. Pergamon, 1969.
- [164] Stanley I. Sandier and Hasan Orbey. 9 MIXING AND COMBINING RULES. *Experimental Thermodynamics*, 5:321–357, 2000.
- [165] Manson Benedict, George B Webb, and Louis C Rubin. An empirical equation for thermodynamic properties of light hydrocarbons and their mixtures ii. mixtures of methane, ethane, propane, and n-butane. *The Journal of Chemical Physics*, 10(12):747–758, 1942.
- [166] PR Bishnoi and DB Robinson. New mixing rules for the bwr parameters to predict mixture properties. *The Canadian Journal of Chemical Engineering*, 50(1):101–107, 1972.
- [167] Kenneth E Starling. *Fluid thermodynamic properties for light petroleum systems*. Gulf Pub. Co., 1973.
- [168] Kenneth R. Hall, Gustavo a. Iglesias-Silva, and G. Ali Mansoori. Quadratic mixing rules for equations of state. Origins and relationships to the virial expansion. *Fluid Phase Equilibria*, 91:67–76, 1993.

- [169] Michael S.-W. Wei, Trent S. Brown, Arthur J. Kidnay, and E. Dendy Sloan. Vapor + liquid equilibria for the ternary system methane + ethane + carbon dioxide at 230 k and its constituent binaries at temperatures from 207 to 270 k. *Journal of Chemical & Engineering Data*, 40(4):726–731, 1995.
- [170] HH Reamer, RH Olds, BH Sage, and WN Lacey. Phase equilibria in hydrocarbon systems. *Industrial & Engineering Chemistry*, 34(12):1526–1531, 1942.
- [171] W. C. Edmister. Applied Hydrocarbon Thermodynamics, Part 4, Compressibility Factors and Equations of State. *Petroleum Refiner*, 37:173–179, 1958.
- [172] F. W. Winn. Physical Properties by Nomogram. *Petroleum Refiners*, 36(21):157, 36(21):157, 1957.
- [173] R. H. Cavett. Physical Data for Distillation Calculation, Vapor-Liquid Equilibria. In *27th Midyear Meeting, API Division of Refining*, San Francisco, CA, 1964.
- [174] M. R. Riazi and T. E. Daubert. Simplify Property Predictions. *Hydrocarbon Processing*, pages 115–116, 1980.
- [175] C. Tsonopoulos, J. L. Heidman, and S. C. Hwang. Thermodynamics and Transport Properties of Coal Liquids. *Chemical Engineering Science*, 42(5), 1987.
- [176] H. Korsten. Internally consistent prediction of vapor pressure and related properties. *Industrial and Engineering Chemistry Research*, 39:813–820, 2000.
- [177] M. R. Riazi and T. E. Daubert. Characterization parameters for petroleum fractions. *Ind. Eng. Chem. Res.*, 26(4):755–759, 1987.
- [178] G. F. Sancet. Heavy Fraction C7+ Characterization for PR-EOS. *SPE-13026-STU*, pages 1–10, 2007.
- [179] M. Jamialahmadi, H. Zangeneh, and S. S. Hosseini. A generalized set of correlations for plus fraction characterization. *Petroleum Science*, 9(3):370–378, aug 2012.
- [180] M. R. Riazi, H. A. Al-Adwani, and A. Bishara. The impact of characterization methods on properties of reservoir fluids and crude oils: Options and restrictions. *Journal of Petroleum Science and Engineering*, 42(2-4):195–207, apr 2004.
- [181] R. Nokay. Estimate Petrochemical Properties. *Chem. Eng.*, pages 147–48, 1959.
- [182] T. E. Daubert and R. P. Danner. *Technical Data Book - Petroleum Refining*. American Petroleum Institute (API), Washington, DC, 6th editio edition, 1997.
- [183] Zh. Jianzhong, Zh. Biao, Zh. Souqi, W. Renan, and Y. Guanghua. Simplified prediction of physical properties for non-polar compounds, petroleum and coal liquid fractions. *Industrial and Engineering Chemistry Research*, 37(5):2059–2060, 1998.
- [184] Zh. Jianzhong, Zh. Biao, Zh. Suoqi, W. Renan, and Y. Guanghua. Prediction of critical properties of non-polar compounds, petroleum and coal-tar liquids. *Fluid Phase Equilibria*, 149:103–109, 1998.

-
- [185] M. R. Riazi, T. A. Al-sahhaf, and M. A. Al-shammari. A generalized method for estimation of critical constants. *Fluid Phase Equilibria*, 147:1–6, 1998.
- [186] G. N. Nji, W. Y. Svrcek, H. W. Yarranton, and M. A. Satyro. Characterization of Heavy Oils and Bitumens . 1 . Vapor Pressure and Critical Constant Prediction Method for Heavy Hydrocarbons. *Energy & Fuels*, 22:455–462, 2008.
- [187] G. N. Nji, W. Y. Svrcek, H. Yarranton, and M. A. Satyro. Characterization of Heavy Oils and Bitumens 2 . Improving the Prediction of Vapor Pressures for Heavy Hydrocarbons at Low Reduced Temperatures Using the Peng - Robinson Equation of State. *Energy & Fuels*, 23:366–373, 2009.
- [188] A. Kumar and R. Okuno. Critical parameters optimized for accurate phase behavior modeling for heavy n-alkanes up to C100 using the Peng–Robinson equation of state. *Fluid Phase Equilibria*, 335:46–59, dec 2012.

A | Parameter Estimation for Thermodynamic Models

In this section we would briefly review the available correlations for acentric factor and critical properties such as T_c and P_c .

A.1 Acentric Factor Correlations

The following correlations are used along with correlations for critical properties to find the model parameters for thermodynamic models such as SRK and PR. It should be mentioned that some of the methods have their own correlation for acentric factor. In such cases none of the following correlations are used.

- Edmister Correlation [171]:

Edmister [171] presented the following correlation to estimate the acentric factor of pure liquids and petroleum fractions:

$$\omega = \frac{3}{7} \left(\frac{\log(P_c)}{T_c/T_b - 1} \right) - 1 \quad (\text{A.1})$$

In this correlation T_b and T_c are in K and P_c is in atm.

- Lee-Kesler/Kesler-Lee Correlations [114, 115]:

Lee and Kesler correlated the acentric factor as follows.

For $T_{br} < 0.8$:

$$\omega = \frac{\ln(P_{br}) - 5.92714 + \frac{6.09648}{T_{br}} + 1.28862 \ln(T_{br}) - 0.169347T_{br}^6}{15.2518 - \frac{15.6875}{T_{br}} - 13.4721 \ln(T_{br}) + 0.43577T_{br}^6} \quad (\text{A.2})$$

For $T_{br} \geq 0.8$:

$$\omega = -7.904 + 0.1352K - 0.007465K^2 + 8.359T_{br} + \frac{1.408 - 0.01063K}{T_{br}} \quad (\text{A.3})$$

In these correlations T_b and T_c are in °R and P_c is in atm. $T_{br} = T_b/T_c$, $P_{br} = 1/P_c$, and $K = T_{br}^{1/3}/SG$

A.2 Critical Temperature and Pressure Correlations

T_c is perhaps the most reliably correlated critical property for petroleum fractions, while P_c correlations are less reliable than T_c . In this section we present some of the most used correlations in calculation of critical properties of SCN fractions. Most of the correlations are summarized from references [87, 90, 108].

- Winn [172] Correlations :

In 1957, Winn [172] developed a correlation for T_c as a function of T_b and SG :

$$T_c = \frac{\exp(4.2009T_b^{0.08615}SG^{0.04614})}{1.8} \quad (\text{A.4})$$

This correlation is used together with the following correlation for P_c :

$$P_c = 6.1483 \times 10^{12} T_b^{-2.3177} SG^{2.4853} \quad (\text{A.5})$$

In these correlations T_b and T_c are in K and P_c is in Pa.

- Cavett Correlations [173]:

$$\begin{aligned} T_c = & 768.071 + 1.7134T_b - 0.10834 \times 10^{-2}T_b^2 \\ & + 0.3889 \times 10^{-6}T_b^3 - 0.89213 \times 10^{-2}T_b \times API \\ & + 0.53095 \times 10^{-6}T_b^2 \times API + 0.32712 \times 10^{-7}T_b^2 \times API^2 \end{aligned} \quad (\text{A.6})$$

$$\begin{aligned} \log(P_c) = & 2.829 + 0.9412 \times 10^{-3}T_b - 0.30475 \times 10^{-5}T_b^2 \\ & + 0.15141 \times 10^{-8}T_b^3 - 0.20876 \times 10^{-4}T_b \times API \\ & + 0.11048 \times 10^{-7}T_b^2 \times API + 0.1395 \times 10^{-9}T_b^2 \times API^2 \\ & - 0.4827 \times 10^{-7}T_b \times API^2 \end{aligned} \quad (\text{A.7})$$

where

$$API = \frac{141.5}{SG} - 131.5 \quad (\text{A.8})$$

In these correlations T_b and T_c are in °F and P_c is in psia.

- Kesler and Lee Correlations [115]:

In addition to the correlation Kesler and Lee [115] developed for acentric factor, they proposed two correlations for T_c and P_c :

$$T_c = 341.7 + 811SG + (0.4244 + 0.1174SG)T_b + (0.4669 - 3.2623SG) \times 10^5 T_b^{-1} \quad (\text{A.9})$$

$$\begin{aligned} \ln P_c = & 8.3634 - \frac{0.0566}{SG} - \left[\left(0.24244 + \frac{2.2898}{SG} + \frac{0.11857}{SG^2} \right) \times 10^{-3} \right] T_b \\ & + \left[\left(1.4685 + \frac{3.648}{SG} + \frac{0.47227}{SG^2} \right) \times 10^{-7} \right] T_b^2 \\ & - \left[\left(0.42019 + \frac{1.6977}{SG^2} \right) \times 10^{-10} \right] T_b^3 \end{aligned} \quad (\text{A.10})$$

where T_b and T_c are in °R and P_c is in psia.

- Riazi-Daubert Correlations [174]:

$$T_c = 24.27871T_b^{0.58848} SG^{0.3596} \quad (\text{A.11})$$

$$P_c = 3.12281 \times 10^9 T_b^{-2.3125} SG^{2.3201} \quad (\text{A.12})$$

where T_b and T_c are in °R and P_c is in psia. (2.30)

- Twu's Correlations [113]:

Twu's correlations estimate the critical properties in two steps. In the first step, the properties of the n-alkanes (T_{cp} , P_{cp}) at the T_b of the SCN component are calculated using the following correlations where T_b and T_{cp} are in °R and P_{cp} is in psia.

$$T_{cp} = T_b \left(\frac{0.53327 + 0.19102 \times 10^{-3} T_b + 0.77968 \times 10^{-7} T_b^2}{-0.28438 \times 10^{-10} T_b^3 + \frac{0.95947 \times 10^{28}}{T_b^{13}}} \right)^{-1} \quad (\text{A.13})$$

$$\begin{cases} \alpha = 1 - T_b/T_{cp} \\ P_{cp} = (3.83354 + 1.19629\alpha^{0.5} + 34.8888\alpha + 36.1952\alpha^2 + 104.193\alpha^4)^2 \end{cases} \quad (\text{A.14})$$

$$V_{cp} = \left(1 - (0.419869 - 0.505839\alpha - 1.56436\alpha^3 - 9481.7\alpha^{14}) \right)^{-8} \quad (\text{A.15})$$

In the second perturbation step, the properties of the SCN component are estimated by using ΔSG as the perturbation parameter. The calculated T_c and P_c are in °R and

psia respectively.

$$\left\{ \begin{array}{l}
 SG_0 = 0.843593 - 0.128624\alpha - 3.36159\alpha^3 - 13749.5\alpha^{12} \\
 \Delta SG_T = \exp(5(SG_0 - SG)) - 1 \\
 f_T = \Delta SG_T \left(-0.362456/T_b^{0.5} + (0.0398285 - 0.948125/T_b^{0.5}) \Delta SG_T \right) \\
 T_c = T_{cp} \left((1 + 2f_T)/(1 - 2f_T) \right)^2 \\
 \\
 \Delta SG_V = \exp(4(SG_0^2 - SG^2)) - 1 \\
 f_V = \Delta SG_V \left(0.466590/T_b^{0.5} + (-0.182421 + 3.01721/T_b^{0.5}) \Delta SG_V \right) \\
 V_c = V_{cp} \left((1 + 2f_v)/(1 - 2f_v) \right)^2 \\
 \\
 \Delta SG_P = \exp(0.5(SG_0 - SG)) - 1 \\
 f_P = \Delta SG_P \left(\begin{array}{l} (2.53262 - 46.1955/T_b^{0.5} - 0.00127885T_b) + \\ (-11.4277 + 252.14/T_b^{0.5} + 0.00230535T_b) \Delta SG_P \end{array} \right) \\
 P_c = P_{cp} (T_c/T_{cp}) (V_{cp}/V_c) \left((1 + 2f_P)/(1 - 2f_P) \right)^2
 \end{array} \right. \quad (A.16)$$

- Tsonopoulos et al. [175] + Korsten [176] Correlations:

In 1987, Tsonopoulos et al. [175] developed the correlations for T_c and P_c as a function of MW :

$$\log(T_c) = 1.20016 + 0.61954 \log(T_b) + 0.48262 \log(SG) + 0.67365 (\log(SG))^2 \quad (A.17)$$

$$\log(P_c) = 7.37498 - 2.15833 \log(T_b) + 3.35417 \log(SG) + 5.64019 (\log(SG))^2 \quad (A.18)$$

They also used the correlation developed by Korsten [176] for ω which is very similar to the Edmister correlation with slight difference in the exponent of T_b :

$$\omega = \log\left(\frac{1}{P_c}\right) \left(\frac{1 - \left(\frac{10}{7}\right)^{1.3}}{\left(\frac{T_c}{T_b}\right)^{1.3} - 1} \right) - 1 \quad (A.19)$$

In these correlations T_b and T_c are in K and P_c is in bar.

- Riazi-Daubert Correlations (T_b and SG) [177]:

$$\begin{aligned}
 T_c &= 9.5233 \exp\left(-9.3140 \times 10^{-4} T_b - 0.54444 SG + 6.4791 \times 10^{-4} T_b SG\right) \\
 &\quad \times T_b^{0.81067} SG^{0.53691}
 \end{aligned} \quad (A.20)$$

$$\begin{aligned}
 P_c &= 3.1958 \times 10^5 \exp\left(-8.5050 \times 10^{-3} T_b - 4.8014 SG + 5.7490 \times 10^{-3} T_b SG\right) \\
 &\quad \times T_b^{-0.4844} SG^{4.0846}
 \end{aligned} \quad (A.21)$$

where T_b and T_c are in K and P_c is in atm.

- Riazi-Daubert Correlations (MW and SG) [177]:

$$T_c = 3.0800 \times 10^2 \exp(-1.3478 \times 10^{-4} MW - 0.61641 SG) MW^{0.2998} SG^{1.0555} \quad (\text{A.22})$$

$$P_c = 3.1166 \times 10^3 \exp(-1.8078 \times 10^{-3} MW - 0.3048 SG) MW^{-0.8063} SG^{1.6015} \quad (\text{A.23})$$

where T_c is in K and P_c is in atm.

- Pedersen et al. Correlations [16]:

In 1989, Pedersen et al. [16] developed a set of correlations for T_c , P_c , and ω as a function of MW and SG :

$$T_c = c_1 SG + c_2 \ln MW + c_3 MW + \frac{c_4}{MW} \quad (\text{A.24})$$

$$\ln P_c = d_1 + d_2 SG + \frac{d_3}{MW} + \frac{d_4}{MW^2} \quad (\text{A.25})$$

$$m = e_1 + e_2 MW + e_3 SG + e_4 MW^2 \quad (\text{A.26})$$

$$\omega = -\frac{(-1.574 + \sqrt{1.574 \times 10^2 + 4(0.48 - m) \times 0.176})}{2 \times 0.176} \quad (\text{A.27})$$

where T_c is in K and P_c is in atm. The coefficients in eqs. (A.24)–(A.26) can be found in the original article. Recently Pedersen et al. [89] updated these correlated coefficients for high pressure and high temperature applications, meanwhile they proposed to use temperature dependent Peneloux volume translation for HPHT conditions and heavy oils.

- Sancet Correlations [178]:

Sancet developed a set of correlations for T_c and P_c and slightly modified the acentric factor correlation by Edmister [171]. The proposed correlations are as follows:

$$T_c = -778.5 + 383.5 \times \log(MW - 4.075) \quad (\text{A.28})$$

$$P_c = 82.82 + 653 \times \exp(-0.007427 MW) \quad (\text{A.29})$$

$$\omega = \frac{3}{7} \left(\frac{\log(P_c)}{T_c/T_b - 1} \right) - 1, \quad T_b = 194 + 0.001241 \times T_c^{1.869} \quad (\text{A.30})$$

where T_b and T_c are in °R and P_c is in psia.

- *Jamialahmadi et al. Correlations [179]:*

Jamialahmadi et al. [179] developed a set of correlations for T_c and P_c and slightly modified the acentric factor correlation by Edmister [171]. The proposed correlations are as follows:

$$T_c = 239.4 \log(MW) - 555.3 \quad (\text{A.31})$$

$$P_c = 36.02 \exp(-0.01323MW) + 26.12 \exp(-0.002561MW) \quad (\text{A.32})$$

$$\omega = \frac{3}{7} \left(\frac{\log(P_c)}{T_c/T_b - 1} \right) - 1, \quad T_b = 0.0004989T_c^2 + 0.3639T_c + 20.92 \quad (\text{A.33})$$

where T_b and T_c are in K and P_c is in atm.

Riazi et al. [180] presented various options for characterization of different types of reservoir fluids and crude oils with respect to the type of available data and their limitations. Aladwani and Riazi [88] compared most of the available correlations for prediction of critical properties of pure components from C_5 to C_{25} where the Twu and Kesler-Lee methods were more successful in prediction of T_c and P_c compared to other correlations. They also mentioned one should be careful that use of these methods outside of the ranges that they have been recommended usually result in less accurate predictions of thermodynamic properties.

Whitson and Brule [90] made a good analysis of correlations for the critical properties and their effects on characterization of C_{7+} of reservoir fluids and suggested the use of Riazi and Daubert for petroleum cuts up to C_{25} . For fractions heavier than C_{25} , he recommended the use of Kesler-Lee or Twu.

A.3 Comparison of Critical Properties Correlations

To evaluate the performance of the mentioned correlations, as well as other correlations in the literature [181–188], we calculated the deviation in T_c , P_c and ω of different pure components using the experimental data from the DIPPR database [105]. We used 21 correlation sets and found the deviation in T_c , P_c and ω for n-alkanes from C₅ up to C₃₆ and for 328 other hydrocarbons:

1. T_c and P_c : Winn [172], and ω : Edmister [171]
2. T_c : Nokay [181], P_c : Riazi-Daubert [174], and ω : Edmister [171]
3. T_c and P_c : Cavett [173], and ω : Edmister [171]
4. T_c and P_c : Cavett [173], and ω : Lee-Kesler/Kesler-Lee [114, 115]
5. T_c and P_c : Kesler-Lee [115], and ω : Edmister [171]
6. T_c , P_c , and ω : Kesler-Lee [115]
7. T_c and P_c : Riazi-Daubert [174], and ω : Edmister [171]
8. T_c and P_c : Twu [113], and ω : Kesler-Lee [115]
9. T_c and P_c : Tsonopoulos et al. [175], and ω : Korsten [176]
10. T_c and P_c : Riazi-Daubert (T_b , SG) [177], and ω : Kesler-Lee [115]
11. T_c and P_c : Riazi-Daubert (MW , SG) [177], and ω : Kesler-Lee [115]
12. T_c , P_c , and ω : Pedersen et al. [16]
13. T_c : API [182], P_c : Riazi-Daubert [174], and ω : Edmister [171]
14. T_c and P_c : Jianzhong et al. [183], and ω : Edmister [171]
15. T_c and P_c : Jianzhong et al. [184], and ω : Edmister [171]
16. T_c and P_c : Riazi et al. [185], and ω : Edmister [171]
17. T_c , P_c , and ω : Pedersen et al. [89]
18. T_c , P_c , and ω : Sancet [178]
19. T_c , P_c , and ω : Nji et al. [186, 187]
20. T_c , P_c , and ω : Kumar and Okuno [188]
21. T_c , P_c , and ω : Jamialahmadi et al. [179]

Table A.1 and Figures A.1–A.3 summarize the Absolute Average Deviations (AAD%) in T_c , P_c , and ω of n-alkanes and other hydrocarbons with 21 different correlation sets. Most of the correlations predict T_c of n-alkanes with rather good accuracy except Cavett [173], Pedersen et al. [16, 89], Kumar and Okuno [188] and Jamialahmadi et al. [179] correlations which give higher deviations. Although Sancet correlation [178] gives low deviations for n-alkanes, it gives very large deviations for other hydrocarbons. Correlations like those of Pedersen et al. [16] which are developed by directly fitting oil and gas PVT data rather than critical properties of pure components, give large deviations in critical properties estimation for individual fractions as it is shown in Figures A.1–A.2.

Table A.1 AAD% in the calculated critical properties of pure components using different correlations set.

Correlation Set No.	n-Alkanes			All HC Components		
	T_c	P_c	ω	T_c	P_c	ω
1	0.69	4.89	8.01	1.17	5.85	19.03
2	0.84	4.63	11.12	0.92	5.39	12.80
3	3.54	51.03	30.96	1.45	11.56	20.23
4	3.54	51.03	23.27	1.45	11.56	18.48
5	0.83	11.26	16.84	1.00	6.45	14.48
6	0.83	11.26	15.61	1.00	6.45	13.94
7	0.61	4.63	9.35	0.93	5.39	10.97
8	0.28	2.93	4.85	0.79	5.40	9.79
9	0.96	11.64	3.40	1.14	8.22	11.74
10	0.87	7.60	10.28	0.94	6.23	11.09
11	2.35	8.95	21.53	1.83	5.13	27.93
12	6.28	52.00	8.51	5.70	25.92	23.66
13	1.06	4.63	26.34	1.20	5.39	19.67
14	0.70	6.10	6.44	0.92	5.48	10.15
15	0.54	4.93	5.84	1.23	7.80	19.91
16	1.30	16.14	16.00	1.18	6.92	16.27
17	5.45	40.22	19.03	4.92	23.33	19.78
18	1.09	3.43	16.54	6.81	17.12	27.80
19	1.00	4.79	4.74	2.24	7.55	17.66
20	3.23	16.07	7.51	6.58	14.36	24.16
21	3.76	13.87	19.43	6.35	12.90	18.90

Among all the correlations for T_c , Twu's method [113] gives the lowest deviation for both n-alkanes and other hydrocarbon components. For P_c , Twu's method gives the lowest deviation for n-alkanes and slightly higher deviation than that of Riazi-Daubert correlation [174] for other hydrocarbons.

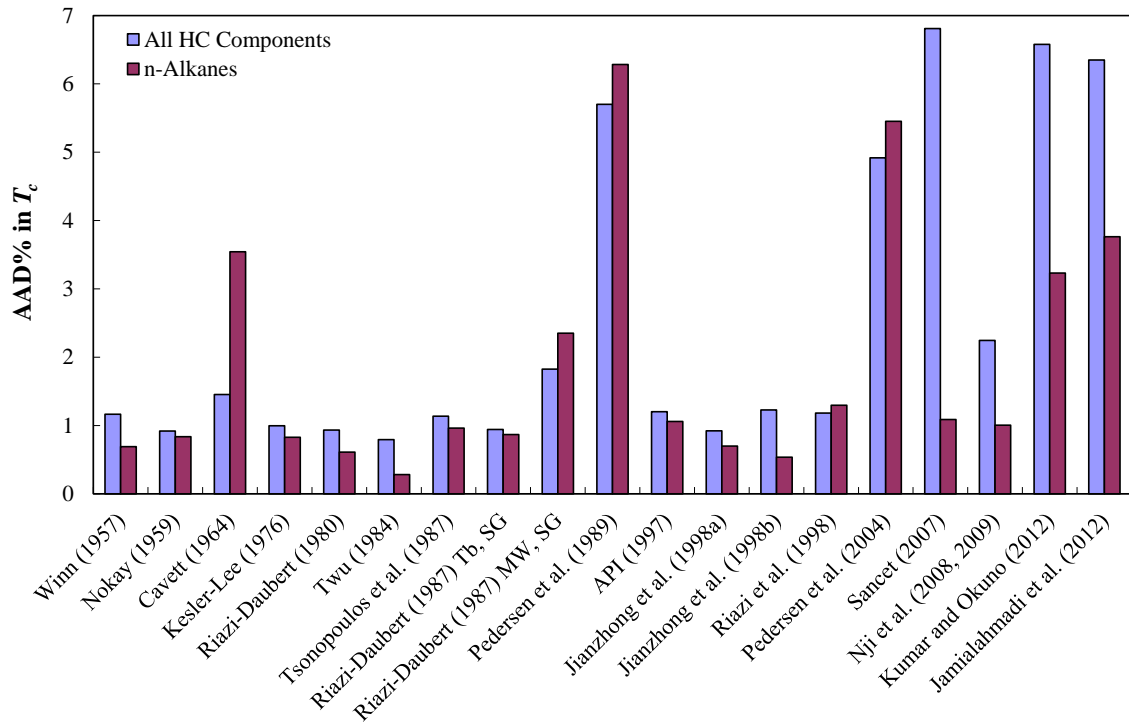


Figure A.1 AAD% in T_c using different correlations.

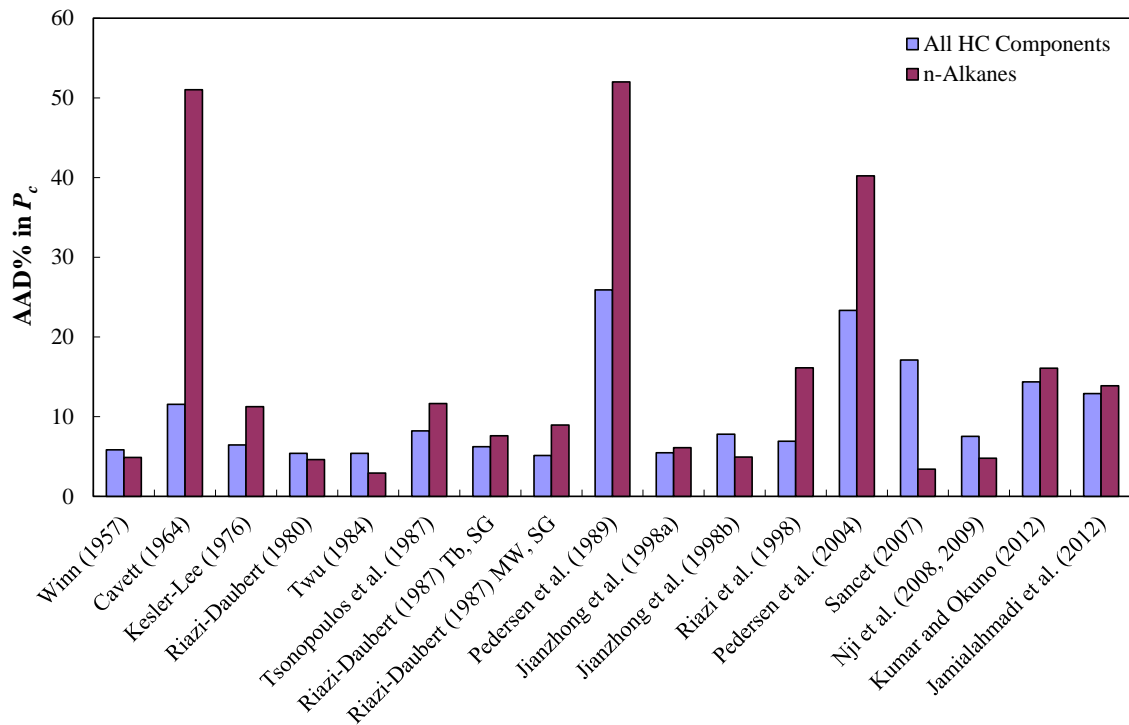


Figure A.2 AAD% in P_c using different correlations.

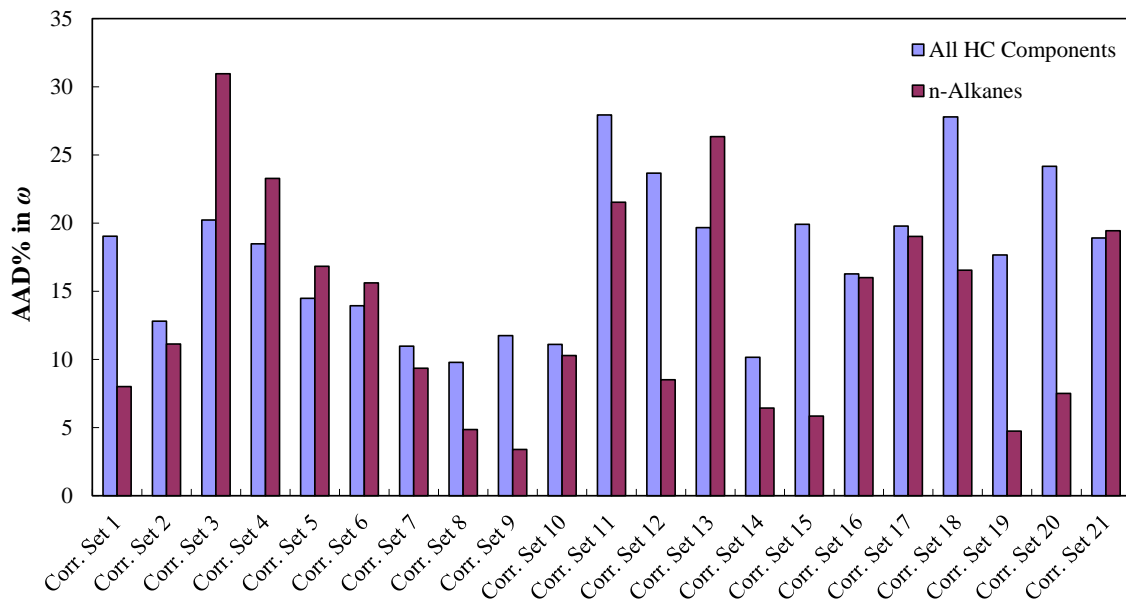


Figure A.3 AAD% in ω using different correlations set.

Using T_c and P_c from Twu's method in the Kesler-Lee correlations to calculate ω (correlations set 8), gives slightly larger deviation for n-alkanes compared to correlation set 9, where Tsonopoulos et al. [175] correlations are used together with Korsten's correlation for ω . However, the AAD% for all the hydrocarbon components is lower for the correlation set 8 than the correlation set 9 as shown in Figure A.3.

In summary, Twu's method [113] with Lee-Kesler/Kesler-Lee correlations [114, 115] for ω seems to be the best set of correlations for calculation of critical properties for both n-alkanes and other hydrocarbons as also suggested by Whitson and Brule [90].

B | PVT Database and Deviations in Saturation Pressure, Density and STO Density

B.1 Petroleum Fluid Database

Table B.1 An overview of the reservoir fluid systems tested.

Fluid no.	%N ₂	%CO ₂	%C ₁	%C ₇₊	MW ₇₊	SG ₇₊	Type	<i>T</i> (K)	<i>P</i> ^{sat} (bar)
Fluid 1	0.34	0.84	49.23	31.45	230.34	0.8656	OIL	366.45	274.50
Fluid 2	0.00	1.81	49.83	30.53	227.66	0.8755	OIL	337.25	289.70
Fluid 3	0.08	0.27	49.71	40.22	251.22	0.8853	OIL	337.85	270.40
Fluid 4	0.00	1.43	49.97	44.04	270.86	0.8998	OIL	337.25	282.30
Fluid 5	0.01	1.38	32.10	48.21	212.22	0.8655	OIL	346.15	133.60
Fluid 6	0.02	0.96	32.03	61.38	283.46	0.9174	OIL	333.15	137.80
Fluid 7	0.18	0.82	22.92	44.00	257.71	0.8742	OIL	374.85	96.90
Fluid 8	0.00	0.20	23.64	45.80	254.44	0.8734	OIL	372.05	117.70
Fluid 9	0.00	0.45	45.85	29.02	216.04	0.8527	OIL	387.35	255.60
Fluid 10	0.00	0.35	54.26	21.27	200.91	0.8328	OIL	388.15	320.20
Fluid 11	0.38	0.45	26.58	42.72	245.43	0.8864	OIL	394.25	145.80
Fluid 12	0.00	0.00	36.20	34.40	219.98	0.8568	OIL	383.15	172.90
Fluid 13	0.00	0.00	31.28	36.78	201.48	0.8354	OIL	393.15	153.90
Fluid 14	0.00	0.08	32.16	35.47	208.07	0.8354	OIL	393.15	153.00
Fluid 15	0.00	2.25	44.66	50.45	290.30	0.9185	OIL	322.65	232.20
Fluid 16	0.13	0.09	41.32	53.81	291.72	0.9226	OIL	344.95	198.70
Fluid 17	0.81	0.08	42.14	54.64	299.54	0.9268	OIL	346.05	208.70
Fluid 18	0.16	0.23	39.45	51.13	248.24	0.9170	OIL	346.15	202.30

Continued on next page

Table B.1 – continued from previous page.

Fluid no.	%N ₂	%CO ₂	%C ₁	%C ₇₊	MW ₇₊	SG ₇₊	Type	<i>T</i> (K)	<i>P</i> ^{sat} (bar)
Fluid 19	0.05	2.25	23.21	72.97	236.22	0.9226	OIL	329.75	105.10
Fluid 20	0.00	2.65	41.99	53.54	288.86	0.9214	OIL	319.55	207.10
Fluid 21	0.07	3.59	35.53	53.76	268.57	0.9185	OIL	339.85	174.80
Fluid 22	0.99	1.41	34.66	33.74	182.36	0.8238	OIL	427.60	186.23
Fluid 23	0.67	1.31	39.55	30.58	194.70	0.8326	OIL	418.10	224.30
Fluid 24	2.18	3.15	74.71	6.39	150.96	0.7932	GC	323.15-469.15	375.20-336.70
Fluid 25	0.70	2.47	63.68	12.47	162.04	0.8036	GC	423.15-455.15	322.31-313.86
Fluid 26	0.81	2.42	63.45	11.13	167.74	0.8070	GC	423.15-460.15	311.27-303.99
Fluid 27	2.66	2.48	63.43	11.46	166.80	0.7986	GC	323.15-460.15	299.40-310.60
Fluid 28	1.13	0.03	27.86	68.15	343.11	0.9400	OIL	345.93	107.85
Fluid 29	0.00	4.70	38.64	53.59	276.63	0.9268	OIL	318.15	185.20
Fluid 30	0.50	0.04	21.50	56.52	317.15	0.9195	OIL	331.15	76.70
Fluid 31	0.15	0.82	32.81	65.83	350.86	0.9747	OIL	329.15	141.20
Fluid 32	2.32	0.25	47.64	25.12	212.74	0.8298	OIL	303.25-417.85	219.20-276.60
Fluid 33	0.36	0.40	47.24	27.18	214.21	0.8451	OIL	394.25	245.70
Fluid 34	0.00	0.67	46.63	28.94	217.29	0.8568	OIL	373.75	245.70
Fluid 35	1.49	0.32	45.29	25.92	222.70	0.8590	OIL	299.85-394.25	212.40-275.00
Fluid 36	0.08	0.27	49.71	40.23	250.15	0.8813	OIL	337.85	270.40
Fluid 37	0.24	2.10	26.13	71.43	260.97	0.8923	OIL	318.35	90.40
Fluid 38	0.09	2.28	30.08	67.33	279.08	0.9096	OIL	318.15	108.60
Fluid 39	0.12	2.08	28.46	69.09	273.23	0.9020	OIL	317.95	94.20
Fluid 40	0.10	3.84	46.77	39.98	256.08	0.8915	OIL	331.15	259.80
Fluid 41	0.07	3.85	45.46	41.67	258.79	0.8900	OIL	331.55	239.90
Fluid 42	0.38	0.14	18.79	50.59	246.49	0.8521	OIL	362.25	72.30
Fluid 43	1.64	1.95	44.40	24.50	209.50	0.8528	OIL	377.95	276.20
Fluid 44	0.01	1.37	32.09	48.21	210.39	0.8725	OIL	346.15	133.60
Fluid 45	0.01	3.87	33.36	55.95	267.64	0.9087	OIL	339.85	155.40
Fluid 46	0.23	0.05	37.62	53.43	257.79	0.9034	OIL	342.15	156.90
Fluid 47	0.00	0.18	36.35	60.22	273.53	0.9094	OIL	335.15	142.60
Fluid 48	0.00	0.14	50.21	34.33	221.50	0.8575	OIL	344.35	267.50
Fluid 49	0.17	0.08	44.72	38.18	235.17	0.8749	OIL	335.25	219.20
Fluid 50	0.23	0.16	35.13	52.20	299.31	0.8659	OIL	318.75	119.50
Fluid 51	0.10	0.09	46.95	38.08	249.18	0.8815	OIL	338.35	260.60
Fluid 52	0.32	0.97	30.18	68.14	314.82	0.9641	OIL	329.15	143.80
Fluid 53	0.00	1.81	49.83	30.53	226.51	0.8616	OIL	337.25	289.70

Continued on next page

Table B.1 – continued from previous page.

Fluid no.	%N ₂	%CO ₂	%C ₁	%C ₇₊	MW ₇₊	SG ₇₊	Type	<i>T</i> (K)	<i>P</i> ^{sat} (bar)
Fluid 54	0.00	1.43	49.97	44.05	270.11	0.9004	OIL	337.85	282.30
Fluid 55	0.07	3.81	40.24	52.58	280.56	0.9094	OIL	331.15	210.40
Fluid 56	0.24	2.54	40.82	49.53	284.34	0.9029	OIL	323.35	235.80
Fluid 57	3.57	20.78	21.99	36.53	232.93	0.8816	OIL	401.05	233.30
Fluid 58	3.82	21.24	22.99	35.00	239.23	0.8804	OIL	401.05	251.30
Fluid 59	0.00	0.20	36.34	42.31	203.78	0.8550	OIL	347.15	149.60
Fluid 60	0.00	0.45	48.76	30.15	196.37	0.8478	OIL	358.15	264.10
Fluid 61	5.50	33.53	18.58	30.73	200.38	0.8416	OIL	409.15	276.90
Fluid 62	0.43	0.06	25.25	52.97	202.39	0.8249	OIL	395.15	103.77
Fluid 63	0.04	0.06	39.89	42.76	221.79	0.8428	OIL	323.15	150.42
Fluid 64	0.10	0.56	30.65	57.97	183.89	0.8680	OIL	334.80	123.40
Fluid 65	0.55	0.15	61.24	13.04	175.74	0.8156	OIL	347.04	338.86
Fluid 66	0.25	0.01	22.56	38.31	238.00	0.9040	OIL	341.48	96.44
Fluid 67	0.19	0.00	23.10	44.43	207.00	0.8829	OIL	341.48	96.78
Fluid 68	0.07	0.02	33.27	54.95	204.06	0.8498	OIL	323.15	113.76
Fluid 69	0.24	0.02	36.88	51.77	211.46	0.8368	OIL	325.15	116.52
Fluid 70	0.65	0.14	40.77	28.01	203.82	0.8446	OIL	335.15	182.37
Fluid 71	0.02	0.05	34.21	57.61	208.21	0.8372	OIL	321.15	122.02
Fluid 72	1.22	0.01	38.36	26.42	200.00	0.8170	OIL	344.26	181.93
Fluid 73	1.11	0.08	28.50	41.06	189.39	0.8053	OIL	384.85	131.00
Fluid 74	1.17	0.05	28.65	40.86	188.76	0.8048	OIL	384.85	132.00
Fluid 75	0.97	1.46	29.78	40.79	190.80	0.8215	OIL	378.15	148.35
Fluid 76	0.96	0.18	27.56	41.10	187.77	0.8218	OIL	382.04	134.08
Fluid 77	0.00	2.35	47.22	38.15	216.82	0.8381	OIL	355.37	247.29
Fluid 78	0.00	0.00	28.07	60.69	192.00	0.8400	OIL	319.26	103.40
Fluid 79	0.26	8.95	43.32	26.93	224.49	0.8448	OIL	359.26	268.39
Fluid 80	0.15	2.04	44.59	39.17	206.00	0.8410	OIL	353.15	218.82
Fluid 81	0.11	3.35	43.44	34.55	191.00	0.8380	OIL	349.82	214.82
Fluid 82	0.14	0.00	35.85	62.51	226.98	0.8719	OIL	328.15	141.87
Fluid 83	0.29	1.70	45.39	40.04	211.00	0.8400	OIL	352.04	223.78
Fluid 84	0.19	1.82	42.39	44.01	205.00	0.8365	OIL	350.93	209.30
Fluid 85	0.21	1.88	44.80	42.28	208.00	0.8430	OIL	350.93	216.41
Fluid 86	0.10	5.58	42.64	31.63	178.00	0.8290	OIL	347.59	242.74
Fluid 87	0.13	5.13	42.47	33.69	186.00	0.8330	OIL	347.59	232.68
Fluid 88	0.62	0.16	26.67	51.15	195.67	0.8295	OIL	398.15	116.57

Continued on next page

Table B.1 – continued from previous page.

Fluid no.	%N ₂	%CO ₂	%C ₁	%C ₇₊	MW ₇₊	SG ₇₊	Type	<i>T</i> (K)	<i>P</i> ^{sat} (bar)
Fluid 89	0.21	5.01	45.97	25.89	182.56	0.8202	OIL	357.04	273.77
Fluid 90	0.20	6.51	44.14	27.38	220.00	0.8429	OIL	359.15	257.08
Fluid 91	4.94	0.82	42.41	37.63	228.41	0.8589	OIL	389.82	296.82
Fluid 92	4.14	0.12	42.81	31.23	226.24	0.8665	OIL	381.48	274.83
Fluid 93	3.64	1.17	38.42	32.74	201.20	0.8496	OIL	403.15	251.11
Fluid 94	3.06	0.23	36.02	32.39	181.76	0.8220	OIL	377.59	194.36
Fluid 95	1.42	0.07	9.59	41.89	156.99	0.7840	OIL	364.82	49.16
Fluid 96	1.94	1.11	10.95	44.76	154.00	0.7970	OIL	394.26	80.92
Fluid 97	1.69	0.03	7.50	75.15	229.43	0.8299	OIL	359.26	34.11
Fluid 98	7.18	0.68	40.28	27.00	169.45	0.8145	OIL	398.71	266.83
Fluid 99	1.89	2.26	35.79	25.20	168.00	0.7916	OIL	439.26	198.20
Fluid 100	7.37	2.51	51.58	15.05	164.97	0.8108	OIL	382.04	379.21
Fluid 101	5.82	0.47	42.24	30.52	195.89	0.8366	OIL	402.04	293.72
Fluid 102	0.26	0.01	2.26	44.19	168.40	0.7916	OIL	372.59	15.10
Fluid 103	6.16	0.83	28.88	39.94	184.63	0.8247	OIL	399.82	196.82
Fluid 104	4.94	0.31	35.60	27.99	179.80	0.8376	OIL	386.48	215.19
Fluid 105	2.10	0.03	20.18	36.43	139.91	0.7859	OIL	369.82	101.35
Fluid 106	2.54	0.57	38.96	32.71	206.00	0.8540	OIL	395.93	230.26
Fluid 107	3.72	2.94	48.69	17.95	169.50	0.8220	OIL	402.59	296.20
Fluid 108	3.22	0.95	39.02	28.11	195.26	0.8509	OIL	383.15	244.05
Fluid 109	2.39	0.13	43.63	17.54	145.76	0.7949	OIL	377.59	232.15
Fluid 110	4.89	0.26	32.40	34.52	185.74	0.8307	OIL	390.37	210.61
Fluid 111	6.88	0.13	40.06	27.97	179.26	0.8217	OIL	409.82	284.75
Fluid 112	3.50	0.46	49.96	20.19	188.15	0.8082	OIL	407.59	326.12
Fluid 113	2.00	0.08	10.81	58.57	198.30	0.8430	OIL	382.04	63.29
Fluid 114	3.35	0.32	42.55	23.66	195.75	0.8364	OIL	405.37	257.17
Fluid 115	8.46	7.19	36.77	13.24	126.06	0.7845	OIL	413.15	201.86
Fluid 116	3.44	0.04	37.89	20.96	133.49	0.7792	OIL	379.82	182.02
Fluid 117	7.71	0.97	37.93	16.16	178.67	0.8149	OIL	392.04	230.68
Fluid 118	1.64	0.54	23.24	38.18	190.96	0.8327	OIL	385.93	123.42
Fluid 119	4.86	0.54	44.64	21.65	176.31	0.8205	OIL	414.26	272.94
Fluid 120	7.26	0.48	34.38	29.21	166.40	0.8007	OIL	402.04	191.40
Fluid 121	3.16	0.21	22.75	26.91	160.30	0.7899	OIL	377.59	119.42
Fluid 122	5.82	0.46	41.55	31.39	204.00	0.8545	OIL	393.15	284.18
Fluid 123	6.60	0.09	16.61	59.73	233.07	0.8433	OIL	360.93	128.91

Continued on next page

Table B.1 – continued from previous page.

Fluid no.	%N ₂	%CO ₂	%C ₁	%C ₇₊	MW ₇₊	SG ₇₊	Type	<i>T</i> (K)	<i>P</i> ^{sat} (bar)
Fluid 124	2.55	0.02	13.50	32.32	157.60	0.7850	OIL	372.04	76.12
Fluid 125	0.28	0.06	33.29	41.32	208.00	0.8349	OIL	316.48	119.88
Fluid 126	3.85	2.67	46.45	26.34	196.83	0.8365	OIL	397.04	294.87
Fluid 127	9.06	0.61	42.73	29.12	153.93	0.7993	OIL	395.37	248.21
Fluid 128	4.42	0.04	44.15	14.23	154.10	0.7866	OIL	379.82	222.63
Fluid 129	4.25	0.00	37.92	25.28	126.95	0.7692	OIL	390.37	195.47
Fluid 130	0.83	0.02	18.16	55.79	256.00	0.8801	OIL	309.82	63.69
Fluid 131	3.11	0.04	17.11	29.53	156.50	0.7842	OIL	372.04	88.46
Fluid 132	4.61	0.70	22.69	38.22	165.64	0.8022	OIL	399.82	133.39
Fluid 133	2.15	0.22	24.77	45.17	196.02	0.8381	OIL	409.26	132.98
Fluid 134	4.95	0.52	43.21	21.31	165.75	0.8128	OIL	400.93	246.47
Fluid 135	3.73	0.00	41.47	28.00	213.81	0.8490	OIL	401.48	263.72
Fluid 136	4.66	2.10	29.26	31.67	149.98	0.7967	OIL	394.26	189.61
Fluid 137	8.28	1.02	48.69	18.57	175.09	0.8150	OIL	397.04	296.34
Fluid 138	3.19	7.13	51.17	14.54	157.07	0.8065	OIL	401.48	305.07
Fluid 139	5.53	3.50	30.92	34.38	181.70	0.8239	OIL	417.59	205.93
Fluid 140	3.60	0.92	45.33	21.18	179.92	0.8269	OIL	395.37	292.34
Fluid 141	4.88	1.86	40.34	27.79	199.25	0.8361	OIL	404.26	298.66
Fluid 142	5.31	0.85	45.91	18.94	170.00	0.8090	OIL	400.37	247.50
Fluid 143	0.30	0.67	24.44	46.59	240.00	0.8703	OIL	300.93	80.23
Fluid 144	2.75	0.10	32.00	30.91	128.29	0.7724	OIL	382.04	156.51
Fluid 145	4.38	0.24	39.08	30.21	183.20	0.8411	OIL	397.59	257.59
Fluid 146	4.51	0.74	50.88	16.32	172.50	0.8264	OIL	395.93	316.75
Fluid 147	4.31	0.13	19.61	59.33	227.12	0.8369	OIL	342.59	109.81
Fluid 148	0.69	2.75	35.24	26.33	182.78	0.8300	OIL	384.00	200.64
Fluid 149	3.37	3.73	54.29	14.78	145.93	0.7926	OIL	397.59	299.92
Fluid 150	14.89	0.18	34.99	27.79	200.80	0.8567	OIL	378.15	427.96
Fluid 151	4.55	0.00	16.31	45.31	213.00	0.8711	OIL	375.37	114.11
Fluid 152	8.22	0.71	15.43	46.64	199.00	0.8540	OIL	398.71	164.01
Fluid 153	7.11	0.63	45.99	16.79	143.00	0.7920	OIL	391.48	239.57
Fluid 154	3.61	1.04	39.27	23.14	203.78	0.8501	OIL	388.00	244.97
Fluid 155	3.59	1.63	49.97	22.57	196.79	0.8259	OIL	388.71	304.06
Fluid 156	5.84	0.43	12.03	53.74	198.87	0.8324	OIL	405.37	120.98
Fluid 157	5.05	0.28	36.83	25.92	126.91	0.7704	OIL	406.00	210.98
Fluid 158	4.79	1.09	46.91	24.66	161.78	0.8068	OIL	395.00	269.59

Continued on next page

Table B.1 – continued from previous page.

Fluid no.	%N ₂	%CO ₂	%C ₁	%C ₇₊	MW ₇₊	SG ₇₊	Type	<i>T</i> (K)	<i>P</i> ^{sat} (bar)
Fluid 159	5.03	0.33	38.11	33.94	195.00	0.8520	OIL	400.93	260.46
Fluid 160	5.25	0.17	41.63	33.99	218.87	0.8579	OIL	391.48	298.18
Fluid 161	2.47	0.22	22.93	49.67	122.76	0.7597	OIL	405.37	115.47
Fluid 162	0.23	0.63	36.24	52.77	300.00	0.9243	OIL	344.82	160.56
Fluid 163	0.77	0.11	47.34	33.64	214.89	0.8442	OIL	345.95	243.00
Fluid 164	0.69	0.12	47.06	33.86	213.64	0.8436	OIL	345.95	238.00
Fluid 165	0.16	0.91	36.47	33.29	218.00	0.8515	OIL	377.60	181.70
Fluid 166	0.60	0.14	39.21	35.73	247.40	0.8900	OIL	335.93	188.57
Fluid 167	0.36	0.17	27.23	42.38	271.00	0.8790	OIL	327.59	94.11
Fluid 168	0.29	0.48	28.36	42.31	252.00	0.8800	OIL	329.26	112.52
Fluid 169	0.33	0.22	25.56	46.01	222.00	0.8780	OIL	329.26	109.97
Fluid 170	0.35	0.47	26.52	46.57	253.00	0.8920	OIL	330.37	103.42
Fluid 171	0.12	0.51	28.81	47.70	250.00	0.8760	OIL	329.82	111.35
Fluid 172	0.16	0.30	24.66	49.61	239.00	0.8750	OIL	329.82	96.53
Fluid 173	0.21	0.15	27.77	49.94	228.00	0.8630	OIL	329.82	109.63
Fluid 174	0.11	0.28	27.53	48.90	245.00	0.8790	OIL	330.37	106.18
Fluid 175	0.79	0.10	24.79	47.85	227.00	0.8840	OIL	329.82	96.46
Fluid 176	0.04	0.17	31.22	50.44	264.00	0.8890	OIL	330.37	116.52
Fluid 177	0.00	0.17	28.56	44.68	249.00	0.8620	OIL	329.82	106.73
Fluid 178	0.45	0.08	29.35	39.62	227.00	0.8630	OIL	329.82	117.56
Fluid 179	0.56	0.07	29.90	43.10	242.00	0.8770	OIL	329.26	113.97
Fluid 180	0.03	0.30	27.80	44.88	254.00	0.8800	OIL	329.82	113.42
Fluid 181	0.06	0.81	31.34	47.60	270.00	0.8920	OIL	328.71	120.73
Fluid 182	0.00	0.15	19.50	51.22	225.00	0.8490	OIL	328.71	70.67
Fluid 183	0.15	0.19	31.15	40.32	221.00	0.8480	OIL	330.37	113.76
Fluid 184	0.50	0.87	29.72	45.99	271.00	0.8820	OIL	329.82	112.66
Fluid 185	0.68	1.02	25.49	46.03	264.00	0.9020	OIL	329.82	105.70
Fluid 186	0.22	1.37	27.92	52.13	255.00	0.8930	OIL	330.37	106.73
Fluid 187	0.20	1.23	26.54	49.22	290.00	0.9100	OIL	328.71	110.11
Fluid 188	0.44	0.83	27.75	45.72	272.00	0.9020	OIL	329.26	107.90
Fluid 189	0.14	0.54	29.44	44.68	290.00	0.9010	OIL	329.82	108.94
Fluid 190	0.26	1.26	28.27	47.50	274.00	0.9080	OIL	329.82	115.83
Fluid 191	0.20	0.80	31.42	44.91	251.00	0.8890	OIL	328.71	119.83
Fluid 192	0.54	0.50	27.79	46.70	214.00	0.8870	OIL	329.26	114.11
Fluid 193	0.41	0.65	30.21	40.47	247.00	0.8750	OIL	330.37	129.62

Continued on next page

Table B.1 – continued from previous page.

Fluid no.	%N ₂	%CO ₂	%C ₁	%C ₇₊	MW ₇₊	SG ₇₊	Type	<i>T</i> (K)	<i>P</i> ^{sat} (bar)
Fluid 194	0.20	1.19	32.26	42.16	134.00	0.8790	OIL	329.26	123.28
Fluid 195	0.10	1.16	32.93	41.62	279.00	0.8790	OIL	329.26	124.45
Fluid 196	0.15	0.65	30.48	49.54	239.00	0.8660	OIL	327.59	115.14
Fluid 197	0.45	0.51	30.56	41.10	268.00	0.8920	OIL	330.37	119.62
Fluid 198	0.23	1.06	24.75	46.12	256.00	0.9050	OIL	329.82	105.49
Fluid 199	0.19	0.12	28.62	44.78	274.00	0.9250	OIL	330.37	121.76
Fluid 200	0.08	1.37	35.97	39.71	274.00	0.8980	OIL	348.71	172.71
Fluid 201	0.13	1.45	36.02	37.30	230.10	0.8960	OIL	347.59	198.09
Fluid 202	0.00	1.12	26.95	40.81	249.00	0.8760	OIL	370.93	129.41
Fluid 203	0.00	1.25	33.35	43.29	252.00	0.8510	OIL	383.15	145.48
Fluid 204	0.05	0.85	41.05	29.01	198.00	0.8480	OIL	389.26	229.94
Fluid 205	0.06	0.94	44.44	28.38	195.00	0.8460	OIL	388.71	250.28
Fluid 206	0.04	0.78	40.91	31.34	202.00	0.8450	OIL	389.26	215.12
Fluid 207	0.06	0.85	40.70	31.36	195.00	0.8470	OIL	390.37	219.25
Fluid 208	0.03	0.97	41.64	29.08	208.00	0.8500	OIL	389.26	211.60
Fluid 209	0.03	1.04	41.88	29.07	200.00	0.8480	OIL	385.93	222.98
Fluid 210	0.02	0.99	38.78	33.37	210.00	0.8490	OIL	388.71	208.15
Fluid 211	0.24	0.39	5.82	83.21	304.00	0.9420	OIL	344.26	21.58
Fluid 212	0.06	5.01	23.03	38.82	254.00	0.8770	OIL	365.37	139.35
Fluid 213	0.10	1.32	8.86	68.67	243.00	0.9340	OIL	354.26	46.68
Fluid 214	0.11	2.35	35.21	34.97	213.00	0.8410	OIL	394.26	175.61
Fluid 215	0.30	0.90	53.47	16.92	173.00	0.8360	OIL	353.15	307.51
Fluid 216	0.45	0.44	35.05	48.24	225.00	0.9000	OIL	355.37	173.75
Fluid 217	0.55	1.02	36.25	30.25	200.00	0.8370	OIL	385.37	189.33
Fluid 218	1.64	0.08	28.40	35.97	252.00	0.8430	OIL	328.15	116.80
Fluid 219	0.00	0.00	52.00	36.84	199.00	0.8410	OIL	366.48	264.69
Fluid 220	0.25	0.24	40.91	28.58	182.00	0.8000	OIL	422.04	209.81
Fluid 221	1.67	2.18	60.51	16.29	181.00	0.7890	OIL	392.04	332.53
Fluid 222	0.16	0.91	36.47	33.29	218.00	0.8520	OIL	377.59	180.64
Fluid 223	0.00	0.00	57.52	19.11	203.00	0.8100	OIL	373.15	349.22
Fluid 224	0.56	3.55	45.33	36.11	253.00	0.8360	OIL	365.93	267.86
Fluid 225	1.64	0.08	28.40	35.97	252.00	0.8430	OIL	328.15	117.76
Fluid 226	0.40	1.00	45.40	45.08	250.00	0.8880	OIL	344.26	238.97
Fluid 227	0.67	2.11	34.93	35.15	230.00	0.8550	OIL	387.59	187.81
Fluid 228	0.34	0.84	49.23	31.45	230.00	0.8650	OIL	366.48	274.48

Continued on next page

Table B.1 – continued from previous page.

Fluid no.	%N ₂	%CO ₂	%C ₁	%C ₇₊	MW ₇₊	SG ₇₊	Type	<i>T</i> (K)	<i>P</i> ^{sat} (bar)
Fluid 229	0.44	0.38	49.10	28.00	231.00	0.8360	OIL	365.93	257.79
Fluid 230	0.90	0.16	47.12	33.00	217.00	0.8500	OIL	347.59	234.01
Fluid 231	0.36	1.06	50.50	39.00	291.00	0.9010	OIL	342.04	254.42
Fluid 232	0.33	0.19	35.42	57.73	255.00	0.9170	OIL	343.71	159.06
Fluid 233	0.41	0.44	40.23	31.23	210.00	0.8450	OIL	370.93	198.98
Fluid 234	0.25	2.19	16.33	52.27	249.00	0.8800	OIL	374.82	86.94
Fluid 235	0.32	3.69	21.55	43.41	243.00	0.8690	OIL	388.15	109.70
Fluid 236	0.21	0.75	6.05	64.81	231.00	0.8570	OIL	337.59	24.27
Fluid 237	0.88	1.34	5.63	67.03	224.00	0.8550	OIL	326.48	25.92
Fluid 238	0.30	0.01	7.14	67.15	233.00	0.8600	OIL	333.15	25.79
Fluid 239	0.31	0.28	6.80	66.76	237.00	0.8580	OIL	335.37	25.79
Fluid 240	0.33	0.35	6.72	71.06	225.00	0.8580	OIL	332.04	24.82
Fluid 241	0.41	0.26	6.14	69.51	225.00	0.8600	OIL	329.82	23.86
Fluid 242	0.53	0.12	22.80	46.04	242.00	0.8640	OIL	342.04	91.36
Fluid 243	0.78	0.10	20.64	47.67	237.00	0.8570	OIL	342.59	83.36
Fluid 244	0.60	0.12	23.71	44.81	238.00	0.8680	OIL	342.04	95.56
Fluid 245	1.13	0.13	25.45	41.02	237.00	0.8510	OIL	342.59	99.70
Fluid 246	0.54	0.18	21.62	47.54	236.00	0.8630	OIL	342.04	86.67
Fluid 247	1.39	0.28	21.32	47.03	257.00	0.8700	OIL	342.04	84.12
Fluid 248	0.68	0.16	22.84	47.90	226.00	0.8640	OIL	342.04	97.01
Fluid 249	0.39	0.14	21.40	50.39	245.00	0.8420	OIL	338.15	77.50
Fluid 250	1.02	0.12	19.76	54.66	247.00	0.8500	OIL	344.54	79.43
Fluid 251	1.67	1.38	26.68	40.41	217.00	0.8550	OIL	372.04	134.72
Fluid 252	0.65	0.02	45.02	22.44	184.00	0.8100	OIL	333.15	206.98
Fluid 253	0.00	0.00	46.79	26.41	158.00	0.7660	OIL	373.15	202.77
Fluid 254	0.00	0.00	36.15	27.79	191.00	0.7720	OIL	373.15	154.30
Fluid 255	0.00	0.00	74.18	10.72	159.00	0.7660	GC	373.15	327.71
Fluid 256	0.00	0.00	73.48	11.20	161.00	0.7670	GC	373.15	326.95
Fluid 257	0.33	3.03	41.33	33.69	200.00	0.8480	OIL	366.48	220.63
Fluid 258	0.31	0.69	47.69	34.64	234.00	0.8690	OIL	384.26	262.00
Fluid 259	0.03	8.39	47.43	18.61	180.00	0.8300	OIL	419.26	275.79
Fluid 260	0.38	7.03	48.73	20.26	181.00	0.8050	OIL	427.04	286.55
Min	0.00	0.00	2.26	6.39	122.76	0.7597	-	299.85	15.10
Max	14.89	33.53	74.71	83.21	350.86	0.9747	-	469.15	427.96

B.2 Deviations in Saturation Pressure, Density and STO Density

The percent average absolute deviations AAD% of saturation pressure, density, and STO density for the 260 petroleum fluids are listed in Table B.2, where we have compared the performance of PC-SAFT EoS with Yan et al.'s characterization method [119] (eq. (4.31) and eqs. (4.34)–(4.35)) with SRK, PR, and Soave-BWR EoSs.

Table B.2 Summary of AAD% in predicted saturation pressures, reservoir fluid densities and stock tank oil densities (PC-SAFT eq. (4.31) and eqs. (4.34)–(4.35)).

Fluid no.	Saturation Pressure			Density			Stock Tank Oil Density					
	SRK	PR	PC-SAFT	SBWR	SRK	PR	PC-SAFT	SBWR	SRK	PR	PC-SAFT	SBWR
Fluid 1	3.47	5.88	6.15	8.59	13.03	3.00	2.56	2.54	18.55	8.89	0.36	5.66
Fluid 2	7.54	10.42	0.11	7.15	13.26	3.14	1.14	3.31	-	-	-	-
Fluid 3	5.13	8.28	0.54	6.25	13.96	3.94	1.65	4.58	-	-	-	-
Fluid 4	4.02	7.80	2.08	8.57	13.75	3.76	1.39	6.35	-	-	-	-
Fluid 5	3.21	1.31	0.14	1.93	13.16	2.73	1.41	4.26	-	-	-	-
Fluid 6	4.09	0.14	3.14	11.90	11.88	1.58	2.44	11.06	-	-	-	-
Fluid 7	0.49	2.18	6.03	5.53	18.97	9.58	3.18	3.43	20.11	10.70	0.78	4.24
Fluid 8	14.84	16.25	1.88	10.48	16.52	6.85	0.37	0.57	-	-	-	-
Fluid 9	10.02	11.87	11.67	0.45	13.63	4.05	3.50	3.25	20.18	10.71	0.48	2.60
Fluid 10	7.89	10.30	17.84	14.30	10.68	1.16	7.21	2.68	20.98	11.55	0.31	0.73
Fluid 11	5.09	6.40	9.45	0.42	12.37	2.28	1.92	2.13	15.22	5.17	2.64	9.92
Fluid 12	0.66	0.60	8.66	6.77	15.11	5.38	0.87	3.04	18.64	8.95	0.60	4.19
Fluid 13	10.79	11.46	0.58	5.89	-	-	-	-	21.71	12.36	1.81	1.25
Fluid 14	7.14	7.88	5.72	1.44	-	-	-	-	20.41	10.91	0.21	0.88
Fluid 15	0.65	5.33	10.30	19.22	11.43	1.16	4.08	11.45	12.44	2.17	4.85	18.25

Continued on next page

Table B.2 – continued from previous page.

Fluid no.	Saturation Pressure				Density				Stock Tank Oil Density			
	SRK	PR	PC-SAFT	SBWR	SRK	PR	PC-SAFT	SBWR	SRK	PR	PC-SAFT	SBWR
Fluid 16	4.99	0.79	5.17	7.27	10.45	0.20	2.93	12.01	11.66	1.29	4.46	19.06
Fluid 17	9.42	4.73	10.47	3.61	9.84	0.58	3.53	13.44	11.74	1.39	4.28	19.66
Fluid 18	1.41	2.24	3.26	8.62	7.49	3.40	4.35	12.28	8.87	1.93	5.74	18.13
Fluid 19	0.13	3.73	6.39	11.07	7.41	3.64	6.31	14.57	8.42	2.46	7.41	17.94
Fluid 20	1.60	3.28	12.28	19.82	10.96	0.64	4.30	11.61	11.89	1.55	5.01	18.83
Fluid 21	4.53	0.58	4.85	7.98	9.34	1.24	3.75	12.21	10.64	0.10	5.02	18.32
Fluid 22	4.88	5.16	0.90	1.94	12.17	2.21	2.83	1.73	18.65	8.83	0.59	0.75
Fluid 23	6.24	7.03	0.37	1.89	11.46	1.54	3.97	1.05	19.65	10.01	0.07	1.03
Fluid 24	8.50	2.48	17.62	11.79	-	-	-	-	18.11	8.16	1.88	0.15
Fluid 25	6.88	1.39	20.20	10.11	-	-	-	-	18.28	8.37	1.87	0.08
Fluid 26	9.94	4.09	22.05	13.42	-	-	-	-	18.01	8.09	2.72	0.87
Fluid 27	11.35	5.81	27.36	18.81	8.95	0.83	4.51	20.77	-	-	-	-
Fluid 28	21.84	16.66	18.18	1.56	-	-	-	-	-	-	-	-
Fluid 29	7.03	1.66	16.07	16.03	8.51	2.09	5.29	14.15	9.00	1.71	6.54	21.13
Fluid 30	16.48	12.36	28.73	0.78	12.74	2.50	3.32	12.17	13.99	3.93	4.25	17.45
Fluid 31	19.66	12.23	24.32	8.78	1.92	9.39	8.61	26.20	-	-	-	-
Fluid 32	8.45	10.44	22.61	7.23	18.28	9.31	2.01	8.40	24.54	15.58	0.74	2.88
Fluid 33	0.38	2.16	21.68	9.48	13.71	4.20	4.99	2.90	19.66	10.10	1.31	2.87
Fluid 34	4.87	6.93	14.29	2.48	12.81	3.03	3.50	2.09	16.96	7.09	3.31	6.24
Fluid 35	4.87	7.37	25.47	12.20	15.24	5.73	1.99	4.18	18.11	8.38	1.44	5.37
Fluid 36	8.09	10.96	1.40	8.06	15.53	5.70	0.92	2.47	16.91	7.09	2.39	9.33
Fluid 37	7.78	4.27	8.52	5.11	14.39	4.42	4.13	7.96	-	-	-	-

Continued on next page

Table B.2 – continued from previous page.

Fluid no.	Saturation Pressure				Density				Stock Tank Oil Density			
	SRK	PR	PC-SAFT	SBWR	SRK	PR	PC-SAFT	SBWR	SRK	PR	PC-SAFT	SBWR
	Fluid 38	11.34	7.05	14.17	6.78	12.15	1.96	5.20	10.98	-	-	-
Fluid 39	16.05	11.89	18.13	0.75	13.33	3.25	4.75	9.51	-	-	-	-
Fluid 40	6.25	9.50	1.94	11.31	13.21	3.16	1.87	2.94	-	-	-	-
Fluid 41	4.91	8.02	2.84	10.65	13.85	3.87	1.87	2.79	-	-	-	-
Fluid 42	1.65	2.93	2.05	1.25	21.06	11.81	1.07	4.29	-	-	-	-
Fluid 43	8.05	9.63	1.35	4.83	15.54	5.67	0.72	3.03	16.77	6.81	2.26	5.32
Fluid 44	5.66	3.59	1.87	0.32	11.95	1.38	2.18	5.42	12.76	2.33	4.17	10.18
Fluid 45	2.61	0.83	2.78	8.85	-	-	-	-	13.43	3.23	3.32	14.90
Fluid 46	11.57	7.94	10.18	1.09	10.92	0.45	3.21	9.92	12.77	2.47	3.89	14.73
Fluid 47	13.45	9.43	11.67	2.42	11.64	1.36	3.53	9.07	12.94	2.69	4.83	16.33
Fluid 48	11.12	13.12	5.22	9.04	16.12	6.30	0.75	2.22	18.11	8.37	1.80	5.33
Fluid 49	4.27	6.83	2.05	6.60	13.90	3.88	1.32	0.59	-	-	-	-
Fluid 50	5.93	8.09	10.19	17.13	25.60	16.94	0.91	3.40	27.11	18.61	0.72	0.26
Fluid 51	12.66	15.25	5.37	12.73	-	-	-	-	16.29	6.39	2.73	9.76
Fluid 52	5.90	0.36	7.72	17.19	4.70	6.40	4.86	7.21	5.35	5.73	6.22	7.86
Fluid 53	15.57	17.76	6.04	13.23	17.77	8.19	1.43	3.82	18.51	8.83	1.12	5.16
Fluid 54	4.21	7.94	2.09	8.14	13.71	3.72	1.81	6.33	15.03	5.03	3.02	13.40
Fluid 55	2.90	6.53	1.39	16.39	12.32	2.07	3.88	10.14	13.57	3.41	5.05	16.21
Fluid 56	19.31	22.36	10.29	31.27	14.85	4.94	1.92	6.84	16.42	6.61	2.44	12.68
Fluid 57	8.73	9.85	7.69	0.53	11.87	1.48	2.49	4.12	13.91	3.67	3.56	10.75
Fluid 58	11.31	12.52	10.16	0.66	12.06	2.04	2.95	0.55	15.11	5.03	3.07	10.01
Fluid 59	1.89	0.26	1.35	1.60	13.91	3.78	0.72	0.63	16.27	6.24	1.55	5.41

Continued on next page

Table B.2 – continued from previous page.

Fluid no.	Saturation Pressure				Density				Stock Tank Oil Density			
	SRK	PR	PC-SAFT	SBWR	SRK	PR	PC-SAFT	SBWR	SRK	PR	PC-SAFT	SBWR
Fluid 60	10.58	12.08	7.05	12.62	13.21	3.26	0.23	3.16	16.09	6.02	1.93	5.06
Fluid 61	9.90	10.60	7.47	5.29	16.18	6.22	1.58	1.98	18.34	8.56	1.63	3.28
Fluid 62	6.90	7.28	5.03	0.57	20.54	11.31	0.78	6.16	24.36	15.35	1.34	3.69
Fluid 63	4.29	5.90	1.49	8.98	18.16	8.49	1.80	1.89	21.18	11.81	1.30	1.91
Fluid 64	7.25	5.05	0.85	2.67	9.96	0.88	3.43	5.32	10.78	0.02	5.07	9.64
Fluid 65	8.31	11.16	7.39	3.80	15.27	5.91	1.80	3.03	18.81	9.02	1.65	1.07
Fluid 66	1.43	0.90	1.93	4.74	7.28	3.93	4.66	10.52	9.01	1.86	5.61	14.79
Fluid 67	2.22	0.20	3.34	4.59	7.44	3.81	4.93	9.09	9.17	1.74	5.85	12.87
Fluid 68	1.73	0.38	3.48	6.63	16.16	6.23	0.88	1.06	18.26	8.49	0.61	3.50
Fluid 69	14.37	12.40	14.22	5.54	15.95	6.05	2.08	1.48	18.52	8.80	1.44	4.33
Fluid 70	1.69	3.14	6.52	4.90	12.07	1.99	4.18	1.45	17.57	7.70	2.30	4.22
Fluid 71	8.58	10.30	5.77	15.67	21.03	11.71	1.51	3.88	22.66	13.46	1.17	0.71
Fluid 72	11.60	12.31	6.57	13.48	16.40	6.36	0.61	2.81	19.73	10.09	0.67	1.25
Fluid 73	12.16	12.48	6.74	7.03	20.78	11.46	0.84	7.75	24.49	15.46	0.96	4.87
Fluid 74	12.20	12.54	6.46	7.03	20.86	11.56	0.87	7.88	24.80	15.80	1.29	5.27
Fluid 75	14.27	14.88	9.71	11.13	18.54	8.74	0.29	3.61	21.31	11.88	0.04	1.24
Fluid 76	13.63	14.18	9.91	10.80	18.25	8.37	0.47	3.58	20.84	11.34	0.38	1.29
Fluid 77	13.54	14.61	7.38	6.99	20.23	10.83	0.83	3.85	23.49	14.41	0.65	0.60
Fluid 78	9.30	11.18	12.82	18.01	13.67	3.28	2.48	4.16	14.83	4.60	2.92	6.45
Fluid 79	11.52	12.84	0.28	3.64	17.41	7.87	1.32	3.83	21.61	12.30	1.85	2.01
Fluid 80	0.73	2.19	0.33	0.64	13.54	3.22	3.06	3.33	17.22	7.34	2.12	5.80
Fluid 81	0.02	1.30	0.85	4.64	12.69	2.24	2.22	2.56	15.30	5.13	2.62	6.05

Continued on next page

Table B.2 – continued from previous page.

Fluid no.	Saturation Pressure				Density				Stock Tank Oil Density			
	SRK	PR	PC-SAFT	SBWR	SRK	PR	PC-SAFT	SBWR	SRK	PR	PC-SAFT	SBWR
Fluid 82	2.80	0.39	0.91	6.83	14.52	4.40	3.23	4.99	16.95	7.09	2.82	7.57
Fluid 83	3.94	5.35	2.84	3.06	15.67	5.66	1.11	2.07	17.95	8.17	1.88	5.32
Fluid 84	8.19	9.38	8.63	8.92	15.17	5.07	1.65	1.99	18.18	8.41	1.46	4.55
Fluid 85	0.89	2.43	0.92	1.40	14.01	3.79	2.49	2.75	16.63	6.68	2.81	6.74
Fluid 86	12.44	13.41	11.08	19.40	12.86	2.44	1.27	2.64	15.31	5.09	1.96	4.59
Fluid 87	9.22	10.33	7.79	14.56	11.71	1.16	3.33	3.14	15.45	5.27	2.42	5.42
Fluid 88	3.47	3.74	4.61	1.14	16.95	6.82	1.21	1.44	19.98	10.39	0.88	0.77
Fluid 89	18.06	18.82	12.55	21.52	21.66	12.29	5.84	9.78	20.61	11.05	0.54	1.25
Fluid 90	6.93	8.42	3.46	1.25	16.03	6.11	1.14	2.72	18.52	8.82	1.77	5.24
Fluid 91	4.44	6.27	1.85	7.84	12.51	2.62	2.16	0.40	16.60	6.69	2.68	8.22
Fluid 92	3.33	1.24	7.87	12.28	10.23	1.21	4.02	3.78	15.30	5.20	2.54	8.64
Fluid 93	2.74	3.78	0.41	0.53	11.20	1.21	2.39	2.14	15.17	4.99	2.24	6.49
Fluid 94	0.84	1.48	3.00	1.28	14.78	4.75	0.53	3.51	15.66	5.49	3.55	4.56
Fluid 95	5.14	5.00	5.99	4.60	12.97	2.33	1.54	0.84	16.13	5.82	0.23	0.37
Fluid 96	18.05	17.60	3.52	16.84	-	-	-	-	16.94	6.74	1.64	1.43
Fluid 97	1.70	2.73	2.37	3.95	21.17	11.85	1.25	1.39	22.30	13.09	0.11	1.14
Fluid 98	0.30	0.69	4.26	4.29	7.05	3.12	5.35	0.38	16.47	6.33	0.60	1.99
Fluid 99	6.59	7.01	0.25	5.03	-	-	-	-	19.66	9.88	1.54	1.95
Fluid 100	7.19	9.50	0.08	17.01	-	-	-	-	16.02	5.80	1.00	2.22
Fluid 101	2.16	3.58	1.74	0.95	6.65	3.70	7.25	2.80	16.47	6.45	1.91	5.02
Fluid 102	7.41	7.00	6.24	11.32	13.98	3.43	1.23	1.61	17.95	7.87	1.78	2.38
Fluid 103	9.13	9.37	8.22	7.72	12.55	2.22	1.69	1.69	16.60	6.51	1.03	2.84

Continued on next page

Table B.2 – continued from previous page.

Fluid no.	Saturation Pressure				Density				Stock Tank Oil Density			
	SRK	PR	PC-SAFT	SBWR	SRK	PR	PC-SAFT	SBWR	SRK	PR	PC-SAFT	SBWR
Fluid 104	1.37	0.78	3.38	2.85	10.28	0.58	2.42	2.06	13.54	3.04	2.46	5.30
Fluid 105	10.43	10.08	12.34	13.85	10.08	0.76	1.78	1.25	13.64	2.94	0.73	0.62
Fluid 106	2.98	1.80	5.25	5.75	10.56	0.24	3.14	2.20	15.06	4.89	2.42	7.17
Fluid 107	1.26	0.45	13.00	6.51	5.72	4.86	9.39	4.08	15.52	5.23	0.74	2.65
Fluid 108	1.70	2.82	1.71	3.91	9.26	1.00	2.58	0.45	14.76	4.50	1.81	6.09
Fluid 109	13.69	13.87	10.98	21.23	9.79	3.73	3.06	4.22	15.74	5.34	1.02	0.71
Fluid 110	4.23	4.79	1.97	4.41	9.66	0.63	3.54	0.13	16.27	6.18	1.34	3.89
Fluid 111	8.32	9.21	4.54	9.85	-	-	-	-	16.85	6.79	0.57	2.31
Fluid 112	15.76	17.02	8.24	15.45	11.62	2.26	1.07	4.88	19.81	10.12	0.55	0.34
Fluid 113	4.69	5.16	7.59	3.05	11.41	0.68	3.54	4.82	15.23	5.03	2.09	5.34
Fluid 114	0.48	1.60	6.55	0.27	-	-	-	-	15.74	5.57	2.11	4.80
Fluid 115	5.68	4.03	26.63	0.17	5.76	4.00	5.04	1.83	13.18	2.35	0.07	0.02
Fluid 116	2.62	2.58	0.78	10.26	-	-	-	-	14.86	4.31	0.57	0.90
Fluid 117	8.72	7.47	26.07	3.51	7.12	2.73	5.31	1.50	17.83	7.85	0.27	0.75
Fluid 118	0.97	1.19	2.80	0.34	9.87	1.97	4.83	2.96	17.05	7.04	0.37	2.77
Fluid 119	3.80	2.25	11.53	0.02	8.14	1.49	3.40	2.08	16.42	6.30	1.12	2.89
Fluid 120	4.17	4.03	6.79	2.11	11.48	1.55	1.05	3.46	16.80	6.63	0.02	0.20
Fluid 121	3.30	2.98	1.01	5.12	11.95	1.27	2.18	2.20	16.12	5.83	0.59	0.26
Fluid 122	4.11	2.31	6.93	7.52	9.59	0.98	4.02	3.42	14.25	3.97	3.16	8.05
Fluid 123	14.46	15.60	10.72	13.88	17.51	7.96	0.79	0.37	19.90	10.39	0.99	3.94
Fluid 124	6.05	4.81	4.03	5.34	12.89	2.19	1.36	2.70	16.62	6.36	0.41	0.95
Fluid 125	0.63	2.30	1.92	7.99	16.65	6.73	0.26	1.87	17.97	8.16	1.73	4.29

Continued on next page

Table B.2 – continued from previous page.

Fluid no.	Saturation Pressure				Density				Stock Tank Oil Density			
	SRK	PR	PC-SAFT	SBWR	SRK	PR	PC-SAFT	SBWR	SRK	PR	PC-SAFT	SBWR
Fluid 126	3.00	1.24	12.40	5.83	6.69	3.45	7.66	2.21	16.68	6.68	1.79	4.85
Fluid 127	16.55	15.31	18.13	7.31	6.22	4.00	6.09	0.82	15.79	5.51	0.82	1.38
Fluid 128	2.20	2.84	4.63	9.64	14.95	5.34	3.19	8.19	18.34	8.31	2.12	2.38
Fluid 129	6.05	6.07	5.12	13.26	8.41	1.60	1.87	2.45	15.47	4.97	1.42	2.07
Fluid 130	0.33	2.87	5.97	11.64	14.11	3.91	2.80	7.84	16.33	6.43	1.81	9.36
Fluid 131	1.37	0.97	0.14	2.68	12.09	1.41	1.59	2.41	14.77	4.28	1.72	1.18
Fluid 132	4.31	3.96	3.02	4.33	13.72	3.38	0.45	2.90	15.88	5.62	1.11	1.43
Fluid 133	1.31	1.18	0.05	4.77	10.65	0.37	3.39	1.41	15.43	5.27	2.65	5.73
Fluid 134	5.14	4.06	11.29	1.66	8.16	1.62	3.05	2.21	15.97	5.74	0.72	1.99
Fluid 135	1.66	2.99	4.40	4.00	12.41	2.68	0.76	2.90	17.27	7.37	1.02	4.96
Fluid 136	7.35	7.29	15.00	11.53	7.76	2.69	5.59	0.23	15.92	5.62	0.03	0.32
Fluid 137	13.80	11.38	22.31	6.79	6.62	3.02	6.15	2.07	17.28	7.25	0.36	1.61
Fluid 138	0.59	1.65	27.56	9.24	9.77	0.87	5.02	5.30	15.33	4.98	1.13	2.17
Fluid 139	2.79	3.07	9.66	1.68	12.41	2.59	0.79	3.54	15.44	5.21	2.35	4.20
Fluid 140	7.66	8.78	1.65	12.14	9.77	1.68	3.78	3.11	16.52	6.40	0.39	2.47
Fluid 141	9.91	11.09	2.45	6.77	11.08	1.30	1.85	2.54	17.26	7.33	1.42	4.36
Fluid 142	12.11	10.54	20.96	5.53	7.23	2.41	6.14	2.34	14.50	4.11	3.55	4.44
Fluid 143	2.21	5.15	3.43	15.17	14.38	4.17	2.39	5.65	16.63	6.72	1.36	7.50
Fluid 144	11.15	10.74	12.40	16.76	8.55	1.99	2.17	1.69	15.88	5.41	2.47	2.99
Fluid 145	4.42	5.26	3.13	7.09	11.61	1.88	1.12	2.54	14.27	3.90	2.00	5.34
Fluid 146	2.44	4.18	3.98	10.83	13.45	4.98	3.19	7.08	14.87	4.50	1.18	3.28
Fluid 147	10.73	12.11	7.08	13.43	18.25	8.72	0.75	0.25	20.82	11.40	0.34	2.53

Continued on next page

Table B.2 – continued from previous page.

Fluid no.	Saturation Pressure				Density				Stock Tank Oil Density			
	SRK	PR	PC-SAFT	SBWR	SRK	PR	PC-SAFT	SBWR	SRK	PR	PC-SAFT	SBWR
Fluid 148	8.88	9.23	13.40	11.35	9.78	0.61	4.06	1.16	15.54	5.31	1.47	3.79
Fluid 149	3.32	5.19	14.12	13.79	-	-	-	-	15.65	5.29	0.08	0.33
Fluid 150	10.89	13.26	6.33	4.82	-	-	-	-	14.39	4.10	2.16	6.98
Fluid 151	2.94	1.88	2.48	3.59	8.29	2.80	4.92	7.81	11.37	0.74	4.76	10.79
Fluid 152	8.96	9.37	7.51	5.97	10.54	1.92	4.30	6.03	12.84	2.35	3.86	8.34
Fluid 153	6.77	5.76	10.39	3.95	3.86	6.06	6.22	0.65	15.72	5.31	1.03	0.80
Fluid 154	3.03	4.05	3.83	3.92	9.28	0.84	2.57	0.81	15.68	5.51	1.12	4.79
Fluid 155	0.67	1.19	14.67	4.13	11.50	2.16	5.09	1.67	18.51	8.73	0.95	2.85
Fluid 156	13.92	13.89	12.05	8.67	13.55	3.50	1.46	0.15	17.81	7.95	0.86	3.24
Fluid 157	11.46	11.60	10.28	17.02	8.45	1.40	1.12	3.07	15.29	4.78	1.27	1.90
Fluid 158	4.23	3.02	7.77	3.59	-	-	-	-	15.40	5.11	1.76	2.73
Fluid 159	10.24	11.02	7.46	6.77	-	-	-	-	18.33	8.52	0.33	2.65
Fluid 160	4.74	6.46	1.68	3.32	11.34	1.40	2.09	0.29	15.62	5.55	2.79	8.14
Fluid 161	7.62	6.87	9.02	10.70	-	-	-	-	15.30	4.80	0.97	2.11
Fluid 162	11.38	7.18	11.97	2.45	7.95	2.81	5.26	16.05	11.04	0.60	4.65	20.22
Fluid 163	9.26	11.01	0.65	5.58	-	-	-	-	20.11	10.61	1.31	2.81
Fluid 164	8.82	10.54	0.37	5.52	17.55	7.87	1.00	2.44	20.89	11.48	0.28	1.67
Fluid 165	2.03	2.73	0.12	2.02	14.61	4.50	2.31	2.01	17.53	7.67	3.81	5.29
Fluid 166	3.38	0.53	8.32	1.36	11.44	0.92	2.93	8.34	13.46	3.19	3.26	12.28
Fluid 167	12.39	9.66	19.03	4.31	-	-	-	-	17.18	7.40	2.36	9.87
Fluid 168	2.06	0.36	4.95	5.01	-	-	-	-	16.04	6.08	1.80	9.35
Fluid 169	5.39	7.60	7.61	12.93	-	-	-	-	12.71	2.28	3.45	10.53

Continued on next page

Table B.2 – continued from previous page.

Fluid no.	Saturation Pressure				Density				Stock Tank Oil Density			
	SRK	PR	PC-SAFT	SBWR	SRK	PR	PC-SAFT	SBWR	SRK	PR	PC-SAFT	SBWR
Fluid 170	7.61	4.69	8.51	1.69	-	-	-	-	13.69	3.46	2.97	12.21
Fluid 171	2.76	0.31	4.99	5.31	-	-	-	-	15.48	5.47	3.30	10.74
Fluid 172	0.68	3.02	0.92	8.37	-	-	-	-	14.79	4.67	3.08	10.32
Fluid 173	1.12	3.20	1.24	8.19	-	-	-	-	15.67	5.64	2.96	8.85
Fluid 174	2.33	0.17	2.70	6.16	-	-	-	-	14.72	4.61	3.19	10.94
Fluid 175	11.51	8.68	9.66	2.24	-	-	-	-	12.39	1.94	3.63	11.53
Fluid 176	9.05	5.98	11.61	2.20	-	-	-	-	14.92	4.88	3.16	12.64
Fluid 177	0.84	2.82	2.19	6.57	-	-	-	-	18.68	9.05	1.39	6.62
Fluid 178	0.47	2.34	0.59	6.10	-	-	-	-	16.33	6.34	1.51	6.77
Fluid 179	10.28	7.67	12.94	2.33	-	-	-	-	15.05	4.97	2.76	10.20
Fluid 180	4.26	6.55	2.38	11.33	-	-	-	-	16.17	6.23	1.85	9.46
Fluid 181	8.07	4.94	12.79	3.05	-	-	-	-	14.72	4.67	3.31	13.31
Fluid 182	4.41	6.15	5.01	9.46	-	-	-	-	18.62	8.93	0.86	4.67
Fluid 183	5.25	3.58	6.91	0.54	-	-	-	-	18.26	8.51	0.90	4.64
Fluid 184	7.59	4.85	13.33	1.27	-	-	-	-	17.09	7.31	2.04	10.13
Fluid 185	5.47	2.33	8.31	4.59	-	-	-	-	12.97	2.67	3.18	13.66
Fluid 186	11.53	8.28	12.57	0.20	-	-	-	-	12.88	2.58	4.31	14.38
Fluid 187	0.50	2.83	4.70	11.94	-	-	-	-	13.50	3.32	3.11	15.55
Fluid 188	11.70	8.29	15.90	0.43	-	-	-	-	13.34	3.10	3.41	14.43
Fluid 189	11.33	7.99	17.69	0.16	-	-	-	-	15.32	5.35	2.34	13.23
Fluid 190	5.42	2.04	8.04	6.40	-	-	-	-	11.95	1.55	4.21	15.96
Fluid 191	14.31	11.09	17.70	3.74	-	-	-	-	13.64	3.42	3.65	13.16

Continued on next page

Table B.2 – continued from previous page.

Fluid no.	Saturation Pressure				Density				Stock Tank Oil Density			
	SRK	PR	PC-SAFT	SBWR	SRK	PR	PC-SAFT	SBWR	SRK	PR	PC-SAFT	SBWR
Fluid 192	9.65	6.81	5.82	0.84	-	-	-	-	11.11	0.47	3.90	11.84
Fluid 193	5.27	7.35	2.38	11.08	-	-	-	-	16.54	6.63	1.45	8.14
Fluid 194	19.93	18.07	7.78	2.07	-	-	-	-	7.34	4.09	4.75	5.73
Fluid 195	5.18	2.60	13.64	2.05	-	-	-	-	18.75	9.19	1.21	8.59
Fluid 196	3.52	1.18	5.46	4.87	-	-	-	-	16.62	6.74	2.48	8.78
Fluid 197	8.81	5.88	14.27	0.58	-	-	-	-	15.09	5.05	2.49	11.66
Fluid 198	0.37	2.66	0.41	9.47	-	-	-	-	12.04	1.61	3.38	14.05
Fluid 199	10.52	6.42	12.32	2.68	-	-	-	-	9.62	1.05	4.78	18.75
Fluid 200	4.15	1.42	17.31	2.91	-	-	-	-	14.21	4.10	3.24	13.97
Fluid 201	2.89	5.31	4.58	7.51	-	-	-	-	10.79	0.16	4.51	14.01
Fluid 202	1.44	0.08	4.37	4.56	-	-	-	-	16.22	6.29	2.09	9.28
Fluid 203	5.21	4.22	6.30	14.81	-	-	-	-	21.12	11.81	0.89	4.68
Fluid 204	3.77	4.66	1.30	4.08	-	-	-	-	15.33	5.15	1.81	5.89
Fluid 205	1.94	3.06	0.60	2.75	-	-	-	-	15.07	4.86	2.17	6.16
Fluid 206	0.71	0.22	3.08	2.50	-	-	-	-	16.10	6.04	1.92	5.76
Fluid 207	0.41	1.29	0.61	0.97	-	-	-	-	14.97	4.74	2.12	6.17
Fluid 208	6.96	5.80	11.39	9.79	-	-	-	-	16.08	6.02	1.92	6.23
Fluid 209	0.83	0.19	3.93	0.92	-	-	-	-	15.52	5.37	1.89	5.95
Fluid 210	3.17	4.03	1.14	0.06	-	-	-	-	16.53	6.55	1.72	5.92
Fluid 211	12.35	7.68	4.61	6.87	-	-	-	-	7.96	2.86	5.82	23.52
Fluid 212	16.86	17.91	20.08	14.22	-	-	-	-	16.88	7.02	1.36	8.37
Fluid 213	3.86	7.02	0.92	9.07	-	-	-	-	6.36	4.77	6.65	19.61

Continued on next page

Table B.2 – continued from previous page.

Fluid no.	Saturation Pressure				Density				Stock Tank Oil Density			
	SRK	PR	PC-SAFT	SBWR	SRK	PR	PC-SAFT	SBWR	SRK	PR	PC-SAFT	SBWR
Fluid 214	2.56	3.07	0.75	1.61	-	-	-	-	18.59	8.84	0.35	3.28
Fluid 215	3.68	5.72	0.23	12.38	-	-	-	-	13.47	2.98	2.61	5.79
Fluid 216	5.74	3.12	1.06	0.59	-	-	-	-	9.73	1.04	5.04	14.61
Fluid 217	3.34	3.90	0.18	2.41	-	-	-	-	17.56	7.65	0.65	3.42
Fluid 218	5.76	7.34	3.01	7.90	-	-	-	-	23.24	14.16	1.10	0.90
Fluid 219	0.88	0.71	1.08	1.72	-	-	-	-	15.91	5.84	2.67	6.40
Fluid 220	5.14	5.63	0.38	1.95	-	-	-	-	20.52	10.95	0.39	0.59
Fluid 221	0.47	2.32	12.30	4.33	-	-	-	-	21.75	12.35	0.01	1.00
Fluid 222	0.01	0.93	2.06	2.98	-	-	-	-	17.08	7.16	1.32	5.58
Fluid 223	14.89	16.65	3.62	3.98	-	-	-	-	22.09	12.78	0.02	0.01
Fluid 224	20.16	21.29	13.12	7.41	-	-	-	-	24.29	15.38	0.01	1.49
Fluid 225	6.53	8.09	2.17	8.65	-	-	-	-	23.24	14.16	1.10	0.90
Fluid 226	1.63	1.51	3.31	1.60	-	-	-	-	13.06	2.79	4.69	14.42
Fluid 227	4.06	4.93	0.92	1.65	-	-	-	-	18.06	8.30	1.15	5.61
Fluid 228	0.44	1.73	4.57	9.11	-	-	-	-	15.78	5.77	2.75	8.88
Fluid 229	5.57	7.06	3.50	7.04	-	-	-	-	21.49	12.18	0.36	2.58
Fluid 230	1.93	0.06	6.01	3.09	-	-	-	-	17.01	7.11	2.00	6.36
Fluid 231	12.60	8.19	24.59	16.28	-	-	-	-	14.62	4.60	3.64	15.49
Fluid 232	15.26	10.97	9.92	1.55	-	-	-	-	8.10	2.76	6.99	20.67
Fluid 233	0.98	1.97	1.76	0.11	-	-	-	-	17.38	7.49	1.12	4.75
Fluid 234	8.59	9.79	9.71	7.46	-	-	-	-	15.67	5.66	2.01	9.53
Fluid 235	4.12	3.28	13.69	9.76	-	-	-	-	17.18	7.34	1.30	7.38

Continued on next page

Table B.2 – continued from previous page.

Fluid no.	Saturation Pressure				Density				Stock Tank Oil Density			
	SRK	PR	PC-SAFT	SBWR	SRK	PR	PC-SAFT	SBWR	SRK	PR	PC-SAFT	SBWR
Fluid 236	3.53	5.39	25.01	5.79	-	-	-	-	18.32	8.58	0.14	4.48
Fluid 237	2.10	0.18	4.11	1.47	-	-	-	-	18.55	8.83	0.45	3.79
Fluid 238	3.83	5.96	6.42	8.39	-	-	-	-	18.01	8.24	0.26	4.96
Fluid 239	5.43	7.40	6.86	9.33	-	-	-	-	18.77	9.10	0.07	4.45
Fluid 240	0.41	2.65	3.05	4.47	-	-	-	-	17.05	7.16	1.27	6.05
Fluid 241	0.93	3.24	2.68	4.86	-	-	-	-	16.85	6.93	1.12	6.03
Fluid 242	0.92	2.65	0.68	4.42	-	-	-	-	18.06	8.32	0.77	6.05
Fluid 243	2.50	4.07	2.44	5.50	-	-	-	-	18.94	9.29	0.08	4.37
Fluid 244	2.86	1.00	2.93	0.98	-	-	-	-	16.82	6.93	1.34	7.28
Fluid 245	5.60	4.06	8.90	3.94	-	-	-	-	19.74	10.20	0.32	4.00
Fluid 246	0.82	2.54	1.39	4.56	-	-	-	-	17.27	7.43	1.28	6.56
Fluid 247	9.22	7.11	12.11	5.12	-	-	-	-	18.61	8.97	0.58	6.44
Fluid 248	2.28	4.00	3.72	6.40	-	-	-	-	15.73	5.67	2.12	7.69
Fluid 249	3.47	4.90	2.10	6.91	-	-	-	-	22.22	13.01	0.19	2.01
Fluid 250	3.03	4.56	2.12	6.48	-	-	-	-	20.99	11.64	0.38	3.83
Fluid 251	6.85	5.81	8.28	8.83	-	-	-	-	16.21	6.21	2.22	7.12
Fluid 252	6.11	7.01	0.38	12.60	-	-	-	-	19.26	9.53	0.29	0.95
Fluid 253	5.78	6.03	3.49	9.80	-	-	-	-	20.87	11.25	1.62	3.01
Fluid 254	8.80	9.02	4.33	5.06	-	-	-	-	25.49	16.56	2.82	5.35
Fluid 255	10.86	6.69	16.80	0.94	-	-	-	-	20.83	11.25	0.52	1.94
Fluid 256	10.44	6.42	17.11	1.82	-	-	-	-	21.11	11.56	0.68	2.14
Fluid 257	1.18	0.16	3.22	0.20	-	-	-	-	14.85	4.65	3.14	7.57

Continued on next page

Table B.2 – continued from previous page.

Fluid no.	Saturation Pressure				Density				Stock Tank Oil Density			
	SRK	PR	PC-SAFT	SBWR	SRK	PR	PC-SAFT	SBWR	SRK	PR	PC-SAFT	SBWR
Fluid 258	4.74	2.66	6.38	16.33	-	-	-	-	15.43	5.39	3.05	9.95
Fluid 259	8.45	6.35	20.36	4.55	-	-	-	-	15.49	5.27	1.70	4.28
Fluid 260	3.17	4.92	8.07	2.22	-	-	-	-	19.50	9.79	0.16	0.43
Average	6.35	6.26	7.36	6.72	12.62	3.95	2.82	4.46	16.49	6.76	2.03	6.45

B.3 PVT Results using General Characterization Approach for PC-SAFT

The percent average absolute deviations AAD% of saturation pressure, density, and STO density for the 260 petroleum fluids are listed in Table B.3, where we have compared the performance of PC-SAFT EoS with the new general characterization method (eqs. (4.39)–(4.40))) with SRK and PR with volume translation.

Table B.3 Summary of AAD% in predicted saturation pressures, reservoir fluid densities and stock tank oil densities (PC-SAFT with new general characterization eqs. (4.39)–(4.40)).

Fluid no.	Saturation Pressure			Density			Stock Tank Oil Density		
	SRK-VT	PR-VT	PC-SAFT	SRK-VT	PR-VT	PC-SAFT	SRK-VT	PR-VT	PC-SAFT
Fluid 1	3.47	5.88	0.98	1.68	1.55	1.10	0.77	0.97	2.05
Fluid 2	7.54	10.42	5.91	1.57	1.97	1.21	-	-	-
Fluid 3	5.13	8.28	6.12	0.96	1.26	0.84	-	-	-
Fluid 4	4.02	7.80	5.86	0.92	1.20	1.30	-	-	-
Fluid 5	3.21	1.31	4.17	0.84	0.90	0.58	-	-	-
Fluid 6	4.09	0.14	4.84	0.41	0.52	0.80	-	-	-
Fluid 7	0.49	2.18	2.04	2.43	2.59	4.48	0.21	0.53	2.27
Fluid 8	14.84	16.25	5.60	0.77	0.59	1.65	-	-	-
Fluid 9	10.02	11.87	7.20	1.10	0.71	2.32	0.76	0.55	0.58
Fluid 10	7.89	10.30	13.60	1.93	1.25	6.03	0.48	0.63	0.42
Fluid 11	5.09	6.40	4.77	0.73	0.30	0.20	0.17	0.12	0.58
Fluid 12	0.66	0.60	4.69	1.25	1.37	0.97	0.07	0.21	0.70
Fluid 13	10.79	11.46	2.07	-	-	-	1.24	1.55	2.55
Fluid 14	7.14	7.88	2.92	-	-	-	0.15	0.46	0.59
Fluid 15	0.65	5.33	0.26	0.67	0.87	0.64	0.03	0.12	1.46

Continued on next page

Table B.3 – continued from previous page.

Fluid no.	Saturation Pressure				Density				Stock Tank Oil Density			
	SRK-VT		PR-VT		PC-SAFT		SRK-VT		PR-VT		PC-SAFT	
	SRK-VT	PR-VT	PC-SAFT	SRK-VT	PR-VT	PC-SAFT	SRK-VT	PR-VT	PC-SAFT	SRK-VT	PR-VT	PC-SAFT
Fluid 16	4.99	0.79	3.50	0.43	0.47	0.67	0.01	0.11	0.79			
Fluid 17	9.42	4.73	0.79	0.86	0.76	0.38	0.39	0.49	0.47			
Fluid 18	1.41	2.24	9.76	0.83	0.73	0.51	0.13	0.12	1.45			
Fluid 19	0.13	3.73	12.96	0.23	0.31	1.67	0.72	0.79	2.61			
Fluid 20	1.60	3.28	1.38	0.66	0.83	0.57	0.26	0.34	1.40			
Fluid 21	4.53	0.58	3.00	0.50	0.56	0.21	0.19	0.34	1.15			
Fluid 22	4.88	5.16	3.53	2.33	2.00	2.22	0.08	0.39	0.11			
Fluid 23	6.24	7.03	3.38	3.22	2.85	3.21	0.76	1.01	0.74			
Fluid 24	8.50	2.48	12.91	-	-	-	0.80	0.69	1.52			
Fluid 25	6.88	1.39	15.95	-	-	-	0.58	0.35	1.42			
Fluid 26	9.94	4.09	17.73	-	-	-	1.32	1.07	2.27			
Fluid 27	11.35	5.81	24.08	2.12	1.09	3.15	-	-	-			
Fluid 28	21.84	16.66	7.83	-	-	-	-	-	-			
Fluid 29	7.03	1.66	5.26	0.88	0.93	1.01	0.61	0.48	2.22			
Fluid 30	16.48	12.36	20.22	0.94	0.93	0.49	0.45	0.29	1.28			
Fluid 31	19.66	12.23	8.95	2.64	2.45	1.95	-	-	-			
Fluid 32	8.45	10.44	18.65	2.61	3.17	1.47	1.07	1.24	1.20			
Fluid 33	0.38	2.16	17.34	0.12	0.12	3.74	1.03	0.79	0.39			
Fluid 34	4.87	6.93	9.32	0.37	0.68	2.21	0.91	0.69	2.07			
Fluid 35	4.87	7.37	19.29	2.50	3.09	1.41	0.80	0.56	0.14			
Fluid 36	8.09	10.96	7.67	1.39	1.66	1.07	0.46	0.62	0.48			
Fluid 37	7.78	4.27	1.57	0.03	0.16	1.93	-	-	-			

Continued on next page

Table B.3 – continued from previous page.

Fluid no.	Saturation Pressure				Density				Stock Tank Oil Density			
	SRK-VT		PR-VT		PC-SAFT		SRK-VT		PR-VT		PC-SAFT	
	SRK-VT	PR-VT	PC-SAFT	SRK-VT	PR-VT	PC-SAFT	SRK-VT	PR-VT	PC-SAFT	SRK-VT	PR-VT	PC-SAFT
Fluid 38	11.34	7.05	5.38	0.39	0.23	2.31	-	-	-	-	-	-
Fluid 39	16.05	11.89	9.72	0.28	0.29	2.21	-	-	-	-	-	-
Fluid 40	6.25	9.50	5.15	0.73	1.18	0.09	-	-	-	-	-	-
Fluid 41	4.91	8.02	4.14	0.72	1.13	0.07	-	-	-	-	-	-
Fluid 42	1.65	2.93	0.92	1.14	1.14	1.84	-	-	-	-	-	-
Fluid 43	8.05	9.63	2.68	2.84	2.71	1.80	0.25	0.07	0.07	0.07	0.98	0.98
Fluid 44	5.66	3.59	2.65	0.63	0.82	0.46	0.57	0.31	0.31	0.31	1.88	1.88
Fluid 45	2.61	0.83	4.34	-	-	-	1.15	1.29	1.29	1.29	0.16	0.16
Fluid 46	11.57	7.94	2.89	0.77	0.77	0.21	0.26	0.44	0.44	0.44	0.83	0.83
Fluid 47	13.45	9.43	3.41	0.36	0.29	0.52	0.10	0.19	0.19	0.19	1.73	1.73
Fluid 48	11.12	13.12	9.73	1.22	1.48	0.90	0.10	0.33	0.33	0.33	0.50	0.50
Fluid 49	4.27	6.83	3.68	1.02	1.42	0.26	-	-	-	-	-	-
Fluid 50	5.93	8.09	4.92	0.95	0.96	1.82	0.73	0.78	0.78	0.78	1.54	1.54
Fluid 51	12.66	15.25	11.15	-	-	-	0.03	0.17	0.17	0.17	0.78	0.78
Fluid 52	5.90	0.36	3.90	0.36	0.32	1.59	0.44	0.54	0.54	0.54	0.41	0.41
Fluid 53	15.57	17.76	10.88	3.49	3.78	2.84	0.84	1.06	1.06	1.06	0.27	0.27
Fluid 54	4.21	7.94	5.80	0.93	1.21	0.89	0.53	0.65	0.65	0.65	0.40	0.40
Fluid 55	2.90	6.53	6.78	0.59	0.73	0.95	0.15	0.22	0.22	0.22	2.11	2.11
Fluid 56	19.31	22.36	17.47	0.85	1.03	0.47	1.26	1.36	1.36	1.36	0.04	0.04
Fluid 57	8.73	9.85	2.65	0.75	0.91	0.91	0.33	0.06	0.06	0.06	1.31	1.31
Fluid 58	11.31	12.52	4.94	0.27	0.10	0.77	0.20	0.05	0.05	0.05	1.02	1.02
Fluid 59	1.89	0.26	2.59	1.27	1.43	0.61	0.64	0.94	0.94	0.94	0.03	0.03

Continued on next page

Table B.3 – continued from previous page.

Fluid no.	Saturation Pressure				Density				Stock Tank Oil Density			
	SRK-VT		PR-VT		PC-SAFT		SRK-VT		PR-VT		PC-SAFT	
	SRK-VT	PR-VT	PC-SAFT	SRK-VT	PR-VT	PC-SAFT	SRK-VT	PR-VT	PC-SAFT	SRK-VT	PR-VT	PC-SAFT
Fluid 60	10.58	12.08	10.74	1.86	2.27	0.74	0.03	0.34	0.56			
Fluid 61	9.90	10.60	3.32	1.66	1.17	1.32	0.21	0.39	0.65			
Fluid 62	6.90	7.28	7.20	1.38	0.78	1.19	1.39	1.58	1.77			
Fluid 63	4.29	5.90	2.35	0.59	0.55	1.00	0.10	0.08	0.55			
Fluid 64	7.25	5.05	5.17	0.46	0.50	0.72	0.56	0.34	2.16			
Fluid 65	8.31	11.16	3.42	4.17	4.87	1.03	0.84	0.64	1.06			
Fluid 66	1.43	0.90	5.43	1.87	1.65	1.37	0.99	0.43	1.84			
Fluid 67	2.22	0.20	6.66	2.14	2.08	1.97	1.37	0.92	2.53			
Fluid 68	1.73	0.38	0.27	0.77	1.08	1.04	1.15	1.39	1.47			
Fluid 69	14.37	12.40	10.31	1.19	0.84	1.09	0.05	0.18	0.27			
Fluid 70	1.69	3.14	3.12	2.47	2.03	2.84	0.68	0.41	0.51			
Fluid 71	8.58	10.30	9.24	2.37	2.53	2.24	2.34	2.47	1.92			
Fluid 72	11.60	12.31	8.62	1.29	1.34	0.47	0.04	0.29	0.05			
Fluid 73	12.16	12.48	8.29	2.03	1.45	1.15	0.83	1.07	1.20			
Fluid 74	12.20	12.54	8.01	1.94	1.48	1.19	1.10	1.33	1.53			
Fluid 75	14.27	14.88	11.86	1.23	1.15	0.60	0.36	0.66	0.58			
Fluid 76	13.63	14.18	11.99	1.72	1.36	0.94	0.71	1.07	0.96			
Fluid 77	13.54	14.61	10.62	1.01	1.23	0.44	0.12	0.17	0.10			
Fluid 78	9.30	11.18	15.88	1.09	1.00	1.07	0.71	0.44	1.35			
Fluid 79	11.52	12.84	3.54	1.57	1.40	0.95	0.14	0.25	1.14			
Fluid 80	0.73	2.19	3.42	1.73	2.01	1.53	0.04	0.10	0.68			
Fluid 81	0.02	1.30	2.69	0.88	1.15	0.66	0.38	0.16	1.08			

Continued on next page

Table B.3 – continued from previous page.

Fluid no.	Saturation Pressure				Density				Stock Tank Oil Density			
	SRK-VT		PR-VT		PC-SAFT		SRK-VT		PR-VT		PC-SAFT	
	SRK-VT	PR-VT	PC-SAFT	SRK-VT	PR-VT	PC-SAFT	SRK-VT	PR-VT	PC-SAFT	SRK-VT	PR-VT	PC-SAFT
Fluid 82	2.80	0.39	6.43	0.38	0.40	1.47	1.28	1.33	1.08			
Fluid 83	3.94	5.35	6.39	0.91	1.10	0.53	0.17	0.00	0.55			
Fluid 84	8.19	9.38	11.82	0.87	1.07	0.52	0.35	0.50	0.18			
Fluid 85	0.89	2.43	4.76	1.20	1.44	0.91	0.69	0.54	1.31			
Fluid 86	12.44	13.41	13.95	1.35	1.45	1.04	0.12	0.35	0.54			
Fluid 87	9.22	10.33	10.90	1.83	2.08	1.85	0.37	0.15	0.99			
Fluid 88	3.47	3.74	7.09	0.80	1.45	0.42	0.16	0.41	0.19			
Fluid 89	18.06	18.82	15.17	7.70	7.42	6.54	1.84	2.04	1.10			
Fluid 90	6.93	8.42	0.40	1.65	1.87	0.52	0.12	0.06	0.47			
Fluid 91	4.44	6.27	5.96	0.70	0.38	0.77	0.24	0.06	0.87			
Fluid 92	3.33	1.24	3.28	2.24	1.88	2.38	0.36	0.65	0.42			
Fluid 93	2.74	3.78	3.81	0.97	1.00	0.80	0.33	0.65	0.46			
Fluid 94	0.84	1.48	0.27	1.35	1.38	0.79	2.67	2.35	2.63			
Fluid 95	5.14	5.00	7.04	1.97	1.84	1.18	0.61	0.13	0.15			
Fluid 96	18.05	17.60	1.84	-	-	-	1.99	2.60	2.32			
Fluid 97	1.70	2.73	4.81	0.36	0.17	2.02	0.43	0.69	0.88			
Fluid 98	0.30	0.69	1.43	3.69	3.16	4.49	0.64	0.97	0.43			
Fluid 99	6.59	7.01	1.65	-	-	-	1.50	1.93	1.99			
Fluid 100	7.19	9.50	2.82	-	-	-	0.26	0.56	0.01			
Fluid 101	2.16	3.58	1.65	5.41	5.03	6.16	0.05	0.30	0.53			
Fluid 102	7.41	7.00	5.32	2.20	1.81	1.03	1.45	2.31	2.15			
Fluid 103	9.13	9.37	10.62	1.21	1.26	0.75	0.29	0.70	0.06			

Continued on next page

Table B.3 – continued from previous page.

Fluid no.	Saturation Pressure				Density				Stock Tank Oil Density			
	SRK-VT		PR-VT		PC-SAFT		SRK-VT		PR-VT		PC-SAFT	
	SRK-VT	PR-VT	PC-SAFT	SRK-VT	PR-VT	PC-SAFT	SRK-VT	PR-VT	PC-SAFT	SRK-VT	PR-VT	PC-SAFT
Fluid 104	1.37	0.78	0.52	0.98	0.97	0.93	0.31	0.21	0.89			
Fluid 105	10.43	10.08	13.64	1.12	0.92	1.26	0.73	0.00	0.12			
Fluid 106	2.98	1.80	1.50	0.93	1.10	1.42	0.32	0.61	0.53			
Fluid 107	1.26	0.45	9.88	4.32	4.45	7.73	0.85	1.26	0.49			
Fluid 108	1.70	2.82	1.68	0.59	0.26	1.29	0.98	1.31	0.11			
Fluid 109	13.69	13.87	12.65	3.53	2.92	3.10	1.54	2.12	1.78			
Fluid 110	4.23	4.79	4.78	2.35	1.92	2.58	0.47	0.76	0.03			
Fluid 111	8.32	9.21	7.21	-	-	-	0.81	1.18	0.51			
Fluid 112	15.76	17.02	10.47	0.73	0.77	0.68	0.80	1.26	1.14			
Fluid 113	4.69	5.16	10.18	2.88	3.21	2.06	0.12	0.32	0.60			
Fluid 114	0.48	1.60	3.34	-	-	-	0.41	0.04	0.81			
Fluid 115	5.68	4.03	23.84	1.90	1.57	4.38	0.55	1.03	0.85			
Fluid 116	2.62	2.58	2.45	-	-	-	0.64	1.19	1.18			
Fluid 117	8.72	7.47	22.87	2.49	1.44	4.52	1.24	1.69	1.14			
Fluid 118	0.97	1.19	0.33	3.48	3.51	3.76	1.24	1.65	0.86			
Fluid 119	3.80	2.25	8.31	1.47	0.66	2.58	0.43	0.72	0.00			
Fluid 120	4.17	4.03	4.70	0.75	0.36	0.53	0.26	0.89	0.63			
Fluid 121	3.30	2.98	2.28	1.55	1.30	1.71	0.72	0.04	0.13			
Fluid 122	4.11	2.31	2.90	1.95	1.99	2.14	0.30	0.02	1.18			
Fluid 123	14.46	15.60	13.61	1.27	0.80	0.28	0.04	0.25	0.13			
Fluid 124	6.05	4.81	5.07	2.08	1.54	1.14	0.07	0.84	0.79			
Fluid 125	0.63	2.30	1.18	1.13	1.47	0.78	0.29	0.02	0.57			

Continued on next page

Table B.3 – continued from previous page.

Fluid no.	Saturation Pressure				Density				Stock Tank Oil Density			
	SRK-VT		PC-SAFT		SRK-VT		PC-SAFT		SRK-VT		PC-SAFT	
	PR-VT	PR-VT	PC-SAFT	PC-SAFT	SRK-VT	PR-VT	PR-VT	PC-SAFT	SRK-VT	PR-VT	PR-VT	PC-SAFT
Fluid 126	3.00	1.24	8.62	8.62	4.85	4.24	6.39	6.39	0.15	0.40	0.40	0.42
Fluid 127	16.55	15.31	15.03	15.03	4.47	4.05	5.21	5.21	0.05	0.32	0.32	0.03
Fluid 128	2.20	2.84	2.73	2.73	6.25	6.17	3.63	3.63	2.10	2.65	2.65	2.60
Fluid 129	6.05	6.07	6.78	6.78	0.76	0.41	1.48	1.48	1.15	1.62	1.62	1.94
Fluid 130	0.33	2.87	1.29	1.29	0.79	0.53	0.61	0.61	0.82	1.11	1.11	0.44
Fluid 131	1.37	0.97	0.96	0.96	1.60	1.20	1.22	1.22	2.08	1.31	1.31	1.33
Fluid 132	4.31	3.96	4.82	4.82	1.52	0.82	0.69	0.69	0.65	0.14	0.14	0.43
Fluid 133	1.31	1.18	2.82	2.82	2.71	2.51	2.23	2.23	0.68	0.37	0.37	1.23
Fluid 134	5.14	4.06	8.40	8.40	1.00	0.42	2.29	2.29	0.54	0.89	0.89	0.30
Fluid 135	1.66	2.99	0.79	0.79	1.09	1.44	0.42	0.42	0.96	1.30	1.30	0.52
Fluid 136	7.35	7.29	12.56	12.56	2.81	2.68	4.83	4.83	0.82	1.17	1.17	0.84
Fluid 137	13.80	11.38	18.78	18.78	3.06	2.12	5.00	5.00	0.83	1.18	1.18	0.58
Fluid 138	0.59	1.65	24.05	24.05	2.61	3.59	4.36	4.36	0.14	0.42	0.42	0.11
Fluid 139	2.79	3.07	6.76	6.76	0.97	0.96	0.31	0.31	0.86	0.50	0.50	1.22
Fluid 140	7.66	8.78	4.45	4.45	2.13	2.16	2.48	2.48	1.27	1.69	1.69	0.82
Fluid 141	9.91	11.09	5.62	5.62	0.62	0.18	0.97	0.97	0.41	0.65	0.65	0.09
Fluid 142	12.11	10.54	17.79	17.79	2.33	1.74	5.04	5.04	2.57	2.19	2.19	2.68
Fluid 143	2.21	5.15	0.66	0.66	0.27	0.35	0.48	0.48	1.12	1.46	1.46	0.64
Fluid 144	11.15	10.74	13.72	13.72	1.71	1.15	1.75	1.75	2.16	2.83	2.83	2.98
Fluid 145	4.42	5.26	6.10	6.10	2.11	1.93	1.57	1.57	0.41	0.81	0.81	0.30
Fluid 146	2.44	4.18	1.13	1.13	5.62	5.74	3.67	3.67	0.51	1.00	1.00	0.11
Fluid 147	10.73	12.11	9.90	9.90	0.81	0.38	0.29	0.29	0.56	0.82	0.82	0.65

Continued on next page

Table B.3 – continued from previous page.

Fluid no.	Saturation Pressure				Density				Stock Tank Oil Density			
	SRK-VT		PC-SAFT		SRK-VT		PC-SAFT		SRK-VT		PC-SAFT	
	PR-VT	PR-VT	PR-VT	PR-VT	PR-VT	PR-VT	PR-VT	PR-VT	PR-VT	PR-VT	PR-VT	PR-VT
Fluid 148	8.88	9.23	10.55	0.93	0.54	3.03	0.24	0.67	0.20			
Fluid 149	3.32	5.19	11.17	-	-	-	0.62	0.97	0.70			
Fluid 150	10.89	13.26	9.96	-	-	-	0.79	1.16	0.11			
Fluid 151	2.94	1.88	1.03	3.18	3.34	2.65	1.48	0.99	2.28			
Fluid 152	8.96	9.37	10.57	2.87	3.56	2.61	1.12	0.70	1.88			
Fluid 153	6.77	5.76	8.02	4.23	3.21	5.43	1.49	2.04	1.78			
Fluid 154	3.03	4.05	0.58	0.93	0.28	1.48	1.05	1.57	0.52			
Fluid 155	0.67	1.19	11.09	2.01	2.06	3.86	0.34	0.57	0.06			
Fluid 156	13.92	13.89	14.44	1.67	1.47	0.43	0.64	0.94	0.31			
Fluid 157	11.46	11.60	11.96	1.05	0.61	0.73	1.07	1.52	1.82			
Fluid 158	4.23	3.02	4.89	-	-	-	0.66	0.39	0.82			
Fluid 159	10.24	11.02	10.21	-	-	-	1.19	1.49	0.80			
Fluid 160	4.74	6.46	5.62	0.83	0.17	0.73	0.18	0.04	0.88			
Fluid 161	7.62	6.87	10.43	-	-	-	0.49	0.79	1.40			
Fluid 162	11.38	7.18	3.47	2.81	2.77	1.09	0.16	0.00	0.46			
Fluid 163	9.26	11.01	4.71	-	-	-	0.04	0.22	0.38			
Fluid 164	8.82	10.54	4.41	1.09	1.34	0.30	1.09	1.27	0.64			
Fluid 165	2.03	2.73	3.54	0.72	0.84	1.31	1.21	0.93	2.81			
Fluid 166	3.38	0.53	2.53	0.50	0.55	0.27	0.50	0.80	0.33			
Fluid 167	12.39	9.66	13.88	-	-	-	0.34	0.09	0.32			
Fluid 168	2.06	0.36	0.46	-	-	-	0.90	1.22	0.49			
Fluid 169	5.39	7.60	11.22	-	-	-	0.18	0.56	0.76			

Continued on next page

Table B.3 – continued from previous page.

Fluid no.	Saturation Pressure			Density			Stock Tank Oil Density		
	SRK-VT	PR-VT	PC-SAFT	SRK-VT	PR-VT	PC-SAFT	SRK-VT	PR-VT	PC-SAFT
Fluid 170	7.61	4.69	3.39	-	-	-	0.54	0.86	0.07
Fluid 171	2.76	0.31	0.30	-	-	-	0.50	0.27	1.08
Fluid 172	0.68	3.02	4.99	-	-	-	0.11	0.17	0.76
Fluid 173	1.12	3.20	5.14	-	-	-	0.28	0.05	0.98
Fluid 174	2.33	0.17	1.85	-	-	-	0.08	0.18	0.78
Fluid 175	11.51	8.68	5.03	-	-	-	0.35	0.69	0.68
Fluid 176	9.05	5.98	5.62	-	-	-	0.02	0.19	0.51
Fluid 177	0.84	2.82	1.61	-	-	-	0.37	0.62	0.21
Fluid 178	0.47	2.34	2.95	-	-	-	0.97	1.33	0.37
Fluid 179	10.28	7.67	8.00	-	-	-	0.27	0.54	0.40
Fluid 180	4.26	6.55	6.60	-	-	-	0.79	1.09	0.43
Fluid 181	8.07	4.94	6.56	-	-	-	0.29	0.08	0.59
Fluid 182	4.41	6.15	7.84	-	-	-	0.91	1.18	0.54
Fluid 183	5.25	3.58	3.49	-	-	-	0.86	1.17	0.50
Fluid 184	7.59	4.85	7.87	-	-	-	0.17	0.41	0.12
Fluid 185	5.47	2.33	2.87	-	-	-	0.70	1.03	0.07
Fluid 186	11.53	8.28	6.60	-	-	-	0.52	0.30	1.27
Fluid 187	0.50	2.83	1.48	-	-	-	0.38	0.63	0.23
Fluid 188	11.70	8.29	9.61	-	-	-	0.23	0.50	0.23
Fluid 189	11.33	7.99	11.11	-	-	-	0.44	0.71	0.47
Fluid 190	5.42	2.04	1.93	-	-	-	0.26	0.05	0.73
Fluid 191	14.31	11.09	11.57	-	-	-	0.02	0.18	0.76

Continued on next page

Table B.3 – continued from previous page.

Fluid no.	Saturation Pressure				Density				Stock Tank Oil Density			
	SRK-VT		PR-VT		PC-SAFT		SRK-VT		PR-VT		PC-SAFT	
	SRK-VT	PR-VT	PC-SAFT	SRK-VT	PR-VT	PC-SAFT	SRK-VT	PR-VT	PC-SAFT	SRK-VT	PR-VT	PC-SAFT
Fluid 192	9.65	6.81	1.30	-	-	-	0.68	1.02	0.47			
Fluid 193	5.27	7.35	6.37	-	-	-	1.14	1.48	0.66			
Fluid 194	19.93	18.07	6.44	-	-	-	1.26	1.68	0.75			
Fluid 195	5.18	2.60	8.18	-	-	-	0.52	0.76	0.71			
Fluid 196	3.52	1.18	0.93	-	-	-	0.07	0.14	0.54			
Fluid 197	8.81	5.88	8.58	-	-	-	0.61	0.91	0.18			
Fluid 198	0.37	2.66	4.46	-	-	-	0.96	1.31	0.18			
Fluid 199	10.52	6.42	5.46	-	-	-	0.50	0.81	0.17			
Fluid 200	4.15	1.42	10.74	-	-	-	0.08	0.31	0.28			
Fluid 201	2.89	5.31	0.39	-	-	-	0.27	0.57	0.85			
Fluid 202	1.44	0.08	0.34	-	-	-	0.62	0.89	0.10			
Fluid 203	5.21	4.22	2.88	-	-	-	0.02	0.16	0.31			
Fluid 204	3.77	4.66	4.53	-	-	-	0.70	1.02	0.06			
Fluid 205	1.94	3.06	2.78	-	-	-	0.37	0.66	0.43			
Fluid 206	0.71	0.22	0.33	-	-	-	0.38	0.65	0.33			
Fluid 207	0.41	1.29	2.69	-	-	-	0.46	0.77	0.35			
Fluid 208	6.96	5.80	7.53	-	-	-	0.48	0.76	0.22			
Fluid 209	0.83	0.19	0.45	-	-	-	0.61	0.92	0.17			
Fluid 210	3.17	4.03	4.44	-	-	-	0.48	0.76	0.11			
Fluid 211	12.35	7.68	2.81	-	-	-	0.18	0.05	0.51			
Fluid 212	16.86	17.91	15.87	-	-	-	1.06	1.38	0.76			
Fluid 213	3.86	7.02	5.99	-	-	-	0.51	0.85	0.58			

Continued on next page

Table B.3 – continued from previous page.

Fluid no.	Saturation Pressure				Density				Stock Tank Oil Density			
	SRK-VT		PR-VT		PC-SAFT		SRK-VT		PR-VT		PC-SAFT	
	SRK-VT	PR-VT	PC-SAFT	SRK-VT	PR-VT	PC-SAFT	SRK-VT	PR-VT	PC-SAFT	SRK-VT	PR-VT	PC-SAFT
Fluid 214	2.56	3.07	3.57	-	-	-	1.13	1.47	1.47	1.13	1.47	0.89
Fluid 215	3.68	5.72	2.44	-	-	-	0.04	0.32	0.32	0.04	0.32	0.83
Fluid 216	5.74	3.12	5.97	-	-	-	0.22	0.55	0.55	0.22	0.55	1.03
Fluid 217	3.34	3.90	3.01	-	-	-	1.10	1.44	1.44	1.10	1.44	0.63
Fluid 218	5.76	7.34	0.18	-	-	-	1.44	1.71	1.71	1.44	1.71	2.02
Fluid 219	0.88	0.71	4.79	-	-	-	0.46	0.26	0.26	0.46	0.26	1.13
Fluid 220	5.14	5.63	1.65	-	-	-	0.62	0.85	0.85	0.62	0.85	0.91
Fluid 221	0.47	2.32	9.75	-	-	-	0.24	0.15	0.15	0.24	0.15	0.36
Fluid 222	0.01	0.93	1.30	-	-	-	0.73	1.06	1.06	0.73	1.06	0.27
Fluid 223	14.89	16.65	6.25	-	-	-	0.22	0.38	0.38	0.22	0.38	0.58
Fluid 224	20.16	21.29	15.78	-	-	-	0.14	0.03	0.03	0.14	0.03	0.76
Fluid 225	6.53	8.09	0.63	-	-	-	1.44	1.71	1.71	1.44	1.71	2.02
Fluid 226	1.63	1.51	3.02	-	-	-	0.84	0.69	0.69	0.84	0.69	1.77
Fluid 227	4.06	4.93	4.27	-	-	-	0.81	1.10	1.10	0.81	1.10	0.40
Fluid 228	0.44	1.73	0.16	-	-	-	0.01	0.22	0.22	0.01	0.22	0.73
Fluid 229	5.57	7.06	0.08	-	-	-	0.31	0.50	0.50	0.31	0.50	0.58
Fluid 230	1.93	0.06	1.72	-	-	-	0.12	0.36	0.36	0.12	0.36	0.41
Fluid 231	12.60	8.19	15.24	-	-	-	0.71	0.57	0.57	0.71	0.57	0.72
Fluid 232	15.26	10.97	2.39	-	-	-	1.08	0.94	0.94	1.08	0.94	2.24
Fluid 233	0.98	1.97	1.54	-	-	-	0.79	1.09	1.09	0.79	1.09	0.33
Fluid 234	8.59	9.79	5.72	-	-	-	0.91	1.22	1.22	0.91	1.22	0.34
Fluid 235	4.12	3.28	9.85	-	-	-	1.06	1.36	1.36	1.06	1.36	0.63

Continued on next page

Table B.3 – continued from previous page.

Fluid no.	Saturation Pressure				Density				Stock Tank Oil Density					
	PR-VT		PC-SAFT		PR-VT		PC-SAFT		SRK-VT		PR-VT		PC-SAFT	
	SRK-VT	PR-VT	PC-SAFT		SRK-VT	PR-VT	PC-SAFT		SRK-VT	PR-VT	PC-SAFT	SRK-VT	PR-VT	PC-SAFT
Fluid 236	3.53	5.39	21.34	-	-	-	-	1.66	2.03	1.40				
Fluid 237	2.10	0.18	0.70	-	-	-	-	2.42	2.77	2.02				
Fluid 238	3.83	5.96	9.54	-	-	-	-	1.61	1.99	1.37				
Fluid 239	5.43	7.40	9.84	-	-	-	-	1.61	1.98	1.44				
Fluid 240	0.41	2.65	6.36	-	-	-	-	0.98	1.30	0.44				
Fluid 241	0.93	3.24	6.02	-	-	-	-	1.22	1.56	0.65				
Fluid 242	0.92	2.65	4.04	-	-	-	-	1.24	1.57	0.94				
Fluid 243	2.50	4.07	5.47	-	-	-	-	1.58	1.94	1.41				
Fluid 244	2.86	1.00	0.73	-	-	-	-	1.09	1.40	0.61				
Fluid 245	5.60	4.06	5.62	-	-	-	-	1.07	1.35	1.00				
Fluid 246	0.82	2.54	4.70	-	-	-	-	0.87	1.19	0.48				
Fluid 247	9.22	7.11	8.00	-	-	-	-	1.27	1.59	1.18				
Fluid 248	2.28	4.00	7.08	-	-	-	-	0.53	0.86	0.15				
Fluid 249	3.47	4.90	4.70	-	-	-	-	0.81	1.06	1.15				
Fluid 250	3.03	4.56	5.13	-	-	-	-	0.68	0.91	0.82				
Fluid 251	6.85	5.81	4.66	-	-	-	-	0.28	0.50	0.42				
Fluid 252	6.11	7.01	2.14	-	-	-	-	0.45	0.68	0.44				
Fluid 253	5.78	6.03	4.50	-	-	-	-	0.67	0.95	1.79				
Fluid 254	8.80	9.02	4.76	-	-	-	-	1.41	1.71	2.91				
Fluid 255	10.86	6.69	14.68	-	-	-	-	0.41	0.28	0.69				
Fluid 256	10.44	6.42	14.98	-	-	-	-	0.26	0.12	0.85				
Fluid 257	1.18	0.16	0.60	-	-	-	-	0.39	0.21	1.32				

Continued on next page

Table B.3 – continued from previous page.

Fluid no.	Saturation Pressure			Density			Stock Tank Oil Density		
	SRK-VT	PR-VT	PC-SAFT	SRK-VT	PR-VT	PC-SAFT	SRK-VT	PR-VT	PC-SAFT
Fluid 258	4.74	2.66	1.59	-	-	-	0.23	0.04	0.87
Fluid 259	8.45	6.35	16.70	-	-	-	0.35	0.64	0.32
Fluid 260	3.17	4.92	5.19	-	-	-	0.40	0.64	0.48
Average	6.35	6.26	6.51	1.63	1.55	1.73	0.66	0.80	0.86

B.4 Deviation in Compressibility Calculations

The AAD% in compressibility for the 260 petroleum fluids in the database are listed in Table B.4, where we have compared the performance of SRK and PR (with/without volume translation), Soave-BWR and PC-SAFT with Yan et al.'s characterization method [119] (eq. (4.31) and eqs. (4.34)–(4.35)), and PC-SAFT with the new general characterization method (eqs. (4.39)–(4.40)).

Table B.4 AAD% in calculated compressibility using different EoSs including PC-SAFT with the new characterization method (eqs. (4.39)–(4.40)). The fluids without density data or few data above saturation pressure are eliminated from table.

Fluid no.	Compressibility						
	SRK	PR	SRK-VT	PR-VT	SBWR	PC-SAFT [119]	PC-SAFT (New Char.)
Fluid 1	20.23	20.68	40.93	42.07	18.94	26.91	25.79
Fluid 6	18.83	16.16	17.10	16.12	9.64	29.76	32.92
Fluid 7	25.09	16.62	8.23	9.10	16.59	15.83	15.56
Fluid 8	45.97	35.11	25.59	27.04	30.16	22.20	24.98
Fluid 9	15.06	13.26	0.79	8.09	5.88	7.10	5.39
Fluid 10	11.39	12.32	5.23	8.09	6.48	8.01	7.37
Fluid 11	18.71	11.33	8.50	9.34	14.92	8.01	10.03
Fluid 12	10.86	14.80	21.78	18.08	22.59	30.67	29.32
Fluid 22	16.52	15.58	14.01	13.85	6.89	8.36	7.60
Fluid 23	13.10	12.70	13.98	11.89	6.83	6.50	6.00
Fluid 27	24.40	24.12	31.77	24.53	21.60	22.16	22.05
Fluid 32	20.92	22.61	22.80	20.30	23.37	25.78	25.29
Fluid 33	19.88	19.56	24.70	21.63	20.18	18.36	18.62
Fluid 34	20.29	17.34	9.75	17.81	8.06	6.04	5.47
Fluid 35	21.56	22.87	17.41	17.39	22.28	17.76	21.53
Fluid 36	27.49	17.99	12.12	14.13	19.86	17.00	19.38
Fluid 62	26.19	21.18	20.10	18.89	20.54	10.93	13.03
Fluid 63	58.81	43.69	34.73	33.11	38.78	39.88	42.71
Fluid 64	29.68	14.55	17.87	15.67	22.12	29.51	31.57
Fluid 65	4.02	3.54	17.60	8.58	16.57	17.95	19.58
Fluid 68	27.69	15.79	13.11	10.57	17.68	23.17	23.23
Fluid 69	20.23	15.68	16.83	15.70	16.97	22.42	24.22
Fluid 70	9.70	5.18	9.72	5.85	8.75	14.80	14.96
Fluid 71	25.15	11.94	8.63	6.30	17.10	25.55	28.12
Fluid 73	35.00	28.28	15.21	17.31	17.81	6.07	7.75
Fluid 74	25.76	20.02	10.76	12.28	10.23	4.74	4.94
Fluid 79	11.88	9.02	5.63	6.08	5.72	3.21	2.08
Fluid 82	30.33	13.85	13.91	9.19	22.13	40.77	44.29
Fluid 91	14.39	9.89	1.95	7.57	14.19	4.39	5.71
Fluid 92	18.67	14.53	6.54	13.76	18.58	8.65	9.56
Fluid 93	8.34	5.38	2.52	4.85	6.63	7.28	7.07
Fluid 94	13.09	8.88	3.91	6.43	6.88	7.34	6.77
Fluid 95	30.53	18.15	14.17	14.16	13.01	10.92	12.16
Fluid 97	13.12	14.63	19.04	21.84	2.91	15.52	17.32
Fluid 98	12.80	12.10	3.09	11.11	4.17	3.34	5.05
Fluid 101	3.96	3.21	7.81	2.90	6.50	12.63	11.70
Fluid 102	34.10	26.14	26.01	24.22	16.05	16.25	17.54

Continued on next page

Table B.4 – continued from previous page.

Fluid no.	Compressibility						
	SRK	PR	SRK-VT	PR-VT	SBWR	PC-SAFT [119]	PC-SAFT (New Char.)
Fluid 103	11.54	8.26	6.48	7.22	4.10	3.76	3.33
Fluid 104	28.85	25.12	17.25	26.44	16.73	12.13	12.66
Fluid 105	43.29	38.75	37.15	38.83	29.95	28.15	28.84
Fluid 106	16.70	12.94	6.06	12.67	4.52	6.29	5.71
Fluid 107	11.01	13.12	3.20	14.53	3.81	3.23	3.31
Fluid 108	9.96	12.57	18.02	11.72	19.18	24.59	23.97
Fluid 109	11.48	11.10	18.15	8.62	26.04	26.17	25.61
Fluid 110	16.30	11.91	4.45	10.50	7.88	4.66	4.77
Fluid 112	23.07	24.50	10.18	22.66	11.56	7.94	8.51
Fluid 113	15.67	19.14	19.87	20.19	17.07	16.21	15.64
Fluid 115	9.23	12.55	4.82	17.37	7.19	11.30	11.59
Fluid 117	11.36	12.23	6.25	12.45	7.55	7.32	8.37
Fluid 118	30.21	22.78	15.93	18.66	17.80	14.90	15.41
Fluid 119	9.90	11.27	4.01	12.21	5.72	5.60	5.52
Fluid 120	10.43	8.94	5.39	8.13	6.77	8.62	8.14
Fluid 121	19.14	14.02	7.90	12.80	6.19	8.12	7.51
Fluid 122	9.90	7.02	1.89	7.50	5.62	3.33	3.17
Fluid 123	8.98	8.26	12.50	12.62	15.26	21.04	22.91
Fluid 124	28.99	20.10	14.09	17.67	11.42	7.57	8.03
Fluid 125	31.18	18.42	16.12	14.54	14.88	17.24	18.79
Fluid 126	16.24	15.59	14.12	17.55	12.07	8.95	9.20
Fluid 127	4.05	3.76	5.62	3.83	7.97	10.42	9.49
Fluid 128	14.43	16.19	5.73	18.75	6.94	6.76	6.75
Fluid 129	15.34	15.71	6.94	17.73	6.94	6.77	6.71
Fluid 131	23.22	16.35	15.25	17.36	4.84	3.71	4.29
Fluid 132	18.88	13.55	9.25	11.79	6.35	3.24	3.62
Fluid 133	20.95	14.49	9.57	11.97	14.40	8.07	9.19
Fluid 134	4.67	4.40	7.98	4.74	12.55	13.94	13.27
Fluid 135	49.41	46.72	33.84	44.90	38.37	26.37	27.62
Fluid 136	51.69	48.30	34.39	45.15	31.17	30.78	32.21
Fluid 137	6.62	8.42	4.27	8.21	5.45	5.81	5.21
Fluid 138	9.50	12.52	5.57	12.28	5.47	9.22	8.51
Fluid 139	19.58	16.89	7.77	15.15	9.19	6.64	6.98
Fluid 140	26.29	26.75	15.44	28.15	9.74	7.28	7.53
Fluid 141	10.77	9.51	1.71	8.14	7.59	6.23	6.13
Fluid 142	7.47	8.80	3.66	9.84	5.55	6.11	5.59
Fluid 144	42.12	37.71	29.40	39.02	16.08	12.46	13.86
Fluid 146	12.85	15.04	6.23	15.31	4.67	4.52	4.52
Fluid 147	18.76	11.47	12.39	11.16	18.68	28.62	30.62
Fluid 148	39.13	35.41	24.33	33.88	19.90	16.28	17.50
Fluid 151	3.82	8.00	9.14	8.03	10.01	9.33	9.60
Fluid 153	8.33	9.30	5.90	11.81	8.35	7.28	7.18
Fluid 154	14.69	12.57	4.72	13.39	4.77	4.42	4.17
Fluid 155	8.60	8.40	3.99	5.77	1.44	3.73	5.77
Fluid 156	13.17	9.48	10.44	9.32	7.16	4.12	5.14
Fluid 157	15.04	16.05	6.60	18.05	7.00	6.71	6.56
Fluid 160	9.01	5.49	2.81	3.77	12.86	6.92	7.19
Fluid 165	21.35	14.89	6.53	10.68	4.84	3.86	3.48
Average	19.38	16.28	12.67	15.40	12.91	12.97	13.49

C | C_p and μ_{JT} Calculated using Different EoSs for Light and Heavy n-alkanes

Table C.1 Heat capacity at constant pressure, C_p , calculated using SRK EoS in $\text{Jg}^{-1}\text{K}^{-1}$.

T/K	P/MPa											
	0.14	10.09	0.1	10.13	0.12	10.17	0.1	10.18	0.12	10.12	0.13	10.09
	n-hexane		n-octane		n-decane		n-dodecane		n-tetradecane		n-hexadecane	
323.15	2.359	2.307	2.268	2.239	2.225	2.205	2.204	2.189	2.179	2.166	2.166	2.155
328.15	2.388	2.332	2.293	2.262	2.248	2.227	2.226	2.210	2.201	2.188	2.188	2.177
333.15	2.417	2.357	2.318	2.285	2.272	2.250	2.248	2.231	2.224	2.210	2.211	2.199
338.15	-	2.383	2.343	2.309	2.296	2.273	2.269	2.252	2.247	2.232	2.233	2.221
343.15	-	2.408	2.369	2.333	2.320	2.295	2.291	2.273	2.270	2.255	2.256	2.243
348.15	-	2.434	2.394	2.356	2.344	2.318	2.313	2.294	2.293	2.277	2.279	2.265
353.15	-	2.460	2.420	2.380	2.368	2.341	2.335	2.315	2.316	2.299	2.301	2.288
358.15	-	2.486	2.447	2.403	2.392	2.364	2.358	2.337	2.338	2.321	2.324	2.310
363.15	-	2.512	2.473	2.427	2.416	2.387	2.380	2.358	2.361	2.343	2.346	2.331
368.15	-	2.538	2.499	2.451	2.441	2.409	2.402	2.379	2.384	2.365	2.369	2.353
373.15	-	-	2.526	2.475	2.465	2.432	2.425	2.400	2.407	2.387	2.391	2.375
378.15	-	-	2.553	2.498	2.490	2.455	2.447	2.422	2.429	2.409	2.414	2.397
383.15	-	-	2.580	2.522	2.514	2.477	2.470	2.443	2.452	2.431	2.436	2.418
388.15	-	-	-	2.546	2.539	2.500	2.492	2.464	2.474	2.452	2.458	2.439
393.15	-	-	-	2.569	2.563	2.522	2.515	2.485	2.497	2.473	2.480	2.461
398.15	-	-	-	2.593	2.588	2.545	2.537	2.506	2.519	2.495	2.502	2.482
403.15	-	-	-	-	2.612	2.567	2.560	2.527	2.541	2.516	2.523	2.502
408.15	-	-	-	-	-	2.589	2.582	2.548	2.563	2.537	2.545	2.523
413.15	-	-	-	-	-	2.611	2.605	2.569	2.585	2.557	2.566	2.544
418.15	-	-	-	-	-	2.633	2.627	2.590	2.607	2.578	2.588	2.564
423.15	-	-	-	-	-	2.655	2.650	2.611	2.629	2.598	2.609	2.584
428.15	-	-	-	-	-	2.677	2.673	2.631	2.651	2.619	2.630	2.604
433.15	-	-	-	-	-	-	2.695	2.652	2.672	2.639	2.651	2.624
438.15	-	-	-	-	-	-	2.718	2.672	2.694	2.659	2.672	2.644
443.15	-	-	-	-	-	-	-	2.692	2.715	2.679	2.693	2.663
448.15	-	-	-	-	-	-	-	2.712	2.737	2.698	2.713	2.683
453.15	-	-	-	-	-	-	-	2.732	2.758	2.718	2.734	2.702
458.15	-	-	-	-	-	-	-	-	2.779	2.737	-	2.721
463.15	-	-	-	-	-	-	-	-	2.801	2.756	-	2.740
468.15	-	-	-	-	-	-	-	-	-	2.775	-	2.758
473.15	-	-	-	-	-	-	-	-	-	2.794	-	2.777
478.15	-	-	-	-	-	-	-	-	-	2.813	-	-
483.15	-	-	-	-	-	-	-	-	-	2.831	-	-

Table C.2 Heat capacity at constant pressure, C_p , calculated using PR EoS in $\text{Jg}^{-1}\text{K}^{-1}$.

T/K	P/MPa											
	0.14	10.09	0.1	10.13	0.12	10.17	0.1	10.18	0.12	10.12	0.13	10.09
	n-hexane		n-octane		n-decane		n-dodecane		n-tetradecane		n-hexadecane	
323.15	2.306	2.260	2.219	2.194	2.178	2.161	2.159	2.146	2.134	2.123	2.121	2.111
328.15	2.335	2.285	2.245	2.218	2.202	2.184	2.181	2.167	2.157	2.145	2.143	2.134
333.15	2.365	2.311	2.270	2.242	2.226	2.207	2.202	2.188	2.180	2.168	2.166	2.156
338.15	-	2.337	2.296	2.265	2.250	2.230	2.225	2.209	2.203	2.191	2.189	2.179
343.15	-	2.363	2.321	2.289	2.274	2.253	2.247	2.231	2.226	2.213	2.212	2.201
348.15	-	2.390	2.348	2.314	2.299	2.276	2.269	2.252	2.249	2.236	2.235	2.224
353.15	-	2.416	2.374	2.338	2.323	2.300	2.291	2.274	2.273	2.258	2.258	2.246
358.15	-	2.443	2.400	2.362	2.348	2.323	2.314	2.296	2.296	2.281	2.281	2.268
363.15	-	2.470	2.427	2.386	2.372	2.346	2.337	2.317	2.319	2.303	2.303	2.290
368.15	-	2.496	2.454	2.410	2.397	2.369	2.359	2.339	2.342	2.325	2.326	2.313
373.15	-	-	2.481	2.434	2.421	2.392	2.382	2.360	2.365	2.348	2.349	2.335
378.15	-	-	2.508	2.459	2.446	2.415	2.404	2.382	2.387	2.370	2.371	2.357
383.15	-	-	2.535	2.483	2.471	2.438	2.427	2.404	2.410	2.392	2.394	2.378
388.15	-	-	-	2.507	2.496	2.461	2.450	2.425	2.433	2.413	2.416	2.400
393.15	-	-	-	2.531	2.520	2.484	2.473	2.447	2.455	2.435	2.438	2.421
398.15	-	-	-	2.555	2.545	2.507	2.495	2.468	2.478	2.457	2.460	2.443
403.15	-	-	-	-	2.570	2.529	2.518	2.490	2.500	2.478	2.482	2.464
408.15	-	-	-	-	-	2.552	2.541	2.511	2.523	2.499	2.504	2.485
413.15	-	-	-	-	-	2.575	2.564	2.532	2.545	2.520	2.526	2.506
418.15	-	-	-	-	-	2.597	2.586	2.553	2.567	2.541	2.547	2.526
423.15	-	-	-	-	-	2.619	2.609	2.574	2.589	2.562	2.569	2.547
428.15	-	-	-	-	-	2.641	2.632	2.595	2.611	2.583	2.590	2.567
433.15	-	-	-	-	-	-	2.655	2.616	2.633	2.603	2.611	2.587
438.15	-	-	-	-	-	-	2.678	2.636	2.654	2.623	2.632	2.607
443.15	-	-	-	-	-	-	-	2.657	2.676	2.643	2.653	2.627
448.15	-	-	-	-	-	-	-	2.677	2.698	2.663	2.674	2.647
453.15	-	-	-	-	-	-	-	2.698	2.719	2.683	2.695	2.666
458.15	-	-	-	-	-	-	-	-	2.741	2.703	-	2.686
463.15	-	-	-	-	-	-	-	-	2.762	2.722	-	2.705
468.15	-	-	-	-	-	-	-	-	-	2.741	-	2.724
473.15	-	-	-	-	-	-	-	-	-	2.761	-	2.742
478.15	-	-	-	-	-	-	-	-	-	2.780	-	-
483.15	-	-	-	-	-	-	-	-	-	2.798	-	-

Table C.3 Heat capacity at constant pressure, C_p , calculated using PC-SAFT EoS in $\text{Jg}^{-1}\text{K}^{-1}$.

T/K	P/MPa											
	0.14	10.09	0.1	10.13	0.12	10.17	0.1	10.18	0.12	10.12	0.13	10.09
	n-hexane		n-octane		n-decane		n-dodecane		n-tetradecane		n-hexadecane	
323.15	2.367	2.338	2.306	2.293	2.287	2.279	2.271	2.266	2.254	2.251	2.249	2.248
328.15	2.390	2.359	2.327	2.312	2.306	2.297	2.288	2.282	2.272	2.269	2.267	2.265
333.15	2.414	2.380	2.347	2.331	2.325	2.315	2.305	2.299	2.290	2.286	2.285	2.282
338.15	-	2.402	2.368	2.350	2.344	2.333	2.323	2.316	2.309	2.304	2.303	2.300
343.15	-	2.424	2.389	2.370	2.364	2.352	2.340	2.333	2.327	2.322	2.322	2.318
348.15	-	2.446	2.411	2.390	2.384	2.371	2.358	2.350	2.346	2.341	2.340	2.336
353.15	-	2.469	2.432	2.410	2.404	2.390	2.376	2.367	2.365	2.359	2.359	2.354
358.15	-	2.492	2.454	2.430	2.424	2.409	2.395	2.385	2.384	2.377	2.377	2.372
363.15	-	2.515	2.477	2.451	2.445	2.429	2.413	2.403	2.403	2.396	2.396	2.390
368.15	-	2.538	2.499	2.471	2.465	2.448	2.432	2.421	2.422	2.414	2.415	2.409
373.15	-	-	2.522	2.492	2.486	2.468	2.451	2.439	2.442	2.433	2.434	2.427
378.15	-	-	2.545	2.513	2.507	2.487	2.470	2.457	2.461	2.451	2.453	2.445
383.15	-	-	2.568	2.534	2.528	2.507	2.489	2.475	2.480	2.470	2.472	2.464
388.15	-	-	-	2.555	2.549	2.527	2.509	2.493	2.499	2.488	2.491	2.482
393.15	-	-	-	2.576	2.571	2.547	2.528	2.512	2.519	2.507	2.510	2.500
398.15	-	-	-	2.597	2.592	2.566	2.548	2.530	2.538	2.526	2.529	2.519
403.15	-	-	-	-	2.614	2.586	2.567	2.549	2.558	2.544	2.548	2.537
408.15	-	-	-	-	-	2.606	2.587	2.567	2.577	2.562	2.567	2.555
413.15	-	-	-	-	-	2.626	2.607	2.586	2.596	2.581	2.586	2.573
418.15	-	-	-	-	-	2.646	2.627	2.604	2.616	2.599	2.605	2.591
423.15	-	-	-	-	-	2.666	2.647	2.623	2.635	2.618	2.623	2.609
428.15	-	-	-	-	-	2.686	2.667	2.642	2.654	2.636	2.642	2.627
433.15	-	-	-	-	-	-	2.687	2.660	2.674	2.654	2.661	2.645
438.15	-	-	-	-	-	-	2.707	2.679	2.693	2.672	2.680	2.663
443.15	-	-	-	-	-	-	-	2.697	2.712	2.690	2.698	2.681
448.15	-	-	-	-	-	-	-	2.716	2.731	2.708	2.717	2.698
453.15	-	-	-	-	-	-	-	2.735	2.751	2.726	2.736	2.716
458.15	-	-	-	-	-	-	-	-	2.770	2.744	-	2.733
463.15	-	-	-	-	-	-	-	-	2.789	2.762	-	2.751
468.15	-	-	-	-	-	-	-	-	-	2.779	-	2.768
473.15	-	-	-	-	-	-	-	-	-	2.797	-	2.785
478.15	-	-	-	-	-	-	-	-	-	2.815	-	-
483.15	-	-	-	-	-	-	-	-	-	2.832	-	-

Table C.4 Heat capacity at constant pressure, C_p , calculated using Soave-BWR EoS in $\text{Jg}^{-1}\text{K}^{-1}$.

T/K	P/MPa											
	0.14	10.09	0.1	10.13	0.12	10.17	0.1	10.18	0.12	10.12	0.13	10.09
	n-hexane		n-octane		n-decane		n-dodecane		n-tetradecane		n-hexadecane	
323.15	2.381	2.349	2.315	2.298	2.288	2.278	2.283	2.277	2.275	2.271	2.284	2.282
328.15	2.405	2.371	2.337	2.318	2.307	2.296	2.299	2.291	2.289	2.285	2.296	2.294
333.15	2.430	2.394	2.358	2.339	2.327	2.315	2.315	2.307	2.305	2.300	2.310	2.307
338.15	-	2.416	2.380	2.359	2.346	2.334	2.331	2.323	2.322	2.316	2.324	2.321
343.15	-	2.439	2.402	2.380	2.367	2.353	2.348	2.339	2.338	2.332	2.339	2.335
348.15	-	2.461	2.424	2.401	2.387	2.373	2.366	2.356	2.356	2.349	2.355	2.351
353.15	-	2.484	2.447	2.422	2.408	2.392	2.384	2.374	2.374	2.366	2.371	2.366
358.15	-	2.507	2.469	2.444	2.429	2.412	2.403	2.392	2.392	2.384	2.388	2.383
363.15	-	2.530	2.492	2.465	2.450	2.433	2.421	2.410	2.410	2.402	2.405	2.399
368.15	-	2.553	2.515	2.486	2.471	2.453	2.440	2.428	2.429	2.420	2.423	2.416
373.15	-	-	2.538	2.507	2.492	2.473	2.460	2.446	2.448	2.438	2.441	2.434
378.15	-	-	2.561	2.529	2.514	2.493	2.479	2.465	2.467	2.457	2.459	2.451
383.15	-	-	2.584	2.550	2.535	2.514	2.498	2.484	2.487	2.476	2.477	2.469
388.15	-	-	-	2.571	2.557	2.534	2.518	2.502	2.506	2.494	2.495	2.487
393.15	-	-	-	2.592	2.578	2.554	2.538	2.521	2.525	2.513	2.514	2.505
398.15	-	-	-	2.613	2.600	2.575	2.558	2.540	2.545	2.532	2.533	2.523
403.15	-	-	-	-	2.621	2.595	2.578	2.559	2.564	2.550	2.551	2.541
408.15	-	-	-	-	-	2.615	2.598	2.578	2.584	2.569	2.570	2.559
413.15	-	-	-	-	-	2.635	2.618	2.597	2.604	2.588	2.589	2.577
418.15	-	-	-	-	-	2.655	2.638	2.616	2.623	2.607	2.608	2.595
423.15	-	-	-	-	-	2.675	2.658	2.635	2.642	2.625	2.627	2.613
428.15	-	-	-	-	-	2.695	2.678	2.653	2.662	2.644	2.645	2.631
433.15	-	-	-	-	-	-	2.698	2.672	2.681	2.662	2.664	2.649
438.15	-	-	-	-	-	-	2.718	2.691	2.701	2.680	2.683	2.667
443.15	-	-	-	-	-	-	-	2.709	2.720	2.699	2.701	2.685
448.15	-	-	-	-	-	-	-	2.728	2.739	2.717	2.720	2.703
453.15	-	-	-	-	-	-	-	2.746	2.758	2.735	2.739	2.720
458.15	-	-	-	-	-	-	-	-	2.777	2.753	-	2.738
463.15	-	-	-	-	-	-	-	-	2.796	2.770	-	2.755
468.15	-	-	-	-	-	-	-	-	-	2.788	-	2.773
473.15	-	-	-	-	-	-	-	-	-	2.805	-	2.790
478.15	-	-	-	-	-	-	-	-	-	2.823	-	-
483.15	-	-	-	-	-	-	-	-	-	2.840	-	-

Table C.5 Joule-Thomson coefficient, μ_{JT} , calculated using SRK EoS in K.MPa^{-1} .

T/K	P/MPa											
	0.14	10.09	0.1	10.13	0.12	10.17	0.1	10.18	0.12	10.12	0.13	10.09
	n-hexane		n-octane		n-decane		n-dodecane		n-tetradecane		n-hexadecane	
323.15	-0.380	-0.459	-0.497	-0.543	-0.563	-0.596	-0.610	-0.636	-0.663	-0.686	-0.695	-0.715
328.15	-0.360	-0.445	-0.483	-0.532	-0.552	-0.586	-0.600	-0.627	-0.652	-0.676	-0.685	-0.706
333.15	-0.339	-0.432	-0.469	-0.521	-0.540	-0.576	-0.589	-0.618	-0.642	-0.667	-0.674	-0.696
338.15	-	-0.418	-0.455	-0.511	-0.528	-0.567	-0.579	-0.609	-0.631	-0.658	-0.664	-0.687
343.15	-	-0.403	-0.440	-0.500	-0.516	-0.557	-0.568	-0.601	-0.621	-0.649	-0.654	-0.678
348.15	-	-0.389	-0.425	-0.489	-0.504	-0.547	-0.558	-0.592	-0.610	-0.640	-0.644	-0.669
353.15	-	-0.374	-0.409	-0.477	-0.491	-0.538	-0.547	-0.583	-0.600	-0.631	-0.634	-0.660
358.15	-	-0.359	-0.393	-0.466	-0.479	-0.528	-0.536	-0.574	-0.589	-0.622	-0.624	-0.652
363.15	-	-0.343	-0.376	-0.455	-0.466	-0.518	-0.525	-0.565	-0.579	-0.613	-0.614	-0.643
368.15	-	-0.327	-0.359	-0.444	-0.453	-0.508	-0.514	-0.557	-0.568	-0.604	-0.604	-0.635
373.15	-	-	-0.341	-0.432	-0.439	-0.499	-0.503	-0.548	-0.558	-0.596	-0.594	-0.626
378.15	-	-	-0.322	-0.420	-0.426	-0.489	-0.491	-0.539	-0.547	-0.587	-0.584	-0.618
383.15	-	-	-0.303	-0.409	-0.412	-0.479	-0.480	-0.530	-0.536	-0.579	-0.574	-0.610
388.15	-	-	-	-0.397	-0.398	-0.469	-0.468	-0.522	-0.526	-0.570	-0.564	-0.601
393.15	-	-	-	-0.384	-0.383	-0.459	-0.456	-0.513	-0.515	-0.562	-0.554	-0.593
398.15	-	-	-	-0.372	-0.368	-0.450	-0.444	-0.504	-0.504	-0.553	-0.543	-0.585
403.15	-	-	-	-	-0.352	-0.440	-0.431	-0.495	-0.492	-0.545	-0.533	-0.577
408.15	-	-	-	-	-	-0.429	-0.418	-0.487	-0.481	-0.537	-0.523	-0.569
413.15	-	-	-	-	-	-0.419	-0.405	-0.478	-0.470	-0.529	-0.513	-0.562
418.15	-	-	-	-	-	-0.409	-0.392	-0.469	-0.458	-0.520	-0.502	-0.554
423.15	-	-	-	-	-	-0.399	-0.378	-0.460	-0.446	-0.512	-0.492	-0.546
428.15	-	-	-	-	-	-0.388	-0.364	-0.451	-0.434	-0.504	-0.481	-0.538
433.15	-	-	-	-	-	-	-0.349	-0.442	-0.422	-0.496	-0.470	-0.531
438.15	-	-	-	-	-	-	-0.333	-0.433	-0.409	-0.488	-0.459	-0.523
443.15	-	-	-	-	-	-	-	-0.424	-0.396	-0.479	-0.448	-0.515
448.15	-	-	-	-	-	-	-	-0.414	-0.383	-0.471	-0.436	-0.508
453.15	-	-	-	-	-	-	-	-0.405	-0.369	-0.463	-0.424	-0.500
458.15	-	-	-	-	-	-	-	-	-0.354	-0.455	-	-0.493
463.15	-	-	-	-	-	-	-	-	-0.340	-0.446	-	-0.485
468.15	-	-	-	-	-	-	-	-	-	-0.438	-	-0.477
473.15	-	-	-	-	-	-	-	-	-	-0.429	-	-0.470
478.15	-	-	-	-	-	-	-	-	-	-0.421	-	-
483.15	-	-	-	-	-	-	-	-	-	-0.412	-	-

Table C.6 Joule-Thomson coefficient, μ_{JT} , calculated using PR EoS in K.MPa⁻¹.

T/K	P/MPa											
	0.14	10.09	0.1	10.13	0.12	10.17	0.1	10.18	0.12	10.12	0.13	10.09
	n-hexane		n-octane		n-decane		n-dodecane		n-tetradecane		n-hexadecane	
323.15	-0.359	-0.423	-0.464	-0.500	-0.523	-0.548	-0.565	-0.585	-0.613	-0.630	-0.641	-0.657
328.15	-0.340	-0.410	-0.451	-0.490	-0.512	-0.539	-0.555	-0.577	-0.603	-0.621	-0.632	-0.648
333.15	-0.321	-0.397	-0.438	-0.480	-0.501	-0.530	-0.546	-0.568	-0.593	-0.613	-0.622	-0.640
338.15	-	-0.384	-0.425	-0.470	-0.491	-0.521	-0.536	-0.560	-0.583	-0.604	-0.613	-0.631
343.15	-	-0.370	-0.412	-0.459	-0.480	-0.512	-0.527	-0.552	-0.574	-0.596	-0.604	-0.623
348.15	-	-0.356	-0.398	-0.449	-0.469	-0.503	-0.517	-0.544	-0.564	-0.587	-0.594	-0.614
353.15	-	-0.342	-0.384	-0.439	-0.457	-0.494	-0.507	-0.535	-0.555	-0.579	-0.585	-0.606
358.15	-	-0.328	-0.369	-0.428	-0.446	-0.485	-0.497	-0.527	-0.545	-0.570	-0.576	-0.598
363.15	-	-0.313	-0.354	-0.418	-0.434	-0.476	-0.487	-0.519	-0.535	-0.562	-0.567	-0.590
368.15	-	-0.298	-0.339	-0.407	-0.422	-0.467	-0.477	-0.511	-0.526	-0.554	-0.558	-0.582
373.15	-	-	-0.322	-0.396	-0.410	-0.458	-0.467	-0.503	-0.516	-0.546	-0.548	-0.574
378.15	-	-	-0.306	-0.385	-0.398	-0.448	-0.457	-0.494	-0.507	-0.538	-0.539	-0.566
383.15	-	-	-0.288	-0.374	-0.385	-0.439	-0.446	-0.486	-0.497	-0.530	-0.530	-0.558
388.15	-	-	-	-0.363	-0.373	-0.430	-0.436	-0.478	-0.487	-0.522	-0.521	-0.551
393.15	-	-	-	-0.351	-0.359	-0.421	-0.425	-0.470	-0.477	-0.514	-0.512	-0.543
398.15	-	-	-	-0.339	-0.346	-0.411	-0.414	-0.462	-0.467	-0.507	-0.503	-0.536
403.15	-	-	-	-	-0.331	-0.402	-0.403	-0.454	-0.457	-0.499	-0.494	-0.528
408.15	-	-	-	-	-	-0.393	-0.391	-0.445	-0.447	-0.491	-0.484	-0.521
413.15	-	-	-	-	-	-0.383	-0.379	-0.437	-0.437	-0.484	-0.475	-0.514
418.15	-	-	-	-	-	-0.373	-0.367	-0.429	-0.426	-0.476	-0.466	-0.507
423.15	-	-	-	-	-	-0.364	-0.355	-0.420	-0.416	-0.468	-0.456	-0.499
428.15	-	-	-	-	-	-0.354	-0.342	-0.412	-0.405	-0.461	-0.446	-0.492
433.15	-	-	-	-	-	-	-0.328	-0.404	-0.394	-0.453	-0.437	-0.485
438.15	-	-	-	-	-	-	-0.315	-0.395	-0.382	-0.445	-0.427	-0.478
443.15	-	-	-	-	-	-	-	-0.386	-0.371	-0.438	-0.417	-0.471
448.15	-	-	-	-	-	-	-	-0.378	-0.359	-0.430	-0.406	-0.464
453.15	-	-	-	-	-	-	-	-0.369	-0.346	-0.422	-0.396	-0.457
458.15	-	-	-	-	-	-	-	-	-0.334	-0.414	-	-0.449
463.15	-	-	-	-	-	-	-	-	-0.320	-0.406	-	-0.442
468.15	-	-	-	-	-	-	-	-	-	-0.399	-	-0.435
473.15	-	-	-	-	-	-	-	-	-	-0.391	-	-0.428
478.15	-	-	-	-	-	-	-	-	-	-0.383	-	-
483.15	-	-	-	-	-	-	-	-	-	-0.374	-	-

Table C.7 Joule-Thomson coefficient, μ_{JT} , calculated using PC-SAFT EoS in K.MPa^{-1} .

T/K	P/MPa											
	0.14	10.09	0.1	10.13	0.12	10.17	0.1	10.18	0.12	10.12	0.13	10.09
	n-hexane		n-octane		n-decane		n-dodecane		n-tetradecane		n-hexadecane	
323.15	-0.356	-0.393	-0.396	-0.415	-0.406	-0.418	-0.414	-0.423	-0.416	-0.423	-0.418	-0.424
328.15	-0.345	-0.384	-0.388	-0.409	-0.400	-0.414	-0.409	-0.419	-0.411	-0.419	-0.414	-0.420
333.15	-0.332	-0.376	-0.380	-0.403	-0.394	-0.409	-0.404	-0.415	-0.407	-0.415	-0.410	-0.417
338.15	-	-0.367	-0.373	-0.397	-0.388	-0.404	-0.400	-0.411	-0.402	-0.411	-0.406	-0.413
343.15	-	-0.357	-0.364	-0.390	-0.382	-0.399	-0.394	-0.407	-0.398	-0.407	-0.402	-0.410
348.15	-	-0.347	-0.356	-0.384	-0.375	-0.394	-0.389	-0.403	-0.393	-0.403	-0.397	-0.406
353.15	-	-0.337	-0.347	-0.377	-0.369	-0.388	-0.384	-0.398	-0.388	-0.399	-0.393	-0.402
358.15	-	-0.327	-0.338	-0.370	-0.362	-0.383	-0.378	-0.394	-0.383	-0.395	-0.388	-0.398
363.15	-	-0.316	-0.328	-0.363	-0.355	-0.377	-0.373	-0.389	-0.378	-0.391	-0.384	-0.394
368.15	-	-0.305	-0.318	-0.356	-0.347	-0.372	-0.367	-0.385	-0.373	-0.387	-0.379	-0.390
373.15	-	-	-0.308	-0.348	-0.340	-0.366	-0.361	-0.380	-0.368	-0.383	-0.374	-0.386
378.15	-	-	-0.297	-0.341	-0.332	-0.360	-0.355	-0.375	-0.363	-0.378	-0.369	-0.382
383.15	-	-	-0.286	-0.333	-0.324	-0.354	-0.348	-0.370	-0.357	-0.374	-0.365	-0.378
388.15	-	-	-	-0.325	-0.316	-0.348	-0.342	-0.365	-0.352	-0.369	-0.359	-0.374
393.15	-	-	-	-0.317	-0.307	-0.341	-0.335	-0.360	-0.346	-0.365	-0.354	-0.370
398.15	-	-	-	-0.308	-0.298	-0.335	-0.328	-0.355	-0.341	-0.360	-0.349	-0.366
403.15	-	-	-	-	-0.289	-0.328	-0.321	-0.349	-0.335	-0.356	-0.344	-0.362
408.15	-	-	-	-	-	-0.322	-0.314	-0.344	-0.329	-0.351	-0.339	-0.357
413.15	-	-	-	-	-	-0.315	-0.306	-0.338	-0.322	-0.346	-0.333	-0.353
418.15	-	-	-	-	-	-0.308	-0.299	-0.333	-0.316	-0.341	-0.327	-0.349
423.15	-	-	-	-	-	-0.301	-0.291	-0.327	-0.310	-0.336	-0.322	-0.344
428.15	-	-	-	-	-	-0.293	-0.282	-0.321	-0.303	-0.332	-0.316	-0.340
433.15	-	-	-	-	-	-	-0.274	-0.315	-0.296	-0.327	-0.310	-0.335
438.15	-	-	-	-	-	-	-0.265	-0.309	-0.289	-0.321	-0.304	-0.330
443.15	-	-	-	-	-	-	-	-0.303	-0.282	-0.316	-0.297	-0.326
448.15	-	-	-	-	-	-	-	-0.296	-0.274	-0.311	-0.291	-0.321
453.15	-	-	-	-	-	-	-	-0.290	-0.267	-0.306	-0.284	-0.316
458.15	-	-	-	-	-	-	-	-	-0.259	-0.300	-	-0.311
463.15	-	-	-	-	-	-	-	-	-0.250	-0.295	-	-0.306
468.15	-	-	-	-	-	-	-	-	-	-0.289	-	-0.301
473.15	-	-	-	-	-	-	-	-	-	-0.283	-	-0.296
478.15	-	-	-	-	-	-	-	-	-	-0.277	-	-
483.15	-	-	-	-	-	-	-	-	-	-0.271	-	-

Table C.8 Joule-Thomson coefficient, μ_{JT} , calculated using Soave-BWR EoS in K.MPa⁻¹.

T/K	P/MPa											
	0.14	10.09	0.1	10.13	0.12	10.17	0.1	10.18	0.12	10.12	0.13	10.09
	n-hexane		n-octane		n-decane		n-dodecane		n-tetradecane		n-hexadecane	
323.15	-0.331	-0.370	-0.377	-0.399	-0.394	-0.409	-0.401	-0.413	-0.415	-0.426	-0.414	-0.423
328.15	-0.319	-0.361	-0.369	-0.393	-0.388	-0.404	-0.396	-0.409	-0.411	-0.422	-0.411	-0.421
333.15	-0.307	-0.351	-0.361	-0.386	-0.381	-0.399	-0.391	-0.405	-0.407	-0.419	-0.408	-0.418
338.15	-	-0.342	-0.352	-0.379	-0.375	-0.393	-0.386	-0.401	-0.402	-0.415	-0.404	-0.415
343.15	-	-0.332	-0.344	-0.372	-0.368	-0.388	-0.381	-0.396	-0.398	-0.411	-0.401	-0.412
348.15	-	-0.323	-0.335	-0.365	-0.361	-0.382	-0.376	-0.392	-0.393	-0.407	-0.397	-0.409
353.15	-	-0.313	-0.325	-0.358	-0.354	-0.376	-0.370	-0.387	-0.388	-0.403	-0.393	-0.405
358.15	-	-0.302	-0.316	-0.350	-0.347	-0.370	-0.365	-0.383	-0.383	-0.399	-0.389	-0.402
363.15	-	-0.292	-0.306	-0.343	-0.340	-0.365	-0.359	-0.378	-0.378	-0.394	-0.384	-0.398
368.15	-	-0.281	-0.296	-0.336	-0.333	-0.359	-0.353	-0.373	-0.373	-0.390	-0.380	-0.394
373.15	-	-	-0.286	-0.328	-0.325	-0.353	-0.347	-0.368	-0.368	-0.385	-0.375	-0.390
378.15	-	-	-0.275	-0.321	-0.317	-0.347	-0.341	-0.363	-0.362	-0.381	-0.371	-0.386
383.15	-	-	-0.264	-0.313	-0.309	-0.340	-0.335	-0.358	-0.357	-0.376	-0.366	-0.382
388.15	-	-	-	-0.305	-0.301	-0.334	-0.328	-0.353	-0.351	-0.372	-0.361	-0.378
393.15	-	-	-	-0.297	-0.293	-0.328	-0.322	-0.347	-0.345	-0.367	-0.356	-0.374
398.15	-	-	-	-0.289	-0.284	-0.322	-0.315	-0.342	-0.339	-0.362	-0.351	-0.370
403.15	-	-	-	-	-0.276	-0.315	-0.308	-0.337	-0.333	-0.357	-0.346	-0.366
408.15	-	-	-	-	-	-0.309	-0.301	-0.331	-0.327	-0.353	-0.340	-0.361
413.15	-	-	-	-	-	-0.302	-0.294	-0.326	-0.321	-0.348	-0.335	-0.357
418.15	-	-	-	-	-	-0.295	-0.286	-0.320	-0.315	-0.343	-0.329	-0.353
423.15	-	-	-	-	-	-0.289	-0.278	-0.315	-0.308	-0.338	-0.324	-0.348
428.15	-	-	-	-	-	-0.282	-0.271	-0.309	-0.302	-0.333	-0.318	-0.344
433.15	-	-	-	-	-	-	-0.263	-0.303	-0.295	-0.328	-0.312	-0.339
438.15	-	-	-	-	-	-	-0.254	-0.298	-0.288	-0.323	-0.307	-0.335
443.15	-	-	-	-	-	-	-	-0.292	-0.281	-0.318	-0.301	-0.330
448.15	-	-	-	-	-	-	-	-0.286	-0.274	-0.313	-0.294	-0.326
453.15	-	-	-	-	-	-	-	-0.280	-0.266	-0.307	-0.288	-0.321
458.15	-	-	-	-	-	-	-	-	-0.259	-0.302	-	-0.317
463.15	-	-	-	-	-	-	-	-	-0.251	-0.297	-	-0.312
468.15	-	-	-	-	-	-	-	-	-	-0.291	-	-0.307
473.15	-	-	-	-	-	-	-	-	-	-0.286	-	-0.302
478.15	-	-	-	-	-	-	-	-	-	-0.280	-	-
483.15	-	-	-	-	-	-	-	-	-	-0.275	-	-

D | Academic Activities

D.1 Peer Reviewed Journal Articles

1. F. Varzandeh, E. H. Stenby, W. Yan. “Comparison of GERG-2008 and Simpler EoS Models in Calculation of Phase Equilibrium and Physical Properties of Natural Gas Related Systems”. *Fluid Phase Equilibria*, (2017), 434, 21-43.
2. F. Varzandeh, E. H. Stenby, W. Yan. “General Approach to Characterizing Reservoir Fluids for EoS Models using a Large PVT Database”. *Fluid Phase Equilibria*, (2017), 433, 97-111.
3. T. Regueira, F. Varzandeh, E. H. Stenby, W. Yan. “Heat capacity and Joule-Thomson Coefficient of Selected n-alkanes at 0.1 and 10 MPa in Broad Temperature Ranges”. *The Journal of Chemical Thermodynamics*, (2017), 111, 250-264.
4. T. Regueira, Y. Liu, A. A. Wibowo, M. Ashrafi, F. Varzandeh, G. Pantelide, E. H. Stenby, W. Yan. “High pressure phase equilibrium of ternary and multicomponent alkane mixtures in the temperature range from (283 to 473) K”. *Fluid Phase Equilibria*, (2017), 449, 186-196.
5. W. Yan, F. Varzandeh, E. H. Stenby. “PVT Modeling of Reservoir Fluids using PC-SAFT EoS and Soave-BWR EoS”. *Fluid Phase Equilibria*, (2015), 386, 96-124.

D.2 Conference Presentations

1. F. Varzandeh, E. H. Stenby, W. Yan. “Evaluation of the Impact of Compositional Characterization of Reservoir Fluids on Modeling”. DHRTC Technology Conference, 16-17 November 2016, Helsingør, Denmark. (*Poster*)

2. F. Varzandeh, W. Yan, E. H. Stenby. “General Approach to Characterize Reservoir Fluids For EoS Models Using a Large PVT Database”. CERE Annual Discussion Meeting, 15-17 June 2016, Denmark. (*Oral*)
3. F. Varzandeh, W. Yan, E. H. Stenby. “Challenges in PVT Modeling and Thermal Properties Calculation of Natural Gas Systems using GERG-2008”. CERE Annual Discussion Meeting, 15-17 June 2016, Denmark. (*Poster*)
4. F. Varzandeh, W. Yan, E. H. Stenby. “General Approach to Characterize Reservoir Fluids Using a Large PVT Database”. *SPE-180082-MS*, SPE EUROPEC (2016), 30 May - 2 June, Vienna, Austria. (*Oral*)
5. F. Varzandeh, W. Yan, E. H. Stenby. “Comparison of GERG-2008 and Soave-BWR in PVT Modeling and Thermal Properties Calculation of Natural Gas Systems”. European Gas Technology Conference (EGATEC 2015), 25-26 November, Vienna, Austria. (*Poster + 5 min oral presentation*)
6. F. Varzandeh, W. Yan, E. H. Stenby. “Comparison of GERG-2008 and Soave-BWR in Thermal Properties Calculation of Natural Gas Systems”. DTU-Kemi PhD Symposium, 5-6 November 2015, Denmark. (*Oral*)
7. F. Varzandeh, W. Yan, E. H. Stenby. “Comparison of GERG-2008 and Soave-BWR in Modeling of Pure, Binary and Natural Gas Mixtures”. Thermodynamics Conference (2015), 15-18 September, Copenhagen, Denmark. (*Poster + 5 min oral presentation*)
8. F. Varzandeh, E. H. Stenby, W. Yan. “Application of Non-Cubic EoS in PVT Calculation and Thermal Properties of HPHT Reservoir Fluids”. CERE Annual Discussion Meeting, 17-19 June 2015, Denmark. (*Oral*)
9. F. Varzandeh, E. H. Stenby, W. Yan. “Comparison of GERG-2008 and Soave-BWR in PVT Modeling of Natural Gas Related Systems”. CERE Annual Discussion Meeting, 17-19 June 2015, Denmark. (*Poster*)
10. F. Varzandeh, E. H. Stenby, W. Yan. “Uncertainty and Sensitivity Analysis of Critical Properties Correlations for Petroleum Fractions”. CERE Annual Discussion Meeting, 17-19 June 2015, Denmark. (*Poster*)
11. F. Varzandeh, E. H. Stenby, W. Yan. “Sensitivity Analysis and Comparison of Critical Properties Correlations for Petroleum Fractions”. DTU-Kemi PhD Symposium, 20 November 2014, Denmark. (*Poster*)
12. F. Varzandeh, E. H. Stenby, W. Yan. “Modeling of HPHT Reservoir Fluids with Non-cubic EoS”. CERE Annual Discussion Meeting, 25-27 June 2014, Denmark. (*Poster*)

D.3 Teaching Assistance/Supervisory of M.Sc. Projects

1. Chairman of DTU SPE Student Chapter, 2014-2016.
2. Co-Supervision of the following M.Sc. Projects during 2014-2016:
 - Joule-Thomson coefficients of hydrocarbon mixtures at high pressures
 - PVT study of model reservoir fluids at HPHT conditions
 - PVT study of hydrocarbon mixtures at high pressure and high temperature conditions
 - Comparison of Equations of State for PVT modeling by use of a large database
3. Teaching Assistant in Enhanced Oil Recovery M.Sc. course (28515), Autumn 2014.
4. Member of organization committee for Thermodynamics Conference, Summer 2015.